MARINE EMISSIONS OF HALOGENATED TRACE GASES FROM THE TROPICAL OCEAN

Dissertation
zur Erlangung des Doktorgrades
der Mathematisch-Naturwissenschaftlichen Fakultät
der Christian-Albrechts-Universität zu Kiel

vorgelegt von
Dipl.-Umweltwiss. Helmke Hepach

Kiel 2014

Erster Gutachter: Prof. Dr. Arne Körtzinger
Zweite Gutachterin: Prof. Dr. Christa Marandino

Tag der mündlichen Prüfung: 23.6.2014
Zum Druck genehmigt: 23.06.2014

Gez. Prof. Dr. Wolfgang J. Duschl, Dekan

Die vorliegende Arbeit wurde am GEOMAR Helmholtz-Zentrum für Ozeanforschung Kiel an der Christian-Albrechts-Universität zu Kiel von November 2009 bis Juni 2014 unter der Anleitung von Dr. Birgit Quack durchgeführt.

„*Man merkt nie, was schon getan wurde, man sieht immer nur, was noch zu tun bleibt*.“

Marie Curie

This thesis is based on the following manuscripts:

1. **Manuscript 1:** H. Hepach, B. Quack, S. Raimund, T. Fischer, and A. Bracher: "*Halocarbon sources and budget in the equatorial Atlantic Cold Tongue*"

   Contribution: Helmke Hepach measured the halocarbons in the sea surface water and from depth profiles, took the phytoplankton pigment samples, evaluated the data, made the calculations, and wrote the manuscript. Birgit Quack assisted with the campaign preparation and postprocessing, and provided input during the manuscript preparation. Stefan Raimund measured together with H. Hepach halocarbons in the sea surface water and the depth. Tim Fischer conducted the microstructure measurements, processed these data and provided the microstructure part in the method section. Astrid Bracher wrote the phytoplankton pigment analysis part in the method section, made the phytoplankton measurements available, calculated the fluorescence sensor data and determined the phytoplankton group composition. T. Fischer and A. Bracher both provided input during the manuscript preparation.

2. **Manuscript 2:** H. Hepach, B. Quack, F. Ziska, S. Fuhlbrügge, E. L. Atlas, K. Krüger, I. Peeken, and D. W. R. Wallace: "*Drivers of diel and regional variations of halocarbon emissions from the tropical North East Atlantic*" Atmos. Chem. Phys., 14, 1255-1275, doi:10.5194/acp-14-1255-2014, 2014.

   Contribution: Helmke Hepach measured the halocarbons in the sea surface water, evaluated the data, made the calculations, and wrote the manuscript. Birgit Quack contributed to the manuscript preparation and the review process. Franziska Ziska took the air samples and conducted the radio sonde launches during the campaign. Steffen Fuhlbrügge evaluated the meteorological data. Elliot L. Atlas measured the atmospheric samples and Ilka Peeken measured and calculated the phytoplankton pigment data. F. Ziska, S. Fuhlbrügge, E. L. Atlas, I. Peeken, K. Krüger and D. W. R. Wallace helped revising the manuscript.

3. **Manuscript 3**: S. Fuhlbrügge, K. Krüger, B. Quack, E. Atlas, H. Hepach, and F. Ziska: "*Impact of the marine atmospheric boundary layer conditions on VSLS abundances in the eastern tropical and subtropical North Atlantic Ocean*" Atmos. Chem. Phys., 13, 6345-6357, doi:10.5194/acp-13-6345-2013, 2013.

   Contribution: Steffen Fuhlbrügge evaluated the data and wrote the manuscript. Kirstin Krüger and Birgit Quack provided input during manuscript preparation and the review process. Elliot Atlas measured and calculated the atmospheric samples. Helmke Hepach measured the sea water samples, calculated the sea-to-air fluxes, and wrote section 3.4. Franziska Ziska took the atmospheric samples and conducted the radio sonde launches. E. Atlas, H. Hepach, and F. Ziska helped revising the manuscript.

4. **Manuscript 4**: F. Ziska, B. Quack, K. Abrahamsson, S. D. Archer, E. Atlas, T. Bell, J. H. Butler, L. J. Carpenter, C. E. Jones, N. R. P. Harris, H. Hepach, K. G. Heumann, C. Hughes, J. Kuss, K. Krüger, P. Liss, R. M. Moore, A. Orlikowska, S. Raimund, C. E. Reeves, W. Reifenhäuser, A. D. Robinson, C. Schall, T. Tanhua, S. Tegtmeier, S. Turner, L. Wang, D. Wallace, J. Williams, H. Yamamoto, S. Yvon-Lewis, and Y. Yokouchi: "*Global sea-to-air flux climatology for bromoform, dibromomethane and methyl* iodide*" Atmos. Chem. Phys., 13, 8915-8934, doi:10.5194/acp-13-8915-2013, 2013.*
   Contribution*:* Franziska Ziska collected and evaluated the data, made the calculations, and wrote the manuscript. Birgit Quack helped collecting and evaluating the data, and assisted in the manuscript preparation and the review process. Helmke Hepach provided halocarbon sea surface data from two campaigns. K. Abrahamsson, S. Archer, E. Atlas, T. Bell, J. Butler, L. Carpenter, C. Jones, N. Harris, K. Heumann, C. Hughes, J. Kuss, P. Liss, R. Moore, A. Orlikowska, S. Raimund, C. Reeves, W. Reifenhäuser, A. Robinson, C. Schall, T. Tanhua, S. Turner, L. Wang, D. Wallace, J. Williams, H. Yamamoto, S. Yvon-Lewis, and Y. Yokouchi provided sea surface water and atmospheric halocarbon data, and together with H. Hepach helped revising the manuscript. Kirstin Krüger and Susann Tegtmeier provided input during the manuscript preparation and the review process.

5. **Manuscript 5**: I. Stemmler, M. Rothe, I. Hense, and H. Hepach: "Numerical modeling of methyl iodide in the eastern tropical Atlantic" Biogeosciences, 10, 4211-4225, doi:10.5194/bg-10-4211-2013, 2013.
   Contribution: Irene Stemmler performed and evaluated the simulations, and wrote the manuscript. Matthias Rothe assisted with the modeling, and Inga Hense provided Input during the manuscript preparation and review process. Helmke Hepach provided methyl iodide data from depth profiles for validation. M. Rothe and H. Hepach helped revising the manuscript.

6. **Manuscript 6**: S. Tegtmeier, K. Krüger, B. Quack, E. Atlas, D. R. Blake, H. Boenisch, A. Engel, H. Hepach, R. Hossaini, M. A. Navarro, S. Raimund, S. Sala, Q. Shi, and F. Ziska: "*The contribution of oceanic methyl iodide to stratospheric iodine*" Atmos. Chem. Phys. Discuss., 13, 11427-11471, doi:10.5194/acpd-13-11427-2013, 2013.

   Contribution: Susann Tegtmeier evaluated the data, performed the calculations, and wrote the manuscript. Kirstin Krüger and Birgit Quack provided input during the manuscript preparation and the review process. Helmke Hepach measured methyl iodide during two campaigns, and calculated the fluxes from one campaign. Stefan Raimund and Qiang Shi provided methyl iodide sea surface data from one campaign. E. Atlas, D. R. Blake, H. Boenisch, A. Engel, H. Hepach, R. Hossaini, M. A. Navarro, S. Raimund, S. Sala, Q. Shi, and F. Ziska helped revising the manuscript.

TABLE OF CONTENTS

I. Summary....3
II. Zusammenfassung....7
III. Introduction....11
  1. Halocarbons in the ocean....12
  1.1. Bromoform and dibromomethane in the ocean....13
    1.1.1. Marine sources....13
    1.1.1.1. Anthropogenic sources....13
    1.1.1.2. Biological sources....14
    1.1.2. Sinks....18
  1.2. Methyl iodide in the ocean....19
    1.2.1. Marine sources....20
    1.2.1.1. Biological production....20
    1.2.1.2. Photochemical formation....22
    1.2.2. Sinks....23
  1.3. Diiodomethane in the ocean....24
    1.3.1. Marine sources....24
    1.3.2. Sinks....26
  2. Air-sea gas exchange....27
  3. Atmospheric bromo- and iodocarbons....30
  3.1. Chemical fate....31
    3.1.1. Bromocarbons....31
    3.1.2. Iodocarbons....32
  3.2. Transport into the stratosphere....34
  4. Study regions....35
  4.1. The equatorial Atlantic upwelling....35
  4.2. The subtropical North East Atlantic....37
  5. Objectives and outline of this dissertation....38
IV. Results and Discussion....43
  1. Manuscript 1....43
  2. Manuscript 2....81
  3. Manuscript 3....105
  4. Manuscript 4....121

  - 5. Manuscript 5 143
  - 6. Manuscript 6 161

V. Conclusions and outlook 183

VI. References 191

VII. Lists 205
  - 1. List of Figures 205
  - 2. List of Tables 207
  - 3. List of Abbreviations 208

VIII. Dansagung 211

IX. Curriculum Vitae 213

X. Eidesstattliche Erklärung 217

SUMMARY

I. Summary

Oceanic bromoform ($CHBr_3$) and dibromomethane (CH_2Br_2) are the largest contributors to organic bromine in the atmosphere, while atmospheric organoiodine is significantly influenced by marine methyl iodide (CH_3I) and diiodomethane (CH_2I_2). Halogenated hydrocarbons (halocarbons) and their degradation products are involved in ozone chemistry in both the troposphere and stratosphere. With decreasing anthropogenic atmospheric halocarbons, the impact of naturally produced halocarbons on atmospheric processes will likely increase. Many uncertainties still exist with regard to their production and degradation in the ocean, as well as to their emissions. While macroalgae have been identified as important sources of them, microalgae were shown to be halocarbon producers as well. Hence, oceanic upwelling systems might play a crucial role for open ocean emissions. The tropical ocean has not only been hypothesized to contribute largely to global halocarbon emissions, but it also may contribute to their transport into upper atmospheric layers. They may be transported in significant amounts into the tropical stratosphere by tropical deep convection. This thesis aims at reducing some of the uncertainties regarding halocarbon emissions from the tropical ocean to understand their role in a future climate.

Two campaigns are covered here: MSM18/3 onboard RV *Maria S. Merian* investigating the Eastern tropical equatorial Atlantic during the cooling season in June and July 2011, and **DRIVE** (**D**iurnal and **R**eg**I**onal **V**ariability of halogen **E**missions) onboard RV *Poseidon*, which focused on the Mauritanian upwelling region in June 2010. Oceanic and atmospheric halocarbon data, biological, meteorological and oceanographic parameters were collected to investigate impact factors on halocarbon emissions. The oceanic and atmospheric data were also included in the most complete halocarbon database so far, **HalOcAt** (**Hal**ocarbons in the **Oc**ean and **At**mosphere). Manuscripts, prepared and published on the basis of this data set, include the first manuscript (Hepach et al., in prep) that focuses on the first measurements of $CHBr_3$, CH_2Br_2, CH_3I and CH_2I_2 in the surface and the water column of the equatorial Atlantic during the Atlantic Cold Tongue (ACT) season. The second (Hepach et al., 2014) and third manuscript (Fuhlbrügge et al., 2013) cover oceanic and atmospheric abundances of $CHBr_3$, CH_2Br_2 and CH_3I in the Mauritanian upwelling region on a diel and regional scale. While the second manuscript investigates impact factors on emissions of these compounds, the third manuscript analyzes meteorological constraints on atmospheric halocarbons. The fourth manuscript (Ziska et al., 2013) uses the HalOcAt database to determine global emissions of $CHBr_3$, CH_2Br_2 and CH_3I, and estimates global contributions from different regions. In the fifth manuscript (Stemmler et al., 2013), depth profiles of CH_3I measured during the DRIVE campaign are used to validate modeled profiles from the tropical open ocean using the **G**eneral **O**cean **T**urbulence **M**odel (**GOTM**). The transport of emissions

of CH_3I into the stratosphere is calculated in the sixth manuscript (Tegtmeier et al., 2013), indicating that CH_3I from the DRIVE campaign is entrained in small amounts into the stratosphere.

Both upwelling systems, the Mauritanian upwelling and the equatorial Atlantic, were shown here to be source regions for $CHBr_3$ and CH_2Br_2, contributing to the large emissions of these compounds from the tropical ocean. While CH_3I has been found to be ubiquitously distributed in the Mauritanian upwelling region hinting towards photochemical formation there, strong implications for biological formation were found in the ACT. This agrees well to the modeled depth profiles of CH_3I indicating they may be influenced both by photochemical and biological formation of this compound. Although it has been hypothesized that the tropical ocean may not contribute to CH_2I_2 emissions to the atmosphere due to its very rapid photolysis, CH_2I_2 could be detected in low concentrations in the surface water of the ACT. The first determination of diapycnal fluxes of $CHBr_3$, CH_2Br_2, CH_3I and CH_2I_2 in the ACT indicate that their production takes place within the mixed layer regardless of deeper biomass maxima, which may be very important for their emissions. In the Mauritanian upwelling, oceanic halocarbon production was identified as the main driver of halocarbon emissions with wind speed having impact on a diel scale. For the first time, the height of the Marine Atmospheric Boundary Layer (MABL) has been found to indirectly impact halocarbon emissions due to its decreasing and increasing effect on atmospheric halocarbons. Together with enhanced emissions of halocarbons, the largely elevated atmospheric halocarbons above the Mauritanian upwelling could be explained solely by local emissions in contrast to previous hypotheses. This process could be of importance in other coastal upwelling systems as well.

ZUSAMMENFASSUNG

II. Zusammenfassung

Bromoform ($CHBr_3$) und Dibrommethan (CH_2Br_2) aus dem Meer tragen entscheidend zum organischen Bromgehalt der Atmosphäre bei. Methyljodid (CH_3I) und Dijodmethan (CH_2I_2) sind wichtige Komponenten organischen Jods in der Atmosphäre. Sobald sie aus dem Meer in die Atmosphäre eingetragen werden, sind diese Verbindungen und ihre Zerfallsprodukte an der Ozonzerstörung in der Tropos- und Stratosphäre beteiligt. Ihre Bedeutung für die Ozonchemie wird vermutlich mit abnehmenden atmosphärischen Konzentrationen anthropogener Fluorchlorkohlenwasserstoffe zunehmen. Allerdings sind viele ihrer Produktions- und Zerfallsprozesse im Meer immer noch nicht bekannt und stellen somit Unsicherheiten im Bezug auf ihre Emissionen dar. Mehrere Studien konnten zeigen, dass Makroalgen stark zu ihrer Produktion beitragen, aber auch Mikroalgen wurden als Produzenten identifiziert. Da diese verstärkt in marinen Auftriebsgebieten verbreitet sind, könnten diese Gebiete wichtige Quellregionen von Halogenkohlenwasserstoffen sein. Der tropische Ozean ist vermutlich nicht nur für ihre Emissionen von Bedeutung, sondern aufgrund tropischer Konvektion auch für den Transport halogenierter Kohlenwasserstoffe in die Stratosphäre. Die Ergebnisse dieser Arbeit sollen dazu beitragen, Prozesse, die zu Emissionen halogenierter Spurengase beitragen, näher zu bestimmen und ihre Rolle in einem sich zukünftig ändernden Klima zu verstehen.

Diese Arbeit beruht auf zwei Kampagnen. Die MSM18/3-Fahrt an Bord der FS *Maria S. Merian* im Juni und Juli 2011 fand im östlichen äquatorialen Atlantik während der Kältesaison statt. Die **DRIVE**-Kampagne (**D**iurnal and **R**eg**I**onal **V**ariability of halogen **E**missions) von Juni 2010 an Bord der FS *Poseidon* hingegen untersuchte das mauretanische Auftriebsgebiet. Messungen von Halogenkohlenwasserstoffen im Meer und in der Atmosphäre, sowie biologische, meteorologische und ozeanographische Parameter wurden verwendet, um Einflussfaktoren auf Emissionen halogenierter Spurengase zu bestimmen. Diese Daten wurden auch in die **HalOcAt**-Datenbank (**Hal**ocarbons in the **Oc**ean and **At**mosphere) integriert, die die bisher größte Sammlung von Konzentrationen mariner Halogenkohlenwasserstoffe darstellt. Auf der Grundlage dieser Daten sind sechs Manuskripte erstellt und publiziert worden. Das erste Manuskript (Hepach et al., in prep) basiert auf den ersten Oberflächen- und Tiefenprofil-Messungen von $CHBr_3$, CH_2Br_2, CH_3I und CH_2I_2 im äquatorialen Ostatlantik während der Kältesaison im äquatorialen Atlantik. Das zweite (Hepach et al., 2014) und das dritte Manuskript (Fuhlbrügge et al., 2013) stellen tageszeitliche und regionale Messungen von $CHBr_3$, CH_2Br_2 und CH_3I im Oberflächenwasser und der Atmosphäre des mauretanischen Auftriebsgebietes vor, wobei das zweite Manuskript sich auf Einflussfaktoren von Emissionen konzentriert. Das dritte Manuskript hat vor allem Zusammenhänge meteorologischer Variablen und atmosphärischer

Konzentrationen der Halogenkohlenwasserstoffe zum Thema. Im vierten Manuskript (Ziska et al., 2013) werden globale Emissionen von $CHBr_3$, CH_2Br_2 und CH_3I basierend auf den Daten der HalOcAt-Datenbank berechnet. Im fünften Manuskript (Stemmler et al., 2013) werden Tiefenprofile von CH_3I, die während der DRIVE-Kampagne gemessen wurden, zur Validierung von modellierten Tiefenprofilen benutzt. Im letzten Manuskript (Tegtmeier et al., 2013) dieser Arbeit wird der Eintrag von CH_3I in die Stratosphäre basierend auf Emissionen der DRIVE-Kampagne berechnet. Diese Berechnungen zeigen, dass zumindest geringe Beträge von CH_3I aus dem tropischen Atlantik die Stratosphäre erreichen.

Beide Auftriebsgebiete wurden als Quellregionen von $CHBr_3$ und CH_2Br_2 identifiziert und tragen daher zu ihren hohen Emissionen aus dem tropischen Ozean bei. CH_3I war gleichmäßig im Oberflächenwasser des mauretanischen Auftriebsgebietes verteilt, was auf photochemische Bildung hinweist. Im Gegenteil dazu wurden mehrere Hinweise auf die biologische Produktion von CH_3I im äquatorialen Ostatlantik gefunden. Beide Mechanismen stimmen gut mit den modellierten Profilen überein. Vorhergehende Studien nahmen an, dass aufgrund seiner starken Photolyse kein CH_2I_2 im Oberflächenwasser des tropischen Ozeans beobachtet werden kann. Allerdings konnte diese Verbindung während der MSM18/3-Kampagne im Oberflächenwasser gemessen werden. Diapyknische Flüsse dieser Verbindungen sind als Teil dieser Arbeit zum ersten Mal berechnet worden. Im Vergleich zu anderen Senken weisen diese darauf hin, dass die Produktion der Halogenkohlenwasserstoffe vermutlich in der gesamten durchmischten Oberflächenschicht stattfindet und somit ihre Emissionen in die Atmosphäre beeinflusst. Biologische und photochemische Produktion von $CHBr_3$, CH_2Br_2 und CH_3I im Oberflächenwasser wurde als wichtigster Einflussfaktor auf ihre Emissionen aus dem mauretanischen Auftriebsgebiet identifiziert, wobei tageszeitliche Variationen der Windgeschwindigkeit ebenfalls eine Rolle spielen können. Es wurde zum ersten Mal festgestellt, dass die Höhe der atmosphärischen Grenzschicht zusätzlich Einfluss auf Emissionen halogenierter Kohlenwasserstoffe von küstennahen Auftriebsgebieten haben kann. Im Gegensatz zu vorherigen Hypothesen können die stark erhöhten atmosphärischen $CHBr_3$ und CH_2Br_2 in diesem Gebiet durch lokale ozeanische Produktion erklärt werden. Entscheidend dafür ist die Kombination der niedrigen Grenzschichthöhe mit verstärkten Emissionen. Dies könnte auch in anderen küstennahen Gebieten ein wichtiger Prozess sein.

INTRODUCTION

III. Introduction

Halocarbons, hydrocarbons in which one or more hydrogen atoms are substituted by one or more halogen (bromine, chlorine, fluorine or iodine) atoms, receive more and more attention due to their involvement in ozone depletion in both the troposphere and the stratosphere. Especially manmade chlorofluorocarbons (CFCs), where hydrogen atoms have been replaced by chlorine and fluorine atoms, have attracted much attention in previous years due to the discovery of the ozone hole in 1985. They have been commercially used since the 1930s as refrigerants, propellants, blowing agents, solvents, and cleaning agents due to their low toxicity, non-flammability, odorlessness, and their persistence. However, this persistence proved to be one of the major environmental problems associated with CFCs. CFCs have very long lifetimes, e.g. 45 yr for CFC-11 and 640 yr for CFC-13 (Montzka and Reimann, 2011), and are practically inert in the troposphere (Solomon, 1999). They can be transported into the stratosphere where they have strong implications for stratospheric ozone chemistry. Molina and Rowland (1974) proposed that chlorine, released from CFCs when exposed to solar radiation could be involved in ozone destruction in the stratosphere via a catalytic chain reaction. Farman et al. (1985) were the first to observe the ozone hole above Antarctica, which confirmed the suggestions that CFCs could have serious implications for the ozone layer. With the Montreal Protocol coming into effect January 1 1989, the production and application of CFCs was banned. Since then, their atmospheric abundance has been slowly decreasing. However, nine years after their ban, about 62 % of total tropospheric chlorine was still coming from CFCs (Montzka and Reimann, 2011) as a result of their long lifetimes. They have now been replaced by compounds such as hydrofluorocarbons (HFCs), perfluorocarbons (PFCs), or sulfur hexafluoride (SF6). The London amendment from 1990 also added tetrachloromethane (CCl_4) to the banned substances.

With decreasing CFCs and a changing global climate, the significance of naturally produced organic halogenated compounds for atmospheric processes might strongly increase. Lovelock et al. (1973) detected methyl iodide (CH_3I) as first natural halogenated compound suggesting the ocean to be its main source. It was hypothesized to be a very important carrier of iodine to the atmosphere, supported by the study of Liss and Slater (1974). Studies on natural halocarbons conducted by Singh (1983), Rasmussen (1984), Penkett (1985), and Cicerone (1988), for example, focusing mainly on their atmospheric abundances, followed in the 1980s. During these investigations, also brominated natural hydrocarbons were investigated and proposed to be of significance for tropospheric and stratospheric ozone chemistry. Fewer studies in the 1970s and 1980s covered the oceanic distributions and sources of these compounds. Burreson et al. (1975) found a number of halocarbons including bromoform ($CHBr_3$) in essential oil extracted from a red algal species, suggesting that these compounds could be emitted into the ocean by macroalgae. Polyhalogenated compounds produced by a red macroalgae species were later hypothesized to be involved in defense mechanisms against bacterial activity (McConnell and Fenical, 1979). Until the 1990s, microalgae were not studied as extensively. Only CH_3I had been observed previously in cultural phytoplankton studies (Fenical, 1981; Gschwend et al., 1985). Tokarczyk and Moore (1994) published the first study showing the production of several halocarbons including $CHBr_3$ and dibromomethane (CH_2Br_2) from cultured phytoplankton species. This study implicated that not only the coastal ocean with a rich quantity of macroalgae was a potential source region, but also more open ocean regions. In comparison to the manmade CFCs, these compounds have very short lifetimes in the atmosphere from 0.003 (diiodomethane) to 123 days (CH_2Br_2) (Montzka and Reimann, 2011), and have therefore been assumed to be only significant for tropospheric processes. However, Solomon et al. (1994) could show that CH_3I can be transported into the stratosphere where it may take part in stratospheric chemical processes, including ozone destruction. $CHBr_3$ and CH_2Br_2 and their degradation products were shown to be transported into the stratosphere as well (Dvortsov et al., 1999; Sinnhuber and Folkins, 2006; Kerkweg et al., 2008). Bromine and iodine may be far more efficient in ozone destruction than chlorine (Daniel et al., 1999). Many uncertainties still exist with regard to naturally occurring halocarbons in the marine environment, including their sources, sinks and fate. It is crucial to continue to study these processes to estimate the significance of halocarbons in a changing future climate.

1. Halocarbons in the ocean

This thesis focuses on four naturally produced halocarbons that contribute significantly to atmospheric organobromine and -iodine: bromoform ($CHBr_3$), dibromomethane (CH_2Br_2), methyl iodine (CH_3I) and diiodomethane (CH_2I_2). While the polyhalogenated $CHBr_3$, CH_2Br_2 and CH_2I_2 have been suggested to be biologically formed by similar pathways, different processes may be involved in the biogenic production of CH_3I. Apart from macroalgae, microalgae could be identified as producers for all four halocarbons. Additionally, photochemical formation with the involvement of organic precursors may play a crucial role in the formation of CH_3I. Rates of degradation processes in the ocean differ for each of the four compounds. While the main sink for $CHBr_3$ and CH_2Br_2 may be air-sea gas exchange, nucleophilic halogen substitution may compete with air-sea gas exchange as sink of CH_3I. Photolysis of CH_2I_2 is very rapid, and is hence the most dominant loss process for this compound. Measurements of these compounds in the field are still very sparse, and emissions have so far only been estimated for few campaigns. Many data gaps exist especially for CH_2I_2.

1.1. Bromoform and dibromomethane in the ocean

$CHBr_3$ and CH_2Br_2 are compounds that find application in industrial processes as solvents, sedatives, flame retardants, and as gauge fluid, and both are used or can be intermediates in organic synthesis. They are odorless and liquid at room temperature. $CHBr_3$ and CH_2Br_2 from the ocean are the largest contributors to atmospheric organic bromine (Hossaini et al., 2012).

1.1.1. Marine sources

1.1.1.1. Anthropogenic sources

Formation of $CHBr_3$ during drinking water treatment by chlorination was first published by Rook (1974), after which it can enter estuaries and coastal waters by riverine discharge (Helz and Hsu, 1978). Additionally to disinfection of drinking-, sea- and wastewater by chlorination and ozonation, cooling water of power plants is chlorinated to prevent biofouling (Fogelqvist et al., 1982; Fogelqvist and Krysell, 1991; Jenner et al., 1997). Chlorination of seawater leads to larger concentrations of $CHBr_3$ than chlorination of freshwater due to the larger amount of bromide (Br^-) present. Chlorination using hypochlorous acid (HOCl) results in hypobromous acid (HOBr) in the presence of Br^- (Jenner et al., 1997).

$ClO^- + Br^- \rightarrow BrO^- + Cl^-$ (reaction equation 1)

$BrO^- + H^+ \rightarrow HOBr$ (reaction equation 2)

HOBr then reacts with reactive dissolved organic matter (DOM) to a brominated organic intermediate which finally reacts rapidly to $CHBr_3$ (Jaworske and Helz, 1985; Lin and Manley, 2012).

$3HOBr + DOM_{react} \rightarrow DOM\text{-}Br_3$ (reaction equation 3)

$DOM\text{-}Br_3 \rightarrow CHBr_3 + DOM$ (reaction equation 4)

Production of $CHBr_3$ may vary with season due to changes in temperature and salinity, radiation, and dissolved organic carbon (DOC) content (Jenner et al., 1997; Allonier et al., 1999). Quack and Wallace (2003) assessed anthropogenic sources of $CHBr_3$ and their contribution to the ocean. Based on references therein, a total of ~0.35 Gmol Br yr^{-1} (0.25 – 1.4 Gmol Br yr^{-1}) were estimated from anthropogenic sources. This includes around 290 Mmol Br ($CHBr_3$) yr^{-1} from fossil fuel generating capacity, 38 Mmol Br ($CHBr_3$) yr^{-1} from nuclear power plants, including inland, 0.04 (+~2) Mmol Br ($CHBr_3$) yr^{-1} from desalination/power plants, and 12 Mmol Br yr^{-1} from disinfection of wastewater, drinking water, and recreational water. The total contribution was estimated to be small on a global scale, but with potentially large significant influence on a local scale in coastal regions.

Less is known about anthropogenic sources of CH_2Br_2. It has several industrial applications, among others as solvent or gauge fluid. Industrial wastewater can be transported into rivers and estuaries which would transport anthropogenic CH_2Br_2 into the ocean. CH_2Br_2 may be produced from the reactions 3 and 4 as well (Lin and Manley, 2012). However, concentrations in drinking water, groundwater and wastewater have been shown to be very low (Perry et al., 1979; Fielding et al., 1981; Page, 1981).

1.1.1.2. Biological sources

1.1.1.2.1. Macroalgal production of $CHBr_3$ and CH_2Br_2

Coastal regions have been assumed to be important sources regions for both $CHBr_3$ and CH_2Br_2 due to large macroalgal populations. Several species of brown, green and red algae could be identified as producers with brown algae contributing about 60 % to the global macroalgae $CHBr_3$ budget due to their large biomass (Carpenter and Liss, 2000). Before the study of Gschwend et al. (1985), the release from macroalgal sources had not been further assessed. The total possible contribution from temperate macroalgae to organic atmospheric bromine based on this study was ~10,000 t yr^{-1}, equivalent to ~0.13 Gmol Br yr^{-1}. Carpenter and Liss (2000) calculated a global contribution of around 1.6 Gmol Br yr^{-1} alone from macroalgal $CHBr_3$, which is about one order of magnitude higher as the previous estimate. Quack and Wallace (2003) estimated a total global coastal flux of 2.3 (0.9 - 3.4) Gmol Br ($CHBr_3$) yr^{-1} in a similar range, which also includes anthropogenic sources that could be occasionally large in comparison to macroalgal emissions. Macroalgal production of halocarbons was mainly investigated in polar (Schall et al., 1994; Laturnus, 1996; Laturnus et al., 1997) and temperate regions (Nightingale et al., 1995; Jones et al., 2009; Bravo-Linares et al., 2010). Up to now, only one incubation study has focused on the tropics (Leedham et al., 2013) with comparable production rates of $CHBr_3$ to temperate and polar algae. This suggests that a previously proposed larger emission of $CHBr_3$ from the tropical coastal ocean (Yokouchi et al., 2005) may rather be a result of the larger biomass of bromocarbon producing species, both macro- and microalgae, than production rates themselves (Leedham et al., 2013).

1.1.1.2.2. Bromocarbon production by phytoplankton

Butler et al. (2007) estimated open ocean contributions for $CHBr_3$ and CH_2Br_2 from several cruises conducted in different regions (Figure III-1). The tropical ocean seems to play an important role for bromocarbon fluxes into the atmosphere contributing about 66 (CH_2Br_2) to

70 % ($CHBr_3$). Of a total global $CHBr_3$ flux of 10 Gmol Br yr^{-1}, the open ocean contribution was calculated to be 19 %, while of a global CH_2Br_2 flux of 3.5 Gmol Br yr^{-1}, 17 % were open ocean emissions. However, these estimates include large uncertainties, because they are only based on seven cruises. The cruise that covered the Atlantic did not cross the Atlantic upwelling systems, which leads to the low estimated Atlantic contribution. Quack and Wallace (2003) assessed a similar global $CHBr_3$ flux of 10 Gmol Br yr^{-1} with 29 % coming from the open ocean. Total emissions of $CHBr_3$ reported so far range between 4.8 (Pyle et al., 2011) from a top-down approach and 10.3 Gmol Br yr^{-1} (Yokouchi et al., 2005; O'Brien et al., 2009) both from bottom-up approaches.

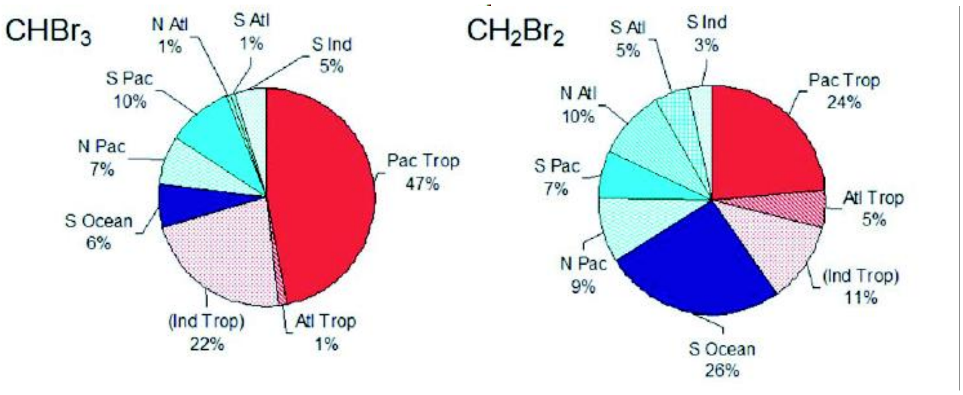

Figure III-1. Contributions of different open ocean regions to emissions of $CHBr_3$ and CH_2Br_2 (warm colors – tropical regions, cold colors – temperate and polar regions). Modified from Butler et al. (2007).

Elevated concentrations in open ocean regions with enhanced biological activity, and correlations of $CHBr_3$ and CH_2Br_2 with chlorophyll *a* (Chl *a*) found in several studies supported first suggestions of an additional microalgal source that would explain the open ocean contributions to emissions of these compounds (Fogelqvist, 1985; Class and Ballschmiter, 1988; Krysell, 1991; Klick and Abrahamsson, 1992; Moore and Tokarczyk, 1993; Schall and Heumann, 1993). Tokarczyk and Moore (1994) conducted the first incubation study investigating halocarbon production with warm and cold water phytoplankton species. Halocarbon production seemed to be species dependent: of 10 investigated species, only two *diatom* species produced $CHBr_3$ and CH_2Br_2. *Diatoms* were then the focus of all mono-cultural incubation studies of $CHBr_3$ and CH_2Br_2 (Moore et al., 1996; Cota and Sturges, 1997; Hill and Manley, 2009; Hughes et al., 2013). Some other algal species have been linked to $CHBr_3$ and CH_2Br_2 production in the field by correlating environmental measurements with phytoplankton pigments and -groups. These include among others *cyanobacteria* (Quack et al., 2007a; Karlsson et al., 2008), *chlorophytes* and *prymnesiophytes* (Raimund et al., 2011).

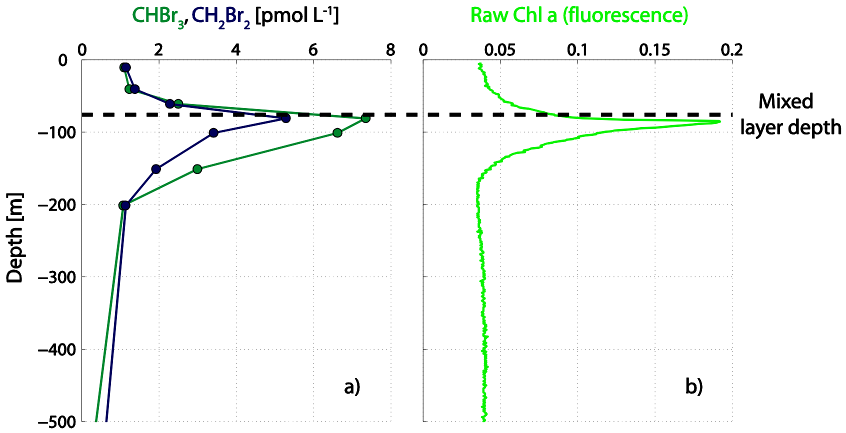

Figure III-2. Exemplary profiles of $CHBr_3$ and CH_2Br_2 in the open ocean (a) and Chl *a* (b) at the Cape Verde Ocean Observatory (CVOO) from June 2010 (unpublished data).

Depth profiles of $CHBr_3$ and CH_2Br_2 in the open ocean were often observed to exhibit a common distinct maximum in the upper layers (Quack et al., 2004; Carpenter et al., 2007; Hughes et al., 2009) (Figure III-2). These maxima are usually found in the vicinity of the Chl *a* maximum, likely as a result of their biological production. The distribution of $CHBr_3$ and CH_2Br_2 depends on several factors such as production and sink processes, advection and diapycnal mixing. Many uncertainties exist in how these factors come together to form the observed profiles.

It is generally assumed that $CHBr_3$ and CH_2Br_2 have related sources (Moore et al., 1996; Schall et al., 1997; Quack et al., 2007a; Karlsson et al., 2008), which supposedly leads to very good correlations of oceanic $CHBr_3$ with CH_2Br_2. The ratio of $CHBr_3$ to CH_2Br_2 leans towards CH_2Br_2 with increasing distance from the source. A possible explanation is that the half-life of CH_2Br_2 is longer than the half-life of $CHBr_3$, which has not been verified yet. Carpenter et al. (2009) offered the explanation that photolysis of $CHBr_3$ is faster than CH_2Br_2 (Carpenter and Liss, 2000). An alternative explanation was proposed by Hughes et al. (2013) who found evidence for biologically-mediated production of CH_2Br_2 from $CHBr_3$.

1.1.1.2.3. Formation of $CHBr_3$ and CH_2Br_2

The formation of $CHBr_3$ and CH_2Br_2 is governed by haloperoxidases which contain iron-heme or vanadium as a cofactor. Chloroperoxidases (CPO) can, in this order, oxidize iodide (I^-), Br^- and chloride (Cl^-), bromoperoxidases (BPO) oxidize I^- and Br^-, while iodoperoxidases (IPO) only oxidize I^-. Haloperoxidases with vanadium as cofactor are present in red and brown macroalgae (Wever and Krenn, 1990; Butler, 1998), while green algae and *diatoms* contain also iron-heme haloperoxidases (Wever and Krenn, 1990; Moore et al., 1996; Hill and Manley, 2009). The location of $CHBr_3$ and CH_2Br_2 production, in- or outside of the cells, is not completely clear yet. Mtolera et al. (1996) and Manley (2002) suggested for example intracellular production due to the location of the haloperoxidases in the chloroplasts.

Theiler et al. (1978) investigated the formation of halocarbons using BPO from the red macroalga *Bonnemaisonia hamifera*. With 3-oxooctanoic acid, hydrogen peroxide (H_2O_2) and

Br^-, they found both $CHBr_3$ and CH_2Br_2 at pH 7.3 with a formation ratio of 10:1. BPO has also been demonstrated to be involved in $CHBr_3$ and CH_2Br_2 formation from phytoplankton (Moore et al., 1996). BPO can brominate β-diketones and β-ketoacids to a polybrominated ketone which can form $CHBr_3$ and CH_2Br_2 by hydrolysis (Theiler et al., 1978; Beissner et al., 1981). This is shown in the following example for $CHBr_3$, reacting in the final step to hexanoic acid.

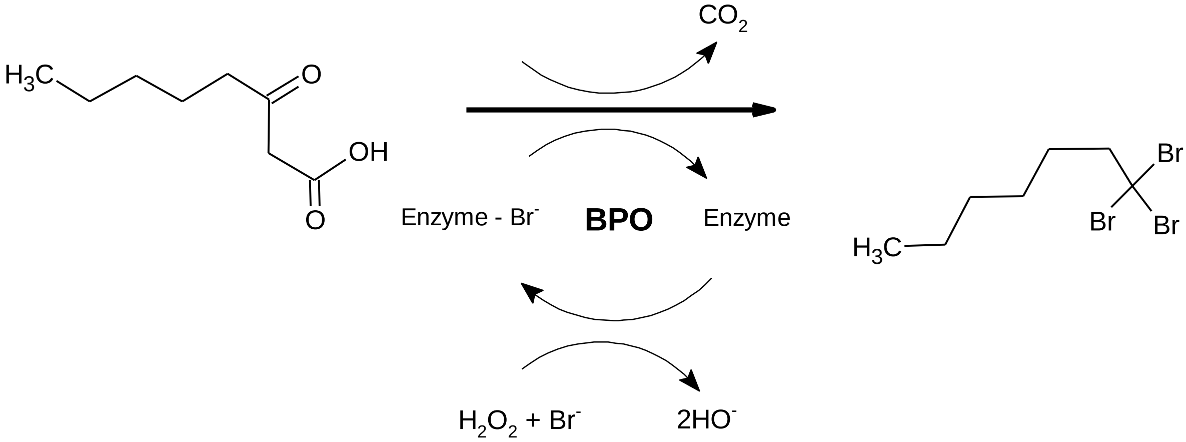

(reaction equation 5)

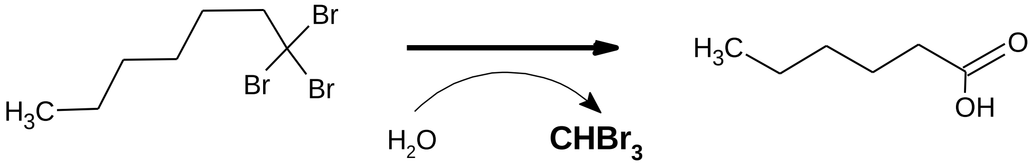

(reaction equation 6)

An alternative extracellular pathway of $CHBr_3$ and CH_2Br_2 production involves DOM in seawater. Wever et al. (1991) investigated vanadium containing BPO that could react to HOBr which is then released by the algae. How much of this is released, is not known. This would yield $CHBr_3$ and CH_2Br_2 in the reaction with DOM present in seawater (Lin and Manley, 2012) according to reactions 3 and 4. $CHBr_3$ is in comparison to CH_2Br_2 the main product of this pathway as well. The production rate at which $CHBr_3$ and CH_2Br_2 are formed from DOM does not only depend on how much HOBr is present, but is also regulated by the quantity and quality of the available DOM (Lin and Manley, 2012).

The function of the haloperoxidases within the macro- and microalgae is still unclear. Halocarbon production has been linked to stress. For instance, Gschwend et al. (1985) proposed that macroalgae use $CHBr_3$ and CH_2Br_2 to protect themselves from grazing/as epiphytic control, later supported by other studies (Nightingale et al., 1995; Paul et al., 2006). Other examples of stress factors that lead to halocarbon release may be changes in pH, as well as changes in light intensities (Mtolera et al., 1996). The connection to higher light intensities might be a result of the potential function of halocarbons to scavenge harmful reactive oxygen species (ROS) such as H_2O_2 out of the cell. These are produced during photosynthesis, photorespiration and respiration (Collén et al., 1994; Pedersén et al., 1996). H_2O_2 is produced within the algae by the Mehler reaction, in which ferredoxine reacts with oxygen (O_2) to yield the superoxide radical (also part of ROS), which then reacts to H_2O_2 with the help of superoxide dismutase (Falkowski and Raven, 2007).

The relationship between photosynthesis and H_2O_2, as well as between H_2O_2 and macroalgal $CHBr_3$/CH_2Br_2 formation has been assumed to lead to diurnal cycles (Pedersén et al., 1996; Goodwin et al., 1997a; Ekdahl et al., 1998; Marshall et al., 1999; Carpenter et al., 2000). It was hypothesized that the production of H_2O_2 is intensified with increased irradiance, and the de-novo formation of $CHBr_3$ and CH_2Br_2 following is quite rapid. However, night production in lower rates during respiration has been observed as well (Pedersén et al., 1996). Diurnal cycles $CHBr_3$ and CH_2Br_2 from microalgae were only observed in the field in one study (Abrahamsson et al., 2004b). Similarly, seasonal cycles of $CHBr_3$ and CH_2Br_2 could be expected due to seasonal changes in biomass and variability in irradiance. Increasing oceanic $CHBr_3$ and CH_2Br_2 concentrations in summer have for example been observed in the Baltic Sea (Orlikowska and Schulz-Bull, 2009).

1.1.2. Sinks

Sinks for $CHBr_3$ and CH_2Br_2 include hydrolysis, reductive dehalogenation, halogen substitution, and photolysis, as well as air-sea gas exchange (Class and Ballschmiter, 1988; Quack and Wallace, 2003; Carpenter et al., 2009). Loss due to air-sea gas exchange may well be one of the most important loss processes for these two compounds.

Hydrolysis is a sink for both $CHBr_3$ and CH_2Br_2 (see example for $CHBr_3$ in reaction equations 7 and 8). Their half-life due to this sink is hundreds to thousands of years in cold water, and it decreases with increasing temperature (Mabey and Mill, 1978; Vogel et al., 1987).

$CHBr_3 + OH^- \rightarrow {}^-CBr_3 + H_2O$ (reaction equation 7)

${}^-CBr_3 \rightarrow CBr_2 + Br^-$ (reaction equation 8)

Reductive dehalogenation mediated by bacteria is a sink for both $CHBr_3$ and CH_2Br_2 (Bouwer and McCarty, 1983; Bouwer et al., 1981; Goodwin et al., 1997b) might be associated with anoxic conditions (Vogel et al., 1987). Transition metal complexes, e.g. containing iron, cobalt or nickel, found in enzymes have been proposed as electron donators in this process (Mohn and Tiedje, 1992).

Halogen substitution of bromine with sea water chlorine in $CHBr_3$ has been suggested to produce dibromochloromethane ($CHBr_2Cl$) and bromodichloromethane ($CHBrCl_2$) (Class and Ballschmiter, 1988) (reaction equations 9 – 11).

$CHBr_3+Cl^- \rightarrow CHBr_2Cl+Br^-$ (reaction equation 9)

$CHBr_2Cl+Cl^- \rightarrow CHBrCl_2+Br^-$ (reaction equation 10)

$CHBrCl_2+Cl^- \rightarrow CHCl_3+Br^-$ (reaction equation 11)

A similar process for CH_2Br_2 can be expected, yielding bromochloromethane (CH_2BrCl). The half-life of $CHBr_3$ due to halogen substitution is similar to hydrolysis dependent on the water temperature, ranging between 5 (25 °C) and 74 (2 °C) years (Geen, 1992).

Photolysis may be the fastest of the mentioned chemical sinks. Carpenter and Liss (2000) calculated a half-life of approximately 9 years for $CHBr_3$ due to photolysis for a mixed layer of 100 m. This may be much shorter, less than a year, for shallower mixed layers (Liu et al., 2011). The shorter half-life of $CHBr_3$ than of CH_2Br_2 indicated by the relationship described in section 1.1.1.2.2. may be a hint for a longer photolysis of CH_2Br_2 than of $CHBr_3$ (Carpenter et al., 2009). The half-lives of $CHBr_3$ and CH_2Br_2 with regard to the other sinks are assumed to be similar. Then, photolysis of $CHBr_3$ needs to be faster than photolysis of CH_2Br_2 to explain the observed relationship only on the basis of bromocarbon sinks. Photolysis in the aqueaous phase is generally characterized by an O-H-insertion reaction of $CHBr_3$ with water producing $CHBr_2OH$ (reaction equation 12) (Kwok et al., 2004).

$CHBr_3+2H_2O \rightarrow CHBr_2OH+HBr+H_2O$ (reaction equation 12)

Similarly to CH_2I_2 (Jones and Carpenter, 2005), the photolysis of CH_2Br_2 would lead to CH_2BrOH and HBr (reaction equation 13).

$CH_2Br_2+H_2O \rightarrow CH_2BrOH+HBr$ (reaction equation 13)

Hughes et al. (2013), who conducted experiments with labeled $CHBr_3$, found evidence for biologically-mediated production of CH_2Br_2 from $CHBr_3$ in *diatom* cultures. This is suggested to be an important source for CH_2Br_2, and is an additional sink for $CHBr_3$ that is potentially faster than the other sinks mentioned, which would also explain the relationship of $CHBr_3$ to CH_2Br_2 in surface water. Additionally, bacterial oxidation of CH_2Br_2 to CO_2 with a half-life of two days was observed in the lab (Goodwin et al., 1998).

1.2. Methyl iodide in the ocean

Terrestrial sources of CH_3I include rice paddies, wetlands, biomass burning, and plants, providing about 0.6 – 0.9 Gmol I (CH_3I) yr^{-1} to the global iodine budget (Bell et al., 2002). It has widely been acknowledged to be the most common organiodine in the marine atmosphere (Saiz-Lopez et al., 2012). Elevated atmospheric CH_3I towards lower latitudes has been found both in the tropical Atlantic and Pacific above open ocean regions (Chuck et al., 2005; Butler et al., 2007; Yokouchi et al., 2008), hence the tropical ocean may be an important source region for CH_3I (Richter and Wallace, 2004; Jones et al., 2010).

1.2.1. Marine sources

Different hypotheses have been established for the production of CH_3I in seawater. Apart from biological production from macroalgae, phytoplankton and bacteria, photochemical pathways have been proposed.

1.2.1.1. Biological production

Macroalgal production of CH_3I was first suggested by Lovelock (1975) who measured largely elevated CH_3I concentrations in the vicinity of a *Laminaria digitata* kelp bed in the North Atlantic. Further macroalgal species were shown to produce CH_3I in the field (Gschwend et al., 1985). Manley and Dastoor (1987) demonstrated CH_3I production from culture experiments with a kelp species, and calculated a global production of 1.6 Mmol I (CH_3I) yr^{-1} from kelp beds. Since this was less than 0.1 % of the annual global emissions (Singh et al., 1983), macroalgae were not considered the dominating source of CH_3I.
Manley and Dastoor (1987) suggested several production pathways for CH_3I: 1) similar production of CH_3I as $CHBr_3$ and CH_2Br_2 using haloperoxidases, although Theiler et al. (1978) proposed only polyhalogenated compounds to be produced this way, hence this does not seem plausible, 2) The reaction of dimethylsulfonium compounds with halides, which has been suggested by White (1982) (reaction equation 14), as well as 3) microbial production by bacteria associated with the kelp.

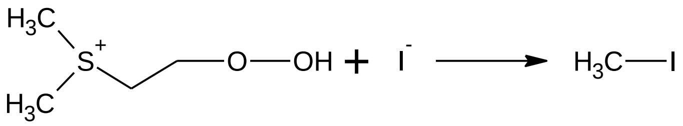

(reaction equation 14)

Several other molecules, e.g. methyl sulfonium compounds (Urhahn and Ballschmiter, 1998) and s-adenosyl-L-methionine (SAM) (Wuosmaa and Hager, 1990), can act as the methyl source (Wuosmaa and Hager, 1990). Additional compounds, for example dimethyl sulfoniopropionate (DMSP) (White, 1982), that could provide the methyl group may be produced from dimethyl sulfide (DMS), which is a trace gas produced by several phytoplankton species throughout the world (Lana et al., 2011). From these compounds, SAM-utilizing methyl transferase may be most significant for methyl halide production in algae (Manley, 2002). Its function is not clear, although it was suggested that it may regulate halide ions in the cell, or methyl halides may act as allelopathic chemicals (Itoh et al., 1997). Furthermore, it was suggested that methyl halide production is only a byproduct or might happen by “accident”, which might apply to the other halocarbons as well (Manley, 2002). Yokouchi et al. (2014) proposed a mechanism for production of CH_3I in marine algae (Figure

III-3): I^- is similarly to Br^- oxidized to hypoiodous acid (HOI) by CPO, BPO or IPO. Iodine is then formed with free I^-, and passes through the cell membrane. In the next step, I^- forms CH_3I from SAM with the help of the halide ion thiol methyl transferase (HTMT), producing S-adenosyl-L-homocysteine (SAH). CH_3I can be transformed into methyl chloride (CH_3Cl) by halogen substitution.

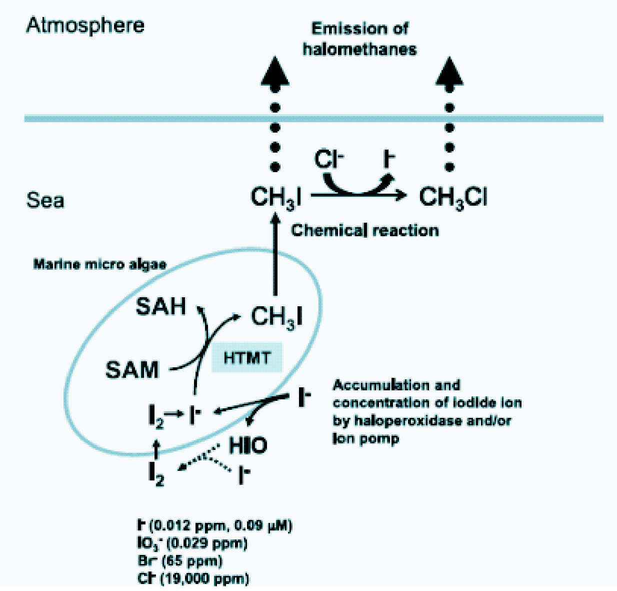
Atmosphere
Emission of halomethanes
Sea
Cl⁻
I⁻
CH₃I
CH₃Cl
Chemical reaction
Marine micro algae
SAH
CH₃I
SAM
HTMT
I₂→I⁻
I⁻
HIO
I₂
I⁻
Accumulation and concentration of iodide ion by haloperoxidase and/or ion pomp
I⁻ (0.012 ppm, 0.09 µM)
IO₃⁻ (0.029 ppm)
Br⁻ (65 ppm)
Cl⁻ (19,000 ppm)

Figure III-3. Methyl iodide biosynthesis using SAM-utilizing methyl transferases (Yokouchi et al., 2014)

Regarding 3): Although these microbes associated with kelp were found to produce CH_3I only in small rates, Manley and Dastoor (1988) estimated a global production from decaying kelp tissue of 2.4 Gmol (CH_3I) l yr^{-1}. Bacterial production of CH_3I was confirmed later in the lab (Amachi et al., 2001; Fuse et al., 2003). Bacteria may also be involved indirectly in the formation of CH_3I. Manley (1994) proposed a formation pathway using methylcobalamin (CH_3-B_{12}), which is a product released by bacteria to seawater (reaction equation 15). The global significance of this source is unclear.

$$CH_3\text{-}B_{12}\left(CO^{3+}\right)+I^-\rightarrow CH_3I+B_{12s}(CO^+) \qquad \text{(reaction equation 15)}$$

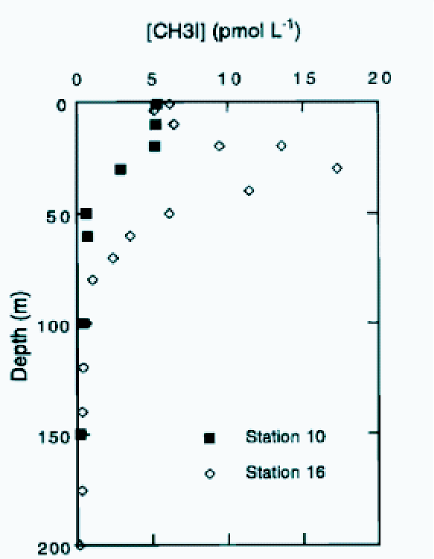

Figure III-4. The production by phytoplankton leads to similar depth profiles as observed for $CHBr_3$ and CH_2Br_2 with pronounced maxima in the Chl *a* maximum (Moore and Groszko, 1999).

Since macroalgae seem to contribute only low amounts to the global CH_3I budget and the contribution from bacterial production is unclear, it was often suggested that production of CH_3I by phytoplankton must add a vast amount to atmospheric CH_3I. The production by phytoplankton leads to similar depth profiles as observed for $CHBr_3$ and CH_2Br_2 with pronounced maxima in the Chl *a* maximum (Figure III-4).

Moore et al. (1996) performed incubation studies testing several *diatom* species for halocarbon production. Of six species, only two produced CH_3I. The low concentration rates of CH_3I were confirmed later on (Manley and de la Cuesta, 1997). A mean global contribution of 9.5 Mmol (CH_3I) l yr^{-1} was calculated from the two phytoplankton species *Phaeocystis sp.*, a *haptophyte*, and *Porosira glacialis*, a *diatom*, in comparison to a corrected global contribution from macroalgae of 4.8 Mmol (CH_3I) I yr^{-1} (Manley et al., 1992). Although the estimates from phytoplankton were larger than the estimated production from macroalgal species, this contribution would still be globally insignificant. However, following this, it was found that certain phytoplankton species seemed to produce CH_3I in much larger amounts than previously reported species (Scarratt and Moore, 1999), thus global estimates based on just few species that have been shown to produce CH_3I (Manley and de la Cuesta, 1997) may be flawed. The differences in the reported CH_3I-production might not only be species related. Although it was often hypothesized that light stress might increase the production of CH_3I, this could not be observed in incubation studies (Scarratt and Moore, 1999; Hughes et al., 2006), leading to the conclusion that in contrast to $CHBr_3$ and CH_2Br_2, production of CH_3I in phytoplankton is not related to protection from oxidative stress.

Additionally, largely elevated concentrations of CH_3I South of 40° N in the Atlantic were found to correlate well with *Prochlorococcus* abundance (Smythe-Wright et al., 2006). From these measurements, a contribution of 4.2 Gmol (CH_3I) I yr^{-1} to the global flux of iodine was estimated. This source would be one order of magnitude larger than the flux calculated by Manley and de la Cuesta (1997). Subsequent incubation studies with *Prochlorococcus* indicated much lower production rates leading to a contribution of 0.6 Mmol (CH_3I) I yr^{-1}, only accounting for 0.03 % of the global CH_3I production (Brownell et al., 2010). Hughes et al. (2011) suggested that the difference in CH_3I production from *Prochlorococcus* in the former two studies may be explained by the physiological state of the CH_3I-producing cell.

1.2.1.2. Photochemical formation

The large discrepancies in reported production rates from macro- and microalgae are unable to close the global CH_3I budget (Bell et al., 2002), which may be explained by additional sources. Moore and Zafiriou (1994) conducted incubation experiments suggesting the photochemical production of CH_3I. The most probable reaction mechanism in their opinion is radical recombination.

$CH_3\cdot + \cdot I \rightarrow CH_3I$ (reaction equation 16)

The methyl radicals were suggested to be a result of photolysis of humic matter from DOC, but these radicals have very short lifetimes due to a very rapid reaction with O_2 (Zafiriou et al., 1990).

$CH_3\cdot + O_2 \rightarrow CH_3OO\cdot$ (reaction equation 17)

The concentration of the iodine radical has to be much larger than the concentration of the methyl radical to favor reaction equation 16. The source of the iodine atoms is supposedly photochemically oxidized I^-. The best oxidant in halide oxidation seem to be one electron oxidants, e.g. OH radicals, and two electron oxidants, e.g. H_2O_2 (Luther, 2011). Other production pathways for photochemical production of CH_3I might exist that solve the problem regarding the very short lifetimes of the methyl radical due to the very rapid reaction with O_2. Wong and Cheng (2001) suggested the involvement of dissolved organic iodine (DOI) in the photochemical formation: methyl- and iodine radicals may be formed in very close proximity to each other providing a possibility for the iodine radical to compete with oxygen for the methyl radical due to the presence of DOI.

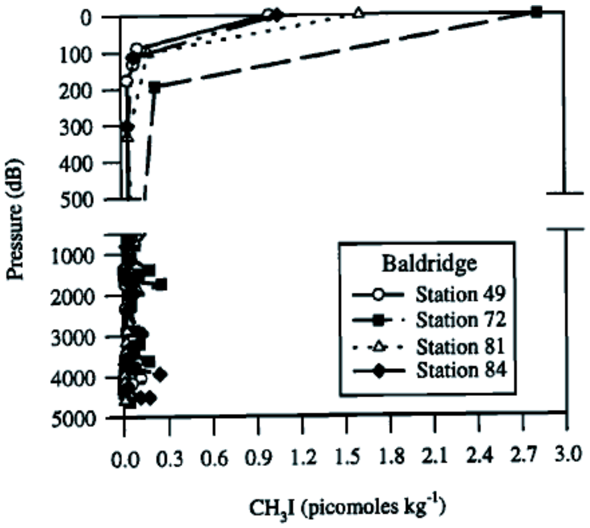

Figure III-5. CH_3I profiles from the tropical Atlantic (Happell and Wallace, 1996)

Happell and Wallace (1996) measured large oversaturations of CH_3I in tropical ocean regions without large biological activity. Typical depth profiles were characterized by pronounced maxima in the surface (Figure III-5). Photochemistry was hypothesized to be the main reason for the large supersaturations and surface maxima, supported by the good linear relationship of CH_3I concentration with photosynthetically active radiation and the undersaturation in the polar region. Furthermore, the distribution of CH_3I in tropical surface water and additional incubation studies using filtered seawater supported the hypothesis that photochemistry might play an important role for CH_3I emissions from the tropical ocean (Richter and Wallace, 2004; Jones et al., 2010; Shi et al., 2014). Bell et al. (2002) modeled the global surface water distribution of CH_3I assuming photochemical production, which proved to be more consistent with the global budget than direct biological sources. From the total global flux of CH_3I of 2.4 Gmol I yr^{-1}, including oceanic, terrestrial and anthropogenic emissions, 70 % were due to photochemical oceanic production. However, photochemical production of CH_3I may not be completely independent of biology, since phytoplankton and bacteria are involved in the release and degradation of DOC (Nagata, 2000).

1.2.2. Sinks

Sinks for CH_3I include photolysis, halogen substitution with Cl^-, hydrolysis, and sea-to-air flux. Although sea-to-air flux is often assumed to be the dominant sink of CH_3I, the substitution with Cl^- competes with the flux in warm waters. Jones and Carpenter (2007) proposed that at low wind speeds and high temperatures, the substitution reaction is the most dominant loss process, while high wind speed regimes favor air-sea gas exchange as the main sink in the tropical ocean. Zafiriou (1975) suggested that CH_3Cl may be produced by the reaction of Cl^- with CH_3I with a half-life of approximately 20 days at 19 °C.

$CH_3+Cl^-\rightarrow CH_3Cl+I^-$ (reaction equation 18)

Zika et al. (1984) compared the substitution of I^- with Cl^- with the photolysis in seawater, and concluded that the influence of photolysis on the CH_3I concentration is very low in comparison to the nucleophilic substitution reaction. Photolysis could be of more significance in high latitudes during summer time due to the slower rates of reaction 18 with increasing latitude. Reaction 18 is strongly temperature-dependent with half-lives between thousands of days in cold water and only 6 days in tropical surface water.

The rate constants of hydrolysis of CH_3I (reaction 19) in sodium chloride solution determined by Elliott and Rowland (1995) yield half-lives from 1600 days at 25 °C to 4000 days at 5 °C.

$CH_3I+H_2O\rightarrow CH_3OH+H^++I^-$ (reaction equation 19)

Furthermore, Moore (2006) determined “non-chemical” losses in incubation experiments due to unknown loss processes. These could potentially contribute <1 to 15 % per day. Possible additional loss processes could be biologic activity or secondary photolytical sink pathways.

1.3. Diiodomethane in the ocean

CH_2I_2 has long been believed to be much less abundant in the atmosphere than CH_3I, and consequently to not contribute as much to the global atmospheric iodine load (Giese et al., 1999) due to its very rapid photolysis in seawater (Jones and Carpenter, 2005; Martino et al., 2006). However, more recent studies have suggested that, together with Chloroiodomethane (CH_2ClI), it may contribute as much organic iodine to the atmosphere as CH_3I (Jones et al., 2011; Yokouchi et al., 2011; Saiz-Lopez et al., 2012).

1.3.1. Marine sources

Similarly to the other three halocarbons, CH_2I_2 is suggested to originate from biogenic sources. Previous studies found largely elevated concentrations of CH_2I_2 in coastal regions (Klick and Abrahamsson, 1992; Schall and Heumann, 1993; Carpenter et al., 1999; Jones et al., 2009), sometimes even exceeding $CHBr_3$ (Klick and Abrahamsson, 1992). Indeed, incubation studies with temperate and tropical macroalgae showed that CH_2I_2 was among the most abundant organoiodine compounds released from macroalgae (Pedersén et al., 1996; Carpenter et al., 2000; Leedham et al., 2013).

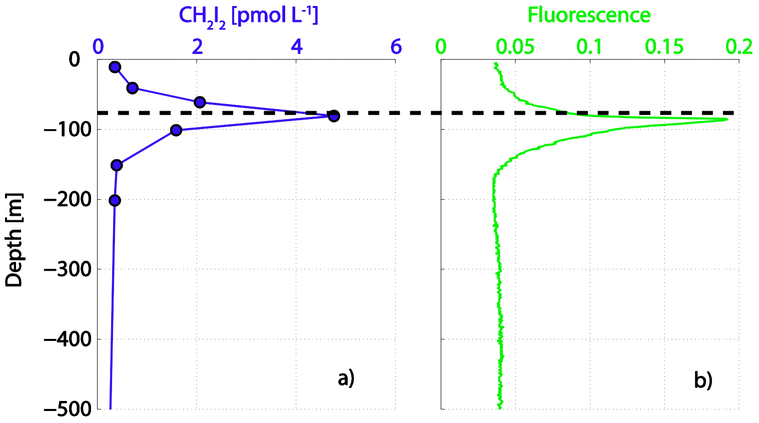

Figure III-6. Typical CH_2I_2 profile in the open ocean (a) in proximity to the Chl *a* maximum (b) at the CVOO from June 2010 (unpublished data).

The large CH_2I_2 production rates from macroalgae indicate that coastal regions are the most important source regions, but CH_2I_2 has also been detected from phytoplankton sources. Moore and Tokarczyk (1993) provided first real evidence for a pelagic source on the basis of depth profiles with distinct maxima in the Chl *a* maximum (see example in Figure III-6). CH_2I_2 was later found to be produced from *diatom* cultures in the laboratory (Moore et al., 1996), but partly from different species than $CHBr_3$ and CH_2Br_2, which was suggested for macroalgal production as well (Schall et al., 1994). Since then, CH_2I_2 has been found in the open ocean during few more field studies (Yamamoto et al., 2001; Abrahamsson et al., 2004b; Carpenter et al., 2007; Jones et al., 2010). Archer et al. (2007) observed a seasonal cycle for CH_2I_2 concentrations with maxima in spring and fall linked to the phytoplankton biomass. Similar observations regarding the seasonality of CH_2I_2 were also made in the Baltic Sea. Its seasonality was hypothesized to be strongly influenced by its very rapid photolysis (Orlikowska and Schulz-Bull, 2009). Martino et al. (2006) modeled depth profiles with only mixed layer production in the Chl *a* maximum and photolysis as major sink. From this, they suggested that CH_2I_2 cannot be measured in tropical surface water. However, Jones et al. (2010) detected CH_2I_2 in low concentrations in surface water of the tropical Atlantic. Additionally to formation from macro- and microalgae, bacterial production of CH_2I_2 was reported (Fuse et al., 2003; Amachi et al., 2005).

Although Collén et al. (1994) did not find increased production of CH_2I_2 after addition of H_2O_2, its production was still hypothesized to being linked to oxidative stress later on. Küpper et al. (1998) suggested that I^- can be oxidized via mediation by e.g. BPO and IPO, producing HOI and finally I_2. The involvement of BPO and IPO in CH_2I_2 formation was also found by Moore et al. (1996).

$I^-+H_2O_2 \leftrightarrow HOI+OH^-$ (reaction equation 20)

$HOI+I^- \leftrightarrow I_2+H_2O$ (reaction equation 21)

HOI can than react with DOM to CH_2I_2. The production of HOI may take place within the cell, while CH_2I_2 is supposedly formed outside by haloform-type reactions (Carpenter et al., 2005) similar to the proposed reactions that yield $CHBr_3$ and CH_2Br_2.

Abiotic formation of CH_2I_2 from ozonation of seawater with DOM has also been observed in the lab (Martino et al., 2009). Ozone (O_3) reacts with I^- in surface seawater.

$O_3+I^-+H_2O \rightarrow HOI+O_2+OH^-$ (reaction equation 22)

$HOI+I^- \leftrightarrow I_2+OH^-$ (reaction equation 23)

HOI and I_2 can further react with DOM. Some parts of the reaction products disproportionate into I^- and iodate (IO_3^-). This process could be of large significance in the oceanic microsurface layer, although its impact on surface concentrations of CH_2I_2 is unknown.

1.3.2. Sinks

Hydrolysis with a very long half-life is also a potential sink for CH_2I_2. Additionally, Class and Ballschmiter (1987) suggested a nucleophilic halogen exchange reaction to yield CH_2ClI induced by light.

$CH_2I_2+Cl^- \rightarrow CH_2ClI+I^-$ (reaction equation 24)

However, the observed production of CH_2ClI by halogen exchange might also have been the result of photolysis of CH_2I_2. Photolysis was investigated further by Jones and Carpenter (2005) who suggested that the photolytic destruction of CH_2I_2 yields 35 % CH_2ClI, which could be the main source of this compound. The following pathway was suggested by Jones and Carpenter (2005) and references therein. The photolytical breakdown of CH_2I_2 leads to a recombination of the photofragments to form a C-I-I linkage, and the photoisomer is then broken down by a water-catalyzed O-H-insertion reaction.

$CH_2I_2 \leftrightarrow CH_2I\cdot+\cdot I \rightarrow CH_2I-I$ (reaction equation 25)

$CH_2I-I+H_2O \rightarrow CH_2IOH+HI$ (reaction equation 26)

$CH_2IOH \rightarrow H_2CO+HI$ (reaction equation 27)

$H_2CO+H_2O \rightarrow CH_2(OH)_2$ (reaction equation 28)

For the formation of CH_2ClI two pathways were suggested: 1) Cl^- may react directly with the CH_2I radical photofragment. 2) Cl^- could attack the photoisomer, or a direct reaction of Cl^- with the photoisomer ion could be possible.

The amount of the CH_2I_2 present in the water column is strongly impacted by its photolysis (Martino et al., 2006; Jones et al., 2010). CH_2I_2 was suggested to have a half-life of less than 10 min in the surface ocean, making photolysis its most significant sink (Jones and Carpenter, 2005; Martino et al., 2005).

2. Air-sea gas exchange

Air-sea gas exchange may be one of the most important sinks out of the mixed layer for $CHBr_3$, CH_2Br_2 and CH_3I, and may also influence surface concentrations of CH_2I_2. In cases where the surface water is not supersaturated, it may also act as a source for these gases. In bioactive regions, $CHBr_3$ and CH_2Br_2 tend to be supersaturated in sea surface water, so fluxes of these compounds may reduce their mixed layer concentrations (Quack et al., 2004; Quack et al., 2007b; Carpenter et al., 2009). Due to its potentially very significant photochemical source, CH_3I is mostly supersaturated in lower and middle latitudes with respect to the atmosphere (Happell and Wallace, 1996; Richter and Wallace, 2004; Jones et al., 2010). Fluxes may therefore also be an important sink for mixed layer concentrations of this compound.

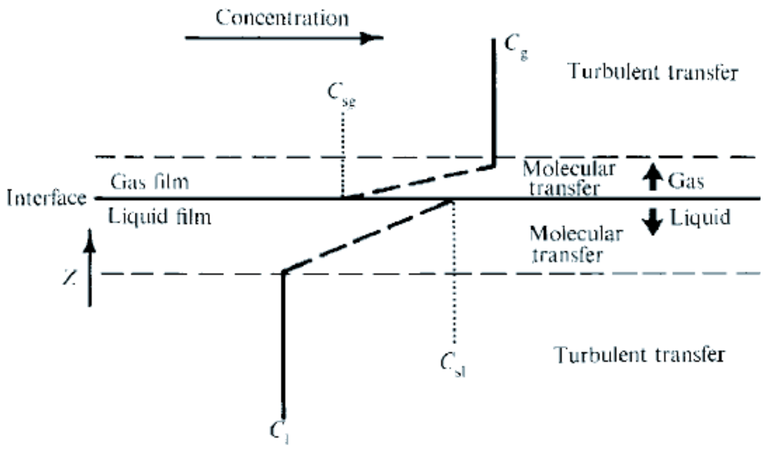

Figure III-7. Two-layer model of a gas-liquid interface, *z* is the thickness of the transfer layer (Liss and Slater, 1974).

First direct flux measurements of CO_2 using eddy covariance techniques have been published by McGillis et al. (2001). Since then, this technique has been mainly applied to CO_2, but also to DMS (Blomquist et al., 2006; Marandino et al., 2007; Miller et al., 2009) and oxygenated volatile organic compounds such as acetone and methanol (Yang et al., 2013a; Yang et al., 2013b). No such measurements exist for $CHBr_3$, CH_2Br_2, CH_3I or CH_2I_2, since these analytical techniques have not been developed yet. The parameterization of air-sea gas exchange has proven to be very difficult (Wanninkhof et al., 2009). One example for a gas-liquid interface model to parameterize gas exchange is the two-layer model proposed by Liss and Slater (1974) (Figure III-7).

The air-sea interface is considered as a flat and solid boundary with stagnant mass boundary layers on the gas- and water side (Garbe et al., 2014). The transport near the interface on the water side supposedly takes place by molecular diffusion. The air-sea gas exchange is generally described with F as the flux across the interface, k as the compound specific transfer coefficient and Δc as the air-sea concentration gradient (Liss and Slater, 1974):

$$F = k \cdot \Delta c \qquad \text{(equation 1)}$$

The compound specific transfer coefficient *k* depends on the degree of turbulence in the fluids on both sides of the interface, and the chemical reactivity of the gas in both the gas and liquid phase. Equation 1 can also be written as:

$$F = k_g \cdot (c_g - c_{sg}) = k_l \cdot (C_{sl} - C_l) \qquad \text{(equation 2)}$$

In this equation, k_g is the gas transfer coefficient for the gas phase, while k_l is the gas transfer coefficient for the liquid phase, c_g is the gas phase concentration, c_{sg} is the gas phase concentration at the interface, C_l is the liquid phase concentration, and C_{sl} is the concentration at the air-sea interface in the liquid phase. The interface concentrations are corrected for their solubility or the degree of disequilibrium between the two phases, respectively (Nightingale, 2009), using the Henry's law coefficients *H*. Then, equation 2 can be written as:

$$F = K_g \cdot (c_g - H \cdot C_l) = K_l \cdot (\frac{c_g}{H} \cdot C_l) \qquad \text{(equation 3)}$$

K_g and K_l are expressed in these equations as total air resistance:

$$\frac{1}{K_g} = \frac{1}{k_g} + \frac{H}{k_l} \qquad \text{(equation 4)}$$

$$\frac{1}{K_l} = \frac{1}{k_l} + \frac{1}{H + k_g} \qquad \text{(equation 5)}$$

Compound	Henry's coefficient
$CHBr_3$	$e^{\frac{-4973}{T+273.15}+13.16}$
CH_2Br_2	$e^{\frac{-4418}{(T+273.15)}+11.7}$
CH_3I	$e^{\frac{-4338}{(T+273.15)}+13.22}$
CH_2I_2	$e^{\frac{-5006}{(t+273.15)}+12.77}$

Table III-1. Henry's law coefficients for $CHBr_3$, CH_2Br_2, CH_3I and CH_2I_2.

Sander (1999) compiled a set of dimensionless Henry's law coefficients for several gases. The ones of the four gases are summarized in Table III-1 as determined by Moore and co-workers (Moore et al., 1995a; Moore et al., 1995b) with *T* for temperature.

The gas-transfer coefficient depends on the molecular diffusion of the gas in the water and gas phases. If the diffusion is very slow in the water, k_w is used and k_g can be neglected, while k_g needs to be considered if the resistance in the gas phase is strong. Gases whose solubility in water is very low are water-side controlled. Then, the coefficient k_w is taken as estimation for K_w (Nightingale, 2009):

$$F = k_l \cdot (\frac{c_g}{H} - C_l) \qquad \text{(equation 6)}$$

The uncertainties in the calculation of the water side controlled transfer coefficient for halocarbons are large due to different approaches for the approximation of their diffusion coefficients, which can only be estimated. The addition of an air side resistance could reduce the overall transfer coefficient for soluble gases (Archer et al., 2007). The uncertainties that come along with the inclusion of air side resistances for heavier halocarbons, which are slightly water soluble, are very large (Quack, personal communication). They have to be parameterized using the transfer coefficient of water (evaporation), which varies with changing meteorological conditions (Isemer et al., 1989; Fairall et al., 2003; Bumke et al., 2013). The application of an algorithm such as TOGA COARE (Fairall et al., 2003) requires a wide set of meteorological parameters, for example air temperature and specific humidity profiles, solar irradiance, downwelling longwave irradiance, and precipitation, that is often not measured. The large uncertainties in deriving the fluxes of these compounds by using parameterizations, both including liquid side and additionally gas side, can only be reduced by the development of direct flux measurement techniques. Since the inclusion of the air-side would add to the uncertainties that come along with the air-side-parameterization, equation 6 was used to calculate sea-to-air fluxes for these four halocarbons.

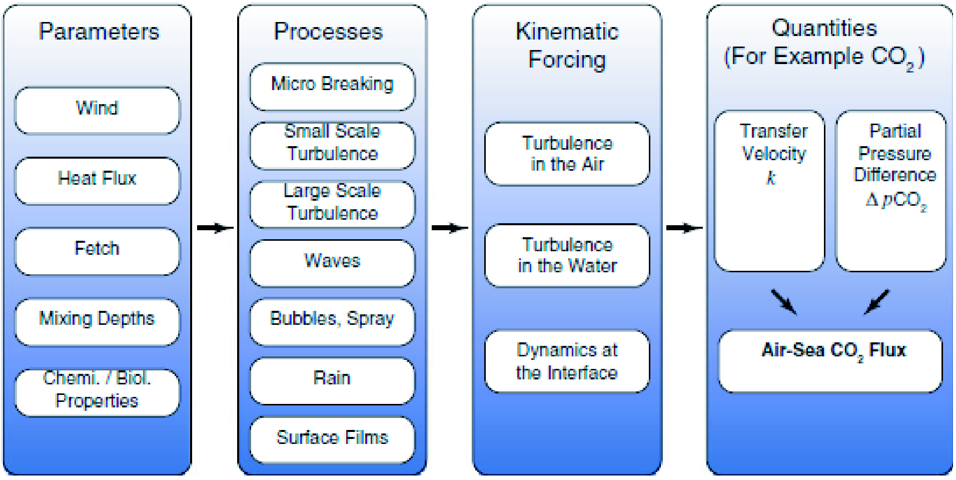
Parameters
Wind
Heat Flux
Fetch
Mixing Depths
Chemi. / Biol. Properties
Processes
Micro Breaking
Small Scale Turbulence
Large Scale Turbulence
Waves
Bubbles, Spray
Rain
Surface Films
Kinematic Forcing
Turbulence in the Air
Turbulence in the Water
Dynamics at the Interface
Quantities (For Example CO₂)
Transfer Velocity k
Partial Pressure Difference ΔpCO₂
Air-Sea CO₂ Flux

Figure III-8. Factors influencing the air-sea gas exchange of CO_2, modified from Garbe et al. (2014).

To calculate *F* here, the wind-speed dependent parameterization of k_w poposed by Nightingale et al. (2000) was used, albeit it may leave out factors that would increase the resistance of one of the two sides. Factors that influence the sea-to-air fluxes of e.g. Carbon dioxide (CO_2), and presumbly also of the four gases covered here, are summarized in Figure III-8 (Wanninkhof et al., 2009; Garbe et al., 2014). The range of measured and parameterized transfer coefficients at very low and high wind speeds is large because they do not consider all these factors (Wanninkhof et al., 2009). Nightingales parameterization (equation 7) is based on a dual tracer method using SF6 and helium-3, and lies well within the range of the fit of all dual tracer data by Ho et al. (2011). Equation 7 is expressed for a Schmidt number *Sc* of 600 (CO_2, 20 °C, fresh water (Nightingale, 2009)) with u_{10m} as the wind speed at 10 m.

$$k_{600} = 0.222 \cdot u_{10m}^2 + 0.333 \cdot u_{10m} \qquad \text{(equation 7)}$$

Compound	**Sc_{hal}**
$CHBr_3$	$\frac{\nu}{1.93\cdot10^{9}\cdot T^{2}+1.686\cdot10^{-7}\cdot T+4.0342\cdot10^{-6}}$
CH_2Br_2	$\frac{\nu}{2.23\cdot10^{-9}\cdot T^{2}+1.9699\cdot10^{-7}\cdot T+4.71321\cdot10^{-6}}$
CH_3I	$\frac{\nu}{2.5\cdot10^{-9}\cdot T^{2}+2.199\cdot10^{-7}\cdot T+5.2612\cdot10^{-6}}$
CH_2I_2	$\frac{\nu}{2\cdot10^{-9}\cdot T^{2}+1.76\cdot10^{-7}\cdot T+4.2\cdot10^{-6}}$

Table III-2. Schmidt numbers for all four halocarbons

Sc describes the viscosity of seawater, which depends on temperature, salinity and density, in relation to the molecular diffusivity of the compound, also temperature dependent. They were determined as a mean between the methods of Hayduk and Laudie (1974) and Wilke and Chang (1955) with *v* as the kinematic viscosity for different temperatures, which finally yields Sc_{hal} for each compound (Table III-2).

Since the diffusion coefficients for $CHBr_3$, CH_2Br_2, CH_3I and CH_2I_2 are not known, they have to be estimated from the relation of *Sc* = 600 of CO_2 to their *Sc* with a power law dependence (Nightingale et al., 2000). The parameterization was converted using a power law dependence of -0.5 at wind speeds above 3.6 m s^{-1} according to Quack and Wallace (2003) and references therein:

$$k_{600hal} = k_{600}\cdot\left(\frac{600}{Sc_{hal}}\right)^{\frac{1}{2}} \qquad \text{(equation 8)}$$

Hence, the final equation from which sea-to-air fluxes in this thesis were derived is with direction from the ocean to the atmosphere:

$$F = k_{600hal}\cdot\left(c_l-\frac{c_g}{H}\right) \qquad \text{(equation 9)}$$

Compound	**Local lifetime [days]**
$CHBr_3$	24
CH_2Br_2	123
CH_3I	7
CH_2I_2	0.003

Table III-3. Local lifetimes of the four halocarbons (Montzka and Reimann, 2011).

3. Atmospheric bromo- and iodocarbons

$CHBr_3$ and CH_2Br_2 are the largest contributors to atmospheric organic bromine (Penkett et al., 1985; Hossaini et al., 2012), while CH_3I and CH_2I_2 are significant contributors to atmospheric organic iodine (Saiz-Lopez et al., 2012). These compounds take part in numerous chemical processes in the troposphere, and they have been shown to be even important for stratospheric processes. Their lifetimes (Table III-3) are very short with iodocarbons having shorter lifetimes than bromocarbons (Montzka and Reimann, 2011).

3.1. Chemical fate

3.1.1. Bromocarbons

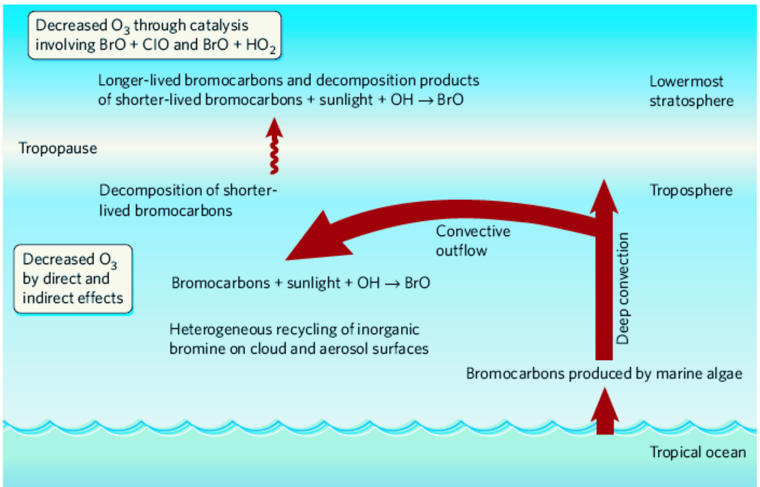
Decreased O_3 through catalysis involving BrO + ClO and BrO + HO_2
Longer-lived bromocarbons and decomposition products of shorter-lived bromocarbons + sunlight + OH → BrO
Lowermost stratosphere
Tropopause
Decomposition of shorter-lived bromocarbons
Troposphere
Convective outflow
Decreased O_3 by direct and indirect effects
Bromocarbons + sunlight + OH → BrO
Deep convection
Heterogeneous recycling of inorganic bromine on cloud and aerosol surfaces
Bromocarbons produced by marine algae
Tropical ocean

Figure III-9. Bromocarbons degrade on their way into the stratosphere. The decomposition products can react with e.g. clouds to form BrO which further can take part in ozone chemistry in the stratosphere (Salawitch, 2006).

Atmospheric $CHBr_3$ and CH_2Br_2 undergo numerous chemical transformations. The general pathway of bromocarbons from the ocean to the atmosphere is illustrated in Figure III-9. Once $CHBr_3$ and CH_2Br_2 are transported into the atmosphere, they are decomposed rather rapidly. They contribute to the production of bromine oxide (BrO), which is involved in ozone chemistry in both the troposphere and stratosphere (Salawitch, 2006). Tropospheric O_3 can be reduced from 5 to 30 % from $CHBr_3$ and CH_2Br_2 due to two processes: direct catalytic loss of O_3 reacting with BrO, and/or reduced O_3 production as a result of decreased levels of nitrogen (Yang et al., 2005).

$CHBr_3$ and CH_2Br_2 are oxidized by OH or Cl, or they are photolyzed. CH_2Br_2 tends to react mainly with OH, while photolysis is the most important loss process for $CHBr_3$ (Ko and Poulet, 2002). Both further react very rapidly with O_2. Following this, the peroxy radicals that are formed, react with nitric oxide (NO), nitrogen dioxide (NO_2), the hydroperoxyl radical (HO_2) and the methyldioxy radical (CH_3O_2) (Krysztofiak et al., 2012). The major degradation products from $CHBr_3$ are carbonyl bromide (CBr_2O) and formyl bromide (CHBrO), which are then further photolyzed. Photolysis of these products yields HBr, HOBr and BrO, together considered as Br_y. Similar reactions are assumed for CH_2Br_2. The major degradation product of CH_2Br_2 in the troposphere is CHBrO, which is produced during photolysis (Hossaini et al., 2010; Krysztofiak et al., 2012, and references therein). It is generally acknowledged that these processes are faster for $CHBr_3$ than for CH_2Br_2 (Table III-3). Ozone destruction involving Br_y has been shown to be 45 times more effective than chlorine due to its larger reactivity (Daniel et al., 1999). Catalytic ozone destroying reaction cycles involving Br_y include cycles 2, 4, 6 and 8 (the odd-numbered cycles only involve chlorine) (Figure III-10).

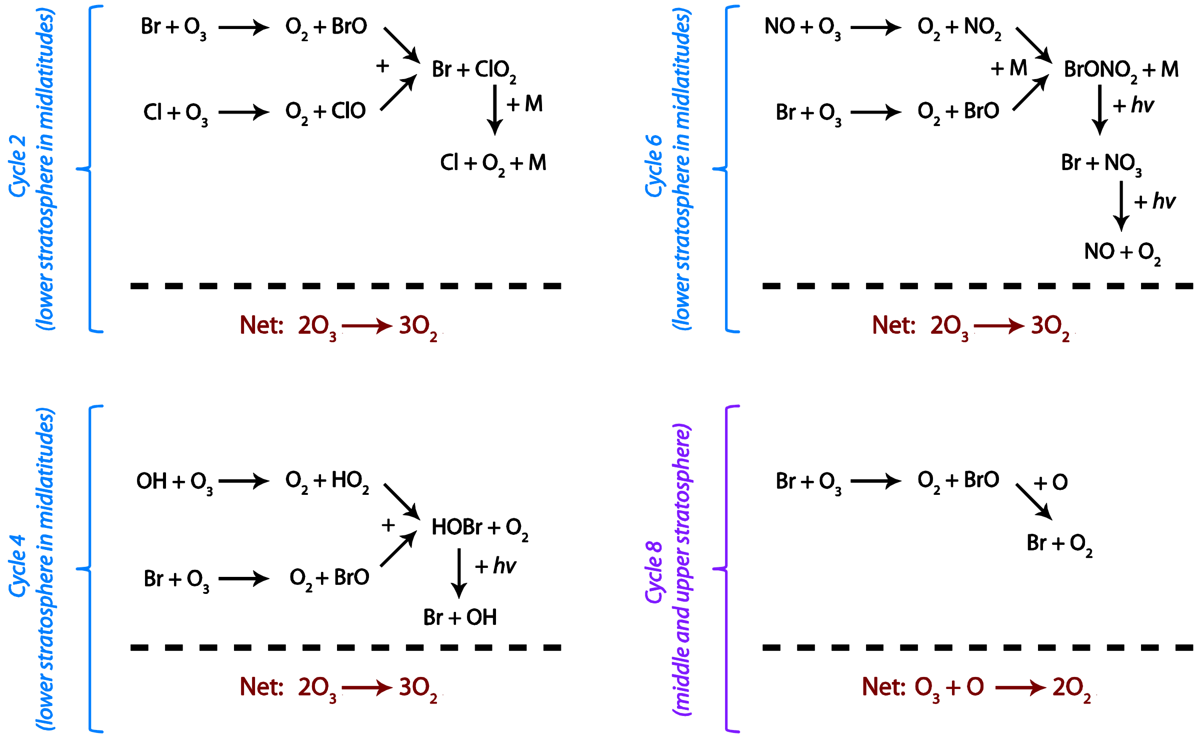
Cycle 2
(lower stratosphere in midlatitudes)
Br + O3 → O2 + BrO
Cl + O3 → O2 + ClO
+
Br + ClO2
+ M
Cl + O2 + M
Net: 2O3 → 3O2
Cycle 6
(lower stratosphere in midlatitudes)
NO + O3 → O2 + NO2
Br + O3 → O2 + BrO
+ M
BrONO2 + M
+ hv
Br + NO3
+ hv
NO + O2
Net: 2O3 → 3O2
Cycle 4
(lower stratosphere in midlatitudes)
OH + O3 → O2 + HO2
Br + O3 → O2 + BrO
+
HOBr + O2
+ hv
Br + OH
Net: 2O3 → 3O2
Cycle 8
(middle and upper stratosphere)
Br + O3 → O2 + BrO
+ O
Br + O2
Net: O3 + O → 2O2

Figure III-10. Catalytic ozone destroying cycles with involvement of bromine according to Daniel et al. (1999). *M* indicates a catalyzer.

3.1.2. Iodocarbons

CH_3I and CH_2I_2 have much shorter lifetimes than $CHBr_3$ and CH_2Br_2 (Table III-3), are very rapidly photolyzed, and then take part in several atmospheric chemical processes (Figure III-11).

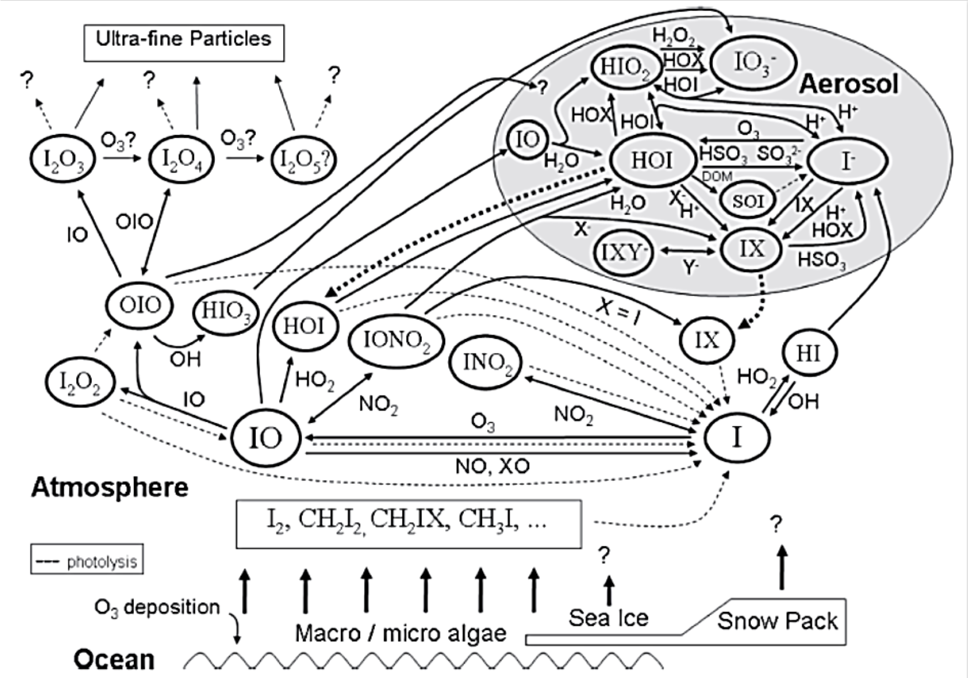
Ultra-fine Particles
?
?
?
I2O3
O3?
I2O4
O3?
I2O5?
IO
OIO
OIO
HIO3
OH
IO
I2O2
HOI
HO2
IONO2
NO2
INO2
O3
NO2
IO
I
NO, XO
X = I
IX
HO2
OH
HI
Aerosol
H2O2
HIO2
HOX
HOI
IO3-
?
IO
H2O
HOX
HOI
HOI
O3
HSO3 SO32-
DOM
H+
H+
I-
H2O
X-
H+
SOI
IX
H+
HOX
X-
IXY
Y-
IX
HSO3
Atmosphere
I2, CH2I2, CH2IX, CH3I, ...
photolysis
?
?
O3 deposition
Macro / micro algae
Sea Ice
Snow Pack
Ocean

Figure III-11. Schematic of the atmospheric iodine photochemistry (Saiz-Lopez et al., 2012) with X and Y as halogen atoms and SOI standing for soluble organic iodine.

The atmospheric photodissociation of CH_3I and CH_2I_2 forms CH_2I radicals and iodine atoms. Iodine atoms can react with O_3 to form iodine oxide (IO). Together, I and IO are called active iodine (IO_x) (Saiz-Lopez et al., 2012). Although it has recently been established that the major formation pathway for IO might be from inorganic iodine from the ocean (Carpenter et al., 2013; Grossmann et al., 2013), CH_3I and CH_2I_2 still represent important sources for IO. The CH_2I radical can also react with O_2, similarly to CH_2Br_2, to form CH_2IO_2, and I and IO in intermediate steps. Reactions of IO_x with organics such as DMS (Nakano et al., 2003) producing DMSO and methyldioxy radicals are also part of the atmospheric iodine chemistry. Once IO_x is produced, it can react again with O_3, taking part in the tropospheric ozone cycle where OIO is formed (Vogt et al., 1999; Saiz-Lopez et al., 2012). Solomon et al. (1994) suggested that iodine could undergo similar ozone destructing cycles in the stratosphere as chlorine and bromine reacting potentially more efficiently with BrO and ClO. CH_3I and CH_2I_2 have also been suggested to be involved in sea-salt and sulfate aerosol formation via the production of HOI and OIO and its self-reaction to I_2O_2 has been suggested (O'Dowd et al., 2002). I_2O_2 is potentially hydrolyzed and then accumulated in aerosols as IO_3^-. HOI can also rapidly react with Cl^- or Br^- to form ICl or IBr in the sea-salt aerosol. This reaction can initiate the autocatalytic release of bromine and chlorine from aerosols (Vogt et al., 1999).

3.2. Transport into the stratosphere

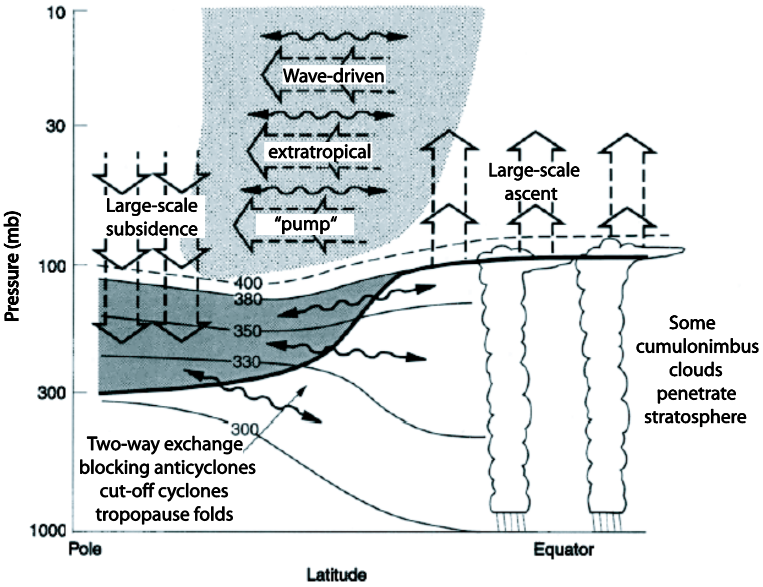
10
30
100
300
1000
Pressure (mb)
Wave-driven
extratropical
"pump"
Large-scale subsidence
Large-scale ascent
400
380
350
330
300
Some cumulonimbus clouds penetrate stratosphere
Two-way exchange
blocking anticyclones
cut-off cyclones
tropopause folds
Pole
Equator
Latitude

Figure III-12. Stratosphere-troposphere exchange modified from Holton et al. (1995). The thick line indicates the tropopause, the dark grey shaded area refers to the "lowermost stratosphere", wavy doubleheaded arrows stand for meridional transport by eddy motions

Once they are produced in the ocean and transported into the lower troposphere, these compounds can further be lifted into the upper troposphere, and finally into the stratosphere. Solomon et al. (1994) and Dvortsov et al. (1999) indicated that, besides the short atmospheric lifetimes of the compounds (Table III-3), significant amounts of CH_3I and $CHBr_3$ could even reach the stratosphere. With regard to their transport, the tropical ocean might be a key region due to convective processes. Tropical deep convection can reach from the surface to up to 15 km, partly reaching the stratosphere. From the tropics, it can be meridionally transported to higher latitudes via the Brewer-Dobson circulation (Figure III-12). It has been suggested that tropical deep convection may be more effective in the Indian and West Pacific Ocean than in the Atlantic (Fueglistaler et al., 2009)

The transport into the upper troposphere and lower stratosphere depends on the speed of vertical transport in comparison to the chemical destruction and washout of the halocarbons emitted from the oceans (abbreviated as SGs – source gases) and their destruction products (abbreviated as PGs – product gases). The atmospheric lifetime plays an important role in how much of a SG reaches the tropical tropopause layer (TTL). Compounds with longer lifetimes may reach the TTL in higher concentrations (Montzka and Reimann, 2011). Since the 2000s, the transport of $CHBr_3$ and CH_2Br_2 into the stratosphere has been studied more thorougly (Sinnhuber and Folkins, 2006; Kerkweg et al., 2008; Laube et al., 2008). Their projected contribution to Br_y differs significantly. Dorf et al. (2008) suggested a stratospheric Br_y amount of 5 ppt from short-lived halocarbons. The modeled contributions from $CHBr_3$ range from 0.7 (Hossaini et al., 2010) to 3 ppt (Aschmann et al., 2009). Recent studies suggest a contribution to stratospheric Br_y of CH_2Br_2 equal to $CHBr_3$ or more (Liang et al., 2010; Hossaini et al., 2010; Aschmann and Sinnhuber, 2013). The modeled entrainment of $CHBr_3$ and CH_2Br_2 into the stratosphere in different regions of the tropical ocean suggest that, although the West Pacific may be of large significance for the Br_y loading, the contribution by $CHBr_3$ and CH_2Br_2 is only moderate, while the contribution from the Atlantic is even lower (Tegtmeier et al., 2012). Fewer studies exist with regard to the transport of CH_3I into the stratosphere. It has generally been assumed that only very small fractions reach the stratosphere due to its short lifetime (Aschmann et al., 2009; Montzka and Reimann, 2011). As a result of the potential involvement of iodine in stratospheric ozone chemistry, it is crucial to constrain its contribution to inorganic iodine. Considering its very short lifetime, CH_2I_2 is probably degraded before it can reach the stratosphere.

4. Study regions

It has been hypothesized that the tropical ocean may play a significant role for halocarbon emissions. Upwelling systems with enhanced primary production may strongly contribute to the significance of the tropical ocean with respect to halocarbon production. Hence, this dissertation focuses on two oceanic upwelling systems in the tropical Atlantic. Two campaigns have been conducted in June and July 2011 and June 2010 in the subtropical and tropical East Atlantic. Cruise MSM18/3 covered the equatorial Atlantic, while the Mauritanian upwelling was part of the **DRIVE** (**D**iurnal and **R**eg**I**onal **V**ariability of halogen **E**missions) campaign (Figure III-13).

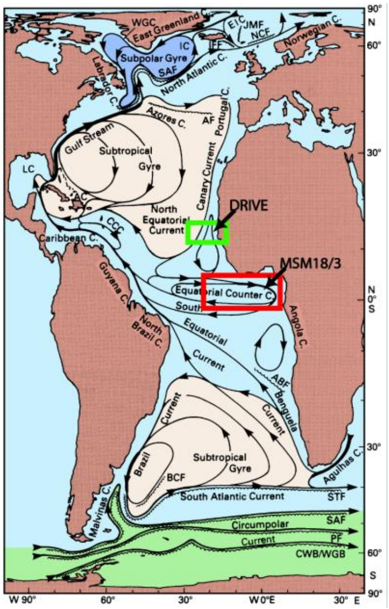
WGC
East Greenland
EIC
JMF
NCF
Norwegian C.
IC
IFF
Subpolar Gyre
SAF
North Atlantic C.
Labrador C.
Azores C.
AF
Portugal C.
Gulf Stream
Subtropical
Gyre
Canary Current
LC
AC
North
Equatorial
Current
DRIVE
CCC
Caribbean C.
MSM18/3
Equatorial Counter C.
South
Equatorial
Current
Guyana C.
North
Brazil C.
Angola C.
ABF
Benguela
Current
Current
Brazil
Subtropical
Gyre
BCF
Agulhas C.
South Atlantic Current
STF
Malvinas C.
SAF
Circumpolar
Current
PF
CWB/WGB
90°
N
60°
30°
N
0°
S
30°
60°
S
90°
W 90°
60°
30°
W 0°E
30° E

Figure III-13. The current system of the Atlantic with the positions of the two study regions of this thesis. Modified from Tomczak and Godfrey (2005).

4.1. The equatorial Atlantic upwelling

The equatorial Atlantic is characterized by a complex current system (Figure III-14). In the surface, a westward directed South Equatorial Current (SEC) spreads between 3° N and at least 15° S, and reaches as deep as 100 m with shallow mixed layers close to the equator (Tomczak and Godfrey, 2005).

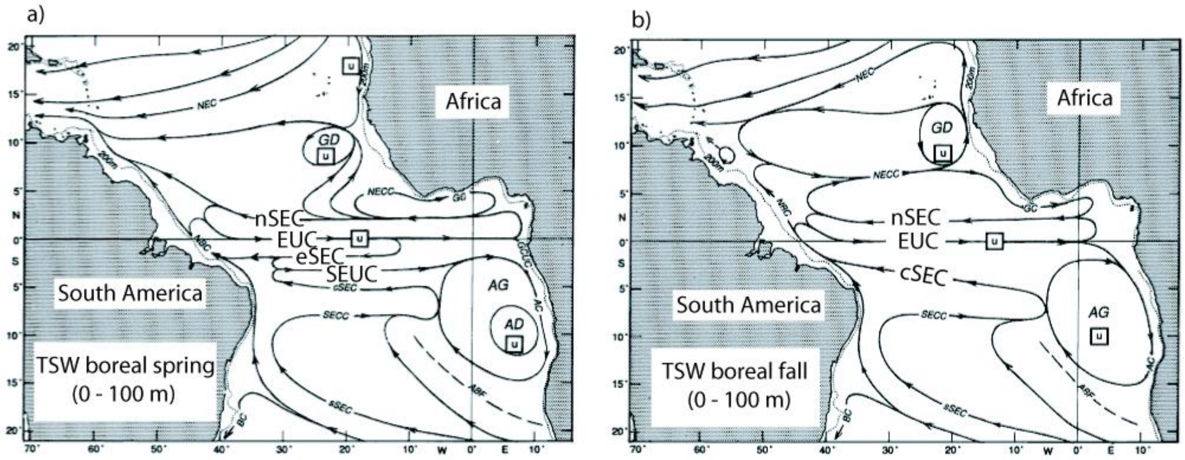
a)
b)
Africa
South America
TSW boreal spring
(0 - 100 m)
TSW boreal fall
(0 - 100 m)
NEC
GD
NECC
GC
nSEC
EUC
eSEC
cSEC
SEUC
sSEC
SECC
AG
AD
AC
ABF
NBC
BC
u
200m
20°
15°
10°
5°
N
0°
S
5°
10°
15°
20°
70°
60°
50°
40°
30°
20°
10°
W
0°
E
10°

Figure III-14. The currents in the Tropical Surface Water (TSW) from 0 – 100 m in boreal spring (a) and boreal fall (b), modified from Stramma and Schott (1999).

The SEC consists of three different branches, which are separated by the South Equatorial Countercurrent (SECC), the South Equatorial Undercurrent (SEUC), and the Equatorial Undercurrent (EUC) (Molinari, 1982). The SEUC with eastward direction is located between 3° S and 5° S and can reach the surface layer east of 35° W with westward flow in July and August (Molinari, 1982; Stramma and Schott, 1999). The EUC is a narrow band between 2° N and 2° S flowing towards the East while reducing speed. Its core is located at 100 m, mostly in the deeper Tropical Surface Water (TSW) and in the shallower Central Water. The position of the core follows the seasonal vertical migration of the thermocline (Stramma and Schott, 1999).

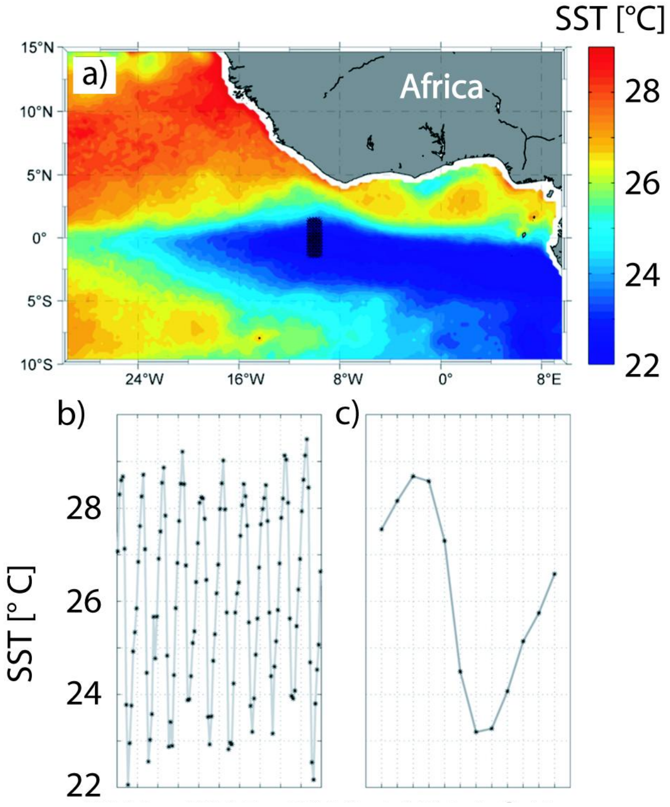

Figure III-15. SST distribution from 2001 from satellite (a), and the SST development from 2000 – 2009 in the section marked by stars (b), and the average annual SST cycle (c). Modified from Hummels et al. (2013).

The Atlantic Cold Tongue (ACT) is a known feature in the equatorial region where SST between 20° W and 5° W can drop by 5 – 7 °C, beginning in May and lasting until September (Weingartner and Weisberg, 1991) (Figure III-15). The development of the ACT has several implications for climate related processes due to its coupling with the African Monsoon (Caniaux et al., 2011). It has been commonly acknowledged that the cooling is linked to the intensifying south-eastern trades in boreal spring and summer as a result of the northward migration of the Intertropical Convergence Zone (ITCZ). Its development is usually associated with phytoplankton blooms in the equatorial region. For example, Grodsky et al. (2008) found a seasonal peak of Chl *a* of 0.6 mg m^{-3} in boreal summer. Many uncertainties remain as to the exact mechanisms that lead to the development of the ACT. Some explanations include advection of cold water upwelled along the African coast (Hastenrath and Lamb, 1978), vertical advection of underlying cold water (Voituriez, 1981), and, the most common is the eastern shallowing of the thermocline (Merle, 1980; Okumura and Xie, 2006). More recently, Jouanno et al. (2011) suggested that the latter is not the primary reason for the cooling, but rather the strong increase of the westward SEC (Philander and Pacanowski, 1986) and the maximum shear above the core of the underlying EUC associated with the ITCZ, confirmed by microstructure measurements (Hummels et al., 2013). Although the shear is maximal at 0° E, maximum cooling appears at 10° W due to the strong stratification in the eastern basin of the equatorial Atlantic (Figure III-15). Jouanno et al. (2011) further proposed that the functions of the EUC include the supply of the background vertical shear to destabilize the upper circulation, and the continuous carriage of cold water to the subsurface, necessary to compensate subsurface warming.

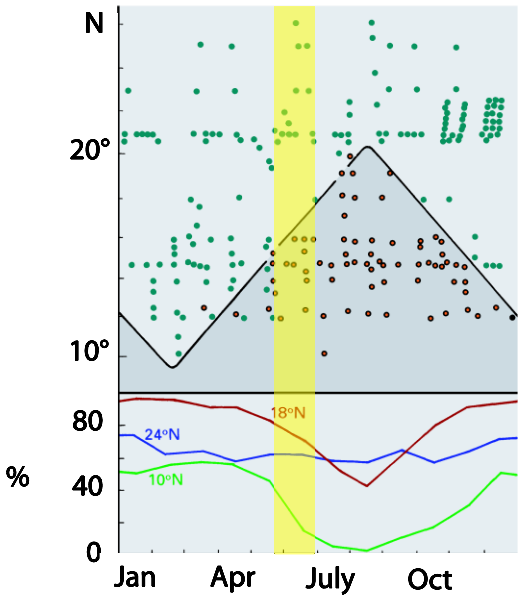

Figure III-16. Tthe seasonal variability of the southern boundary of the Canary Current upwelling system (upper panel) (full dots – observed upwelling, circled dots – observed absence of upwelling), the frequency of occurrence of winds favorable for upwelling (lower panel), modified from Schemainda et al. (1975). The yellow mark indicates the season during which the DRIVE campaign took place.

4.2. The subtropical North East Atlantic

The wind-driven Canary Current extending from 30° N to 10° N with equator ward direction (Fedoseev, 1970) and the North Equatorial Current represent the south-eastern part of the North Atlantic Subtropical Gyre. Part of the Canary Current is the North West African upwelling system on the African shelf area which can be divided into regions with upwelling of varying intensity. Between 12° N and 20° N cold nutrient rich South Atlantic Central Water (SACW), characterized as a straight trend in the T-S diagram between 5 °C and 34.3 and 20 °C and 36.0, is brought up to the surface (Tomczak and Godfrey, 2005). It is transported to the Mauritanian coast by a poleward directed undercurrent, which can take place from late autumn to late spring with regional differences (Minas et al., 1982; Tomczak, 1982; Hagen, 2001) (Figure III-16, upper panel). This is induced by the position of the ITCZ and the trade winds favoring offshore Ekman transport, which leads to upwelling (Mittelstaedt, 1982) (Figure III-16, lower panel). In late spring, the ITCZ starts moving northward, resulting in changing atmospheric conditions south of 20° N. The upwelling consequently starts to cease. Between Cape Blanc (20.8° N and 17.0° W) and Cape Ghir (30.6° N and 9.9° W), upwelling of North Atlantic Central Water (NACW), which is warmer, saltier and contains less nutrients than SACW, (Minas et al., 1982) can be observed throughout the year (Tomczak and Godfrey, 2005).

5. Objectives and outline of this dissertation

Current research is starting to focus on halocarbons and their impact on atmospheric processes in the future. However, many uncertainties still exist regarding their formation and their present emissions. Global estimates of their oceanic concentrations and emissions have been attempted, but until now, many gaps exist in the knowledge on their global coverage. The tropical ocean has been identified as a key region, since global estimates implicate that the tropical ocean is a significant source region for atmospheric mixing ratios of these compounds (Butler et al., 2007; Jones et al., 2010). The tropical region also plays an important role in the halogen transport into the stratosphere.

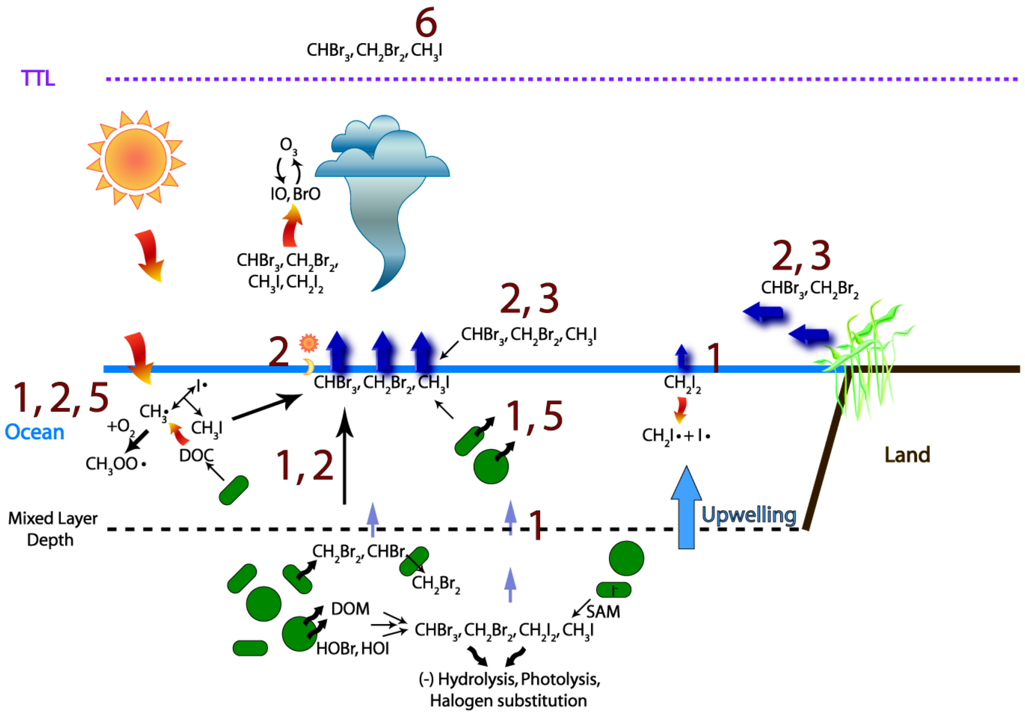
6
$CHBr_3, CH_2Br_2, CH_3I$
TTL
O_3
IO, BrO
$CHBr_3, CH_2Br_2,$
CH_3I, CH_2I_2
2, 3
$CHBr_3, CH_2Br_2$
2, 3
$CHBr_3, CH_2Br_2, CH_3I$
2
1
1, 2, 5
Ocean
$I\cdot$
$CH_3\cdot$
$+O_2$
CH_3I
$CH_3OO\cdot$
DOC
$CHBr_3, CH_2Br_2, CH_3I$
1, 5
1, 2
CH_2I_2
$CH_2I\cdot + I\cdot$
Land
Upwelling
Mixed Layer
Depth
1
$CH_2Br_2, CHBr_3$
CH_2Br_2
I^-
SAM
DOM
HOBr, HOI
$CHBr_3, CH_2Br_2, CH_2I_2, CH_3I$
(-) Hydrolysis, Photolysis,
Halogen substitution

Figure III-17. Summary of the processes that are still subjects of great uncertainty that contribute to halocarbon production and degradation in the tropical ocean as describe above. The numbers at the processes indicate in which manuscript of the thesis they will be investigated.

This thesis investigates some of the processes that impact emissions of $CHBr_3$, CH_2Br_2, CH_3I and CH_2I_2 from productive tropical regions (Figure III-17). The compounds distributions and emissions were investigated during two SOPRAN (**S**urface **O**cean **PR**ocesses in the **AN**thropocene) related campaigns (section 4), a project focusing on atmosphere-ocean interactions of several chemical species. Methods that were used to measure, calculate and evaluate the campaign data are included in the manuscripts in section IV. The main research foci with regard to the six manuscripts are described in the following paragraphs.

Depth profiles of halocarbons often exhibit clear maxima within the Chl *a* maximum that often lie just below the mixed layer. Sea-to-air fluxes however strongly depend on the surface concentrations of these compounds. This leads to the main research questions for the first manuscript *"Halocarbon sources and budget in the equatorial Atlantic Cold Tongue"*:

1. **Is the equatorial Atlantic a source for atmospheric halocarbons and how are they produced?**
2. **How does halocarbon production below the mixed layer influence these emissions?**

Halocarbon supersaturations in the surface ocean will lead to their emissions to the overlying atmosphere. Due to the potential connection of halocarbon production to light due to photosynthetic processes and photochemical production, their concentrations and emissions might exhibit diurnal cycles. This and regional variations in and above the Mauritanian upwelling are investigated in the second manuscript *"Drivers of diel and regional variations of halocarbon emissions from the tropical North East Atlantic"*. The large atmospheric abundances of $CHBr_3$ and CH_2Br_2 found above the upwelling were attributed to coastal sources during previous campaigns (Quack et al., 2007b; Carpenter et al., 2009). This hypothesis is also subject of the second and the third manuscript *"Impact of the marine atmospheric boundary layer conditions on VSLS abundances in the eastern tropical and subtropical North Atlantic Ocean"*. Main questions for these two manuscripts are:

3. **What influences emissions $CHBr_3$, CH_2Br_2 and CH_3I from a tropical upwelling region on a diel and a regional scale?**
4. **Do coastal sources of $CHBr_3$ and CH_2Br_2 influence atmospheric abundances of these compounds in the Mauritanian upwelling?**
5. **What are meteorological constraints on atmospheric abundances and emissions of $CHBr_3$, CH_2Br_2 and CH_3I from coastal upwelling systems?**

Oceanic and atmospheric $CHBr_3$, CH_2Br_2 and CH_3I data from MSM18/3 and DRIVE were also included in the global halocarbon data base **HalOcAt** (**Hal**ocarbons in the **Oc**ean and **At**mosphere). This database was published along with global emission maps in the fourth manuscript *“Global sea-to-air flux climatology for bromoform, dibromomethane and methyl iodide”*. The main focus of this manuscript with regard to this thesis is:

6. **How do concentrations and emissions of the halocarbons from tropical upwelling systems in the Atlantic compare to a global perspective?**

In contrast to the mainly biological production pathways of $CHBr_3$, CH_2Br_2 and CH_2I_2, photochemistry might play a crucial role for the surface and depth distribution of CH_3I in the tropical open ocean. This is investigated in the fifth manuscript *“Numerical modeling of methyl iodide in the eastern tropical Atlantic”* using the one-dimensional “**G**eneral **O**cean **T**urbulence **M**odel” (**GOTM**), and applying it to measurements from the DRIVE campaign. From this, the main research question with respect to this thesis is posed:

7. **Which processes lead to the observed depth profiles of CH_3I in the tropical open ocean?**

The oceanic biogenic and photochemical production pathways lead to the emission of halocarbons into the tropical lower troposphere. They are then degraded, but can also be transported into the stratosphere where they may be involved in ozone chemistry. The transport of halocarbons, which are very patchily distributed in the ocean, can best be resolved with a Lagrangian transport model, which was newly applied on oceanic emissions of CH_3I. The concentrations and emissions of CH_3I from the DRIVE campaign were used along with data from a third campaign, **SHIVA** (**S**tratospheric Ozone: **H**alogen **I**mpacts in a **V**arying **A**tmosphere), in the South China Sea in the sixth manuscript *“The contribution of oceanic methyl iodide to stratospheric iodine”* to calculate its entrainment into the stratosphere. The last question addressed in this thesis is therefore:

8. **How much CH_3I from the Cape Verde and Mauritanian upwelling region can reach the stratosphere and how does this compare to other tropical oceanic regions?**

Finally, an outlook on possible future studies to further address the uncertainties in Figure III-17 will be given.

RESULTS AND DISCUSSION

IV. Results and Discussion

1. Manuscript 1

Halocarbon sources and budget in the equatorial Atlantic Cold Tongue

Helmke Hepach[1], Birgit Quack[1], Stefan Raimund[1], Tim Fischer[1], and Astrid Bracher[2,3]

[1] GEOMAR Helmholtz-Zentrum für Ozeanforschung Kiel, Germany

[2] Helmholtz-University Young Investigators Group PHYTOOPTICS, Alfred-Wegener-Institute (AWI) Helmholtz Center for Polar and Marine Research, Bremerhaven

[3] Institute of Environmental Physics, University of Bremen, Germany

Corresponding author: H. Hepach, GEOMAR Helmholtz-Zentrum für Ozeanforschung Kiel, Germany, Research Division 2: Marine Biogeochemistry, Chemical Oceanography Düsternbrooker Weg 20, 24105 Kiel, Germany (hhepach@geomar.de)

To be submitted

Abstract

Bromoform ($CHBr_3$), dibromomethane (CH_2Br_2), methyl iodide (CH_3I), and diiodomethane (CH_2I_2) from oceanic sources contribute to halogens in the troposphere, and can be transported into the stratosphere where they take part in ozone chemistry. Here, distribution and sources of these four compounds in the equatorial Atlantic from June and July 2011 are presented. Enhanced biological production during the Atlantic Cold Tongue (ACT) season led to elevated concentrations of $CHBr_3$ of up to 44.7 pmol L^{-1} and up to 9.2 pmol L^{-1} for CH_2Br_2 in the surface water, which is comparable to other tropical upwelling systems. While both compounds correlated very well with each other in the surface water, CH_2Br_2 was often more elevated in greater depth than $CHBr_3$, which showed occasional maxima in the vicinity of the deep chlorophyll maximum. The deeper maxima of CH_2Br_2 indicate an additional source in comparison to $CHBr_3$ or a slower degradation of CH_2Br_2 in deeper layers. This may be evidence for the recently hypothesized biologically-mediated conversion of $CHBr_3$ to CH_2Br_2. Concentrations of CH_3I in the surface water were also elevated up to 12.8 pmol L^{-1}, and contrary to expectations of its photochemical formation in the tropical ocean, its distribution was mostly in agreement with biological parameters pointing to biological sources. CH_2I_2 was very low in the near surface water with concentrations of up to 3.7 pmol L^{-1}, and the observed anticorrelation with global radiation was likely due to its strong photolysis. While CH_3I was more elevated in surface water, CH_2I_2 showed distinct maxima in deeper water comparable to CH_2Br_2. For the first time, diapycnal fluxes of the four halocarbons between the upper thermocline and the mixed layer were determined, which acted both as source and sink for the mixed layer. These fluxes were low in comparison to sea-to-air fluxes, which indicates that despite their observed deep maxima, production of the four compounds in the surface mixed layer is the main oceanic source influencing emissions into the atmosphere.

1.1. Introduction

Oceanic upwelling regions where cold nutrient rich water is brought up to the surface are connected to enhanced primary production and elevated halocarbon production (Quack et al., 2007a; Carpenter et al., 2009; Raimund et al., 2011; Hepach et al., 2014). Photochemical formation (Moore and Zafiriou, 1994; Richter and Wallace, 2004) with a possible involvement of organic precursors (Bell et al., 2002; Stemmler et al., 2013a) might be an important methyl iodide (CH_3I) source. An additional abiotic formation pathway involving ozone has been found for diiodomethane (CH_2I_2) in the laboratory (Martino et al., 2009), while it generally has been suggested to be produced biologically. The biogenic production of CH_2I_2 is suggested to occur through different species than the production of $CHBr_3$ and CH_2Br_2 (Moore et al., 1996; Orlikowska and Schulz-Bull, 2009). Additionally, bacterial involvement in the formation of e.g. CH_3I and CH_2I_2 has been observed (Manley and Dastoor, 1988; Amachi et al., 2001; Fuse et al., 2003; Amachi, 2008). Large uncertainties regarding the cycling of halocarbons in the ocean remain. Depth profiles of these compounds might provide insight into the processes participating in their cycling. Elevated concentrations of $CHBr_3$ and CH_2Br_2 at the bottom of the mixed layer and below, mostly close to the chlorophyll *a* (Chl *a*) subsurface maximum, are a common feature in the water column (Yamamoto et al., 2001; Quack et al., 2004; Liu et al., 2013). They are mostly attributed to their production by phytoplankton. While CH_3I maxima close to the Chl *a* maximum were observed as well (Moore and Groszko, 1999; Wang et al., 2009), Happell and Wallace (1996) measured maxima at the surface in different oceanic regions including the equatorial Atlantic which was attributed to a predominantly photochemical source. Elevated CH_2I_2 concentrations associated with the Chl *a* maximum were proposed to be the result of biogenic sources with strong depletion in the surface layers caused by rapid photolysis (Moore and Tokarczyk, 1993; Yamamoto et al., 2001; Carpenter et al., 2007; Kurihara et al., 2010). Not much is known on the actual processes determining the in situ surface water concentrations of these compounds. Potential processes include sources (biogenic and non-biogenic production), sinks (hydrolysis, photolysis, chlorine substitution and air-sea gas exchange), advection, and turbulent mixing in and out of the mixed layer (diapycnal fluxes).

Once they are produced in the ocean, halocarbons can be transported from the oceanic mixed layer into the troposphere via air-sea gas transfer. $CHBr_3$ and CH_2Br_2 are the largest contributors to atmospheric organic bromine from the ocean (Penkett et al., 1985; Schauffler et al., 1998; Hossaini et al., 2012). Marine CH_3I is the most abundant organoiodine in the troposphere, while the very short lived CH_2I_2 together with CH_2ClI contributes potentially as much organic iodine (Saiz-Lopez et al., 2012). Significant amounts of halocarbons and their degradation products can be carried into the stratosphere (Solomon et al., 1994; Hossaini et al., 2010; Aschmann et al., 2011), especially in the tropical regions where surface air can be transported very rapidly into the tropical tropopause layer by tropical deep convection (Tegtmeier et al., 2012; Tegtmeier et al., 2013). The short-lived brominated and iodinated halocarbons produced in the equatorial region may hence play an important role for stratospheric halogens.

This paper characterizes the distribution of brominated and iodinated halocarbons ($CHBr_3$, CH_2Br_2, CH_3I, and CH_2I_2) in the surface water and the water column of the equatorial Atlantic Cold Tongue (ACT). We aim at providing more insight into the biological and physical processes contributing to the mixed layer budget of these compounds in the equatorial Atlantic. Sea-to-air fluxes and, for the first time, diapycnal fluxes from the upper thermocline are calculated. While the first are often an important sink of halocarbons from the ocean, the latter can be both source and sink for the mixed layer. Phytoplankton groups (obtained from pigment concentration) are evaluated as sources of these four compounds. Additionally, surface water halocarbons are correlated to meta data such as temperature, salinity and global radiation to evaluate their origin.

1.2. Methods

Cruise MSM 18/3 onboard the RV *Maria S. Merian* took place from June 21 to July 21 2011. One goal of the campaign was the characterization of the Atlantic equatorial upwelling with regard to halocarbon emissions and their sources. RV *Maria S. Merian* started at Mindelo (Sao Vicente, Cape Verde) at 16.9° N and 25.0° W, and finished at Libreville (Gabon) at 0.4° N and 13.4° E with several transects across the equator. The ship entered the colder waters of the equatorial upwelling several times. Along the cruise track, measurements of halocarbons and phytoplankton pigments were conducted in surface water and at 13 stations where water samples for halocarbon and adjacent parameters were obtained (Figure IV-1). Samples for dissolved halocarbons from sea surface water were taken from a continuously working pump in the ships moon pool at a depth of about 6.5 m every 3 h. Water samples were taken from up to eight different depths per station between 10 and 700 m from 12 l Niskin bottles attached to a 24-bottle-rosette with a CTD (Conductivity Temperature Depth). Halocarbon stations 1 – 4 were located at the first meridional transect at 15° W, stations 5 – 7 were taken during the second transect at 10° W, 8 – 10 were located at the third section at around 5° W, and the last three stations 11 – 13 were taken during the last section at 0° E (Figure IV-1). Water temperature and salinity were recorded with a thermosalinograph. Air pressure and wind speed were derived from sensors in 30 m height, and averaged in 10 min intervals. Global radiation was measured onboard in 19.5 m height with sensors (SMS-1 combined system from MesSen Nord, Germany) measuring downward incoming global radiation (GS, shortwave) and infrared radiation (IR, long-wave).

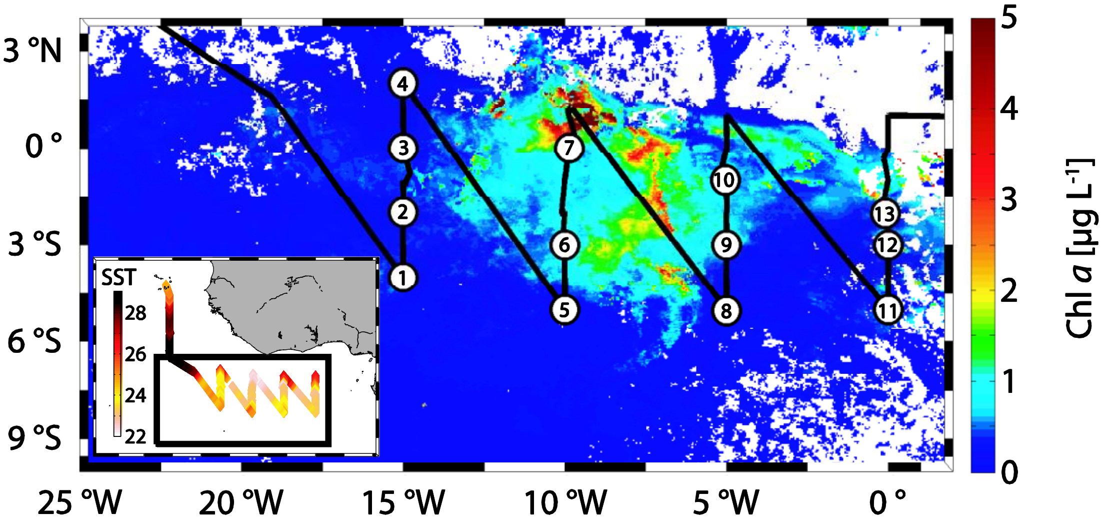

Figure IV-1. Cruise track with measured SST in °C (small box) and the section (large box) during which halocarbons were sampled in both the sea surface and during CTD stations, plotted on monthly average Chl *a* for July 2011 derived from mapped level 3 MODIS Aqua Data.

1.2.1. Sampling and analysis of halocarbons in seawater

A purge and trap system attached to a gas chromatograph with mass spectrometric detection in single ion (GC-MS) mode was used to analyze 50 mL water sample for dissolved halocarbons. Volumetrically prepared standards in methanol were used for quantification. Precision lay within 3 % for $CHBr_3$, 6 % for CH_2Br_2, 15 % for CH_3I and 20 % for CH_2I_2 determined from duplicates. For a detailed description see Hepach et al. (2014).

1.2.2. Phytoplankton pigment analysis and continuous measurement of chlorophyll *a*

Water samples were filtered onto GF/F filters, shock-frozen in liquid nitrogen and stored at -80 °C. Pigments were analyzed using a HPLC technique based on the method by Barlow et al. (1997), slightly modified by Hoffmann et al. (2006), and adapted to the applied instruments as described in Taylor et al. (2011). Samples were measured using a Waters 600 controller combined with a photodiode array detector (PDA, Waters 2998) and an auto sampler (Waters 717plus). As an internal standard, 100 µL canthaxanthin (Roth) was added to each sample. Identification and quantification of the different pigments were carried out using the program EMPOWER by Waters. A list of the pigments used for this study, their abbreviations and their associated phytoplankton groups can be found in Table 2 of Taylor et al. (2011). The pigment data were quality controlled according to Aiken et al. (2009).

As an interpretation of the pigment data the program CHEMTAX® (Mackey et al., 1996) was used, initiated with the pigment ratio matrix proposed by Veldhuis and Kraay (2004) for the subtropical Atlantic Ocean. By using this matrix it can be distinguished between the following phytoplankton groups: *diatoms*, *Synechococcus*-type, *Prochlorococcus* HL (high light adapted) and *Prochlorococcus LL* (low light adapted), *dinoflagellates*, *haptophytes*, *pelagophytes*, *cryptophytes* and *prasinophytes*.

To obtain high resolution TChl *a* data, 10-min-averaged continuous surface maximum fluorescence measured by a microFlu-chl fluorometer from TriOS located in the ships moon pool was used to derive continuous TChl *a* concentrations along the underway transect. This is based on the assumption that active fluorescence F is correlated to the amount of available chlorophyll (Kolber and Falkowski, 1993) as has been used in many active fluorometers. The method is described in details in Taylor et al. (2011) using the correction accounted for non-photochemical quenching as in Strass (1990). Mean conversion factors specific for each zone were determined for collocated F and HPLC-TChl *a* measurements. A linear regression of $r = 0.83$ ($p < 0.01$, $n = 89$) was observed between surface HPLC-derived TChl *a* and F-derived TChl *a*. It shows that F-derived TChl *a* is applicable in this study region.

1.2.3. Correlation analysis of halocarbons

Correlations of different parameters to surface water halocarbons were carried out. Physical influences were investigated with 10 min averages of sea surface temperature (SST), salinity, global radiation and wind speed, and a relationship with location was explored using latitude. Biological parameters used for correlations were the sum of chlorophyll *a* (Chl *a*) and divinyl chlorophyll *a* (div *a*), and the abundances of all phytoplankton groups. Since most of the data sets were not normally distributed and common transformations into normal distributions were not possible, the Spearman's rank correlation coefficient r_s was applied. All correlations with $p < 0.05$ were regarded as significant.

Correlation analysis of the depth profile dataset using the Spearman's rank coefficient did not allow for drawing specific conclusions due to the complexity of the data set. Hence, the mixed influences of water column halocarbon concentrations were examined with principal component analysis (PCA) using MATLAB. Concentrations of all four halocarbons, all phytoplankton groups, the sum of Chl *a* and div *a*, density, temperature, and salinity were included. PCA in comparison to correlation analysis has the advantage that the collective variance of a dataset including several variables can be analyzed.

1.2.4. Mixed layer depth

Mixed layer depths z_{ML} were determined using the method introduced by Kara et al. (2000), which proved to be closest to the visually determined z_{ML} from the temperature, salinity and density profiles. The mixed layer of each CTD profile was calculated as the depth where the temperature from the reference depth in the upper well-mixed temperature region was reduced by a threshold value of 0.8 °C.

1.2.5. Calculation of sea-to-air fluxes of halocarbons

The air-sea gas exchange parameterization of Nightingale et al. (2000) was applied to calculate sea-to-air fluxes F_{as} of halocarbons (equation 1). Schmidt number corrections as reported by Quack and Wallace (2003) were applied to determine the compound specific transfer coefficient k_w. The air-sea concentration gradient was computed from sea surface water measurements and atmospheric background concentrations c_{atm} of 2.50 ppt for $CHBr_3$, 1.20 ppt for CH_2Br_2, and 0.50 ppt for CH_3I determined from 10 atmospheric samples taken during MSM 18/3, and atmospheric mixing ratios of 0.01 ppt for CH_2I_2 as reported by Jones et al. (2010) for the tropical Atlantic. Henry's law constants H of Moore and co-workers (Moore et al., 1995a; Moore et al., 1995b) were used to obtain the equilibrium concentrations c_{atm}/H.

$$F_{as} = k_w \cdot (c_w - \frac{c_{atm}}{H}) \qquad \text{(equation 1)}$$

1.2.6. Calculation of diapycnal fluxes of halocarbons

To estimate the diapycnal flux of halocarbons in the ocean, i.e. the halocarbon transport perpendicular to the stratification, the relation in equation 2 is used with F_{dia} as the diapycnal flux in mol m^{-2} s^{-1}, ρ the seawater density in kg m^{-3}, Δc the diapycnal gradient of the concentration in mol kg^{-1}, and K_{dia} the diapycnal diffusion coefficient in m^2 s^{-1}.

$$F_{dia} = \rho \cdot K_{dia} \cdot \Delta c \qquad \text{(equation 2)}$$

In the equatorial near surface waters, molecular and double diffusion are negligible compared to turbulent mixing. K_{dia} from turbulent mixing can be estimated from measurements of the velocity microstructure (turbulent motions on length scales of centimeters to meters). During MSM18/3, velocity microstructure profiling was performed immediately before or after taking halocarbon profiles, so that local and pointwise in time estimates of diapycnal flux resulted from the combination of the two kinds of profiles via equation 2. The used microstructure profiler was a loosely tethered MSS90 equipped with airfoil shear probes, manufactured by Sea&Sun Technology, Trappenkamp, Germany. In order to calculate K_{dia} from velocity fluctuations measured by the MSS, first the average spectrum of vertical shear for a depth interval of typically 10 to 50 m is calculated and integrated to get an estimate of the average dissipation rate of turbulent kinetic energy (epsilon in W kg^{-1}). The relation in equation 3 first proposed by Osborn (1980) then allows to deduce K_{dia}, with γ a function of the mixing efficiency and N the buoyancy frequency for the chosen depth interval.

$$K_{dia} = \gamma \cdot \frac{\varepsilon}{N^2} \qquad \text{(equation 3)}$$

γ was chosen to be 0.2 following Hummels et al. (2013). A more detailed descriptions of the method to derive K_{dia} below the mixed layer can be found in Schafstall et al. (2010) and Hummels et al. (2013).

1.3. Physical and biological characteristics of the investigation area

1.3.1. Oceanographic description

The equatorial Atlantic is described by a complex current system. The surface is characterized by the westward South Equatorial Current (SEC) spreading between 3° N and 15° S which reaches as deep as 100 m, but has shallow mixed layers close to the equator (Tomczak and Godfrey, 2005). Below the SEC, the Equatorial Undercurrent (EUC) is located (Molinari, 1982). The EUC is a narrow band between 2° N and 2° S flowing towards the east while reducing speed. It carries mostly water with characteristics of deeper tropical surface water (TSW) and of shallower central water. While the core in the West is at 100 m, its position in the East follows the seasonal vertical migration of the thermocline (Stramma and Schott, 1999). Consequently, the mixed layer depth was shallow and ranged only between 10 and 49 m with a mean of 28 m during MSM18/3. The mixed layer was also exposed to diurnal variability. During the day time, it was shallower due to warmer air temperatures and more stratification. In the night time, when the air temperature and SSTs start cooling, water is mixed further down. The shallowest mixed layers were found between 0° N and 3° S in agreement with the location of the EUC. The Atlantic Cold Tongue (ACT) is a known feature in the equatorial region where sea surface temperatures (SST) between 20° and 5° W can drop by 5 – 7 °C from May to September (Weingartner and Weisberg, 1991). TSW around and north of the equator is characterized by high temperatures and comparably low salinities due to enhanced precipitation (Tsuchiya et al., 1992). Many uncertainties remain with respect to the exact mechanisms that lead to the development of the ACT. Jouanno et al. (2011) suggested that the strong increase of the westward SEC associated with the ITCZ (Philander and Pacanowski, 1986), and the maximum shear above the core of the underlying EUC lead to the low SSTs, confirmed later by microstructure measurements (Hummels et al., 2013). Although the shear is maximal at 0° E, maximum cooling appears at 10° W due to the strong stratification in the eastern basin of the equatorial Atlantic. During MSM18/3, maximum SSTs around the equator of 28.5 °C were found at 3° N and 20° W, while the lowest SSTs of 22.1 °C were located at 1° N and 10° W (Figure IV-1, Table IV-1). Generally, high SSTs and low salinities of less than 35.5 were observed north of the equator (TSW). Lower SSTs and higher salinities were measured in the south with the only exception being the 10° W section where both low SSTs and high salinities were also found north of the equator. In total, SSTs during MSM18/3 of mean (range) 24.4 (22.1 – 29.0) °C and salinities of 35.7 (34.5 – 36.3) were measured in the investigated region (Figure IV-2). Wind speed was generally rather low with a mean of 6.1 m s^{-1}, ranging between 0.3 and 11.1 m s^{-1} (Table IV-1).

1.3.2. Biological description

The cooling of SSTs in the ACT region is usually accompanied by a phytoplankton bloom. Grodsky et al. (2008) found a seasonal peak of chlorophyll *a* (Chl *a*) of 0.6 µg L^{-1} in boreal summer. In comparison, surface Chl *a* during MSM18/3 reached values as high as 1.20 µg L^{-1} (around 0.8° N and 0° E), and additionally very high Chl *a* concentrations from the continuous fluorescence sensor measurements above 1 µg L^{-1} around 10° W in agreement to the most intense cooling. HPLC measurements, only taken every three hours, generally agree with the high Chl *a* with maximum values of up to 0.99 µg L^{-1} (Table IV-1).

The most abundant phytoplankton group in the ACT were *chrysophytes* during MSM18/3. *Chrysophytes*, golden algae with flagellar hairs, are thought to be mostly common in freshwater (Round, 1986). However, they have been previously shown to be also the most abundant phytoplankton group in several regions of the Atlantic Ocean, including the lower latitudes around the equator (Kirkham et al., 2011). This group correlated significantly with SST (r_s = -0.45) and salinity (r_s = 0.48) (Table IV-2), it hence seems to be associated with the upwelling water of the EUC. C*hlorophytes, dinoflagellates*, *haptophytes* and *Prochlorococcus* HL include further phytoplankton groups significantly associated with halocarbons in the equatorial Atlantic region. *Chlorophytes* and *Prochlorococcus* HL correlated positively with SST (r_s = 0.13, not significant, and r_s = 0.44, significant) and negatively with salinity (r_s = -0.15, not significant, and r_s = -0.39, significant). They were associated with different water masses than the other three groups. Additionally, *Prochloroccocus* LL were observed in deeper layers and could play a role in comparison to depth profiles of the four halocarbons. These results are in agreement with Johnson et al. (2006), where it was shown that *Prochlorococcus* dominate in oligotrophic tropical waters, especially where the nutrient concentrations are lowest and temperature is high, specifically between 15° S and 15° N of the Atlantic Ocean. *Prochlorococcus* HL dominate among the species, which generally occur from the surface down to 50 m, while the LL dominate from about 75 m downwards in the water column.

Parameter		**Unit**	**Mean** **(min - max)**
SST		[°C]	24.4 (22.1 - 29.0)
Salinity			35.7 (34.5 - 36.3)
Wind speed		[m s^{-1}]	6.1 (0.3 - 11.1)
Biomass proxies	Chlorophyll *a* + Divinyl chlorophyll *a* (HPLC)	[µg L^{-1}]	0.51 (0.10 - 0.99)
	Chlorophyll *a* (sensor)		0.44 (0.06 - 1.20)
$CHBr_3$	Sea surface concentrations	[pmol L^{-1}]	12.9 (1.8 - 44.7)
	Sea-to-air fluxes	[pmol m^{-2} h^{-1}]	644 (-146 - 4285)
CH_2Br_2	Sea surface concentrations	[pmol L^{-1}]	3.7 (0.9 - 9.2)
	Sea-to-air fluxes	[pmol m^{-2} h^{-1}]	187 (-3 - 762)
CH_3I	Sea surface concentrations	[pmol L^{-1}]	5.5 (1.5 - 12.8)
	Sea-to-air fluxes	[pmol m^{-2} h^{-1}]	425 (34 - 1300)
CH_2I_2	Sea surface concentrations	[pmol L^{-1}]	1.1 (0.3 - 3.7)
	Sea-to-air fluxes	[pmol m^{-2} h^{-1}]	82 (3 - 382)

Table IV-1. Mean (minimum – maximum) values of physical parameters (sea surface temperature (SST), salinity, and wind speed), biomass proxies (Chl *a* + Div *a*, and chl *a* determined from the continuously measuring fluorescence sensor), and sea surface concentrations, as well as sea-to-air fluxes of the four halocarbons $CHBr_3$, CH_2Br_2, CH_3I, and CH_2I_2 during the cruise MSM 18/3.

1.4. Results

1.4.1. Surface water

1.4.1.1. $CHBr_3$ and CH_2Br_2

Large regional variations could be observed for $CHBr_3$ in surface water of the tropical Atlantic with a mean of 12.9 (1.8 – 44.7) pmol L^{-1}, and mean CH_2Br_2 of 3.7 (0.9 – 9.2) pmol L^{-1} (Figure IV-2, Table IV-1).

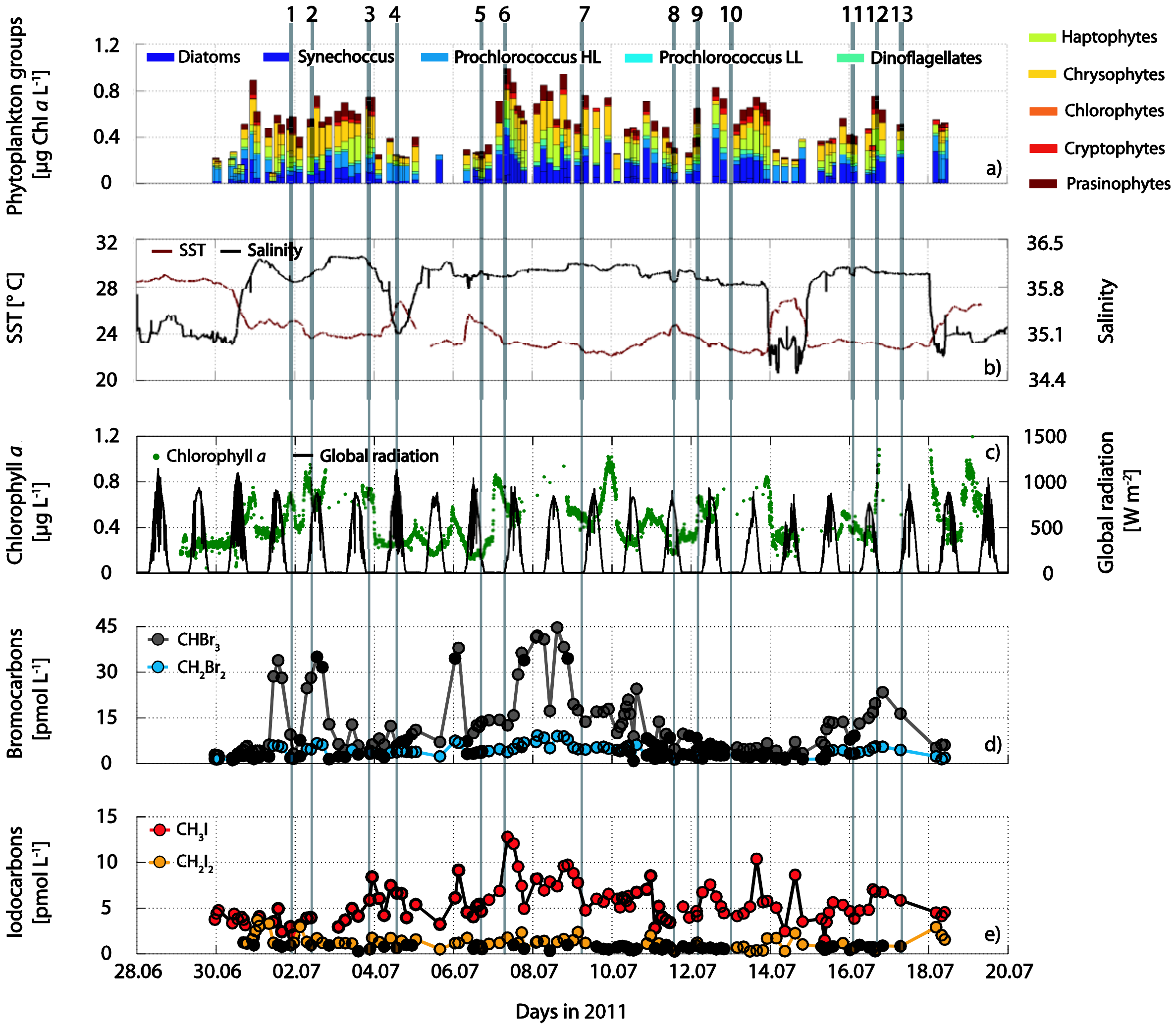

Figure IV-2. Species composition (HL – high light, LL – low light) in a), SST (left side) and salinity (right side) during the cruise in b). In c) Chl *a* from underway sensor measurements (left side), and global radiation (right side). The halocarbon distribution is shown in d) for $CHBr_3$ and CH_2Br_2, and in e) for CH_3I and CH_2I_2. The top numbers mark the halocarbon CTD stations.

Concentrations of the underway measurements and from the shallowest depth from the profiles were included in the evaluation of the surface water concentrations. The observed values are in agreement with data from the tropical oligotrophic Atlantic north of 16° N and the Mauritanian upwelling ranging between 1.0 and 43.6 for $CHBr_3$ and 0.6 – 9.4 pmol L^{-1} for CH_2Br_2 with the largest values close to the coast in the upwelling (Quack et al., 2007a;

Carpenter et al., 2009; Hepach et al., 2014). Quack et al. (2004) observed lower $CHBr_3$ of 2.3 pmol L^{-1} and CH_2Br_2 of 0.2 pmol L^{-1} at 10° N through the tropical Atlantic in boreal fall, while values of 12.8 and 5.3 pmol L^{-1} for $CHBr_3$ and CH_2Br_2 were found at the equator in agreement to this study. Both compounds show the same pattern in surface water throughout the cruise, having hot spots slightly south of the equator.

The very good correlation between $CHBr_3$ and CH_2Br_2 is in agreement to numerous studies from several regions, commonly attributed to related sources for both compounds from macro- and microalgae (Nightingale et al., 1995; Moore et al., 1996; Schall et al., 1997; Laturnus, 2001; Quack et al., 2007b; Karlsson et al., 2008). Significant correlations to SST ($r_s = -0.46$ for both compounds), salinity ($r_s = 0.48$ for $CHBr_3$ and $r_s = 0.41$ for CH_2Br_2), and the sum of Chl *a* and div *a* ($r_s = 0.25$ for $CHBr_3$ and $r_s = 0.27$ for CH_2Br_2) were found, while very low insignificant correlations ($r_s = 0.05$ for $CHBr_3$ and $r_s = 0.04$ for CH_2Br_2) were observed with the 10 min averaged global radiation values (Table IV-2). The most significant correlations were found to *Prochlorococcus* HL with $r_s = -0.70$ for $CHBr_3$ and -0.57 for CH_2Br_2, and to *chrysophytes* with $r_s = 0.43$, and $r_s = 0.41$, respectively.

1.4.1.2. CH_3I and CH_2I_2

The second highest mean sea surface water concentration of the four halocarbons was observed for CH_3I of 5.5 (1.5 – 12.8) pmol L^{-1} (Figure V-2, Table IV-1), which is in the range of earlier studies. The previous measurements of CH_3I in the tropical Atlantic were widely spread between the coasts of South America and Africa with values between 0 and 36.5 pmol L^{-1} in the region south of 25° N and north of 20° S (Happell and Wallace, 1996; Schall et al., 1997; Richter and Wallace, 2004; Jones et al., 2010; Hepach et al., 2014). 7.1 to 16.4 pmol L^{-1} were detected near the region of this study (Richter and Wallace, 2004). Of all four compounds, CH_2I_2 was characterized by the lowest sea surface water concentrations of 1.1 (0.3 – 3.7) pmol L^{-1}. Literature reports of measurements of CH_2I_2 in the tropical Atlantic are very sparse: while Schall et al. (1997) report on average three times higher values of 3.4 (2.1 – 6.8) pmol L^{-1} between 25° N and 20° S than this study, Jones et al. (2010) measured on average 5.8 (0.9 and 17.1) pmol L^{-1} (reported in Ziska et al. (2013)) in the region between 15 and 25° N, which is about five times higher than our mean.

Sea surface CH_3I was similar to $CHBr_3$ and CH_2Br_2 significantly anticorrelated with SST ($r_s = -0.42$), and not significantly correlated with global radiation (Table IV-2). In contrast to the bromocarbons, significant correlations were neither found to salinity, nor to latitude. Additionally, sea surface CH_3I correlated significantly to biomass indicators (sum of Chl *a* and div *a*: $r_s = 0.36$). The regional distribution of CH_3I often followed qualitatively the regional distribution of *haptophytes* ($r_s = 0.39$) with the most elevated concentrations south of the equator. Significant positive correlations were also found to *dinoflagellates* (r_s = 0.29) and *chrysophytes* (r_s = 0.26). A weak, but significant anticorrelation was observed to wind speed (r_s = -0.22). In contrast to the other three halocarbons, CH_2I_2 was significantly positively correlated with SST (r_s = 0.33), and elevated concentrations were observed mostly north of the equator. A weak, but significant anticorrelation of CH_2I_2 was found with global radiation (r_s = -0.25), indicating higher sea surface CH_2I_2 during the night time and lower concentrations during the day. CH_2I_2 correlated significantly both with *chlorophytes* (r_s = 0.32) and *Prochlorococcus* (r_s = 0.27).

	$CHBr_3$	CH_2Br_2	CH_3I	CH_2I_2	SST	Salinity	Global radiation	Latitude	Wind speed	Chl *a* + Div *a*	Chlorophytes	Chrysophytes	Dinoflagellates	Haptophytes
Prochlorococcus (HL)	**-0.70**	**-0.57**	-0.21	**0.27**	**0.44**	**-0.39**	-0.20	**0.49**	**0.26**	-0.01	**0.34**	**-0.28**	-0.14	-0.33
Haptophytes	**0.34**	**0.37**	**0.39**	**-0.25**	**-0.58**	**0.34**	0.16	**-0.21**	**-0.34**	**0.57**	-0.18	**0.37**	**0.53**	
Dinoflagellates	**0.22**	**0.22**	**0.29**	-0.02	**-0.50**	0.10	-0.14	**-0.33**	**-0.37**	**0.72**	0.09	**0.40**		
Chrysophytes	**0.43**	**0.41**	**0.26**	0.13	**-0.45**	**0.48**	**-0.28**	-0.15	-0.15	**0.71**	**0.22**			
Chlorophytes	**-0.29**	**-0.26**	-0.15	**0.32**	0.13	-0.15	**-0.26**	**0.25**	-0.05	0.11				
Ch *a* + Div *a*	**0.23**	**0.27**	**0.36**	0.04	**-0.58**	**0.35**	**-0.22**	-0.13	**-0.27**					

Wind speed	**-0.18**	-0.16	**-0.22**	**0.20**	**0.56**	-0.06	0.12	0.04
Latitude	**-0.38**	**-0.18**	0.03	0.12	0.10	**-0.20**	-0.08	
Global radiation	0.05	0.04	-0.09	**-0.25**	**0.19**	-0.09		
Salinity	**0.48**	**0.41**	-0.09	-0.04	**-0.42**			
SST	**-0.46**	**-0.46**	**-0.42**	**0.33**				
CH_2I_2	0.07	0.09	-0.04					
CH_3I	**0.50**	**0.62**						
CH_2Br_2	**0.90**							

Table IV-2. Spearman's rank correlation coefficients r_s of halocarbons with different parameters and phytoplankton species. Numbers printed in bold are regarded as significant with p < 0.05.

1.4.2. Water column

1.4.2.1. $CHBr_3$ and CH_2Br_2

$CHBr_3$ and CH_2Br_2 exhibited maxima in both the surface and the bottom of and below the mixed layer (Figure IV-3, Table IV-3). Maximum concentration of $CHBr_3$ reached values of up to 19.2 pmol L^{-1}, while up to 10.6 pmol L^{-1} CH_2Br_2 were observed in the deep maxima (profile 4). At stations where $CHBr_3$ was most elevated in the surface (profiles 2, 7, 12, 13), much higher overall $CHBr_3$ concentrations of up to 35.0 pmol L^{-1} were measured. CH_2Br_2 only reached maximum values of up to 6.6 pmol L^{-1} in the surface (profiles 2, 7). In contrast to surface water, $CHBr_3$ and CH_2Br_2 were not always similarly distributed. CH_2Br_2 was elevated 10 m below $CHBr_3$ in several profiles (Figure IV-3e). This can also be seen in the T-S diagrams of these compounds (Figure IV-4a, b): while the most elevated $CHBr_3$ was observed in the density layers between 1024 and 1025 kg m^{-3} (shallower central water of the EUC), CH_2Br_2 was often also elevated in the denser, deeper layers below 30 m (Table IV-3). The maxima of both compounds were mostly in the vicinity of the Chl *a* maximum.

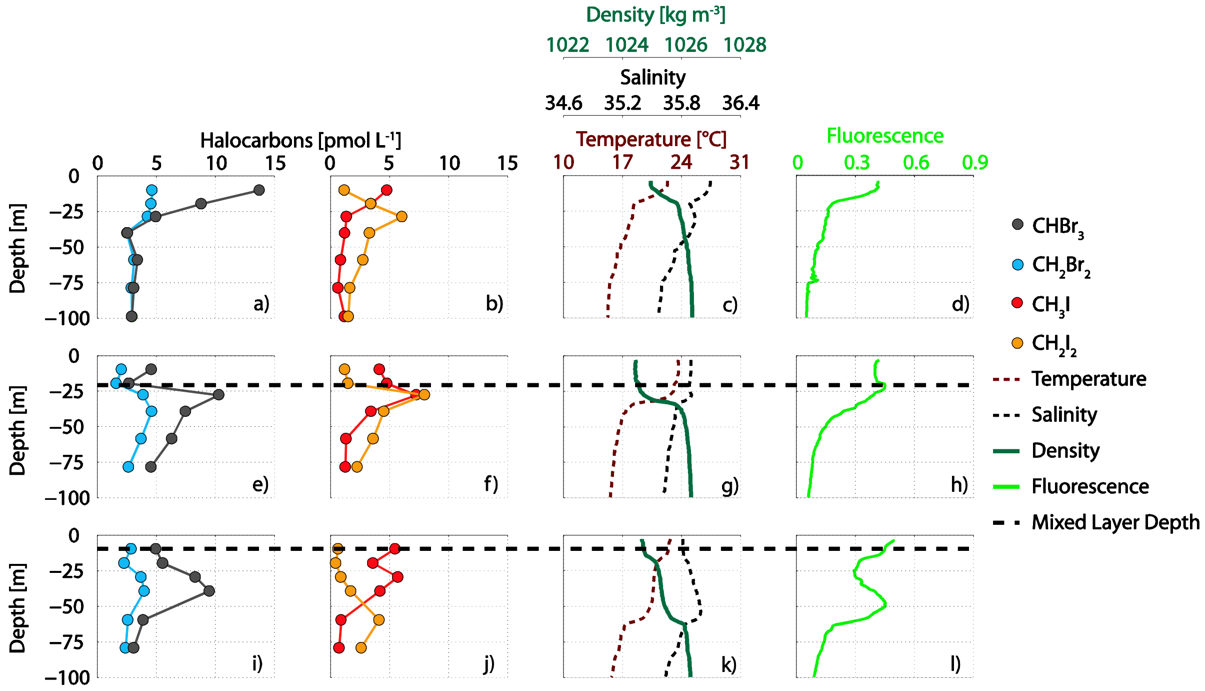

Figure IV-3. Selected CTD profiles (profiles 7, 9 and 10) of $CHBr_3$, CH_2Br_2, CH_3I, and CH_2I_2 in a – b), e – d), and i – j), along with temperature, salinity, and density (c, g and k), as well as raw chlorophyll in d), h), and l), and the mixed layer depth as black dashed line at the same stations.

The PCA can reveal similarities in the variances of several variables in the data set. The results (Figure IV-5) agree with the observations that $CHBr_3$ and CH_2Br_2 display a different distribution: while the variance of $CHBr_3$ seems comparable to several phytoplankton groups such as *chrysophytes* and salinity, CH_2Br_2 exhibits many similarities with the distribution of CH_2I_2 in the water column.

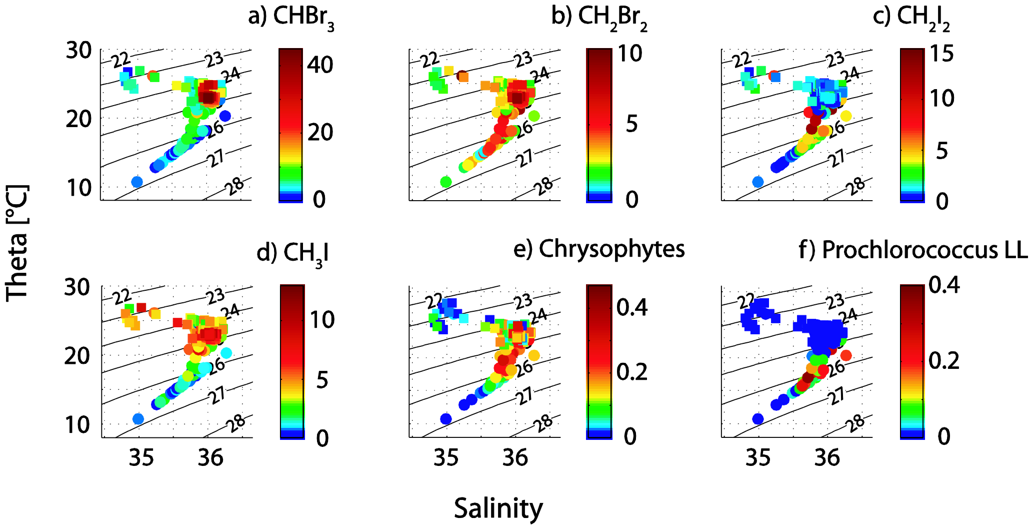

Figure IV-4. Temperature-Salinity (T-S) plots for halocarbons (a – d, in pmol L^{-1}), and phytoplankton species (e – f, in µg Chl *a* L^{-1}). Square markers indicate surface values of halocarbons from underway measurements, circles are depth measurements from CTD profile, and the lines indicate the potential density – 1000.

	z_{ML} m	0 – 30 m Concentrations [pmol L^{-1}]		0 – 30 m Chl *a* + Div *a* [µg L^{-1}]	31 – 60 m Concentrations [pmol L^{-1}]		31 – 60 m Chl *a* + Div *a* [µg L^{-1}]	61 – 100 m Concentrations [pmol L^{-1}]		61 – 100 m Chl *a* + Div *a* [µg L^{-1}]
		CHBr$_3$	CH$_2$Br$_2$		CHBr$_3$	CH$_2$Br$_2$		CHBr$_3$	CH$_2$Br$_2$	
1	34	5.4 (3.2 - 6.5)	1.7 (1.3 - 2.1)	0.60 (0.52 - 0.69)	**5.8** **(3.7 - 7.9)**	**3.0** **(1.8 - 4.2)**	0.59 (0.53 - 0.65)	2.1	1.1	---
2	16	**30.2** **(25.4 - 35.0)**	**6.5** **(6.4 - 6.6)**	0.92 (0.76 - 1.07)	9.0 (7.6 - 10.3)	5.2 (5.1 - 5.4)	0.86 (0.74 - 0.97)	2.4 (1.2 - 4.6)	1.8 (0.8 - 3.6)	0.20 (0.10 - 0.30)
3	37	**6.8** **(6.2 - 7.4)**	**3.9** **(3.6 - 4.2)**	0.80 (0.75 - 0.86)	3.0 (2.6 - 3.2)	2.4 (2.4 - 2.5)	0.65 (0.51 - 0.80)	2.3 (2.2 - 2.5)	2.3 (2.3 - 2.3)	0.18
4	14	**12.5** **(5.8 - 19.2)**	**7.2** **(3.8 - 10.6)**	0.56 (0.26 - 0.86)	5.9 (4.8 - 6.9)	3.1 (3.0 - 3.2)	0.80 (0.79 - 0.81)	2.6 (2.0 - 3.2)	2.5 (1.8 - 3.2)	0.19 (0.13 - 0.26)
5	49	**14.0** **(13.6 - 14.4)**	4.2 (4.0 - 4.3)	0.34 (0.28 - 0.39)	11.7	4.8	0.58	7.6 (6.6 - 8.5)	**7.4** **(6.1 - 8.6)**	0.39 (0.24 - 0.53)
6	12	**13.4** **(12.5 - 14.3)**	**5.0** **(3.8 - 6.3)**	0.99	5.4 (5.1 - 5.7)	4.8 (4.7 - 4.8)	0.30 (0.17 - 0.43)	4.9 (4.7 - 5.1)	4.6 (4.6 - 4.7)	0.10 (0.04 - 0.17)
7	---	**11.2** **(8.8 - 13.7)**	**4.6** **(3.5 - 4.6)**	0.71 (0.65 - 0.76)	3.7 (2.5 - 4.9)	3.4 (2.5 - 4.2)	0.46 (0.44 - 0.48)	3.1 (2.9 - 3.4)	3.0 (2.9 - 3.1)	0.11 (0.06 - 0.17)
8	45	5.0 (4.7 - 5.3)	1.0 (0.6 - 1.4)	0.34 (0.31 - 0.38)	**7.0** **(5.7 - 8.3)**	**2.5** **(1.9 - 3.2)**	0.51 (0.47 - 0.58)	1.1	1.5	0.51
9	21	3.6 (2.7 - 4.5)	1.8 (1.6 - 2.0)	0.75 (0.64 - 0.85)	**8.9** **(7.4 - 10.3)**	**4.2** **(3.9 - 4.6)**	0.77 (0.68 - 0.85)	5.4 (4.5 - 6.3)	3.2 (2.6 - 3.7)	0.24 (0.17 - 0.32)
10	10	5.2 (4.9 - 5.5)	2.6 (2.3 - 2.8)	0.50 (0.41 - 0.59)	**8.9** **(8.3 - 9.5)**	**3.8** **(3.7 - 4.0)**	0.62 (0.51 - 0.73)	3.5 (3.1 - 3.9)	2.5 (2.4 - 2.6)	0.47 (0.32 - 0.62)

11	24	6.0 (4.1 - 7.9)	2.5 (1.8 - 3.3)	0.46 (0.42 - 0.49)	**13.1**	4.3	0.82	4.0 (2.5 - 6.8)	**4.0** **(2.8 - 6.0)**	0.23 (0.04 - 0.44)
12	35	**18.1** **(16.4 - 19.8)**	**5.8** **(5.6 - 6.1)**	0.77 (0.76 - 0.79)	11.6 (9.1 - 14.1)	6.3 (5.4 - 7.1)	0.70 (0.68 - 0.72)	5.3 (4.7 - 6.0)	5.5 (5.3 - 5.8)	0.25
13	41	**11.6** **(6.9 - 16.4)**	3.5 (2.5 - 4.4)	0.55 (0.51 - 0.58	8.9 (8.3 - 9.5)	4.6 (3.0 - 5.6)	0.16 (0 - 0.48)	5.9 (3.3 - 7.6)	**5.2** **(4.1 - 5.7)**	0.12 (0 - 0.30)

Table IV- 3. Concentrations of $CHBr_3$, CH_2Br_2 and the sum of Chl *a* and div *a* averaged over different depths at every CTD station (1 – 13), as well as the mixed layer depth. If a range is not given, only one measurement point exists. Bold numbers indicate the maximum concentrations at this station.

1.4.2.2. CH_3I and CH_2I_2

In agreement with $CHBr_3$ and CH_2Br_2, CH_3I was both elevated in the surface (three profiles 4, 6, 7) (Table IV-4, Figure IV-3b) with values of up to 12.8 pmol L^{-1}, and in the deeper layers in and below the mixed layer (Figure IV-3f) reaching up to 8.5 pmol L^{-1}. In contrast to the other halocarbons, most maxima of CH_3I were observed closer to the surface in the mixed layer (Figure IV-4d). Partly in contrast to $CHBr_3$ and in agreement to the elevated surface concentrations in the third and fourth transect of the cruise, elevated concentrations were also observed in less dense layers of the less biologically active TSW. The PCA revealed that its variance was similar to the variance of *dinoflagellates* and temperature.

		0 – 30 m			**30 – 60 m**			**60 – 100 m**		
	z_{ML} [m]	**Concentrations [pmol L^{-1}]**		**Chl *a* + Div *a* [µg L^{-1}]**	**Concentrations [pmol L^{-1}]**		**Chl *a* + Div *a* [µg L^{-1}]**	**Concentrations [pmol L^{-1}]**		**Chl *a* + Div *a* [µg L^{-1}]**
		CH_3I	CH_2I_2		CH_3I	CH_2I_2		CH_3I	CH_2I_2	
1	34	**2.7** **(2.1 - 3.4)**	4.5 (1.2 - 6.8)	0.60 (0.52 - 0.69)	2.5 (1.8 - 3.2)	**9.9** **(3.9 - 16.0)**	0.59 (0.53 - 0.65)	0.2	1.7	---
2	16	2.8 (0.4 - 5.2)	4.8 (1.7 - 8.0)	0.92 (0.76 - 1.07)	**3.1** **(2.7 - 3.6)**	**12.2** **(11.5 - 12.9)**	0.86 (0.74 - 0.97)	0.6 (0.1 - 1.3)	2.0 (0.7 - 4.3)	0.20 (0.10 - 0.30)
3	37	**8.5** **(8.4 - 8.5)**	4.1 (1.7 - 6.4)	0.80 (0.75 - 0.86)	2.6 (1.0 - 3.5)	**4.6** **(4.3 - 4.9)**	0.65 (0.51 - 0.80)	0.7 (0.4 - 1.1)	3.3 (2.3 - 4.4)	0.18
4	14	**6.1** **(5.5 - 6.6)**	**7.0**	0.56 (0.26 - 0.86)	4.6 (4.6 - 4.7)	2.3 (2.2 - 2.4)	0.80 (0.79 - 0.81)	0.8 (0.7 - 0.9)	1.0 (0.7 - 1.3)	0.19 (0.13 - 0.26)
5	49	**5.4**	0.6 (0.5 - 0.7)	0.34 (0.28 - 0.39)	4.5	4.9	0.58	2.4 (1.9 - 3.0)	**10.5** **(7.1 - 13.8)**	0.39 (0.24 - 0.53)

6	12	**10.4** **(8.0 - 12.8)**	**6.9** **(1.8 - 12.0)**	0.99	1.6 (1.5 - 1.7)	4.0 (3.1 - 4.8)	0.30 (0.17 - 0.43)	1.4 (1.0 - 1.7)	2.4 (1.7 - 3.1)	0.10 (0.04 - 0.17)
7	---	**4.1** **(3.4 - 4.8)**	2.3 (1.2 - 3.4)	0.71 (0.65 - 0.76)	1.3 (1.2 - 1.3)	**4.7** **(3.3 - 6.1)**	0.46 (0.44 - 0.48)	0.9 (0.6 - 1.2)	2.0 (1.5 - 2.7)	0.11 (0.06 - 0.17)
8	45	0.2 (0.1 - 0.4)	0.3 (0.3 - 0.3)	0.34 (0.31 - 0.38)	**4.7** **(3.0 - 7.0)**	1.2 (0.5 - 1.9)	0.51 (0.47 - 0.58)	0.0	**2.4**	0.51
9	21	4.4 (4.1 - 4.8)	1.3 (1.2 - 1.5)	0.75 (0.64 - 0.85)	**5.3** **(3.4 - 7.3)**	**6.2** **(4.5 - 8.0)**	0.77 (0.68 - 0.85)	1.3 (1.3 - 1.3)	2.9 (2.3 - 3.6)	0.24 (0.17 - 0.32)
10	10	4.5 (3.6 - 5.5)	0.5 (0.4 - 0.6)	0.50 (0.41 - 0.59)	**4.9** **(4.2 - 5.7)**	1.3 (0.9 - 1.7)	0.62 (0.51 - 0.73)	0.8 (0.7 - 0.9)	**3.4** **(2.6 - 4.1)**	0.47 (0.32 - 0.62)
11	24	**3.8** **(2.9 - 4.6)**	0.4	0.46 (0.42 - 0.49)	4.4	2.3	0.82	1.7 (1.0 - 2.3)	**1.7** **(0.6 - 3.2)**	0.23 (0.04 - 0.44)
12	35	**7.0** **(6.8 - 7.1)**	1.2 (0.3 - 2.2)	0.77 (0.76 - 0.79)	2.7	**4.1** **(3.8 - 4.3)**	0.70 (0.68 - 0.72)	2.0	2.7 (1.6 - 3.8)	0.25
13	41	**5.1** **(4.3 - 5.9)**	1.5 (0.8 - 2.1)	0.55 (0.51 - 0.58	3.8 (2.0 - 5.6)	**5.9** **(3.9 - 7.4)**	0.16 (0 - 0.48)	1.0 (0.1 - 2.0)	3.4 (1.0 - 4.8)	0.12 (0 - 0.30)

Table IV- 4. Concentrations of CH_3I, CH_2I_2 and the sum of Chl *a* and div *a* averaged over different depths at every CTD station (1 – 13), as well as the mixed layer depth. If a range is not given, only one measurement point exists. Bold numbers indicate the maximum concentrations at this station.

CH_2I_2 was always depleted in the surface with respect to the underlying water column. Maxima of CH_2I_2 were found in different depths, sometimes associated with the Chl *a* maximum (Figure IV-3f), and mostly below the mixed layer (Figure IV-3j). The Maxima in deeper depths were in agreement with the deeper CH_2Br_2 maxima (Figure IV-4), which is also expressed in the similar directed vectors of both compounds in the PCA (Figure IV-5). Values at depth were characterized by much higher concentrations of 16.0 pmol L^{-1} (profile 1) between 30 and 60 m, and 13.8 pmol L^{-1} (profile 5) between 60 and 100 m compared to concentrations of up to 12.0 pmol L^{-1} in the surface (0 and 30 m) (profile 6) (Table IV-4).

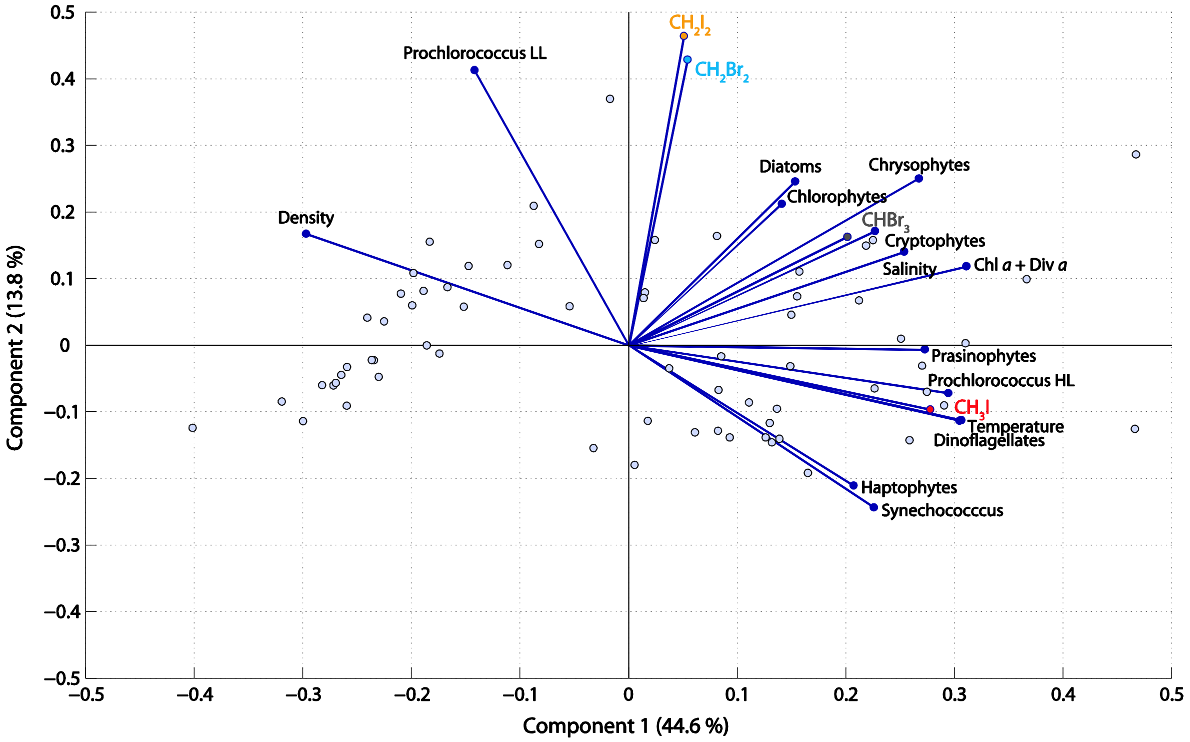

Figure IV-5. Principal component analysis (PCA) of all halocarbon and phytoplankton species composition data, as well as temperature, salinity, and density for the 13 CTD stations.

1.4.3. Fluxes

1.4.3.1. CHBr$_3$ and CH$_2$Br$_2$

Sea-to-air fluxes of CHBr$_3$ and CH$_2$Br$_2$ of 644 (-146 – 4285) and 187 (-3 – 762) pmol m^{-2} h^{-1} during MSM18/3 were larger in the first two transects of the cruise that were characterized by higher seawater concentrations, as well as higher wind speeds (Table IV-1, Figure IV-6). Carpenter et al. (2009) and Hepach et al. (2014) reported -150 and 3504 for open ocean and upwelling CHBr$_3$ fluxes as well as of 5 – 917 pmol m^{-2} h^{-1} for fluxes of CH$_2$Br$_2$ from the Cape Verde and Mauritanian upwelling region. The lower fluxes in the equatorial region in comparison to the other two studies in the Mauritanian region are a result of the lower wind speeds (6.1 (0.3 – 11.1 m s^{-1})) measured during MSM18/3 and the larger concentration gradients of Carpenter et al. (2009). Quack et al. (2004) reported CHBr$_3$ fluxes from the equatorial Atlantic of 2700 (± 800) pmol m^{-2} h^{-1}, to which this study compares well.

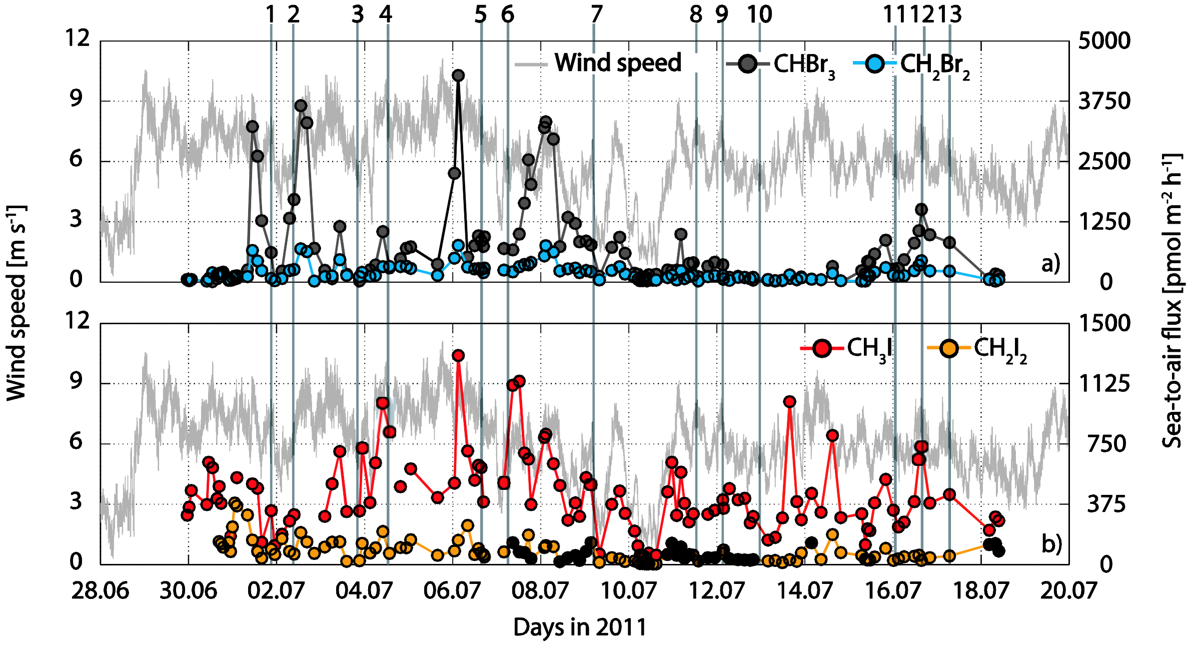

Figure IV-6. Wind speed during the cruise (left side) along with sea-to-air fluxes calculated with sea surface water concentrations and mean atmospheric halocarbons from 10 air samples (right side) in a) for CHBr$_3$ and CH$_2$Br$_2$ and in b) for CH$_3$I and CH$_2$I$_2$. Numbers on the top indicate CTD stations.

Diapycnal fluxes are the fluxes of halocarbons that diffuse out of or into the mixed layer from below the thermocline. Maxima within the mixed layer will lead to fluxes to below the thermocline, while maxima below the mixed layer will have a flux of halocarbon-molecules into the mixed layer as a result. The diapycnal fluxes were generally lower than the sea-to-air fluxes (Table IV-5). They could act both as a source and a sink for halocarbons in the mixed layer. At eight stations, CHBr$_3$ was diffusing into the mixed layer, providing on average 5 (0 – 14) pmol m^{-2} h^{-1} from below to the mixed layer budget of CHBr$_3$. On the other hand, on average 30 (2 – 125) pmol m^{-2} h^{-1}were diffusing out of the mixed layer, which is the highest to below the thermocline of all four halocarbons. This is the result of much larger concentration gradients of CHBr$_3$ at these five stations. Diapycnal fluxes of CH$_2$Br$_2$ were generally lower than for CHBr$_3$ due to the lower concentration gradients. Fluxes into the mixed layer from eight profiles were on average 3 (0 – 8) pmol m^{-2} h^{-1}, while the diapycnal flux reduced the mixed layer budget of CH$_2$Br$_2$ by 2 (0 – 8) pmol m^{-2} h^{-1} at the remaining five stations.

1.4.3.2. CH$_3$I and CH$_2$I$_2$

CH$_3$I fluxes were on average 425 (34 – 1300) pmol m^{-2} h^{-1} throughout the cruise. During the third and fourth transect, they were elevated at several locations mostly during daytime in contrast to the bromocarbons (Table IV-1, Figure IV-6). The fluxes are half the sea-to-air fluxes from the equatorial Atlantic region reported by Richter and Wallace (2004) of 958 ± 750 pmol m^{-2} h^{-1}. They were two times larger than fluxes of Hepach et al. (2014) of on average 246 pmol m^{-2} h^{-1}, and five times lower than fluxes reported from Jones et al. (2010) of on average 2154 pmol m^{-2} h^{-1} from the Cape Verde and Mauritanian upwelling region. CH_2I_2 fluxes were generally larger in the beginning of the cruise where higher wind speeds and higher surface water concentrations were measured. Only few studies have published sea-to-air fluxes of CH_2I_2 from the tropical ocean. CH_2I_2 emissions calculated for MSM18/3 are the lowest of the four halocarbons with only 82 (3 – 382) pmol m^{-2} h^{-1} in comparison to mean fluxes reported by Jones et al. (2010) of on average 541 – 688 pmol m^{-2} h^{-1}. These much higher fluxes are the result of higher oceanic CH_2I_2 concentrations (Jones et al., 2010).

Similarly to the bromocarbons, diapycnal fluxes of CH_3I and CH_2I_2 were generally lower than sea-to-air fluxes (Table IV-5). Due to the larger CH_3I concentrations in the mixed layer compared to the upper thermocline, diapycnal fluxes of 5 (1 – 13) pmol m^{-2} h^{-1} were mostly acting as a sink for the mixed layer budget. Only at three stations, 2 (1 – 5) pmol m^{-2} h^{-1} were transported into the mixed layer. On the other hand, diapycnal fluxes of CH_2I_2 were mostly a source for mixed layer CH_2I_2, providing the mixed layer with on average 12 (0 – 39) pmol m^{-2} h^{-1} due to its much higher concentrations in the water below. This was the highest flux of halocarbons into the mixed layer. The diapycnal flux of CH_2I_2 of 2 (0 – 4) pmol m^{-2} h^{-1} out of the mixed layer was only observed at three stations.

CTD station	**$CHBr_3$**		**CH_2Br_2**		**CH_3I**		**CH_2I_2**	
	Diapycnal flux [pmol m^{-2} h^{-1}]	Sea-to-air flux [pmol m^{-2} h^{-1}]	Diapycnal flux [pmol m^{-2} h^{-1}]	Sea-to-air flux [pmol m^{-2} h^{-1}]	Diapycnal flux [pmol m^{-2} h^{-1}]	Sea-to-air flux [pmol m^{-2} h^{-1}]	Diapycnal flux [pmol m^{-2} h^{-1}]	Sea-to-air flux [pmol m^{-2} h^{-1}]
1	**14**	**14**	**8**	-27	**5**	-119	**39**	-64
2	-125	-3651	-8	-689	-13	-44	**29**	-199
3	**0**	-184	**1**	-195	-6	-703	**7**	-129
4	**8**	-241	**4**	-265	-1	-671	**3**	---
5	-3	-893	**4**	-275	-2	---	**9**	-45
6	**5**	-590	**7**	-185	-13	-988	**27**	-121
7	-16	-68	-0	-25	-5	-38	**7**	-8
8	-2	-110	-0	-25	-1	-4	**0**	-22
9	**3**	-57	**1**	-64	**1**	-337	**3**	-88
10	**2**	-45	-2	-83	-6	-300	-1	-30
11	**4**	-248	**1**	-136	**1**	-316	**0**	-24
12	-4	-1208	-1	-357	-2	-583	-0	-20
13	**1**	-837	**0**	-231	-3	-446	-4	-54

Table IV-5. Diapycnal and sea-to-air fluxes at every CTD stations for the four halocarbons. The fluxes in bold provide the mixed layer with the corresponding halocarbon from below the mixed layer or from the atmosphere, while the negative fluxes losses from the mixed layer to below.

1.5. Discussion

1.5.1. Surface water

1.5.1.1. $CHBr_3$ and CH_2Br_2

The equatorial Atlantic is a source for $CHBr_3$ and CH_2Br_2 during the ACT season with the correlations to biogenic parameters indicating biological formation. $CHBr_3$ and CH_2Br_2 correlated significantly, but weakly with Chl *a*. Weak correlations of bromocarbons with Chl *a* are not an unusual feature (Abrahamsson et al., 2004a; Carpenter et al., 2009; Liu et al., 2011; Hepach et al., 2014). The higher correlations of bromocarbons with SST (higher bromocarbons with lower SST) and salinity (higher bromocarbons with higher salinity) indicate a relationship of bromocarbon abundance with processes within the upwelled water of the EUC, supported by the T-S diagrams (Figure IV-4). The weak, but significant negative correlation with latitude (r_s = -0.38 for $CHBr_3$ and r_s = -0.18 for CH_2Br_2) with maximum values between 2 and 3° S, where water with properties from the EUC is reaching to the surface, underline this hypothesis. Although the correlation analysis of halocarbons with phytoplankton groups cannot directly resolve production and loss processes by algal activity, it is still an indicator for potential sources. Bromocarbon production might exceed loss processes, which leads to the observed statistical link to *chrysophytes*. *Chrysophytes* were to our knowledge not yet among observed halocarbon producers in incubation and field studies. The strong negative correlation of *Prochlorococcus* HL and $CHBr_3$ or CH_2Br_2, respectively, has been observed previously (Hepach et al., 2014). In both cases, this study and Hepach et al. (2014), *Prochlorococcus* HL correlated in contrast to bromocarbons, positively with SST. The negative correlation could then be a result of the bromocarbons being produced by phytoplankton groups associated with water masses of the EUC, while *Prochlorococcus* HL is more associated with warmer, oligotrophic water.

1.5.1.2. CH_3I and CH_2I_2

The anticorrelation of CH_3I concentrations and wind speed has been observed previously (Richter, 2004). The explanation was offered that low wind speed leads to lower sea-to-air fluxes, and thus an accumulation of the produced CH_3I in the sea surface, while high wind speeds deplete the surface concentration. In contrast to Richter (2004) however, indications for biological formation of CH_3I were found in the ACT region. These indications are the anticorrelation with SST, indicating a relationship with the biologically more active upwelled water, the significant correlations with $CHBr_3$ and CH_2Br_2 (Table IV-2) and with pigments as biomass indicators, as well as the lack of correlation to global radiation. Previous studies (Richter and Wallace, 2004; Jones et al., 2010) have attributed CH_3I in the tropical ocean mainly to photochemical formation based on Moore and Zafiriou (1994). However, Stemmler et al. (2013b) modeled depth profiles of CH_3I in the tropical open ocean and suggested that the observed profiles are a combination of photochemical formation and biological production. Similarly, photochemistry and biological production probably both played a role during MSM18/3. *Haptophytes* were the phytoplankton group that correlated most significantly with CH_3I. Correlations additionally indicate *dinoflagellates* and *chrysophytes* as source organisms. Some representatives of *haptophytes* have already been shown to produce CH_3I both in the laboratory (Itoh et al., 1997; Manley and de la Cuesta, 1997; Scarratt and Moore, 1998; Smythe-Wright et al., 2010) and in the field (Abrahamsson et al., 2004b). *Prochlorococcus* have often been discussed as important source for CH_3I in the open ocean (Smythe-Wright et al., 2006; Brownell et al., 2010; Hughes et al., 2011) with production rates varying several orders of magnitude. There is no evidence that *Prochlorococcus* HL had any influence on surface CH_3I concentrations during MSM18/3. In contrast to $CHBr_3$ and CH_2Br_2, some elevated concentrations of CH_3I were also found between the second and third transects during midday (see CH_3I in comparison to global radiation in Figure IV-3), which could be a result of photochemical production.

The very low sea surface concentrations of CH_2I_2 with lowest concentrations during the day are a result of the fast photolysis of this compound. Photolysis of CH_2I_2 can be very rapid with a lifetime of only a few minutes in surface water (Jones and Carpenter, 2005; Martino et al., 2005), which can explain the lower day time concentrations indicated by the negative correlation with global radiation. During MSM18/3, the surface water was not completely depleted, which implicates production in the surface layer. This is in contrast to previously modeled depth profiles at the equatorial Atlantic (Martino et al., 2006) where CH_2I_2 was photolyzed more rapid than it could be transported into the surface water. Although CH_2I_2 is generally assumed to be of biogenic origin in the open ocean (Moore and Tokarczyk, 1993; Yamamoto et al., 2001; Orlikowska and Schulz-Bull, 2009; Hopkins et al., 2013), great uncertainties remain as to which species are involved in its production. The positive correlation of CH_2I_2 with SST during MSM 18/3 could be a result of different sources than for the other three halocarbons (Moore et al., 1996) with indications that *chlorophytes* and *Prochlorococcus* HL might be involved.

1.5.2. Water column

Previous studies focusing on halocarbon profiles from polar to tropical regions usually observed halocarbons in the Chl *a* maximum (Moore and Tokarczyk, 1993; Moore and Groszko, 1999; Yamamoto et al., 2001; Quack et al., 2004; Carpenter et al., 2007; Hughes et al., 2009). This was attributed to biological production of these compounds, while the photochemical formation of CH_3I may lead to surface maxima (Happell and Wallace, 1996).

During MSM18/3, maxima of halocarbons were not always found in the Chl *a* maximum. This could have several reasons. First, the location of the Chl *a* maximum is not necessarily the location of highest biomass or primary production, but rather reflects the photoadaption capability of the predominant phytoplankton groups (Claustre and Marty, 1995). Second, halocarbons could be produced by phytoplankton groups that are not in the biomass maximum distribution in the water column. Third, the location of the halocarbon maximum might be more determined from their sink processes than from their production. For example, sink processes and mixing could be faster or production could have ceased already.

1.5.2.1. $CHBr_3$ and CH_2Br_2

The PCA (Figure IV-5) revealed that in contrast to their surface distribution, the variance in $CHBr_3$ and CH_2Br_2 in the water column is different to each other. Although the first two components of the PCA can together only explain 58.4 % of the total variability in the data set, strong indications for biological sources of $CHBr_3$ exist. *Chrysophytes* as potential source group are in agreement to surface water measurements (Table IV-2, Figure IV-5). Maximum CH_2Br_2 concentrations were occasionally found below $CHBr_3$ maxima, which have already been observed by Quack et al. (2007b). The deeper maxima can have two reasons: 1) CH_2Br_2 could have an additional source such as the biologically mediated conversion from $CHBr_3$ (Hughes et al., 2013). 2) $CHBr_3$ is degraded faster in the depth than CH_2Br_2. Sinks for $CHBr_3$ and CH_2Br_2 include very slow hydrolysis (hundreds to thousands of years) (Mabey and Mill, 1978), slow halogen substitution (5 years) (Geen, 1992), and photolysis (9 years with a mixed layer of 100 m for $CHBr_3$). Photolysis has been suggested to be faster for $CHBr_3$ than for CH_2Br_2 (Carpenter et al., 2009), which would be of more significance in the surface layer. The potential faster degradation of $CHBr_3$ in greater depths is also somewhat contrary to the very fast bacterial degradation of CH_2Br_2 with a half-live of 2 days (Goodwin et al., 1998). An additional source for CH_2Br_2 that involves $CHBr_3$ therefore seems plausible. At four of the 13 stations, $CHBr_3$ was not maximal at the same depth as *chrysophytes*. There, maximum CH_2Br_2 concentrations were found below $CHBr_3$, which could be a result of faster conversion to CH_2Br_2 than production of $CHBr_3$. CH_2Br_2 in denser water is also co-located with *Prochlorococcus* LL, which might be involved in the $CHBr_3$-conversion.

1.5.2.2. CH_3I and CH_2I_2

More elevated CH_3I in surface water in the T-S diagram (Figure IV-4) could be a result of the photochemical formation of this compound. Assuming that CH_3I was solely formed from photochemistry during the cruise, surface maxima would be expected (Happell and Wallace, 1996). Deeper maxima could also occur if the sea-to-air flux in the surface would exceed the photochemical production. The low wind speed, which would not be sufficient to deplete the surface, the relationship with biological parameters, and the partly co-located maxima with the other three biogenic halocarbons (Figure IV-3, Figure IV-5) indicate that CH_3I was at least partly produced directly from phytoplankton, potentially *dinoflagellates* (Table IV-2, Figure IV-5), and/or bacteria. CH_2I_2 was always depleted in the surface with respect to the underlying water column as a result of its strong photolysis (Jones and Carpenter, 2005; Martino et al., 2006). In contrast to previous studies (Moore and Tokarczyk, 1993; Yamamoto et al., 2001), CH_2I_2 was frequently elevated below the Chl *a* maximum and mostly also below the base of the mixed layer (Figure IV-3). The similarity in distribution to CH_2Br_2 (Figure 4, Figure 5) could indicate similar processes for CH_2I_2. The formation of CH_2I_2 seems to have taken place below the formation of $CHBr_3$ and CH_3I, suggesting different sources of CH_2I_2 than for $CHBr_3$ and CH_3I (Moore et al., 1996). With respect to their location within the water column, *Prochlorococcus* LL could, similar to *Prochlorococcus* HL in the surface, be involved in CH_2I_2 production as well (Figure IV-4). Bacterial formation of CH_2I_2 (Fuse et al., 2003; Amachi et al., 2005) could also be an additional source for this compound. Alternatively, CH_2I_2 may not degrade as quickly as $CHBr_3$ and CH_3I in greater depths, which would lead to accumulation below the mixed layer.

1.5.3. Processes contributing to the halocarbon distribution in the mixed layer

Halocarbon emissions into the atmosphere depend strongly on the mixed layer budget of these compounds, which is determined by their sources and sinks. One question that remains to be answered in the field is where halocarbon production occurs. It has been suggested that the production is solely taking place in the Chl *a* maximum (Martino et al., 2006), whereas other model studies assume production of e.g. $CHBr_3$ to be coupled to primary production in the whole water column (Hense and Quack, 2009). Assuming production of halocarbons takes place only in the Chl *a* maximum, which is located below the mixed layer, diapycnal fluxes from below the thermocline could be an important source for mixed layer halocarbons.

To evaluate the significance of halocarbon production below the mixed layer for emissions into the atmosphere, production, loss and transport processes have to be considered. The calculations of diapycnal and sea-to-air fluxes are based on 13 halocarbon gradients determined from the depth profiles, and the joint calculations and measurements of eddy diffusivity (section 1.4.3). With this relatively small number of data, the diapycnal fluxes are subject to some uncertainties. These include a relatively low depth resolution within the water column, thus the concentration gradient may be steeper or less steep than what is assumed from the actual measurements, and a short validity of diffusion coefficients of only 1 h, since the oceanic conditions vary rapidly. Since the depth profiles measured during MSM18/3 agree well to previous studies from the tropical ocean (Yamamoto et al., 2001; Quack et al., 2004), a general idea of the significance of diapycnal fluxes for the mixed layer budget of halocarbons can still be obtained. The loss rates due to chemical sinks were not determined directly during this study, hence they were estimated from literature values. Chemical loss processes for $CHBr_3$, CH_2Br_2 and CH_3I from the mixed layer include hydrolysis, halogen substitution and photolysis. The half-lives of $CHBr_3$ and CH_2Br_2 due to hydrolysis are more than hundreds and thousands of years (Mabey and Mill, 1978), while for CH_3I, the half-life due to hydrolysis can range between 1600 days at 25 °C and 4000 days at 5 °C (Elliott and Rowland, 1995). The half-life of $CHBr_3$ at 25 °C due to halogen substitution is about 5 years and similarly slow for CH_2Br_2 (Geen, 1992). The half-life of $CHBr_3$ with respect to photolysis is 9 years assuming a mixed layer of 100 m, and potentially slower for CH_2Br_2 (Carpenter et al., 2009). Liu et al. (2011) calculated a half-life of $CHBr_3$ due to photolysis in a coastal mixed layer of only 5 m to be 82 days. Since mixed layers during MSM18/3 were much shallower than 100 m, photolysis of bromocarbons in the mixed layer should be similary short. Nevertheless, this time scale is still long in comparison to the one hour that is considered here. As a result of these slow rates, only sea-to-air flux is considered as sink for $CHBr_3$ and CH_2Br_2. In comparison to halide substitution, photolysis of CH_3I is also very slow (Zika et al., 1984). Halide substitution was suggested to be important sink in the tropical ocean with low wind speeds favoring halide substitution as main sink process, and large wind speeds favoring sea-to-air fluxes as main sink (Jones and Carpenter, 2007). For the calculations here, halide substitution is additional to sea-to-air fluxes included for CH_3I, and was determined according to Stemmler et al. (2013b) using the rates published by Elliott and Rowland (1993). For CH_2I_2, photolysis may well be the most significant sink with a half-life of less than 10 min in surface water (Jones and Carpenter, 2005), hence this is also included here. Losses of CH_2I_2 due to photolysis were calculated according to Martino et al. (2006) with a photon flux calculated from the NASA COART model (Jin et al., 2006), a Chl *a* concentration of 0.4 $\mu g\ L^{-1}$, absolute quantum yields from Martino et al. (2006), and absorption cross sections determined by Jones and Carpenter (2005). Advection, which is difficult to estimate, may not play a large role for CH_2Br_2, CH_3I and CH_2I_2, since mixed layer concentrations of these compounds were rather homogeneous in the whole region. $CHBr_3$ concentrations were more variable. Consequently, advection may transport significant amounts from one location to another. The mixed layer was well mixed considering the temperature and salinity profiles. Consequently, halocarbon maxima can only occur within the mixed layer if halocarbon production is faster than mixing. As a consequence, local processes probably play the most important role for their distribution in the water column. All the processes involved are summarized in Figure IV-7.

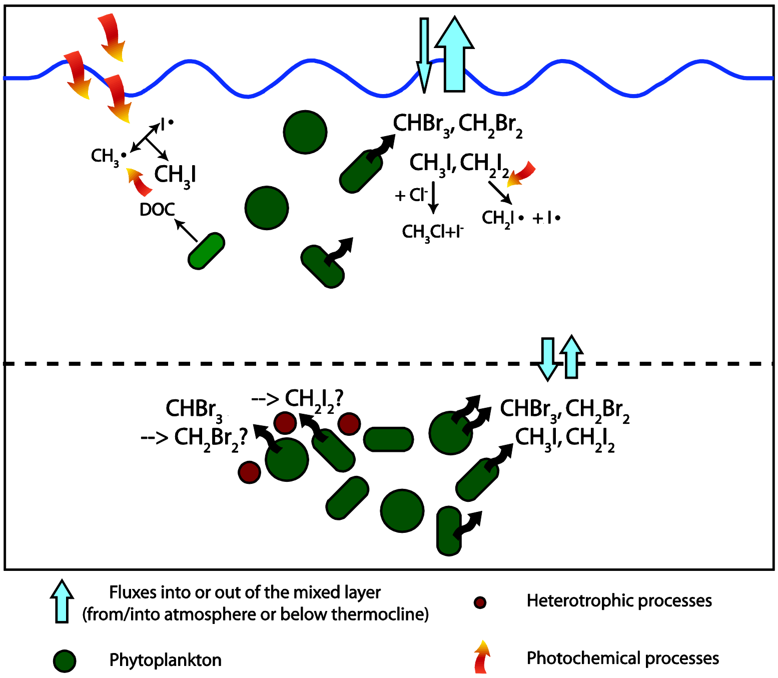
I•
CH3•
CH3I
DOC
CHBr3, CH2Br2
CH3I, CH2I2
+ Cl-
CH3Cl+I-
CH2I• + I•
CHBr3
--> CH2Br2?
--> CH2I2?
CHBr3, CH2Br2
CH3I, CH2I2
Fluxes into or out of the mixed layer (from/into atmosphere or below thermocline)
Heterotrophic processes
Phytoplankton
Photochemical processes

Figure IV-7. Processes that were possibly involved in forming the observed depth profiles during the MSM18/3 cruise, including the processes that were taken into account for assessing the importance of diapycnal fluxes from below the thermocline into the mixed layer (including sea-to-air fluxes, nucleophilic chlorine substitution of CH_3I and photolysis of CH_2I_2).

The sinks were calculated as relative fractions of the total mixed layer concentrations to evaluate the significance of diapycnal fluxes (Table IV-6). Assuming that the conditions during MSM18/3 reflect the general situation in the equatorial upwelling, the results suggest that sea-to-air fluxes are the main sink on short time scales for $CHBr_3$, CH_2Br_2 and CH_3I at each station. The estimation of sea-to-air fluxes using bulk data comprises some uncertainties. However, the parameterization has been successfully applied in several studies, e.g. in Hepach et al. (2014), so we assume that the sea-to-air fluxes are indeed the main sink for mixed-layer-halocarbons.

	Sea-to-air flux	Diapycnal flux	Other sinks	Total	Sea-to-air flux	Diapycnal flux	Other sinks	Total
$CHBr_3$	-1.55	+0.03		**-1.52**	-2.24	-0.07		**-2.31**
CH_2Br_2	-2.10	+0.05		**-2.05**	-2.09	-0.03		**-2.12**
CH_3I	-3.20	+0.08	-4.8×10^{-4}	**-3.12**	-3.30	-0.24	-9.4×10^{-4}	**-3.54**
CH_2I_2	-2.33	+0.31	-22.38	**-24.40**	-1.77	-0.04	-21.75	**-23.56**

Table IV- 6. Averaged percentaged fractions of sinks during MSM18/3 for cases where diapycnal fluxes provided the mixed layer with halocarbons from below (first four columns, stations 1, 3 – 4, 9 – 11, 13 for $CHBr_3$, stations 1, 3 – 6, 9, 11, 13 for CH_2Br_2, stations 1, 9, 11 for CH_3I, and stations 1 – 9, 11 for CH_2I_2) and where halocarbons diffused out of the mixed layer (last four columns, stations 2, 5, 7 – 8, 12 for $CHBr_3$, satations 2, 7 – 8, 10, 12 for CH_2Br_2, stations 2 – 8, 10, 12 – 13 for CH_3I, stations 10, 11 – 12 for CH_2I_2).

On short time scales, diapycnal fluxes of CH_3I may compete with the loss due to chloride substitution from the mixed layer. In comparison to halogen substitution (9.4×10^{-4} % depletion of total mixed layer CH_3I), 0.24 % are lost due to diffusion to below the thermocline. Photolysis may reduce the CH_2I_2 mixed layer budget by on average 22 % (Table IV-6). Diapyknal fluxes along concentration gradients from maxima below the mixed layer can clearly not account for all losses of CH_2I_2 (sea-to-air fluxes and photolysis) during 1 h. Between 1.55 ($CHBr_3$) and 3.20 % (CH_3I) of the mixed layer budget of the four halocarbons are lost due to sea-to-air fluxes, while diapycnal fluxes can only account for 0.03 ($CHBr_3$) to 0.31 % (CH_2I_2). The discrepancy between the large sea-to-air flux and the lower diapycnal flux into the mixed layer for all four halocarbons has to be balanced by mixed layer production and advection. Since we argued that advection potentially plays a minor role, production in the whole mixed layer seems to be the most important process for emissions of halocarbons into the tropical atmosphere, even if maximum production takes place below. The maxima that occasionally evolve in the mixed layer suggest that production of halocarbons is rapid, but it may vary with depth. The relative production of halocarbons in the mixed layer is likely largest for CH_2I_2, because it has to account for its rapid photolysis (on average 22 % loss in 1 h) in comparison to losses of only 1.52 ($CHBr_3$) to 3.54 % (CH_3I) of the other halocarbons. This may be in agreement to earlier studies investigating macroalgal production proposing larger release rates of CH_2I_2 than of $CHBr_3$, CH_2Br_2 and CH_3I (Klick and Abrahamsson, 1992; Carpenter et al., 2000). In addition to the processes discussed above, the diurnal shift of the mixed layer may have an impact on the mixed layer budget of these compounds. For instance, when the mixed layer deepens during night time due to cooling of the SSTs, halocarbons may be introduced into the mixed layer where they are mixed up more efficiently.

The calculations of diapycnal fluxes in comparison to loss processes of halocarbons such as sea-to-air fluxes, nucleophilic halide substitution and photolysis implicate that mixing from below the thermocline into the mixed layer through diffusion is generally not sufficient to account for these losses. Mixed layer production through biological and photochemical pathways may be the main driver for halocarbon emissions from the ocean when halocarbons are supersaturated in surface water, even when main production of halocarbons takes place below the thermocline (Figure IV-7). The largest discrepancy was found for CH_2I_2 due to its very rapid photolysis. When diapycnal fluxes act as a sink for the mixed layer budget of halocarbons, they may compete with nucleophilic halogen substitution as important sink for CH_3I. However, the long-term impact of diapycnal fluxes on the mixed layer budget of halocarbons remains to be investigated.

1.6. Summary and conclusions

The increased biological production during the Atlantic Cold Tongue (ACT) leads to elevated $CHBr_3$ and CH_2Br_2 concentrations within the equatorial surface water with comparable concentrations to other tropical upwelling systems. Both compounds showed similar distributions and maxima in the region where the Equatorial Undercurrent (EUC) influences the surface waters between 2° and 3° S with cooler water and elevated nutrients. *Chrysophytes*, the dominating phytoplankton group in the equatorial surface waters, may be involved in bromocarbon production. In contrast to their surface water distribution, both compounds exhibited different distributions in the water column. While $CHBr_3$ was mostly elevated in shallower layers, CH_2Br_2 frequently showed maxima in deeper water below $CHBr_3$. This may be an indicator for bromocarbon cycling within the water column, for example the biologically mediated conversion of $CHBr_3$ to CH_2Br_2. Elevated maxima of CH_2Br_2 were found where heterotrophic processes dominate. This may be an indicator for processes that are involved in this bromocarbon cycling.

In contrast to other tropical Atlantic regions, the correlation of CH_3I with $CHBr_3$ and with biological parameters indicates at least partly biogenic formation of this compound. Concentrations measured in the ACT lie within previously reported ranges from the tropical Atlantic. In contrast to the other three compounds, CH_2I_2 surface water and mixed layer concentrations were lowest due its strong photolysis, supported by a low, but significant anticorrelation with global radiation. CH_2I_2 maxima could be found in deep layers, where also

CH_2Br_2 was enhanced, suggesting similar formation or loss pathways for CH_2I_2 at depth likely tied to heterotrophic activities below the layers of maximum production.

The estimation of sinks in the mixed layer suggests, that halocarbon production from both biogenic and photochemical pathways in the upper water column is likely the most important factor contributing to marine emissions of these compounds. While sea-to-air fluxes seem to be the most important sink for mixed layer $CHBr_3$, CH_2Br_2 and CH_3I, photolysis influences CH_2I_2 concentrations the most. Diapycnal mixing was found to be a small source and sink for the halocarbon mixed layer budget. Its influence on a larger time scale than 1 h remains to be investigated by for example time series measurements of production and loss rates of halocarbons in combination with measurements of diapycnal mixing.

The results of this study clearly show the need to conduct more process-related studies in the field. Future campaigns need to include diapycnal mixing when assessing halocarbons at depth to evaluate the significance of this process for the mixed layer budget of these compounds more thoroughly. While current studies start to concentrate more and more on changes of emissions of halocarbons in a future climate, investigating the exact mechanisms of formation, degradation and transport of halocarbons in the water column remains an important task, since they have not been resolved yet. Understanding of the actual processes that contribute to their concentrations and distribution within the water column is crucial to predict their emissions. We therefore suggest to do further mono-cultural incubation studies to determine more species-dependent production and consumption rates, as well as more in-situ incubations in different depths within the water column in combination with diapycnal flux measurements. Furthermore, more studies in the tropical ocean in different seasons are needed to evaluate the significance of the halocarbon emissions from the tropical ocean in a global perspective.

Acknowledgements

We thank the chief scientist of the cruise MSM18/3 Arne Körtzinger, as well as the captain, the crew and the scientific crew for all their help. The authors acknowledge Sonja Wiegmann for pigment analysis and Bettina Taylor for CHEMTAX calculations. We thank Björn Fiedler for providing the fluorescence sensor data and Elliot Atlas for analyzing the ten air samples to determine atmospheric background halocarbons. Additionally, the authors acknowledge NASA for providing satellite MODIS-Aqua data. This work was part of the German research project SOPRAN II (grant no. FKZ 03F0611A) funded by the Bundesministerium für Bildung und Forschung (BMBF), and was also supported by the EU project SHIVA (grant no. FP7-ENV-2007-1-226224) and by the HGF Innovative Network Fund (PHYTOOTPICS project).

References

Abrahamsson, K., Bertilsson, S., Chierici, M., Fransson, A., Froneman, P. W., Loren, A., and Pakhomov, E. A.: Variations of biochemical parameters along a transect in the southern ocean, with special emphasis on volatile halogenated organic compounds, Deep-Sea Res. Part II-Top. Stud. Oceanogr., 51, 2745-2756, 10.1016/j.dsr2.2004.09.004, 2004a.

Abrahamsson, K., Lorén, A., Wulff, A., and Wangberg, S. A.: Air-sea exchange of halocarbons: The influence of diurnal and regional variations and distribution of pigments, Deep-Sea Res. Part II-Top. Stud. Oceanogr., 51, 2789-2805, 10.1016/j.dsr2.2004.09.005, 2004b.

Aiken, J., Pradhan, Y., Barlow, R., Lavender, S., Poulton, A., Holligan, P., and Hardman-Mountford, N.: Phytoplankton pigments and functional types in the atlantic ocean: A decadal assessment, 1995-2005, Deep-Sea Res. Part II-Top. Stud. Oceanogr., 56, 899-917, 10.1016/j.dsr2.2008.09.017, 2009.

Amachi, S., Kamagata, Y., Kanagawa, T., and Muramatsu, Y.: Bacteria mediate methylation of iodine in marine and terrestrial environments, Applied and Environmental Microbiology, 67, 2718-2722, 10.1128/aem.67.6.2718-2722.2001, 2001.

Amachi, S., Muramatsu, Y., Akiyama, Y., Miyazaki, K., Yoshiki, S., Hanada, S., Kamagata, Y., Ban-nai, T., Shinoyama, H., and Fujii, T.: Isolation of iodide-oxidizing bacteria from iodide-rich natural gas brines and seawaters, Microb. Ecol., 49, 547-557, 10.1007/s00248-004-0056-0, 2005.

Amachi, S.: Microbial contribution to global iodine cycling: Volatilization, accumulation, reduction, oxidation, and sorption of iodine, Microbes Environ., 23, 269-276, 10.1264/jsme2.ME08548, 2008.

Aschmann, J., Sinnhuber, B. M., Chipperfield, M. P., and Hossaini, R.: Impact of deep convection and dehydration on bromine loading in the upper troposphere and lower stratosphere, Atmos. Chem. Phys., 11, 2671-2687, 10.5194/acp-11-2671-2011, 2011.

Barlow, R. G., Cummings, D. G., and Gibb, S. W.: Improved resolution of mono- and divinyl chlorophylls a and b and zeaxanthin and lutein in phytoplankton extracts using reverse phase c-8 hplc, Marine Ecology Progress Series, 161, 303-307, 10.3354/meps161303, 1997.

Bell, N., Hsu, L., Jacob, D. J., Schultz, M. G., Blake, D. R., Butler, J. H., King, D. B., Lobert, J. M., and Maier-Reimer, E.: Methyl iodide: Atmospheric budget and use as a tracer of marine convection in global models, J. Geophys. Res.-Atmos., 107, 434010.1029/2001jd001151, 2002.

Brownell, D. K., Moore, R. M., and Cullen, J. J.: Production of methyl halides by prochlorococcus and synechococcus, Glob. Biogeochem. Cycle, 24, 10.1029/2009gb003671, 2010.

Carpenter, L. J., Malin, G., Liss, P. S., and Kupper, F. C.: Novel biogenic iodine-containing trihalomethanes and other short-lived halocarbons in the coastal east atlantic, Glob. Biogeochem. Cycle, 14, 1191-1204, 2000.

Carpenter, L. J., Wevill, D. J., Palmer, C. J., and Michels, J.: Depth profiles of volatile iodine and bromine-containing halocarbons in coastal antarctic waters, Mar. Chem., 103, 227-236, 10.1016/j.marchem.2006.08.003, 2007.

Carpenter, L. J., Jones, C. E., Dunk, R. M., Hornsby, K. E., and Woeltjen, J.: Air-sea fluxes of biogenic bromine from the tropical and north atlantic ocean, Atmos. Chem. Phys., 9, 1805-1816, 2009.

Claustre, H., and Marty, J. C.: Specific phytoplankton biomasses and their relation to primary production in the tropical north-atlantic, Deep-Sea Res. Part I-Oceanogr. Res. Pap., 42, 1475-1493, 10.1016/0967-0637(95)00053-9, 1995.

Elliott, S., and Rowland, F. S.: Nucleophilic substitution rates and solubilities for methyl halides in seawater, Geophys. Res. Lett., 20, 1043-1046, 10.1029/93gl01081, 1993.

Elliott, S., and Rowland, F. S.: Methyl halide hydrolysis rates in natural-waters, J. Atmos. Chem., 20, 229-236, 10.1007/bf00694495, 1995.

Fuse, H., Inoue, H., Murakami, K., Takimura, O., and Yamaoka, Y.: Production of free and organic iodine by roseovarius spp, FEMS Microbiology Letters, 229, 189-194, 10.1016/s0378-1097(03)00839-5, 2003.

Geen, C. E.: Selected marine sources and sinks of bromoform and other low molecular weight organobromines, PhD, Dalhousie University, Halifax, Halifax, Nova Scotia, 1992.

Goodwin, K. D., Schaefer, J. K., and Oremland, R. S.: Bacterial oxidation of dibromomethane and methyl bromide in natural waters and enrichment cultures, Applied and Environmental Microbiology, 64, 4629-4636, 1998.

Grodsky, S. A., Carton, J. A., and McClain, C. R.: Variability of upwelling and chlorophyll in the equatorial atlantic, Geophys. Res. Lett., 35, L03610

10.1029/2007gl032466, 2008.

Happell, J. D., and Wallace, D. W. R.: Methyl iodide in the greenland/norwegian seas and the tropical atlantic ocean: Evidence for photochemical production, Geophys. Res. Lett., 23, 2105-2108, 10.1029/96gl01764, 1996.

Hense, I., and Quack, B.: Modelling the vertical distribution of bromoform in the upper water column of the tropical atlantic ocean, Biogeosciences, 6, 535-544, 2009.

Hepach, H., Quack, B., Ziska, F., Fuhlbrügge, S., Atlas, E. L., Krüger, K., Peeken, I., and Wallace, D. W. R.: Drivers of diel and regional variations of halocarbon emissions from the tropical north east atlantic, Atmos. Chem. Phys., 14, 1255-1275, 10.5194/acp-14-1255-2014, 2014.

Hoffmann, L. J., Peeken, I., Lochte, K., Assmy, P., and Veldhuis, M.: Different reactions of southern ocean phytoplankton size classes to iron fertilization, Limnol. Oceanogr., 51, 1217-1229, 2006.

Hopkins, F. E., Kimmance, S. A., Stephens, J. A., Bellerby, R. G. J., Brussaard, C. P. D., Czerny, J., Schulz, K. G., and Archer, S. D.: Response of halocarbons to ocean acidification in the arctic, Biogeosciences, 10, 2331-2345, 10.5194/bg-10-2331-2013, 2013.

Hossaini, R., Chipperfield, M. P., Monge-Sanz, B. M., Richards, N. A. D., Atlas, E., and Blake, D. R.: Bromoform and dibromomethane in the tropics: A 3-d model study of chemistry and transport, Atmos. Chem. Phys., 10, 719-735, 2010.

Hossaini, R., Chipperfield, M. P., Feng, W., Breider, T. J., Atlas, E., Montzka, S. A., Miller, B. R., Moore, F., and Elkins, J.: The contribution of natural and anthropogenic very short-lived species to stratospheric bromine, Atmos. Chem. Phys., 12, 371-380, 10.5194/acp-12-371-2012, 2012.

Hughes, C., Chuck, A. L., Rossetti, H., Mann, P. J., Turner, S. M., Clarke, A., Chance, R., and Liss, P. S.: Seasonal cycle of seawater bromoform and dibromomethane concentrations in a coastal bay on the western antarctic peninsula, Glob. Biogeochem. Cycle, 23, Gb2024

10.1029/2008gb003268, 2009.

Hughes, C., Franklin, D. J., and Malin, G.: Iodomethane production by two important marine cyanobacteria: Prochlorococcus marinus (ccmp 2389) and synechococcus sp (ccmp 2370), Mar. Chem., 125, 19-25, 10.1016/j.marchem.2011.01.007, 2011.

Hughes, C., Johnson, M., Utting, R., Turner, S., Malin, G., Clarke, A., and Liss, P. S.: Microbial control of bromocarbon concentrations in coastal waters of the western antarctic peninsula, Mar. Chem., 151, 35-46, http://dx.doi.org/10.1016/j.marchem.2013.01.007, 2013.

Hummels, R., Dengler, M., and Bourles, B.: Seasonal and regional variability of upper ocean diapycnal heat flux in the atlantic cold tongue, Prog. Oceanogr., 111, 52-74, 10.1016/j.pocean.2012.11.001, 2013.

Itoh, N., Tsujita, M., Ando, T., Hisatomi, G., and Higashi, T.: Formation and emission of monohalomethanes from marine algae, Phytochemistry, 45, 67-73, http://dx.doi.org/10.1016/S0031-9422(96)00786-8, 1997.

Jin, Z. H., Charlock, T. P., Rutledge, K., Stamnes, K., and Wang, Y. J.: Analytical solution of radiative transfer in the coupled atmosphere-ocean system with a rough surface, Appl. Optics, 45, 7443-7455, 10.1364/ao.45.007443, 2006.

Johnson, Z. I., Zinser, E. R., Coe, A., McNulty, N. P., Woodward, E. M. S., and Chisholm, S. W.: Niche partitioning among prochlorococcus ecotypes along ocean-scale environmental gradients, Science, 311, 1737-1740, 10.1126/science.1118052, 2006.

Jones, C. E., and Carpenter, L. J.: Solar photolysis of ch_2i_2, ch_2ici, and ch_2ibr in water, saltwater, and seawater, Environ. Sci. Technol., 39, 6130-6137, 10.1021/es050563g, 2005.

Jones, C. E., and Carpenter, L. J.: Chemical destruction of ch3i, c2h5i, 1-c3h7i, and 2-c3h7i in saltwater, Geophys. Res. Lett., 34, 10.1029/2007gl029775, 2007.

Jones, C. E., Hornsby, K. E., Sommariva, R., Dunk, R. M., Von Glasow, R., McFiggans, G., and Carpenter, L. J.: Quantifying the contribution of marine organic gases to atmospheric iodine, Geophys. Res. Lett., 37, L1880410.1029/2010gl043990, 2010.

Jouanno, J., Marin, F., du Penhoat, Y., Sheinbaum, J., and Molines, J. M.: Seasonal heat balance in the upper 100 m of the equatorial atlantic ocean, J. Geophys. Res.-Oceans, 116, 10.1029/2010jc006912, 2011.

Kara, A. B., Rochford, P. A., and Hurlburt, H. E.: An optimal definition for ocean mixed layer depth, Journal of Geophysical Research: Oceans, 105, 16803-16821, 10.1029/2000jc900072, 2000.

Karlsson, A., Auer, N., Schulz-Bull, D., and Abrahamsson, K.: Cyanobacterial blooms in the baltic - a source of halocarbons, Mar. Chem., 110, 129-139, 10.1016/j.marchem.2008.04.010, 2008.

Kirkham, A. R., Jardillier, L. E., Tiganescu, A., Pearman, J., Zubkov, M. V., and Scanlan, D. J.: Basin-scale distribution patterns of photosynthetic picoeukaryotes along an atlantic meridional transect, Environ. Microbiol., 13, 975-990, 10.1111/j.1462-2920.2010.02403.x, 2011.

Klick, S., and Abrahamsson, K.: Biogenic volatile iodated hydrocarbons in the ocean, J. Geophys. Res.-Oceans, 97, 12683-12687, 10.1029/92jc00948, 1992.

Kurihara, M. K., Kimura, M., Iwamoto, Y., Narita, Y., Ooki, A., Eum, Y. J., Tsuda, A., Suzuki, K., Tani, Y., Yokouchi, Y., Uematsu, M., and Hashimoto, S.: Distributions of short-lived iodocarbons and biogenic trace gases in the open ocean and atmosphere in the western north pacific, Mar. Chem., 118, 156-170, 10.1016/j.marchem.2009.12.001, 2010.

Laturnus, F.: Marine macroalgae in polar regions as natural sources for volatile organohalogens, Environ. Sci. Pollut. Res., 8, 103-108, 10.1007/bf02987302, 2001.

Liu, Y. N., Yvon-Lewis, S. A., Hu, L., Salisbury, J. E., and O'Hern, J. E.: Chbr(3), ch(2)br(2), and chclbr(2) in u.S. Coastal waters during the gulf of mexico and east coast carbon cruise, J. Geophys. Res.-Oceans, 116, C10004

10.1029/2010jc006729, 2011.

Liu, Y. N., Yvon-Lewis, S. A., Thornton, D. C. O., Campbell, L., and Bianchi, T. S.: Spatial distribution of brominated very short-lived substances in the eastern pacific, J. Geophys. Res.-Oceans, 118, 2318-2328, 10.1002/jgrc.20183, 2013.

Mabey, W., and Mill, T.: Critical-review of hydrolysis of organiccompounds in water under environmental-conditions, J. Phys. Chem. Ref. Data, 7, 383-415, 1978.

Mackey, M. D., Mackey, D. J., Higgins, H. W., and Wright, S. W.: Chemtax - a program for estimating class abundances from chemical markers: Application to hplc measurements of phytoplankton, Mar. Ecol.-Prog. Ser., 144, 265-283, 10.3354/meps144265, 1996.

Manley, S. L., and Dastoor, M. N.: Methyl-iodide (ch_3i) production by kelp and associated microbes, Mar. Biol., 98, 477-482, 1988.

Manley, S. L., and de la Cuesta, J. L.: Methyl iodide production from marine phytoplankton cultures, Limnol. Oceanogr., 42, 142-147, 1997.

Martino, M., Liss, P. S., and Plane, J. M. C.: The photolysis of dihalomethanes in surface seawater, Environ. Sci. Technol., 39, 7097-7101, 10.1021/es048718s, 2005.

Martino, M., Liss, P. S., and Plane, J. M. C.: Wavelength-dependence of the photolysis of diiodomethane in seawater, Geophys. Res. Lett., 33, L06606

10.1029/2005gl025424, 2006.

Martino, M., Mills, G. P., Woeltjen, J., and Liss, P. S.: A new source of volatile organoiodine compounds in surface seawater, Geophys. Res. Lett., 36, L01609

10.1029/2008gl036334, 2009.

Molinari, R. L.: Observations of eastwars currents in the tropical south-atlantic ocean - 1978 - 1980, Journal of Geophysical Research-Oceans and Atmospheres, 87, 9707-9714, 10.1029/JC087iC12p09707, 1982.

Moore, R. M., and Tokarczyk, R.: Volatile biogenic halocarbons in the northwest atlantic, Glob. Biogeochem. Cycle, 7, 195-210, 1993.

Moore, R. M., and Zafiriou, O. C.: Photochemical production of methyl-iodide in seawater, J. Geophys. Res.-Atmos., 99, 16415-16420, 10.1029/94jd00786, 1994.

Moore, R. M., Geen, C. E., and Tait, V. K.: Determination of henry law constants for a suite of naturally-occurring halogenated methanes in seawater, Chemosphere, 30, 1183-1191, 10.1016/0045-6535(95)00009-w, 1995a.

Moore, R. M., Tokarczyk, R., Tait, V. K., Poulin, M., and Geen, C. E.: Marine phytoplankton as a natural source of volatile organohalogens, in: Naturally-produced organohalogens, edited by: Grimvall, A., and deLeer, E. W. B., Kluwer Academic Publishers, Dordrecht, 283-294, 1995b.

Moore, R. M., Webb, M., Tokarczyk, R., and Wever, R.: Bromoperoxidase and iodoperoxidase enzymes and production of halogenated methanes in marine diatom cultures, J. Geophys. Res.-Oceans, 101, 20899-20908, 10.1029/96jc01248, 1996.

Moore, R. M., and Groszko, W.: Methyl iodide distribution in the ocean and fluxes to the atmosphere, J. Geophys. Res.-Oceans, 104, 11163-11171, 10.1029/1998jc900073, 1999.

Nightingale, P. D., Malin, G., and Liss, P. S.: Production of chloroform and other low-molecular-weight halocarbons by some species of macroalgae Limnol. Oceanogr., 40, 680-689, 1995.

Nightingale, P. D., Malin, G., Law, C. S., Watson, A. J., Liss, P. S., Liddicoat, M. I., Boutin, J., and Upstill-Goddard, R. C.: In situ evaluation of air-sea gas exchange parameterizations using novel conservative and volatile tracers, Glob. Biogeochem. Cycle, 14, 373-387, 10.1029/1999gb900091, 2000.

Orlikowska, A., and Schulz-Bull, D. E.: Seasonal variations of volatile organic compounds in the coastal baltic sea, Environ. Chem., 6, 495-507, 10.1071/en09107, 2009.

Osborn, T. R.: Estimates of the local-rate of vertical diffusion from dissipation measurements, J. Phys. Oceanogr., 10, 83-89, 10.1175/1520-0485(1980)010<0083:eotlro>2.0.co;2, 1980.

Penkett, S. A., Jones, B. M. R., Rycroft, M. J., and Simmons, D. A.: An interhemispheric comparison of the concentrations of bromine compounds in the atmosphere, Nature, 318, 550-553, 10.1038/318550a0, 1985.

Philander, S. G. H., and Pacanowski, R. C.: A model of the seasonal cycle in the tropical atlantic ocean, Journal of Geophysical Research: Oceans, 91, 14192-14206, 10.1029/JC091iC12p14192, 1986.

Quack, B., and Wallace, D. W. R.: Air-sea flux of bromoform: Controls, rates, and implications, Glob. Biogeochem. Cycle, 17, 102310.1029/2002gb001890, 2003.

Quack, B., Atlas, E., Petrick, G., Stroud, V., Schauffler, S., and Wallace, D. W. R.: Oceanic bromoform sources for the tropical atmosphere, Geophys. Res. Lett., 31, L23s0510.1029/2004gl020597, 2004.

Quack, B., Atlas, E., Petrick, G., and Wallace, D. W. R.: Bromoform and dibromomethane above the mauritanian upwelling: Atmospheric distributions and oceanic emissions, J. Geophys. Res.-Atmos., 112, D0931210.1029/2006jd007614, 2007a.

Quack, B., Peeken, I., Petrick, G., and Nachtigall, K.: Oceanic distribution and sources of bromoform and dibromomethane in the mauritanian upwelling, J. Geophys. Res.-Oceans, 112, C1000610.1029/2006jc003803, 2007b.

Raimund, S., Quack, B., Bozec, Y., Vernet, M., Rossi, V., Garcon, V., Morel, Y., and Morin, P.: Sources of short-lived bromocarbons in the iberian upwelling system, Biogeosciences, 8, 1551-1564, 10.5194/bg-8-1551-2011, 2011.

Richter, U.: Factors influencing methyl iodide production in the ocean and its flux to the atmosphere, PhD, Mathematisch-Naturwissenschaftliche Fakultät der Christian-Albrechts-Universität zu Kiel, Christian-Albrechts-Universität zu Kiel, Kiel, 117 pp., 2004.

Richter, U., and Wallace, D. W. R.: Production of methyl iodide in the tropical atlantic ocean, Geophys. Res. Lett., 31, L23s0310.1029/2004gl020779, 2004.

Round, F. E.: The chrysophyta - a reassessment, in: Chrysophytes: Aspects and problems, edited by: Kristiansen, J., and Andersen, R. A., Cambridge University Press, Cambridge, 1986.

Saiz-Lopez, A., Plane, J. M. C., Baker, A. R., Carpenter, L. J., von Glasow, R., Martin, J. C. G., McFiggans, G., and Saunders, R. W.: Atmospheric chemistry of iodine, Chem. Rev., 112, 1773-1804, 10.1021/cr200029u, 2012.

Scarratt, M. G., and Moore, R. M.: Production of methyl bromide and methyl chloride in laboratory cultures of marine phytoplankton ii, Mar. Chem., 59, 311-320, 10.1016/s0304-4203(97)00092-3, 1998.

Schafstall, J., Dengler, M., Brandt, P., and Bange, H.: Tidal-induced mixing and diapycnal nutrient fluxes in the mauritanian upwelling region, Journal of Geophysical Research: Oceans, 115, C10014, 10.1029/2009jc005940, 2010.

Schall, C., Heumann, K. G., and Kirst, G. O.: Biogenic volatile organoiodine and organobromine hydrocarbons in the atlantic ocean from 42 degrees n to 72 degrees s, Fresenius J. Anal. Chem., 359, 298-305, 1997.

Schauffler, S. M., Atlas, E. L., Flocke, F., Lueb, R. A., Stroud, V., and Travnicek, W.: Measurements of bromine containing organic compounds at the tropical tropopause, Geophys. Res. Lett., 25, 317-320, 1998.

Smythe-Wright, D., Boswell, S. M., Breithaupt, P., Davidson, R. D., Dimmer, C. H., and Diaz, L. B. E.: Methyl iodide production in the ocean: Implications for climate change, Glob. Biogeochem. Cycle, 20, Gb300310.1029/2005gb002642, 2006.

Smythe-Wright, D., Peckett, C., Boswell, S., and Harrison, R.: Controls on the production of organohalogens by phytoplankton: Effect of nitrate concentration and grazing, J. Geophys. Res.-Biogeosci., 115, 10.1029/2009jg001036, 2010.

Solomon, S., Garcia, R. R., and Ravishankara, A. R.: On the role of iodine in ozone depletion, J. Geophys. Res.-Atmos., 99, 20491-20499, 10.1029/94jd02028, 1994.

Stemmler, I., Hense, I., Quack, B., and Maier-Reimer, E.: Methyl iodide production in the open ocean, Biogeosciences Discuss., 10, 17549-17595, 10.5194/bgd-10-17549-2013, 2013a.

Stemmler, I., Rothe, M., Hense, I., and Hepach, H.: Numerical modelling of methyl iodide in the eastern tropical atlantic, Biogeosciences, 10, 4211-4225, 10.5194/bg-10-4211-2013, 2013b.

Stramma, L., and Schott, F.: The mean flow field of the tropical atlantic ocean, Deep-Sea Res. Part II-Top. Stud. Oceanogr., 46, 279-303, 10.1016/s0967-0645(98)00109-x, 1999.

Strass, V. H.: Meridional and seasonal-variations in the satellite-sensed fraction of euphotic zone chlorophyll, J. Geophys. Res.-Oceans, 95, 18289-18301, 10.1029/JC095iC10p18289, 1990.

Taylor, B. B., Torrecilla, E., Bernhardt, A., Taylor, M. H., Peeken, I., Rottgers, R., Piera, J., and Bracher, A.: Bio-optical provinces in the eastern atlantic ocean and their biogeographical relevance, Biogeosciences, 8, 3609-3629, 10.5194/bg-8-3609-2011, 2011.

Tegtmeier, S., Kruger, K., Quack, B., Atlas, E. L., Pisso, I., Stohl, A., and Yang, X.: Emission and transport of bromocarbons: From the west pacific ocean into the stratosphere, Atmos. Chem. Phys., 12, 10633-10648, 10.5194/acp-12-10633-2012, 2012.

Tegtmeier, S., Krüger, K., Quack, B., Atlas, E., Blake, D. R., Boenisch, H., Engel, A., Hepach, H., Hossaini, R., Navarro, M. A., Raimund, S., Sala, S., Shi, Q., and Ziska, F.: The contribution of oceanic methyl iodide to stratospheric iodine, Atmos. Chem. Phys., 13, 11869-11886, 10.5194/acp-13-11869-2013, 2013.

Tomczak, M., and Godfrey, J. S.: Regional oceanography: An introduction, in, 2 ed., Daya Publishing House, Delhi, 2005.

Tsuchiya, M., Talley, L. D., and McCartney, M. S.: An eastern atlantic section from iceland southward across the equator, Deep-Sea Res, 39, 1885-1917, 10.1016/0198-0149(92)90004-d, 1992.

Veldhuis, M. J. W., and Kraay, G. W.: Phytoplankton in the subtropical atlantic ocean: Towards a better assessment of biomass and composition, Deep-Sea Res. Part I-Oceanogr. Res. Pap., 51, 507-530, 10.1016/j.dsr.2003.12.002, 2004.

Wang, L., Moore, R. M., and Cullen, J. J.: Methyl iodide in the nw atlantic: Spatial and seasonal variation, J. Geophys. Res.-Oceans, 114, C07007

10.1029/2007jc004626, 2009.

Weingartner, T. J., and Weisberg, R. H.: On the annual cycle of equatorial upwelling in the central atlantic-ocean, J. Phys. Oceanogr., 21, 68-82, 10.1175/1520-0485(1991)021<0068:otacoe>2.0.co;2, 1991.

Yamamoto, H., Yokouchi, Y., Otsuki, A., and Itoh, H.: Depth profiles of volatile halogenated hydrocarbons in seawater in the bay of bengal, Chemosphere, 45, 371-377, 10.1016/s0045-6535(00)00541-5, 2001.

Zika, R. G., Gidel, L. T., and Davis, D. D.: A comparison of photolysis and substitution decomposition rates of methyl-iodide in the ocean, Geophys. Res. Lett., 11, 353-356, 10.1029/GL011i004p00353, 1984.

Ziska, F., Quack, B., Abrahamsson, K., Archer, S. D., Atlas, E., Bell, T., Butler, J. H., Carpenter, L. J., Jones, C. E., Harris, N. R. P., Hepach, H., Heumann, K. G., Hughes, C., Kuss, J., Krüger, K., Liss, P., Moore, R. M., Orlikowska, A., Raimund, S., Reeves, C. E., Reifenhäuser, W., Robinson, A. D., Schall, C., Tanhua, T., Tegtmeier, S., Turner, S., Wang, L., Wallace, D., Williams, J., Yamamoto, H., Yvon-Lewis, S., and Yokouchi, Y.: Global sea-to-air flux climatology for bromoform, dibromomethane and methyl iodide, Atmos. Chem. Phys., 13, 8915-8934, 10.5194/acp-13-8915-2013, 2013.

2. Manuscript 2

Drivers of diel and regional variations of halocarbon emissions from the tropical North East Atlantic

H. Hepach[1], B. Quack[1], F. Ziska[1], S. Fuhlbrügge[1], E. L. Atlas[2], K. Krüger[1,*], I. Peeken[3,4], and D. W. R. Wallace[1,]**

[1] GEOMAR Helmholtz-Zentrum für Ozeanforschung Kiel, Germany

[2] Rosenstiel School of Marine and Atmospheric Science (RSMAS), University of Miami, USA

[3] Alfred-Wegener-Institut für Polar und Meeresforschung (AWI), Bremerhaven, Germany

[4] MARUM – Center for Marine Environmental Sciences, University Bremen, Bremen, Germany

[*] now at Department of Geosciences, University of Oslo (UiO), Oslo, Norway

[**] now at Department of Oceanography, Dalhousie University, Halifax, Canada

Published in: Atmospheric Chemistry and Physics, 14, 1255-1275, doi:10.5194/acp-14-1255-2014, 2014.

Atmos. Chem. Phys., 14, 1255–1275, 2014
www.atmos-chem-phys.net/14/1255/2014/
doi:10.5194/acp-14-1255-2014
© Author(s) 2014. CC Attribution 3.0 License.

Atmospheric Chemistry and Physics
Open Access

Drivers of diel and regional variations of halocarbon emissions from the tropical North East Atlantic

H. Hepach[1], B. Quack[1], F. Ziska[1], S. Fuhlbrügge[1], E. L. Atlas[2], K. Krüger[1,*], I. Peeken[3,4], and D. W. R. Wallace[1,]**

[1]GEOMAR Helmholtz-Zentrum für Ozeanforschung Kiel, Germany
[2]Rosenstiel School of Marine and Atmospheric Science (RSMAS), University of Miami, USA
[3]Alfred-Wegener-Institut für Polar und Meeresforschung (AWI), Bremerhaven, Germany
[4]MARUM – Center for Marine Environmental Sciences, University Bremen, Bremen, Germany
[*]now at: Department of Geosciences, University of Oslo (UiO), Oslo, Norway
[**]now at: Department of Oceanography, Dalhousie University, Halifax, Canada

Correspondence to: H. Hepach (hhepach@geomar.de)

Received: 15 July 2013 – Published in Atmos. Chem. Phys. Discuss.: 25 July 2013
Revised: 9 December 2013 – Accepted: 10 December 2013 – Published: 3 February 2014

Abstract. Methyl iodide (CH_3I), bromoform ($CHBr_3$) and dibromomethane (CH_2Br_2), which are produced naturally in the oceans, take part in ozone chemistry both in the troposphere and the stratosphere. The significance of oceanic upwelling regions for emissions of these trace gases in the global context is still uncertain although they have been identified as important source regions. To better quantify the role of upwelling areas in current and future climate, this paper analyzes major factors that influenced halocarbon emissions from the tropical North East Atlantic including the Mauritanian upwelling during the DRIVE expedition. Diel and regional variability of oceanic and atmospheric CH_3I, $CHBr_3$ and CH_2Br_2 was determined along with biological and physical parameters at six 24 h-stations. Low oceanic concentrations of CH_3I from 0.1–5.4 pmol L^{-1} were equally distributed throughout the investigation area. $CHBr_3$ and CH_2Br_2 from 1.0 to 42.4 pmol L^{-1} and to 9.4 pmol L^{-1}, respectively were measured with maximum concentrations close to the Mauritanian coast. Atmospheric CH_3I, $CHBr_3$, and CH_2Br_2 of up to 3.3, 8.9, and 3.1 ppt, respectively were detected above the upwelling, as well as up to 1.8, 12.8, and 2.2 ppt at the Cape Verdean coast. While diel variability in CH_3I emissions could be mainly ascribed to oceanic non-biological production, no main driver was identified for its emissions over the entire study region. In contrast, biological parameters showed the greatest influence on the regional distribution of sea-to-air fluxes of bromocarbons. The diel impact of wind speed on bromocarbon emissions increased with decreasing distance to the coast. The height of the marine atmospheric boundary layer (MABL) influenced halocarbon emissions via its influence on atmospheric mixing ratios. Oceanic and atmospheric halocarbons correlated well in the study region, and in combination with high oceanic CH_3I, $CHBr_3$ and CH_2Br_2 concentrations, local hot spots of atmospheric halocarbons could solely be explained by marine sources. This conclusion is in contrast to previous studies that hypothesized elevated atmospheric halocarbons above the eastern tropical Atlantic to be mainly originated from the West-African continent.

1 Introduction

Volatile halogenated hydrocarbons (halocarbons) occur naturally in the oceans from where they are emitted into the atmosphere. Bromine and iodine atoms released from these compounds by photolysis and oxidation can take part in catalytic ozone destroying cycles in both the troposphere and stratosphere (McGivern et al., 2000; Salawitch et al., 2005; Montzka and Reimann, 2011) with iodine also participating in aerosol formation (O'Dowd et al., 2002). Halocarbons comprise brominated and iodinated methanes such as bromoform ($CHBr_3$) and dibromomethane (CH_2Br_2), methyl iodide (CH_3I) and diiodomethane, as well as longer chained and mixed halogenated compounds such as iodoethane, chloroiodomethane, and dibromochloromethane.

While $CHBr_3$ and CH_2Br_2 represent the largest contributors to atmospheric organic bromine from the ocean to the atmosphere (Hossaini et al., 2012a), methyl iodide (CH_3I), originating mostly from marine sources, is the most abundant organoiodine in the atmosphere (Saiz-Lopez et al., 2012). Although these three halocarbons are among those that receive the most attention due to their large contributions to atmospheric organic halogens, many uncertainties remain regarding their formation pathways, influences on their emissions, and their fate in the ocean and the atmosphere.

Elevated halocarbon concentrations, particularly of $CHBr_3$ and CH_2Br_2, occur in coastal regions where macro algae are thought to be the most dominant sources (Carpenter and Liss, 2000; Laturnus, 2001). Elevated concentrations of halocarbons are often observed in upwelling regions with large phytoplankton activity, where cold, nutrient rich water is brought up to the sea surface (Tokarczyk and Moore, 1994; Quack et al., 2004). Abiotic production such as photochemical processes could be of high significance for the marine formation of iodinated organic trace gases (Martino et al., 2009), e.g. CH_3I. Hence, its distribution in the ocean may depend on physical parameters such as insolation (Moore and Groszko, 1999; Richter and Wallace, 2004; Yokouchi et al., 2008; Stemmler et al., 2013).

The subtropical and tropical regions represent the largest contributors to global emission budgets of CH_3I, $CHBr_3$ and CH_2Br_2 (Ziska et al., 2013). The compounds and their degradation products can be carried into the stratosphere in significant quantities (Solomon et al., 1994; Hossaini et al., 2010; Aschmann et al., 2011; Montzka and Reimann, 2011; Tegtmeier et al., 2013), since deep tropical convection can lift surface air very rapidly into the tropical tropopause layer (Tegtmeier et al., 2012). Studies by Pyle et al. (2007) and Hossaini et al. (2012b) projected considerable changes in future inorganic bromine in the tropical troposphere and to the stratosphere from biogenic halocarbon emissions due to strengthening of convection, increasing their importance in the tropics. Coastal upwelling systems might play a crucial role in a changing climate. The tropical Mauritanian upwelling is an example of a recently intensified coastal eastern boundary upwelling (McGregor et al., 2007). Primary production could increase with enhanced entrainment of nutrient rich deep water into the surface ocean leading to amplified production of halocarbons. Increasing wind speeds, caused by enhanced pressure gradients (Bakun, 1990), would also directly influence the sea-to-air fluxes of all trace gases via a faster transfer coefficient (e.g. Nightingale et al., 2000). Thus the identification of factors impacting halocarbon sea-to-air fluxes is crucial for assessing possible effects of climate change on future emissions from coastal upwelling systems.

This paper reports on oceanic and atmospheric halocarbon distributions and sea-to-air fluxes from the DRIVE (Diurnal and RegIonal Variability of halogen Emissions) campaign of RV *Poseidon* in the eastern tropical North Atlantic and the Mauritanian upwelling in June 2010. We present results from six 24 h-stations in different distances from the Mauritanian coast and from two simultaneous diel stations on the Cape Verde island Sao Vincente. We aim at describing and quantifying significant factors that control the concentrations and emission fluxes of CH_3I, $CHBr_3$, and CH_2Br_2 both on a diel and a regional scale, including biological production, wind speed, and atmospheric transport. Previous studies have hypothesized that elevated atmospheric mixing ratios of $CHBr_3$ and CH_2Br_2 above the Mauritanian upwelling area were mainly of continental origin, since sea-to-air fluxes of these compounds appeared not sufficient to explain the observations (Quack et al., 2007a; Carpenter et al., 2009). In contrast, the investigation by Fuhlbrügge et al. (2013) revealed high atmospheric mixing ratios of CH_3I, $CHBr_3$ and CH_2Br_2 close to the coast also in air masses transported from the open ocean, with a significant anticorrelation between the atmospheric mixing ratios and the height of MABL. We therefore examine how oceanic emissions contribute to the mixing ratios of atmospheric halocarbons taking the height of the marine atmospheric boundary layer (MABL) into account. Meteorological constraints on the atmospheric distributions during the cruise are investigated in the accompanying paper by Fuhlbrügge et al. (2013).

2 Methods

The cruise P399/2 (Poseidon 399 leg 2) named DRIVE (Diurnal and RegIonal Variability of halogen Emissions) of RV*Poseidon* took place from May 31 to June 17 in 2010 in the eastern tropical North Atlantic and the Mauritanian upwelling. The ship followed a course from Las Palmas (Canary Islands, 28.1° N and 15.4° W) back to Las Palmas with a short stop at Mindelo (Sao Vicente, Cape Verde, 16.9° N and 25.0° W). The cruise track included six stations located at 17.6° N and 24.3° W (S1), 18.0° N and 21.0° W (S2), 18.0° N and 18.0° W (S3), 18.5° N and 16.5° W (S4), 19.0° N and 16.6° W (S5), and 20.0° N and 17.3° W (S6) where the ship remained at its position for 24 h (Fig. 1). Samples for dissolved halocarbons in sea water, atmospheric halocarbons and phytoplankton pigments were taken at all 24h-stations in parallel, and additionally four radio sonde launches per 24h-station were accomplished to determine the MABL properties. More details on the campaign and the meteorological conditions can be found in Bange et al. (2011) and Fuhlbrügge et al. (2013).

Related to the ship expedition a land-based operation took place from 3 to 8 June 2010 at the Cape Verde Atmospheric Observatory (CVAO) on Sao Vincente close to Mindelo at 17.6° N and 24.3° W (Fig. 1) where samples of atmospheric halocarbons were taken during two days.

Atmospheric halocarbon mixing ratios and meteorological conditions were also determined during a second cruise leg P399/3 from Las Palmas, Spain to Vigo, Spain and are covered in Fuhlbrügge et al. (2013). In contrast, this manuscript focuses only on results from leg P399/2. The words “whole cruise” will refer to leg 2 and “whole campaign” includes leg 2 and the land-based operation at Cape Verde.

2.1 Sampling and analysis of halocarbons in sea surface water and air

Dissolved halocarbons were sampled in 500 mL amber glass bottles from a continuously working pump from the ships moon pool at a depth of 4.4 m. This allowed for nearly hourly sampling of sea surface water at every diel station. In between 24h-stations, the samples were taken every 3 h. The water was analyzed for halocarbons using a purge and trap system attached to a gas chromatograph with mass spectrometric detection (GC-MS). 80 mL of water were purged at 70 °C for 60 min with a stream of helium at 30 mL min^{-1} in a glass chamber with a purge efficiency of more than 98 % for all three halocarbons. The volatilized trace gases were desiccated with a Nafion® dryer and were trapped on glass beads at −100 °C. After purging, the compounds were desorbed at 100° C onto a deactivated capillary in liquid nitrogen as second trap. After three minutes, the sample was injected into the GC-MS, where the trace gases were separated on a Rtx-VGC capillary column with a length of 60 m, a diameter of 0.25 mm and a film thickness of 1.40 µm, and were detected in single ion mode. Quantification was achieved with volumetrically prepared standards in methanol. Four calibration curves were performed using different dilutions, each injected in triplicate. One standard was injected once a day in triplicate to monitor the internal drift of the instrumental set up which was low during the whole cruise. Precision for these measurements lay within 16 % for CH_3I, and 6 % for $CHBr_3$ and CH_2Br_2, determined only from duplicates due to time constraints.

Air samples were taken hourly at the diel stations. They were pumped into stainless steel canisters on the compass deck at a height of 13.7 m with a metal bellows pump. Samples were analyzed within a month at the Rosenstiel School of Marine and Atmospheric Science in Miami with a precision of approximately 5 % using GC-MS (Schauffler et al., 1999). Previous campaigns show that stability of the measured compounds in the canisters is not an issue over this time period. Additionally, air samples were taken at CVAO on an hourly basis parallel to the first two diel stations of the ship. Samples were taken according to the method onboard the RV *Poseidon* in approximately 3 m height above ground and then analyzed along with the other canisters collected during the cruise. Oceanic and atmospheric measurements were intercalibrated against whole air working-standards obtained from the NOAA Global Monitoring Division (Boulder, USA).

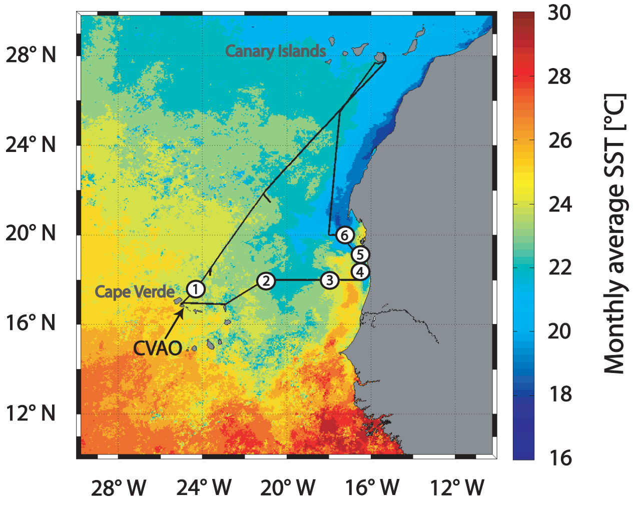

Fig. 1. Cruise track (black line) during DRIVE on SST derived from the monthly composite of June 2010 of MODIS-Aqua level 3 data. White circles with black numbers indicate 24 h-stations. Also marked is the location of the CVAO (Cape Verde Atmospheric Observatory).

2.2 Phytoplankton pigment analysis and flow cytometry

Samples for pigment analysis were taken approximately every 2 h at every diel station. 1 L of sea surface water from the continuously working pump in the ships moon pool was filtered through 25 mm Whatman GF/F filters and stored at −80 °C until analysis. Back in the lab, phytoplankton pigments were analyzed according to Tran et al. (2013) using a Waters high-performance liquid chromatography (HPLC) system at the Alfred Wegener Institute for Polar and Marine Research Bremerhaven (AWI). Apart from chlorophyll *a* (Chl *a*), the 27 marker pigments for which samples were analyzed include various chlorophyll type pigments such as chlorophyll *c1*, *c2* and *c3*, divinyl chlorophyll *b*, chlorophyll *b*, divinyl chlorophyll *a*, and phaeophytin *a*. The following carotenoids were detected: peridin, predinin derivative, 19-butanoyloxyfucoxanthin, fucoxanthin, neoxanthin, 19-hexanoyloxyfucoxanthin, violaxanthin, astaxanthin, prasinoxanthin, diadinoxanthin, alloxanthin, diatoxanthin, anthreaxanthin, zeaxanthin, lutein, α-carotene, and β-carotene. Marker pigments and their relative abundance are indicative for different phytoplankton groups.

For flow cytometry, 4 mL of water from the underway pump system were preserved with glutaraldehyde with a final concentration of 0.1 %, shock frozen in liquid nitrogen and stored at −80 °C. Flow cytometry samples were analyzed for nanoplankton, picoplankton, *Prochlorococcus*, and *Synechococcus* at the AWI according to Taylor et al. (2011). Potential cell loss associated with the sample fixation has not been taken into account.

Table 1. Means and ranges (minimum – maximum) of ambient parameters (SST, salinity, Chl *a*, wind speed, MABL height) during DRIVE for open ocean stations S1–S2 and coastal stations S3–S6.

		S1	S2	S3	S4	S5	S6
Parameter	Unit	17.6° N and 24.3° W	18.0° N and 21.0° W	18.0° N and 18.0° W	18.5° N and 16.5° W	19.0° N and 16.6° W	20.0° N and 17.3° W
SST	°C	24.5 (24.4–24.7)	23.2 (23.0–23.6)	21.7 (21.6–21.8)	23.3 (23.1–23.4)	20.4 (20.2–21.0)	18.6 (18.4–18.7)
Salinity		36.7 (36.7–36.7)	36.4 (36.4–36.5)	35.9 (35.9–35.9)	35.9 (35.9–35.9)	35.8 (35.8–35.8)	35.9 (35.8–35.9)
Chl *a*	$\mu g\,L^{-1}$	0.05 (0 -0.08)	0.30 (0.10–0.43)	1.00 (0.58–1.79)	1.63 (0.81–3.01)	4.50 (1.69–8.12)	4.80 (7.40–6.70)
Wind speed	$m\,s^{-1}$	4.6 (2.0–7.1)	11.0 (7.8–14.8)	6.0 (3.9–9.0)	9.7 (6.7–12.9)	8.9 (4.3–13.7)	11.0 (6.8–14.2)
MABL height	m	950 (850–1100)	540 (400–700)	290 (200–400)	120 (50–200)	25 (surface–100)	190 (100–350)

2.3 Calculation of sea-to-air fluxes and saturation anomaly

Sea-to-air fluxes (F) of CH_3I, $CHBr_3$ and CH_2Br_2 were calculated using the air-sea gas exchange parameterization of Nightingale et al. (2000). Schmidt number (Sc) corrections for the compound specific transfer coefficients k_w derived with the transfer coefficient k_{CO_2} of CO_2 as reported by Quack and Wallace (2003) were applied.

$$\frac{k_w}{k_{CO_2}} = \frac{Sc^{-\frac{1}{2}}}{660} \tag{1}$$

The air-sea concentration gradient was derived from all simultaneous water (c_w) and air (c_{atm}) measurements calculated with the Henry's law constants H of Moore and coworkers (Moore et al., 1995a, b) to obtain the theoretical equilibrium concentration c_{atm}/H.

$$F = k_w \cdot \left(c_w - \frac{c_{atm}}{H}\right) \tag{2}$$

The saturation anomaly S was calculated from the concentration gradient as the percentage of the equilibrium concentration.

$$S = \left(\left(c_w - \frac{c_{atm}}{H}\right) \cdot 100\right) \cdot \left(\frac{c_{atm}}{H}\right)^{-1} \tag{3}$$

Water temperature and salinity were continuously recorded using the ships' thermosalinograph. Air pressure and wind speed were determined by sensors on the compass deck and in 25.5 m height, respectively. Ten minute averages of these four parameters were included in the calculations, and wind speed was corrected to 10 m values.

3 Hydrography and environmental parameters during DRIVE

High SST values between 23.0 and 24.7 °C and high salinities from 36.4 to 36.7 observed at S1 and S2 close to Cape Verde (Figs. 1–2a, Table 1) were consistent with tropical surface water characteristics (Tsuchiya et al., 1992). Low Chl *a* concentrations between 0.00 and 0.43 $\mu g\,L^{-1}$ were a sign of low primary production there. Stations S1 and S2 are hence defined as open ocean. Wind speed had the lowest mean of the whole cruise at S1 with 4.6 $m\,s^{-1}$ and was highest at S2 with a mean of 11.0 $m\,s^{-1}$. The MABL height in this region determined by Fuhlbrügge et al. (2013) ranged between 400 and 1100 m (Table 1). With decreasing distance to the Mauritanian coast, a decrease in SST and salinity and an increase in Chl *a* concentrations were observed. This is a sign of the North West African upwelling system on the African shelf as part of the wind-driven Canary Current extending from 30° N to 10° N (Fedoseev, 1970). South Atlantic Central Water (SACW), characterized as a straight T-S curve between 5 °C and 34.3 and 20 °C and 36.0 (Tomczak and Godfrey, 2005), is transported to the Mauritanian coast by a poleward directed undercurrent. Between 12° N and 20° N upwelling of the cold nutrient rich SACW takes place from late fall to late spring (Minas et al., 1982; Tomczak, 1982; Hagen, 2001) after which the upwelling starts to cease due to changing atmospheric conditions induced by the shift of the Intertropical Convergence Zone (Mittelstaedt, 1982). Although the upwelling already began to cease during our cruise, stations S3–S6 are defined as upwelling and coastal stations (further on called coastal stations) due to the lower SSTs observed there. The lowest SST with 18.4 °C as well as the highest daily mean Chl *a* concentration of 4.80 $\mu g\,L^{-1}$ were found at the northernmost station (S6), while the overall maximum Chl *a* concentration of 8.12 $\mu g\,L^{-1}$ was observed at S5. MABL heights generally ranged between surface and 400 m

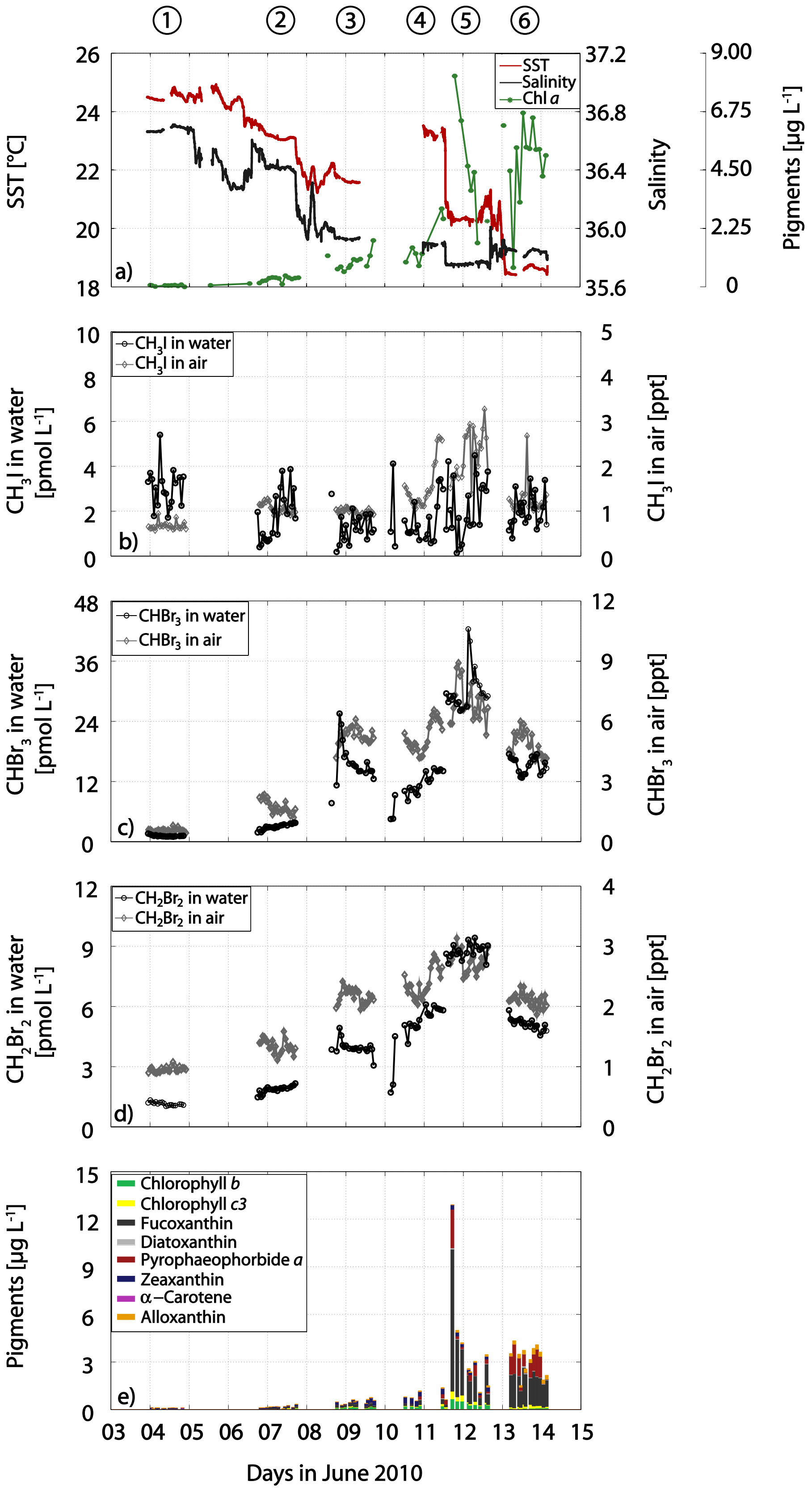

Fig. 2. SST, salinity and Chl *a* **(a)** along with halocarbon concentrations in water and atmospheric mixing ratios of CH_3I **(b)**, $CHBr_3$ **(c)** and CH_2Br_2 **(d)** and pigments significant for the regional distribution of $CHBr_3$ and CH_2Br_2 **(e)** during the DRIVE campaign.

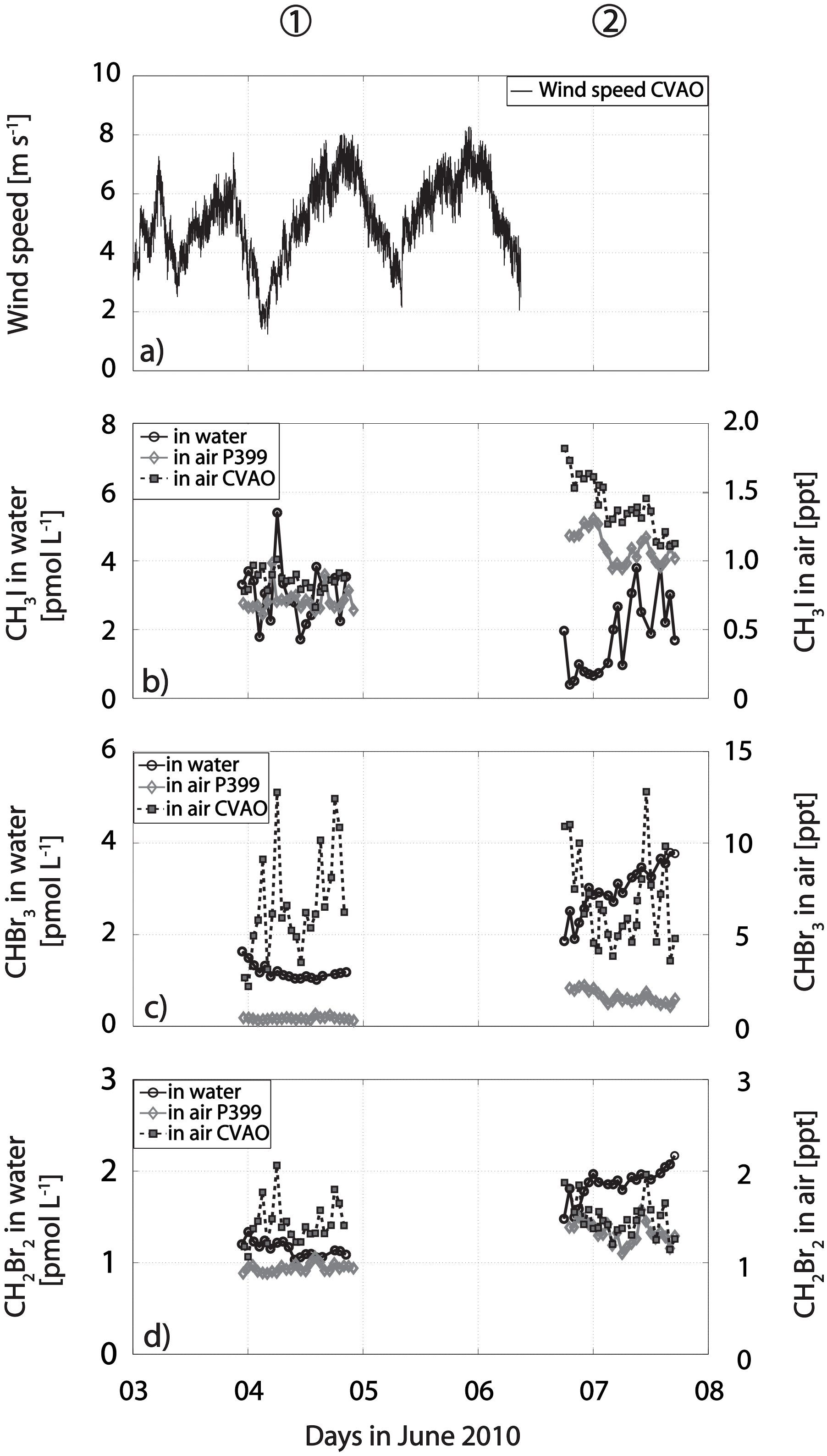

Fig. 3. Open ocean surface water and atmospheric halocarbons during stations S1 and S2 and atmospheric halocarbons measured parallel at CVAO as well as wind speed (wind speed in **a**, CH_3I in **b**, $CHBr_3$ in **c**, and CH_2Br_2 in **d**). Wind speed data for 7 and 8 June in 2010 was not available.

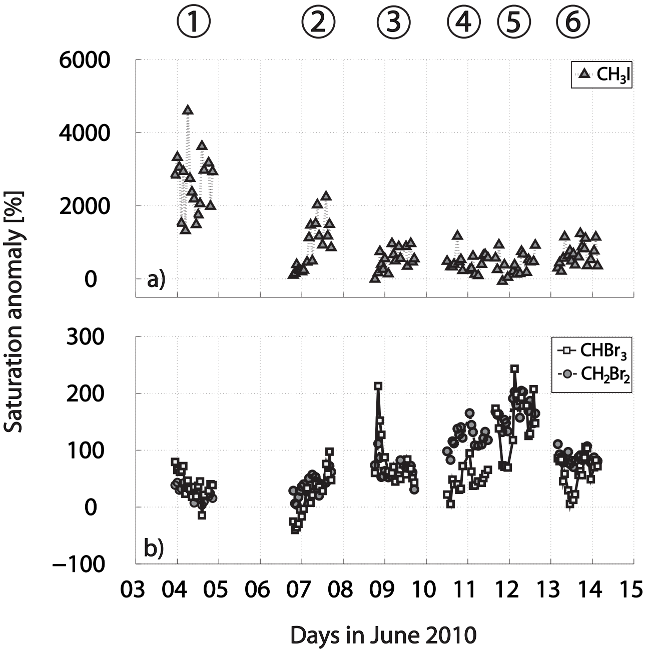

Fig. 4. Saturation anomalies of CH_3I **(a)** and $CHBr_3$ and CH_2Br_2 **(b)** throughout the RV *Poseidon* cruise.

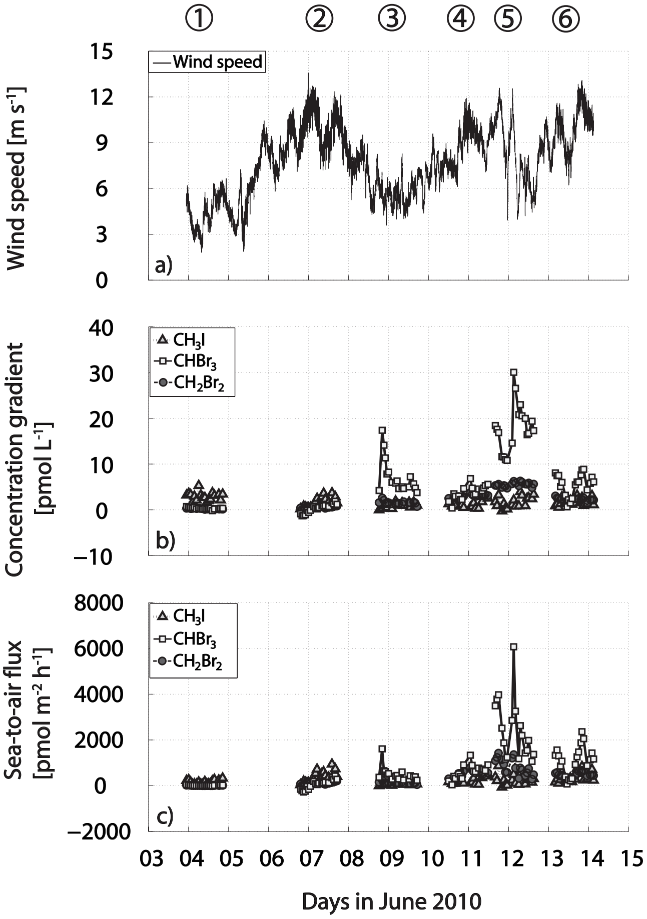

Fig. 5. Wind speed **(a)**, concentration gradients **(b)** and sea-to-air fluxes **(c)** of CH_3I, $CHBr_3$ and CH_2Br_2 during DRIVE.

at S3–S6, while wind speeds varied between 3.9 (S3) and 14.2 m s^{-1} (S6). At S5, the lowest MABL heights (close to the surface) together with the highest relative standard deviation (further on referred to as variability) in wind speed with a mean of 8.9 m s^{-1} and a variability of 27 % was observed at one station in the course of 24 h (Table 1). Due to the classification of the stations into two regions, average values of both open ocean stations together are based on fewer measurements than average values of the four coastal stations.

4 Results

4.1 Methyl iodide (CH_3I)

4.1.1 Regional distribution

At the open ocean stations S1 and S2 higher mean oceanic CH_3I of 2.4 pmol L^{-1} was found than at coastal stations S3–S6 with a mean of 1.8 pmol L^{-1} (Fig. 2b, Table 2). The maximum mean oceanic CH_3I of 3.0 (1.7–5.4) pmol L^{-1} was observed at S1, while S3 showed the lowest mean of 1.2 (0.2–2.1) pmol L^{-1} during 24 h. In total, the regional variability of CH_3I, which is the relative standard deviation between the means of the individual stations, was the lowest of all three halocarbons with 56 %. Correlations to neither phytoplankton pigments nor to picoplankton abundances were found for CH_3I in sea surface water (Table 3).

Atmospheric CH_3I with an overall mean of 1.3 (0.6–3.3) ppt revealed a different distribution in comparison to oceanic CH_3I (Fig. 2a). It was generally lower above the open ocean with 0.9 (0.6–1.3) ppt on average and increased towards the coast with a mean (range) of 1.6 (0.9–3.3) ppt (see also Fuhlbrügge et al., 2013). In total, atmospheric CH_3I had a lower regional variability of 44 % than oceanic CH_3I.

4.1.2 Diel variations

Of all three halocarbons, oceanic CH_3I showed the largest diel variability which was also larger than its regional variability. The lowest and the highest mean variability during 24 h were found at the open ocean stations S1 with 29 % and at S2 with 62 %. At the coastal stations oceanic CH_3I varied between 37 % (S6) and 60 % (S4). While at four stations maxima of CH_3I in the surface water were found in the morning hours, elevations in the afternoon were observed at open ocean station S2 and coastal station S6. Hence, no overall diurnal cycle could be detected.

Low relative diel variability between 9 % (S2) and 11 % (S1) was observed in atmospheric CH_3I above the open ocean. The variability at CVAO at the same time ranged

Table 2. Results of halocarbon measurements (water and air) and calculations (saturation anomalies and sea-to-air fluxes) for all six diel stations and parallel air sampling at CVAO.

			S1	S2	S3	S4	S5	S6
			17.6° N and 24.3° W	18.0° N and 21.0° W	18.0° N and 18.0° W	18.5° N and 16.5° W	19.0° N and 16.6° W	20.0° N and 17.3° W
Compound	Parameter	Unit						
CH_3I	Water	pmol L^{-1}	3.0 (1.7–5.4)	1.8 (0.4–3.9)	1.2 (0.2–2.1)	1.6 (0.6–3.4)	2.2 (0.1–4.5)	2.0 (0.8–3.5)
	Air	ppt	0.7 (0.6–1.0)	1.1 (1.0–1.3)	1.0 (0.9–1.1)	1.6 (1.1–2.7)	2.3 (1.4–3.3)	1.3 (1.1–2.7)
	CVAO air	ppt	0.9 (0.7–1.0)	1.4 (1.1–1.8)	–	–	–	–
	Saturation anomaly	%	2606.3 (1321.1–4597.1)	870.2 (99.4–2243.7)	532.2 (−8.5–967.1)	445.6 (90.8–1167.4)	410.8 (−65.8–928.7)	672.1 (210.1–1242.3)
	Sea-to-air flux	pmol m^{-2} h^{-1}	158.3 (59.3–330.4)	372.6 (39.6–941.6)	79.0 (−1.7–212.2)	227.7 (61.4–500.5)	259.6 (−64.6–871.6)	382.5 (106.1–837.9)
$CHBr_3$	Water	pmol L^{-1}	1.2 (1.0–1.6)	3.0 (1.9–3.8)	16.2 (11.3–25.5)	11.9 (8.1–14.7)	30.6 (26.1–42.4)	15.3 (12.8–17.5)
	Air	ppt	0.6 (0.5–0.8)	1.8 (1.2–2.4)	5.3 (4.2–6.1)	5.3 (4.2–6.6)	7.0 (5.4–8.9)	4.9 (4.1–6.0)
	CVAO air	ppt	6.7 (2.3–12.8)	6.8 (3.7–12.8)	–	–	–	–
	Saturation anomaly	%	39.6 (−14.7–79.3)	17.7 (−40.3–97.3)	80.6 (43.0–212.7)	46.1 (5.2–94.4)	148.0 (69.4–243.1)	59.4 (5.4–105.5)
	Sea-to-air flux	pmol m^{-2} h^{-1}	15.5 (−8.5–45.0)	65.6 (−273.4–426.7)	489.1 (241.4–1610.9)	611.7 (41.7–1333.8)	2423.0 (1063.3–6068.9)	1098.2 (77.8–2360.2)
CH_2Br_2	Water	pmol L^{-1}	1.2 (1.0–1.3)	1.9 (1.5–2.2)	4.0 (3.1–4.9)	5.4 (4.1–6.1)	8.8 (8.1–9.4)	5.1 (4.6–5.8)
	Air	ppt	1.0 (0.9–1.1)	1.4 (1.1–1.6)	2.2 (2.0–2.4)	2.4 (2.0–2.9)	2.8 (2.5–3.1)	2.1 (1.9–2.3)
	CVAO air	ppt	1.4 (1.1–2.1)	1.5 (1.2–2.0)	–	–	–	–
	Saturation anomaly	%	24.7 (3.4–43.2)	37.7 (4.1–72.2)	64.7 (30.9–111.5)	122.0 (82.7–165.0)	169.0 (131.8–204.3)	86.1 (70.1–110.6)
	Sea-to-air flux	pmol m^{-2} h^{-1}	10.6 (1.8–27.9)	118.5 (14.5–214.3)	115.7 (50.0–260.3)	511.8 (207.9–801.0)	815.4 (285.6–1429.4)	470.4 (295.5–671.6)

between 9 % (4 June, parallel to S1) and 14 % (June 6 and 7, parallel to S2) (Fig. 3a, Table 2) with mean mixing ratios of 1.2 ppt (0.7 ppt, 4 June–1.8 ppt, 6 June). At the coastal stations S3–S6, diel variability of 7 (S3) – 33 % (S4) was observed. The highest mean atmospheric variability at S4 coincides with the largest oceanic variability. Similarly to oceanic CH_3I, there is no overall diurnal cycle in atmospheric mixing ratios. Maxima and minima occurred in both day and night hours.

4.1.3 Saturation anomaly, sea-air concentration gradient and sea-to-air fluxes

Saturation anomalies (Fig. 4), concentration gradient (Fig. 5b) as well as sea-to-air fluxes (Fig. 5c) were calculated according to Eqs. (1)–(3) (Table 2). To constrain the atmospheric influence on the concentration gradient, thus on the sea-to-air fluxes, the fraction of the equilibrium concentration c_{atm}/H of the oceanic concentration c_{w} was calculated (Fig. 6a). This is the relative reduction of the sea-to-air flux by the atmospheric mixing ratios compared to an empty atmosphere, which will be referred to as "flux reducing effect" further on.

For CH_3I the highest saturation anomalies with means of 931 (−66–4597) % (Fig. 4a, Table 2) and the lowest concentration gradients of 1.7 (−0.3–5.3) pmol L^{-1} (Fig. 5b) of the three halocarbons were calculated for CH_3I for the whole cruise. Both were consistent with the oceanic distribution: they were highest in the open ocean with maxima at S1 where however no high emissions of this compound were calculated because of the prevailing low wind speeds during that time (Fig. 5c). The open ocean was generally highly supersaturated with mean anomalies of 1715 % on average, decreasing towards the coastal stations to a mean of 522 %. The reducing effect of atmospheric CH_3I on the sea-to-air flux was low, usually less than 50 %. One exception was S5 where low oceanic CH_3I coincided with high atmospheric mixing ratios, and the flux reducing effect reached 300 % leading to a flux into the water. Mainly positive sea-to-air fluxes of CH_3I could be observed with a mean of 254 pmol m^{-2} h^{-1} for the whole cruise (−65 at coastal station S5 to 942 pmol m^{-2} h^{-1} at open ocean station S2) (Fig. 5c, Table 2). Open ocean and mean coastal fluxes of 268 and 246 pmol m^{-2} h^{-1}, respectively were in a similar range though with potentially higher fluxes in the open ocean due to its large supersaturation there.

Table 3. Correlation coefficients R^2 of halocarbons to nano- and picoplankton abundances as well as to phytoplankton pigment data (MLR – Multiple Linear Regression). The correlations to Prochlorococchus are all significant on the p <0.05 level. Negative correlations are printed in italic.

		n	CH_3I	$CHBr_3$	CH_2Br_2
Nano- and picoplankton	Prochlorococcus	72	0.10	*0.39*	*0.26*
	Others	72	< 0.08	< 0.09	< 0.10
Phyotplankton pigments	Chl *a*	61	0.00	0.38	0.49
	MLR	61	None	0.79	0.77

4.1.4 Impact of oceanic CH_3I and wind speed on fluxes

The sea-to-air flux of CH_3I showed significant but low regional correlations with sea surface concentrations ($R^2 = 0.37$) and wind speed ($R^2 = 0.24$) for the whole cruise (Fig. 7a, d, Table 4). Considering each station individually, high significant correlations of oceanic CH_3I and sea-to-air flux were found at open ocean station S2 and at all coastal stations with R^2 ranging between 0.57 and 0.91. Significant correlations of wind speed to the CH_3I sea-to-air flux only existed at coastal station S3 and open ocean station S1 ($R^2 = 0.24$ and 0.76).

4.2 Bromoform ($CHBr_3$) and dibromomethane (CH_2Br_2)

4.2.1 Regional distribution

$CHBr_3$ and CH_2Br_2 were both lower in the open ocean with means of 2.3 (1.0–3.8) pmol L^{-1} for $CHBr_3$ and 1.6 (1.0–2.2) pmol L^{-1} for CH_2Br_2 with minimum concentrations occurring at S1 (Fig. 2c, d, Table 2). Both compounds had higher coastal concentrations of 18.3 (8.1–42.4) pmol L^{-1} for $CHBr_3$ and 5.8 (3.1–9.4) pmol L^{-1} for CH_2Br_2 with maxima at S5 and a much more pronounced increase in oceanic $CHBr_3$ than in CH_2Br_2. $CHBr_3$ and CH_2Br_2 in sea surface water demonstrated much higher relative regional variability of 78 % ($CHBr_3$) and 59 % (CH_2Br_2) than oceanic CH_3I.

Atmospheric $CHBr_3$ and CH_2Br_2 increased towards the coast similarly to their oceanic counterparts (Fig. 2c, d, Table 2). The highest mean regional variability was found for $CHBr_3$ (56 %), while atmospheric CH_2Br_2 showed the lowest (33 %) of the three halocarbons.

4.2.2 Diel variations

Diel variations of both $CHBr_3$ and CH_2Br_2 in sea surface water were generally lower than their regional variations. The variability of $CHBr_3$ ranged between 14 % (S1) and 19 % (S2) in the open ocean, while the variability of CH_2Br_2 was even lower with 7 % (S1) and 9 % (S2). At most of the coastal stations $CHBr_3$ and CH_2Br_2 revealed similar distributions throughout 24 h with maxima in the evening and night hours with the exception of S5 where maxima

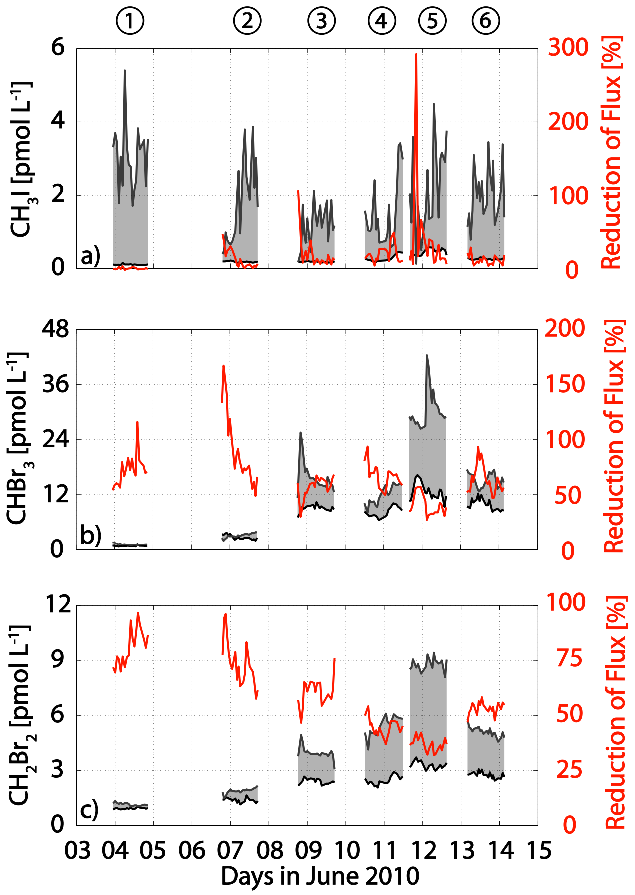

Fig. 6. Influence of atmospheric mixing ratios on the amount of oceanic halocarbons emitted for CH_3I **(a)**, $CHBr_3$ **(b)**, and CH_2Br_2 **(c)**. Oceanic concentrations are plotted in grey (left axis), the equilibrium concentration is delineated in black, and the concentration gradient is shaded in grey. The percentaged reduction of the concentration gradient by the equilibrium concentration (flux reducing effect) derived from the atmospheric measurements (equilibrium concentration in percent in relation to the water concentrations) is shown in red (right axis). Values above 100 % refer to fluxes from the atmosphere into the ocean.

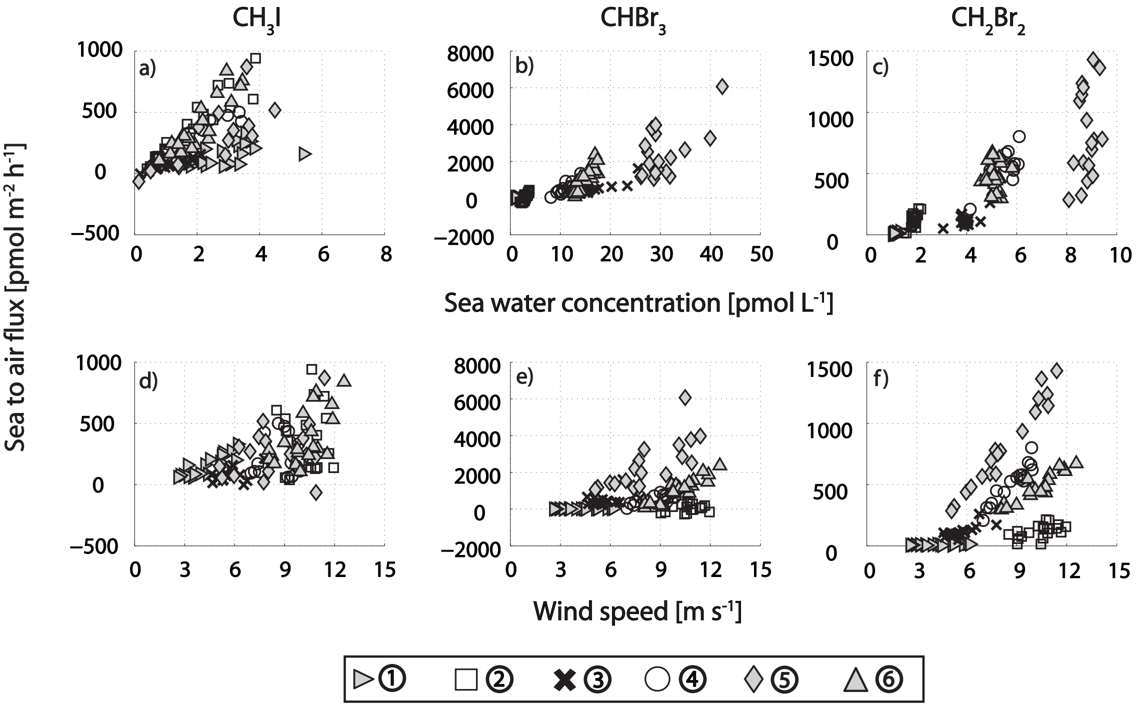

Fig. 7. Sea-to-air fluxes versus sea water concentrations of CH_3I **(a)**, $CHBr_3$ **(b)** and CH_2Br_2 **(c)** and wind speed **(d–f)** during DRIVE.

of 42.4 pmol L^{-1} ($CHBr_3$) and 9.4 pmol L^{-1} (CH_2Br_2) were found in the morning hours. The highest diel variation of 23 % was found at coastal station S3 for oceanic $CHBr_3$, while CH_2Br_2 was generally less variable ranging from 4 (S5) to 10 % (S4).

Atmospheric mixing ratios of bromocarbons were low at the open ocean stations S1–S2 with means between 0.6 and 1.78 ppt and relative standard deviations of 13–19 % for $CHBr_3$ and atmospheric CH_2Br_2 ranging on average between 1.0 and 1.4 ppt with a relative standard deviation of 5–9 %. At CVAO mean mixing ratios of 6.7–6.8 ppt $CHBr_3$ and of 1.4–1.5 ppt CH_2Br_2 were higher than at S1–S2, as was their diel variability ranging from 35–43 % for $CHBr_3$ and 14–16 % for CH_2Br_2 (Fig. 3b, c, Table 2). The highest atmospheric $CHBr_3$ during the whole campaign of 12.8 ppt was measured at CVAO on 7 June. The diel variability of atmospheric $CHBr_3$ at the coastal stations S3–S6 was generally lower than what was observed above the open ocean with 7 (S3)–14 % (S4) and means of 4.8 (S6)–7.0 ppt (S5). The diel variability of atmospheric CH_2Br_2 at the coast was similar to the open ocean with 5 (S6)–10 % (S4) and means of 2.1 (S6)–2.8 ppt (S5). Atmospheric $CHBr_3$ and CH_2Br_2 showed no overall diurnal cycles above neither open ocean nor coastal stations with maxima during both day and night hours.

4.2.3 Correlations of $CHBr_3$ and CH_2Br_2 with phytoplankton pigments

Surface water concentrations of $CHBr_3$ and CH_2Br_2 correlated significantly with Chl *a* at the 95 % level with correlation coefficients R^2 of 0.38 and 0.49 (Table 3, Figure 2a). Multiple linear regressions (MLR) of brominated halocarbons to all phytoplankton marker pigments were carried out for the whole cruise. All pigment data related to $CHBr_3$ or CH_2Br_2 with $p < 0.05$ was regarded as significant. The six pigments chlorophyll *b*, chlorophyll *c3*, fucoxanthin, diatoxanthin, pyrophaeophorbide *a* and zeaxanthin were found to describe the regional distribution of $CHBr_3$ best (Fig. 2e, Table 3). Chlorophyll *b*, fucoxanthin, α-carotene (negatively correlated) and alloxanthin were important for CH_2Br_2 in the order of explanatory power. Additionally, significant but low correlations of $CHBr_3$ and CH_2Br_2 were found to *Prochlorococcus* with $R^2 = 0.39$ and $R^2 = 0.26$ (negatively correlated).

4.2.4 Saturation anomaly, sea-air concentration gradients and sea-to-air fluxes

The ocean was generally supersaturated with $CHBr_3$ and CH_2Br_2 (Fig. 4, Table 2). The overall saturation anomaly of 65 (−40 – 243) % for $CHBr_3$ was slightly lower than the mean of CH_2Br_2 with 84 (3–204) % (Fig. 4b). Both displayed similar trends opposite to CH_3I: lower anomalies of around 30 % in the open ocean stations, increasing towards the coastal stations S3 – S6 with means of

83 % for $CHBr_3$ and 110 % for CH_2Br_2. Maximum saturation anomalies coincided with maximum oceanic and atmospheric bromocarbons at S5 with daily means of 148 % for $CHBr_3$ and 169 % for CH_2Br_2. The concentration gradient $c_{\mathrm{w}} - c_{\mathrm{atm}}/H$ of $CHBr_3$ was the highest of all three halocarbons with a total mean of 5.8 (−1.3–30.0) pmol L^{-1}, followed by CH_2Br_2 with a mean of 2.2 (0–6.3) pmol L^{-1} and minima in the open ocean region (Fig. 5b). The reducing effect of atmospheric $CHBr_3$ and CH_2Br_2 on the sea-to-air flux was > 75 % in the open ocean where both compounds were close to equilibrium and decreases simultaneously with the strongly increasing concentration gradient towards the coast (Fig. 6b, c). For $CHBr_3$ and CH_2Br_2 the flux reducing effect was around 50 % at the four coastal stations (S3–S6). Sea-to-air fluxes of $CHBr_3$ and CH_2Br_2 for the whole cruise were on average higher than CH_3I fluxes with 787 (−273–6069) pmol m^{-2} h^{-1} and 341 (2–1429) pmol m^{-2} h^{-1}, respectively (Fig. 5c, Table 2). Fluxes of both compounds were low in the open ocean region with means of 41 pmol m^{-2} h^{-1} for $CHBr_3$ and of 66 pmol m^{-2} h^{-1} for CH_2Br_2. Higher sea-to-air fluxes of $CHBr_3$ and CH_2Br_2 with means of 1171 and 483 pmol m^{-2} h^{-1} were observed at the coastal stations S3–S6. The maximum fluxes of both compounds were found at coastal station 5.

Table 4. Correlation coefficients for water concentrations of halocarbons and wind speed with sea-to-air fluxes of halocarbons for the whole cruise and for the individual stations. Coefficients printed in bold represent significant correlations with $p < 0.05$.

Station	R^2 of		with F of		n
		CH_3I	$CHBr_3$	CH_2Br_2	
Whole cruise	Water conc.	**0.37**	**0.68**	**0.71**	109
	Wind speed	**0.24**	**0.14**	**0.29**	
S1	Water conc.	**0.24**	**0.66**	**0.35**	18
	Wind speed	**0.73**	**0.28**	0.21	
S2	Water conc.	**0.89**	**0.78**	**0.64**	19
	Wind speed	0.00	0.00	0.15	
S3	Water conc.	**0.67**	**0.66**	**0.42**	17
	Wind speed	**0.24**	0.21	**0.56**	
S4	Water conc.	**0.91**	**0.60**	**0.53**	17
	Wind speed	0.02	**0.67**	**0.93**	
S5	Water conc.	**0.57**	**0.34**	0.09	18
	Wind speed	0.02	**0.55**	**0.95**	
S6	Water conc.	**0.79**	**0.70**	0.00	20
	Wind speed	0.06	**0.82**	**0.78**	

4.2.5 Impact of oceanic $CHBr_3$ and CH_2Br_2 and wind speed on fluxes

Sea surface water concentrations of $CHBr_3$ and CH_2Br_2 correlated regionally to sea-to-air fluxes with $R^2 = 0.68$ ($CHBr_3$) and 0.71 (CH_2Br_2) for the whole cruise (Fig. 7, Table 4). Significant correlations of $CHBr_3$ fluxes with sea surface water concentrations were found at all 24h-stations (R^2 from 0.34 to 0.78). The highest correlations of sea surface CH_2Br_2 to its sea-to-air fluxes were found at open ocean station S2 (0.64) and coastal stations S3 and S4 (0.42, 0.53). No significant correlations could be observed at coastal stations S5 and S6. In contrast, wind speed showed low but regionally significant correlations to the overall sea-to-air fluxes with $R^2 = 0.14$ ($CHBr_3$) and $R^2 = 0.29$ (CH_2Br_2). Considering the stations individually, $CHBr_3$ and CH_2Br_2 revealed high correlations of wind speed with sea-to-air flux at coastal stations S4–S6 with R^2 from 0.56 to 0.95.

5 Discussion

5.1 Sea-to-air fluxes of CH_3I

5.1.1 Oceanic and atmospheric CH_3I as drivers of the regional and diel variability of the concentration gradient

The ocean was highly supersaturated with CH_3I throughout most of the cruise which is underlined by the low impact of atmospheric CH_3I on its concentration gradient (Fig. 6a). Regional and diel variability in the concentration gradient was primarily a result of varying oceanic CH_3I. The oceanic concentrations during DRIVE (0.1 to 5.4 pmol L^{-1}, Table 2) compare well to the measurements by Schall et al. (1997) of 0–3 pmol L^{-1} in the Atlantic, north of 42° N during boreal wintertime. In contrast, Richter and Wallace (2004) measured 3–5 times higher oceanic CH_3I with 7.1–16.4 pmol L^{-1} in boreal fall south of 15° N, and Jones et al. (2010) reported even 6 times higher concentrations (total range from min to max: 1.0–36.5 pmol L^{-1}, data from Jones et al., 2010; Ziska et al., 2013) in the same region and season. Similarly to DRIVE, Jones et al. (2010) found no significant difference between open ocean and coastal regions which was ascribed to photochemical sources supported by the incubation experiments of Richter and Wallace (2004) from the equatorial Atlantic. Richter (2004) found a relationship of oceanic CH_3I with wind speed within this data which was not found during DRIVE: lower wind speeds led to elevated oceanic CH_3I. The much more elevated oceanic CH_3I of Jones et al. (2010) was measured in our study region and season. A possible explanation for their largely elevated CH_3I concentrations compared to our and other open ocean values (Ziska et al., 2013) might be enhanced photochemistry, but more detailed information is not given in the study of Jones et al. (2010). Smythe-Wright et al. (2006) measured CH_3I as high as 45 pmol L^{-1} in the Atlantic region south of 40° N in late summer which was accompanied by high *Prochlorococcus* abundance. In contrast, no outstanding relationship of CH_3I with picoplankton including *Prochlorococcus* or the marker pigment divinyl chlorophyll *a* indicative of these species was found during DRIVE. Additionally, no correlation with diatom pigments as suggested by Lai et al. (2011) for the production of open ocean CH_3I was observed, supporting photochemistry as important production pathway for its formation as suggested by Moore and Zafiriou (1994). The likely non-biological formation of CH_3I also leads to high saturation anomalies in open ocean surface waters. The lower saturation anomalies in the coastal zone might likely be a result of upwelled water diluting the more concentrated surface water (Happell and Wallace, 1996) combined with the elevated atmospheric CH_3I above the upwelling. The large supersaturation of CH_3I in surface water of the open ocean region indicates their potential for largely elevated sea-to-air fluxes in contrast to the coastal area. However, CH_3I production may not be completely independent of biological parameters. Lacking correlations of CH_3I concentrations with pigment and flow cytometry data does not necessarily allow for excluding a biological source completely. The concentrations are a result of production and loss processes, which may partly be temporally and spatially decoupled. Another possible source for CH_3I involves bacteria (Manley and Dastoor, 1998; Amachi et al., 2001; Fuse et al., 2003) which has not been taken into account during DRIVE. Additionally, Bell et al. (2002) suggested that organic precursors from phytoplankton production could be involved in the photochemical formation of CH_3I in the surface ocean.

Atmospheric CH_3I (0.6 to 3.3 ppt) measured during DRIVE falls well within the range of tropical Atlantic values reported by Williams et al. (2007) of 1.4 (0.6–3.0) ppt. Air mass back trajectory analysis and similar ranges of atmospheric CH_3I at open ocean station S1 and parallel at CVAO on Cape Verde indicate open ocean air masses at both locations on 4 June (Fuhlbrügge et al., 2013). Wind speed at Cape Verde was highly variable on June 6 (Fig. 3d) leading to high variations in local sea-to-air fluxes likely causing the observed higher mean variability in atmospheric CH_3I at CVAO parallel to open ocean station S2 (Sect. 4.1.2, Fig. 3a). Atmospheric CH_3I during DRIVE at CVAO (0.7–1.8 ppt) was generally lower than the 1.2–13.8 ppt detected by O'Brien et al. (2009) in a similar season.

Non-biological or indirect biological formation mechanisms in the surface water seem likely since the variability in oceanic CH_3I was not correlated to the measured biological variables. Although a biological source cannot completely be excluded, the abiotic formation thus appears as main driver for variations of its concentration gradient across the air-sea interface with negligible influence from atmospheric CH_3I on oceanic concentrations.

5.1.2 The relative influence of concentration gradient and wind speed on sea-to-air fluxes of CH_3I

Applying the parameterization of Nightingale et al. (2000), sea water concentrations and wind speed were almost equally important as driving factors for the variations in the CH_3I sea-to-air flux for the whole cruise region (Fig. 7) based on their similar regional variability (see the scatter in Fig. 8a and similar error bars at the plot that includes all data points in Figure 8b). Diel variability in fluxes could be mainly ascribed to variations in oceanic CH_3I, since they were much higher than the diel variability in wind speed (Fig. 8a, b). Significant correlations of wind speed with sea-to-air fluxes of CH_3I were only found at two 24h-station. The high correlation to wind speed at S1 was caused by the large variability of the generally low speeds in combination with a relatively constant high concentration gradient. Here we note that although the parameterization of Nightingale et al. (2000) is a commonly applied parameterization for k_w in oceanic trace gas emissions, it might not include all factors influencing sea-to-air fluxes. Stability of the atmosphere and the ocean, sea state, bubble transfer, as well as surfactants might influence the transfer across the air-sea interface as well. Some of these factors are included in the TOGA COARE algorithm representing an alternative method for deriving transfer coefficients, which involves an additional set of meteorological parameters such as air temperature and specific humidity profiles, solar irradiance, downwelling longwave irradiance, and precipitation (Fairall et al., 2003).

Our mean (10^{th}–90^{th} percentile) fluxes of 268 (64–550) in the open ocean and 246 (42–523) $\mathrm{pmol\,m^{-2}\,h^{-1}}$ in the coastal region are 7.5 and 8.7 lower than the fluxes of Jones et al. (2010) of 2021 (417–4046) and 2154 (321–4096) $\mathrm{pmol\,m^{-2}\,h^{-1}}$. Although the spatial resolution of the measurements by Jones et al. (2010) in the same region was higher than during DRIVE, the difference in emission strength can be mainly explained by their large sea water concentrations and very low atmospheric mixing ratios compared to our study. The fluxes reported here were 3.8 times lower than fluxes reported by Richter and Wallace (2004) ($958.3 \pm 750.0\,\mathrm{pmol\,m^{-2}\,h^{-1}}$) using a similar flux parameterization which are a result of higher oceanic CH_3I as well.

5.2 Sea-to-air fluxes of $CHBr_3$ and CH_2Br_2

5.2.1 Oceanic and atmospheric $CHBr_3$ and CH_2Br_2 as drivers of regional and diel variability of the concentration gradient

The oceanic concentrations of both compounds were generally driving factors for their concentration gradients during DRIVE. Only in the open ocean atmospheric $CHBr_3$ and CH_2Br_2 reduced the sea-to-air fluxes significantly (Fig. 6) where the low oceanic concentrations were close to equilibrium with the atmosphere and even led to undersaturation of $CHBr_3$ at S2. The concentration gradient increased towards the Mauritanian upwelling with a much more pronounced increase in oceanic $CHBr_3$ and CH_2Br_2 than in the atmosphere. The oceanic and atmospheric concentrations as well as the concentration gradients of both bromocarbons peaked simultaneously at coastal station S5. Open ocean $CHBr_3$ (1.0–3.8 $\mathrm{pmol\,L^{-1}}$) and CH_2Br_2 (1.0–2.2 $\mathrm{pmol\,L^{-1}}$), increasing towards the coast of Mauritania to 8.1–42.4 $\mathrm{pmol\,L^{-1}}$ and

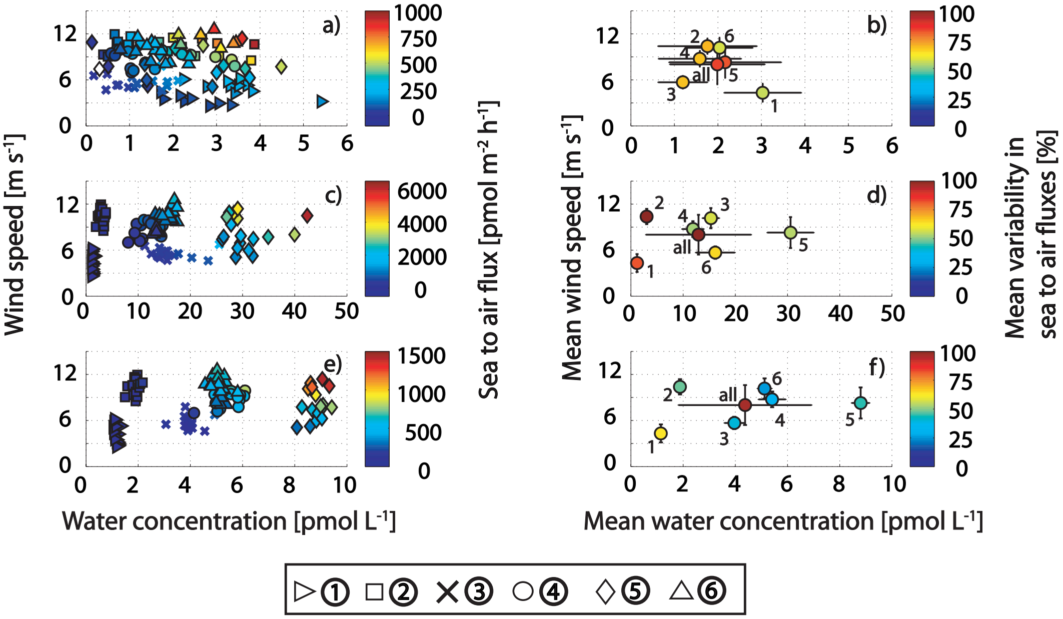

Fig. 8. Left side – wind speed versus CH_3I **(a)**, $CHBr_3$ **(c)** and CH_2Br_2 **(e)** water concentrations. Symbols are filled according to their sea-to-air flux (see color bars). Right side – mean wind speed versus mean CH_3I **(b)**, $CHBr_3$ **(d)** and CH_2Br_2 **(f)** water concentrations with their standard deviations which is expressed in error bars (horizontal for water concentrations and vertical for wind speed) for each diel station (S1–S6) and for all stations together. Symbols are filled with the relative standard deviations of the sea-to-air fluxes (see color bars).

Table 5. Phytoplankton pigments that were found to be significant at $p < 0.05$ and what they are indicative for.

Pigment	Indicative for	$CHBr_3$	CH_2Br_2
Chlorophyll *b*	Chlorophytes	x	x
Chlorophyll *c3*	Haptophytes	x	
Fucoxanthin	Diatoms	x	x
Diatoxanthin		x	
Zeaxanthin	Cyanobacteria	x	
α-carotene	Cryptophytes		x
Alloxanthin			x
Pyrophaephorbide a	Grazing	x	

3.1–9.4 pmol L^{-1}, respectively were in good agreement to earlier studies conducted in the oligotrophic tropical and subtropical Atlantic. Class and Ballschmiter (1988) reported 3.2–23.7 pmol L^{-1} for $CHBr_3$ and 1.7–5.8 pmol L^{-1} for CH_2Br_2 in March, Schall et al. (1997) found 3.2–8.0 for $CHBr_3$ and 1.0–1.8 pmol L^{-1} for CH_2Br_2 in boreal wintertime, while Carpenter et al. (2009) published values from the same season as DRIVE of 2.1–43.6 for $CHBr_3$ and 0.7–8.7 pmol L^{-1} for CH_2Br_2 with the highest values in the Mauritanian upwelling and close to the coast. In contrast to oceanic CH_3I during DRIVE, oceanic $CHBr_3$ and CH_2Br_2 was elevated in the biological active regions and correlated with phytoplankton pigments.

Possible biological sources during DRIVE were identified by using pigments indicative for various phytoplankton groups which were investigated with MLR more thoroughly. However it should be noted that, for example, fucoxanthin, which mainly occurs in diatoms, is also present in other phytoplankton groups to a certain extent (Jeffrey and Vesk, 1997). Production of halocarbons and the occurrence of the phytoplankton pigments may also take place on different time scales, which may obscure or stimulate a correlation. $CHBr_3$ and CH_2Br_2 showed a relationship to *Chlorophytes* and *Diatoms* while $CHBr_3$ also correlated significantly with *Cyanobacteria* and CH_2Br_2 with *Cryptophytes* (Tables 3, 5). Similar biological sources for both bromocarbons are in agreement to previous studies (Manley et al., 1992; Tokarczyk and Moore, 1994). The regional distribution of *Chlorophytes* and $CHBr_3$ and CH_2Br_2 were in best agreement to each other. *Diatoms*, although they were the dominant species in the Mauritanian upwelling and have been shown to produce halocarbons in the laboratory (Moore et al., 1996), appeared not as major contributors to bromocarbons which is in agreement to Quack et al. (2007b). Additionally, pyrophaeophorbide *a* was shown to be significant for the $CHBr_3$ distribution. This chlorophyll degradation product is specific for grazing which could lead to release of bromocarbons (Nightingale et al., 1995) produced within the algae (Moore et al., 1996). The correlations with phytoplankton pigments indicate a potential biological production of $CHBr_3$ and CH_2Br_2, which is also supported by their regional distribution. However, these correlations can neither resolve the rates of production and loss processes of bromocarbons in the ocean, nor their temporal and spatial distribution. Thus, the correlations found during DRIVE only represent indicators to possible source organisms.

Diel variability in the open ocean for both bromocarbons was very low and increased towards the coast. No relationship of halocarbons to either light, SST or salinity was found during 24 h. Elevated $CHBr_3$ and CH_2Br_2 were usually observed during evening (S3, S4 and S6) and night hours (S5). In contrast, many laboratory and field studies with both macroalgae and phytoplankton have shown maxima of $CHBr_3$ and CH_2Br_2 during the day which was attributed to light induced oxidative stress on the organisms (Ekdahl et al., 1998; Carpenter et al., 2000; Abrahamsson et al., 2004). Bromocarbon production from phytoplankton is still poorly characterized. Elevated bromocarbon production during night may indicate formation during respiration in contrast to light linked production during photosynthesis (Ekdahl et al., 1998; Abrahamsson et al., 2004) or other stress factors such as grazing. Alternatively, $CHBr_3$ and CH_2Br_2 could also be stored in the algal cells during light production and released later during the night time (Ekdahl et al., 1998) which would obscure a correlation to light in the field.

In conclusion, the regional variability of the concentration gradients of both bromocarbons was probably a result of the regional differences in primary production supported by their relationship to SST and phytoplankton pigment data (Sect. 4.2.3).

5.2.2 The relative influence of concentration gradient and wind speed on sea-to-air fluxes of $CHBr_3$ and CH_2Br_2

The regional distribution of sea-to-air fluxes of both bromocarbons was strongly determined by the most likely biologically produced oceanic $CHBr_3$ and CH_2Br_2. The regional variability in oceanic bromocarbons was much larger than the regional variations in wind speed (Fig. 8c–f). However, within individual stations, the variability in oceanic $CHBr_3$ and CH_2Br_2 was mostly lower than the variations in wind speed. At the open ocean stations, only very low oceanic bromocarbons were measured leading to very low concentration gradients and thus to very low sea-to-air fluxes, since the wind speed did not have a large impact on the variability of sea-to-air fluxes. With increasing oceanic $CHBr_3$ and CH_2Br_2 concentrations, the diel impact of changes in wind speed on the sea-to-air flux variability increased which is expressed in high correlation coefficients (Table 4, Fig. 8c, e). This effect was most pronounced for CH_2Br_2 which showed the lowest diel concentration variability of all three halocarbons (see the scatter in Fig. 8e). The influences of wind speed and concentration gradient on the emissions of bromocarbons are discussed based on the parameterization of Nightingale et al. (2000), which may not include all control factors similarly to our discussions concerning CH_3I emissions (Sect. 5.1.2).

Carpenter et al. (2009) derived 8.9 times higher $CHBr_3$ fluxes in the open ocean and 1.3 times higher in the coastal region of mean (10th–90th percentile) 367 (42–625) and 1483 (421–3504) $\mathrm{pmol\,m^{-2}\,h^{-1}}$ in comparison to our study with 41 (-150 – 222) and 1171 (300 – 2463) $\mathrm{pmol\,m^{-2}\,h^{-1}}$. Sea-to-air fluxes of CH_2Br_2 calculated by Carpenter et al. (2009) were 2.4 times higher in the open ocean and in a similar range in the coastal region with 158 (17–288) and 554 (204–917) $\mathrm{pmol\,m^{-2}\,h^{-1}}$ in comparison to 66 (5–155) and 483 (109–809) $\mathrm{pmol\,m^{-2}\,h^{-1}}$ (this study) analyzing the same season and region although with higher spatial resolution. This resulted from larger concentration gradients due to their lower atmospheric mixing ratios and comparable ambient parameters.

5.3 Other impact factors on sea-to-air fluxes: MABL height and SST

Wind speed and concentration gradients are direct factors that influence sea-to-air fluxes. Some more indirect factors that could possibly impact the emissions include SST and the MABL through their intensifying or decreasing effect on the concentration gradient. Possible effects of the changes in SST on the solubility of oceanic halocarbons and therewith their concentration gradients were small during DRIVE compared to the variability in sea water concentrations (Fig. 2).

The MABL height has implications for the atmospheric mixing ratios of halocarbons and their sea-to-air fluxes via the concentration or dilution of atmospheric halocarbons, emitted from the oceans, within a decreasing or increasing MABL height (Fuhlbrügge et al., 2013). In order to understand the possible effect of MABL variations, sea-to-air fluxes of all three halocarbons were calculated with minimum and maximum atmospheric mixing ratios associated with high (S1) and low MABL heights (S5) to cover the range of potential fluxes in the study region (Fig. 9). A different concentration distribution caused by other atmospheric conditions can change the $CHBr_3$ and CH_2Br_2 sea-to-air fluxes on average between 19 % (S5) and 4160 % (S1) for $CHBr_3$ and between 7 % (S5) and 1337 % (S1) for CH_2Br_2 (see the lower and upper limits in Fig. 9b–c; the shading implicates the potential range). The effect on the CH_3I fluxes is from 1 % (S1) to 42 % (S4) (Fig. 9a) lower due to its high supersaturation (Fig. 4a). Considering the large MABL height changes occurring within one day above coastal stations, e.g. from 100 to 350 m at S6, the effect of the entailing varying atmospheric mixing ratios on local emissions has to be taken into account when assessing halocarbon sea-to-air fluxes from coastal upwelling regions.

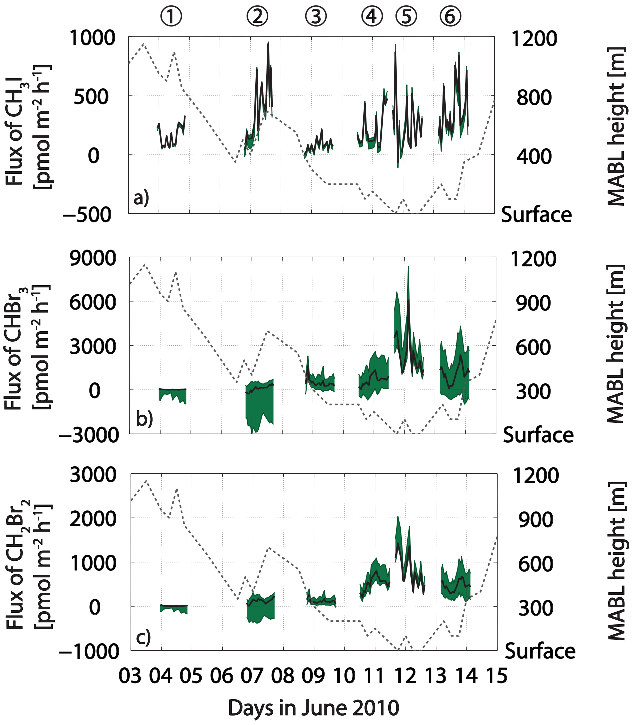

Fig. 9. Sea-to-air fluxes for CH_3I **(a)**, $CHBr_3$ **(b)** and CH_2Br_2 **(c)** during DRIVE and the MABL height, determined by Fuhlbrügge et al. (2013) as the dashed grey line are shown on the right side. The upper and lower value of potential sea-to-air fluxes assuming the lowest MABL (lower range, 3.0 ppt for CH_3I, 3.1 ppt for CH_2Br_2 and 8.9 ppt for $CHBr_3$) and the highest MABL (upper range, 0.6 ppt for CH_3I, 0.9 ppt for CH_2Br_2 and 0.5 ppt for $CHBr_3$) valid for the whole region are shaded in green.

5.4 Oceanic influence on atmospheric mixing ratios of CH_3I, $CHBr_3$ and CH_2Br_2

5.4.1 The contribution of the oceanic emissions to the atmospheric mixing ratios

We have shown in the last sections that the sea-to-air fluxes of halocarbons are dominated by the oceanic production and that the sea water concentrations of bromocarbons are increasing towards the coast. In order to understand the importance of sea-to-air fluxes for the atmospheric halocarbon distribution, we calculated their relative contributions to the atmospheric mixing ratios at the individual 24 h-stations. Previous studies assigned the high $CHBr_3$ and CH_2Br_2 mixing ratios above the coastal upwellling to air masses originating from the North West African continent (Quack et al., 2007a) and very low atmospheric bromocarbons to air masses from the northern open ocean (Carpenter et al., 2009; Lee et al., 2010). Air masses during coastal station S5 also arrived from the northern open ocean (Fuhlbrügge et al., 2013) which contradicts the hypothesis that high atmospheric halocarbons could only be accounted for by continental sources.

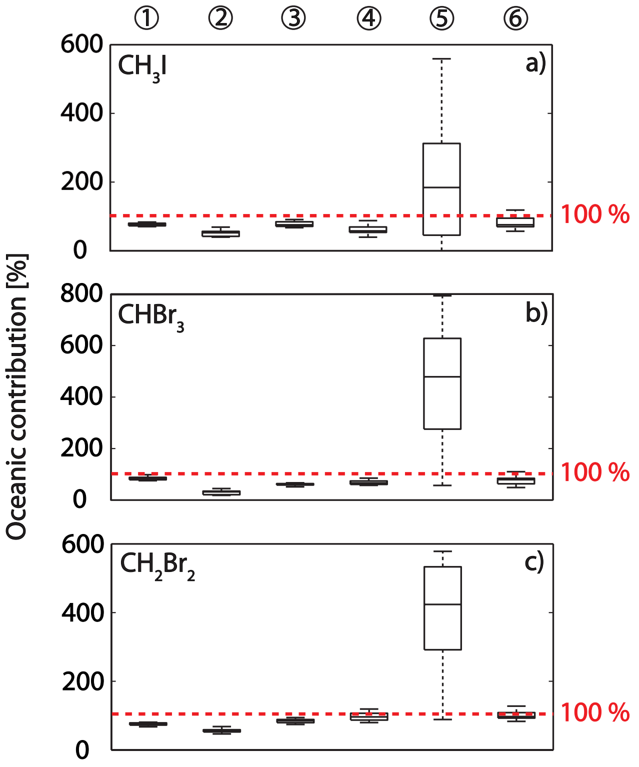

Fig. 10. Oceanic contributions to atmospheric halocarbons assuming a mean distance of 200 km, mean wind speeds, mean sea-to-air fluxes and background mixing ratios for the open ocean (CH_3I = 0.50 ppt, $CHBr_3$ = 0.50 ppt, CH_2Br_2 = 0.75 ppt) and the coastal region (CH_3I = 0.75 ppt, $CHBr_3$ = 3.00 ppt, CH_2Br_2 = 1.80 ppt), and the MABL heights determined by Fuhlbrügge et al. (2013) at every measurement point for CH_3I **(a)**, for $CHBr_3$ **(b)** and for CH_2Br_2 **(c)**, outliers are excluded. The red dashed line marks 100 % in every plot.

For our calculations, we apply a fetch of 200 km (the mean distance between the diel stations), sea-to-air fluxes from Sects. 4.1.5 and 4.2.6, according wind speeds and MABL heights (Table 1). The sea-to-air fluxes and the height of the MABL have numerically the same influence on atmospheric mixing ratios since bromocarbons in the atmosphere are within the calculations a product of both. Applying a fetch of 200 km, the air mass travels approximately 7 h until it arrives at the diel stations. Open ocean background values for S1 and S2 were set to 0.50 ppt for CH_3I and $CHBr_3$, and 0.75 ppt for CH_2Br_2, while higher background values of 0.75 ppt for CH_3I, 1.80 ppt for CH_2Br_2 and 3.00 ppt for $CHBr_3$ were assigned to coastal stations S3–S6. We did not include the tropical atmospheric lifetimes of the three halocarbons (7, 24, 123 days for CH_3I, $CHBr_3$, CH_2Br_2; Montzka and Reimann, 2011) since the degradation during the short-term box-calculation has no substantial influence on the results. The oceanic emissions are nearly sufficient to explain most of the atmospheric halocarbons (Fig. 10a–c). Oceanic halocarbon contributions at S1–S6 (except for S5)

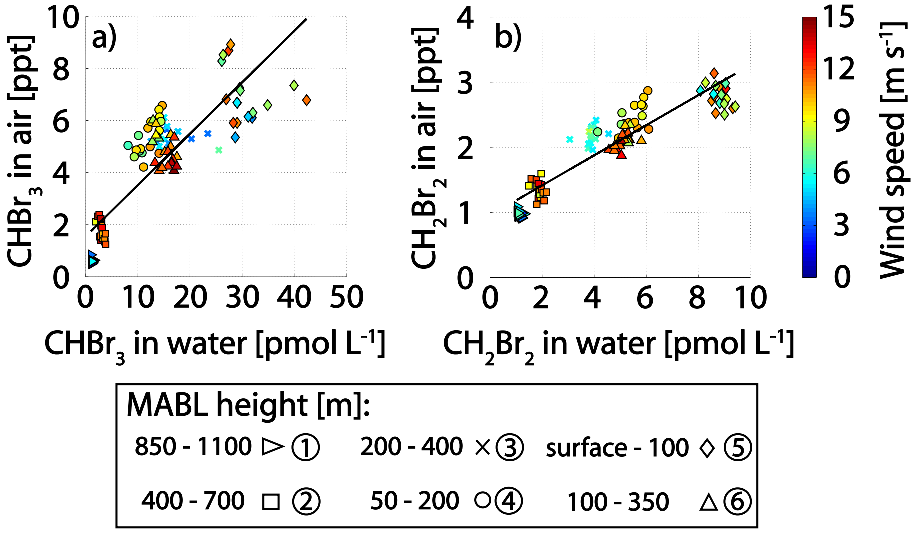

Fig. 11. Correlations of oceanic versus atmospheric halocarbons ($CHBr_3$ in **a** and CH_2Br_2 in **b**) filled with wind speed (see color coding). The black line indicates the regression line for the whole cruise. For the individual correlation coefficients see Table 6.

ranged from 39 to 135 % for CH_3I, between 18 and 126 % for $CHBr_3$ and from 47 to 148 % for CH_2Br_2 with generally lowest contributions at S2 (40–69 % for CH_3I, 18–45 % for $CHBr_3$ and 47–68 % for CH_2Br_2). At S5, the emissions from the assumed 200 km fetch contributed 560 (CH_3I)–800 % ($CHBr_3$) to the observed mixing ratios. At this station high oceanic and atmospheric $CHBr_3$ and CH_2Br_2 coincided with very low MABL heights. These results suggest that (1) atmospheric mixing ratios over the open ocean S1–S2 are derived from regional emissions and distant sources, (2) the source strength in combination with the observed MABL height can nearly maintain the medium range of atmospheric mixing ratios found at S3, S4, and S6, and (3) the high sea-to-air fluxes and low MABL heights leading to the highly elevated atmospheric mixing ratios at S5 are a very local phenomenon, constrained to the boundaries of this station. The large overestimation of mixing ratios within the box model is then a result of the extrapolation of the high sea-to-air fluxes to the fetch of 200 km. Vertical transport has been neglected in this simple model approach, which likely introduces only small errors since the top of the MABL was very stable and isolated above all coastal stations (Fuhlbrügge et al., 2013).

While the Mauritanian upwelling has been identified to contribute to the high atmospheric abundances of all halocarbons in the region, the elevated and highly variable atmospheric mixing ratios of $CHBr_3$ and CH_2Br_2 at Cape Verde can be attributed to local sources. O'Brien et al. (2009) suggested high atmospheric halocarbons at CVAO originating from the coastal region off Mauritania. However, back trajectory analysis revealed air masses at CVAO originating from the open ocean during our investigation (Fuhlbrügge et al., 2013). This together with the considerably lower atmospheric mixing ratios measured at the open ocean stations (0.5 – 2.4 ppt for $CHBr_3$ and 0.9–1.6 ppt for CH_2Br_2) and around the upwelling contradicts upwelling originated halocarbons at Cape Verde during DRIVE. In addition, $CHBr_3$ reached its highest value of the whole campaign at CVAO. Hence, the high and variable atmospheric $CHBr_3$ and CH_2Br_2 at Cape Verde in combination with comparably variable wind speeds suggest local coastal sources for both compounds.

5.4.2 Correlations between oceanic and atmospheric $CHBr_3$ and CH_2Br_2

In contrast to the observations presented in Quack et al. (2007a) and Carpenter et al. (2009), atmospheric $CHBr_3$ and CH_2Br_2 followed the same regional distribution as their oceanic counterparts. Water concentrations and atmospheric mixing ratios of $CHBr_3$ ($R^2 = 0.74$) and CH_2Br_2 ($R^2 = 0.85$) correlated regionally very well during DRIVE (Fig. 11a–b) which has not been observed during the other cruises. This is likely caused by a combination of the stable and isolated marine boundary layer observed over the upwelling, the coinciding high productivity and concentration of the bromocarbons in the upwelling, and the combined effects of air-sea exchange as slowest process (over a considerable fetch) and advection as the fastest (diluting with background air), both influencing the atmospheric signals. We assume biological production of bromocarbons and mixing within the water column also as rapid processes (Ekdahl et al., 1998). Correlations between atmospheric mixing ratios and oceanic concentrations within the individual 24h-stations were only significant at open ocean station S2 for $CHBr_3$ and at coastal stations S4 and S6 for both compounds (Table 6). A diel anti-correlation of atmospheric mixing ratios with water concentrations was also observed at several diel stations (S1, S2, S5,

Table 6. Correlation coefficients R^2 and number of data points n of oceanic versus atmospheric bromocarbons for the whole cruise and each individual station. Bold numbers indicate significant correlations with $p < 0.05$. Italic numbers mark negative correlations.

	Whole cruise	S1 (17.6° N and 24.3° W)	S2 (18.0° N and 21.0° W)	S3 (18.0° N and 18.0° W)	S4 (18.5° N and 16.5° W)	S5 (19.0° N and 16.6° W)	S6 (20.0° N and 17.3° W)
$CHBr_3$	**0.74**	*0.01*	***0.52***	0.01	**0.45**	*0.05*	***0.20***
CH_2Br_2	**0.85**	*0.19*	*0.09*	0.01	**0.40**	*0.18*	**0.28**
n	109	18	19	17	17	18	20

and S6). An explanation for this observation (see Table 6) between the atmospheric and oceanic concentrations on a diel scale is still lacking, since neither wind direction, including land-sea breeze circulation (Fuhlbrügge et al., 2013), nor MABL height variations led to clear correlations.

Positive and negative deviations from the overall good regional correlation of sea water concentrations and atmospheric mixing ratios could also be observed at the individual stations. Atmospheric concentrations can increase with wind speed due to increasing sea-to-air fluxes, while elevated wind speeds also dilute local emissions with background air and vice versa. Thus, low wind speeds in the open ocean led to lower atmospheric mixing ratios at S1 while the higher wind speeds at S2 triggered average mixing ratios (Fig. 11). This may not only be a result of increasing sea-to-air flux and fetch, but may also be partly a result of the reduction of the MABL height. While coastal stations S3, S4 and S6 have similar mean $CHBr_3$ surface water concentrations, S6 showed the largest sea-to-air fluxes of these three stations due to the largest prevailing wind speeds (see Fig. 5), but on average relatively low atmospheric mixing ratios (Fig. 11a, b). We interpret this as intense transport phenomenon and possible dilution of the large sea-to-air fluxes with background air masses due to intensifying winds and increasing MABL height. Although atmospheric mixing ratios for $CHBr_3$ and CH_2Br_2 were highest at S5, they are on average much lower as could be expected from the overall regional correlation and the large sea water concentrations (see the data points below the correlation line in Fig. 11a, b in contrast to most of the data points from other stations that are above the line). We hypothesize regional mixing with background air masses as cause for the lower than average correlation of sea surface $CHBr_3$ and CH_2Br_2 and atmospheric bromocarbons, which supports that the high atmospheric mixing ratios at S5, the high sea-to-air fluxes, and low MABL height are very local phenomena. The good overall correlation between atmospheric and oceanic bromocarbons shows the dominance of sea water production for the atmosphere. The co-correlation of increased productivity and production of bromocarbons during upwelling of cold and nutrient rich water and the high atmospheric mixing ratios in a low and stable MABL over the low sea surface temperature of the upwelled water (Fuhlbrügge et al., 2013) can be explained within the known concepts of wind driven air-sea exchange, advection and MABL variations on a regional scale.

6 Summary and conclusions

We have discussed the temporal and spatial influence of biological productivity, wind speed, MABL height and SST on oceanic emissions and atmospheric mixing ratios of halocarbons in the tropical North East Atlantic.

During DRIVE, oceanic CH_3I neither showed a relationship to phytoplankton pigments nor to cyanobacteria, and its distribution appeared mainly as a result of abiotic or indirect biological formation which seemed to be the main driver of the CH_3I concentration gradient between sea water and air. On a regional scale, neither wind speed nor oceanic CH_3I were dominating the sea-to-air flux, while diel variations in emissions were a result of varying oceanic CH_3I concentrations almost throughout the whole cruise. On the contrary, the oceanic distribution of $CHBr_3$ and CH_2Br_2 and their emissions correlated with phytoplankton pigments which implies a biological source, albeit with no clear diurnal cycles unlike observed in previous studies. The variability in wind speed gained increasing impact on the diel bromocarbon emissions with decreasing distance to the coast, because the diel variability in oceanic $CHBr_3$ and even more pronounced in oceanic CH_2Br_2 was low in comparison to large diel wind speed variations.

MABL height was identified as an additional factor impacting oceanic emissions of halocarbons in the upwelling through its influence on atmospheric halocarbon abundances. Sea-to-air fluxes of CH_3I were hardly influenced by the varying MABL due to its high supersaturation in sea surface water. The sea-to-air fluxes of $CHBr_3$ and CH_2Br_2 however were substantially influenced by atmospheric conditions High atmospheric CH_3I, $CHBr_3$ and CH_2Br_2 mixing ratios at a coastal site on the Cape Verde islands (CVAO) could be attributed to local coastal sources. Regional oceanic bromocarbon emissions from the upwelling, probably driven by biological production, could in combination with varying and low MABL heights and air mass transport explain most of the observed atmospheric halocarbons, contrasting previous hypotheses regarding additional continental bromocarbon sources above the upwelling. As a result, the atmospheric bromocarbons showed significant and high overall correlations with the oceanic concentrations, which is caused by the coincidence of oceanic production in upwelled water and low and stable MABLs over the cold upwelled water. We therefore hypothesize that low MABL heights and high sea-to-air fluxes coinciding with high atmospheric mixing ratios could be a common feature in coastal upwelling systems (this study; Fuhlbrügge et al., 2013).

The temporal and spatial development of biological production, wind speed, SST and changes in atmospheric mixing ratios with MABL height will influence the future sea-to-air fluxes and their corresponding atmospheric mixing ratios, as well as their contribution to atmospheric chemical processes. Surface air and water temperature could play a crucial role in the future development of wind speed via the potentially increased land-sea pressure gradients. A potential future increase of SST in the tropical oligotrophic Atlantic (Hoerling et al., 2001) could lead to enhanced oceanic production of CH_3I (Richter, 2004) and in combination with reduced solubility to elevated emissions of CH_3I. An elevation of atmospheric CH_3I with increasing SST and accompanying physical-biological phenomena on a decadal scale has already been shown by Yokouchi et al. (2012) in the tropical and temperate Pacific region. At the same time, the enhancement of eastern boundary upwelling systems accompanied by increasing primary production (Lachkar and Gruber, 2012) could result in higher production of oceanic bromocarbons. Combined with elevated wind speeds (Bakun, 1990), increased emissions of brominated compounds would be the consequence. Hence, the relevance of the tropical upwelling systems with respect to halocarbon emissions will likely increase and the influence of the diel and regional drivers on the emissions may be intensified. To better understand the current and future roles of halocarbon emissions from marine upwelling regions on global ozone changes and atmospheric chemistry, it is important to continue to better quantify the relative roles and interactions of oceanic halocarbon production, wind speed and MABL height, SST and seasonal variations, as well as other relevant forcings in oceanic upwelling regions around the global ocean.

Acknowledgements. The authors would like to thank the chief scientist of the cruise P399/2 Prof Dr Hermann W. Bange, as well as the captain and the crew of the RV *Poseidon* during P399/2 for all their help and support. We are also very grateful to Karen Stange and Gert Petrick for their technical support before and during the campaign. We would like to acknowledge Carolin Löscher for her help with water sampling for pigment analysis and Bettina Taylor for analysis of the flow cytometry samples. The authors thank Christian Müller and Julian Kinzel for their assistance with air sampling at CVAO. We thank Xiaorong Zhu and Leslie Pope for technical assistance in the air canister analyses. Furthermore, we would like to thank Christa Marandino and Susann Tegtmeier for their helpful input. We acknowledge the National Centre for Atmospheric Science (NCAS) for providing the Cape Verde Atmospheric Observatory wind speed data. Additionally, the authors would like to acknowledge NASA for providing satellite MODIS-Aqua data. We thank the anonymous reviewers for very helpful input and corrections. This work was part of the German research project SOPRAN II (grant no. FKZ 03F0611A) funded by the Bundesministerium für Bildung und Forschung (BMBF), and was also supported by the EU project SHIVA (grant no. FP7-ENV-2007-1-226224), as well as NASA UARP Grant NNX09AJ25G.

The service charges for this open access publication
have been covered by a Research Centre of the
Helmholtz Association.

Edited by: W. T. Sturges

References

Abrahamsson, K., Lorén, A., Wulff, A., and Wangberg, S. A.: Air-sea exchange of halocarbons: The influence of diurnal and regional variations and distribution of pigments, Deep-Sea Res. Part II-Top. Stud. Oceanogr., 51, 2789–2805, doi:10.1016/j.dsr2.2004.09.005, 2004.

Amachi, S., Kamagata, Y., Kanagawa, T., and Muramatsu, Y.: Bacteria mediate methylation of iodine in marine and terrestrial environments, Appl. Environ. Microbiol., 67, 2718–2722, doi:10.1128/aem.67.6.2718-2722.2001, 2001.

Aschmann, J., Sinnhuber, B. M., Chipperfield, M. P., and Hossaini, R.: Impact of deep convection and dehydration on bromine loading in the upper troposphere and lower stratosphere, Atmos. Chem. Phys., 11, 2671–2687, doi:10.5194/acp-11-2671-2011, 2011.

Bakun, A.: Global climate change and intensification of coastal ocean upwelling, Science, 247, 198–201, doi:10.1126/science.247.4939.198, 1990.

Bange, H. W., Atlas, E. L., Bahlmann, E., Baker, A. R., Bracher, A., Cianca, A., Dengler, M., Fuhlbrügge, S., Großmann, K., Hepach, H., Lavric, J., Löscher, C., Krüger, K., Orlikowska, A., Peeken, I., Quack, B., Schafstall, J., Steinhoff, T., Williams, J., and Wittke, F.: Fs poseidon fahrtbericht/cruise report p399 − 2 & 3, Leibniz-Institut für Meereswissenschaften IFM-GEOMAR, Kiel, 74, 2011.

Bell, N., Hsu, L., Jacob, D. J., Schultz, M. G., Blake, D. R., Butler, J. H., King, D. B., Lobert, J. M., and Maier-Reimer, E.: Methyl iodide: Atmospheric budget and use as a tracer of marine convection in global models, J. Geophys. Res.-Atmos., 107, 4340, doi:10.1029/2001jd001151, 2002.

Carpenter, L. J. and Liss, P. S.: On temperate sources of bromoform and other reactive organic bromine gases, J. Geophys. Res.-Atmos., 105, 20539–20547, 2000.

Carpenter, L. J., Malin, G., Liss, P. S., and Kupper, F. C.: Novel biogenic iodine-containing trihalomethanes and other short-lived halocarbons in the coastal east atlantic, Glob. Biogeochem. Cy., 14, 1191–1204, 2000.

Carpenter, L. J., Jones, C. E., Dunk, R. M., Hornsby, K. E., and Woeltjen, J.: Air-sea fluxes of biogenic bromine from the tropical and north atlantic ocean, Atmos. Chem. Phys., 9, 1805–1816, doi:10.5194/acp-9-1805-2009, 2009.

Class, T., and Ballschmiter, K.: Chemistry of organic traces in air viii: Sources and distribution of brom- and bromochloromethanes in marine air and surfacewater of the atlantic ocean, J. Atmos. Chem., 6, 35-46, 1988.

Ekdahl, A., Pedersén, M., and Abrahamsson, K.: A study of the diurnal variation of biogenic volatile halocarbons, Mar. Chem., 63, 1–8, 1998.

Fairall, C. W., Bradley, E. F., Hare, J. E., Grachev, A. A., and Edson, J. B.: Bulk parameterization of air–sea fluxes: Updates and verification for the coare algorithm, J. Clim., 16, 571–591, doi:10.1175/1520-0442(2003)016<0571:bpoasf>,2.0.co;2, 2003.

Fedoseev, A.: Geostrophic circulation of surface waters on the shelf of north-west africa, Rapp. Proc. Verb. Reun. Cons. Inst. Expl. Mer., 159, 32–37, 1970.

Fuhlbrügge, S., Krüger, K., Quack, B., Atlas, E. L., Hepach, H., and Ziska, F.: Impact of the marine atmospheric boundary layer on vsls abundances in the eastern tropical and subtropical north atlantic ocean, Atmos. Chem. Phys., 13, 6345–6357, doi:10.5194/acp-13-6345-2013, 2013.

Fuse, H., Inoue, H., Murakami, K., Takimura, O., and Yamaoka, Y.: Production of free and organic iodine by roseovarius spp, FEMS Microbiology Letters, 229, 189–194, doi:10.1016/s0378-1097(03)00839-5, 2003.

Hagen, E.: Northwest african upwelling scenario, Oceanol. Acta, 24, S113–S128, 2001.

Happell, J. D. and Wallace, D. W. R.: Methyl iodide in the greenland/norwegian seas and the tropical atlantic ocean: Evidence for photochemical production, Geophys. Res. Lett., 23, 2105–2108, doi:10.1029/96gl01764, 1996.

Hoerling, M. P., Hurrell, J. W., and Xu, T. Y.: Tropical origins for recent north atlantic climate change, Science, 292, 90–92, doi:10.1126/science.1058582, 2001.

Hossaini, R., Chipperfield, M. P., Monge-Sanz, B. M., Richards, N. A. D., Atlas, E., and Blake, D. R.: Bromoform and dibromomethane in the tropics: A 3-d model study of chemistry and transport, Atmos. Chem. Phys., 10, 719–735, doi:10.5194/acp-10-719-2010, 2010.

Hossaini, R., Chipperfield, M. P., Feng, W., Breider, T. J., Atlas, E., Montzka, S. A., Miller, B. R., Moore, F., and Elkins, J.: The contribution of natural and anthropogenic very short-lived species to stratospheric bromine, Atmos. Chem. Phys., 12, 371–380, doi:10.5194/acp-12-371-2012, 2012a.

Hossaini, R., Chipperfield, M. P., Dhomse, S., Ordonez, C., Saiz-Lopez, A., Abraham, N. L., Archibald, A., Braesicke, P., Telford, P., Warwick, N., Yang, X., and Pyle, J.: Modelling future changes to the stratospheric source gas injection of biogenic bromocarbons, Geophys. Res. Lett., 39, L20813, doi:10.1029/2012gl053401, 2012b.

Jeffrey, S. W. and Vesk, M.: Introduction to marine phytoplankton and their pigment signatures, in: Phytoplankton pigments in oceanography: Guideline to modern methods., edited by: Jeffrey, S. W., Mantoura, R. F. C., and Wright, S. W., 10, UNESCO Publishing, Paris, 37–84, 1997.

Jones, C. E., Hornsby, K. E., Sommariva, R., Dunk, R. M., Von Glasow, R., McFiggans, G., and Carpenter, L. J.: Quantifying the contribution of marine organic gases to atmospheric iodine, Geophys. Res. Lett., 37, L18804, doi:10.1029/2010gl043990, 2010.

Lachkar, Z. and Gruber, N.: A comparative study of biological production in eastern boundary upwelling systems using an artificial neural network, Biogeosciences, 9, 293–308, doi:10.5194/bg-9-293-2012, 2012.

Lai, S. C., Williams, J., Arnold, S. R., Atlas, E. L., Gebhardt, S., and Hoffmann, T.: Iodine containing species in the remote marine boundary layer: A link to oceanic phytoplankton, Geophys. Res. Lett., 38, L20801, doi:10.1029/2011gl049035, 2011.

Laturnus, F.: Marine macroalgae in polar regions as natural sources for volatile organohalogens, Environ. Sci. Pollut. Res., 8, 103–108, doi:10.1007/bf02987302, 2001.

Lee, J. D., McFiggans, G., Allan, J. D., Baker, A. R., Ball, S. M., Benton, A. K., Carpenter, L. J., Commane, R., Finley, B. D., Evans, M., Fuentes, E., Furneaux, K., Goddard, A., Good, N., Hamilton, J. F., Heard, D. E., Herrmann, H., Hollingsworth, A., Hopkins, J. R., Ingham, T., Irwin, M., Jones, C. E., Jones, R. L., Keene, W. C., Lawler, M. J., Lehmann, S., Lewis, A. C., Long, M. S., Mahajan, A., Methven, J., Moller, S. J., Muller, K., Muller, T., Niedermeier, N., O'Doherty, S., Oetjen, H., Plane, J. M. C., Pszenny, A. A. P., Read, K. A., Saiz-Lopez, A., Saltzman, E. S., Sander, R., von Glasow, R., Whalley, L., Wiedensohler, A., and Young, D.: Reactive halogens in the marine boundary layer (rhamble): The tropical north atlantic experiments, Atmos. Chem. Phys., 10, 1031–1055, doi:10.5194/acp-10-1031-2010, 2010.

Manley, S. L. and Dastoor, M. N.: Methyl-iodide (CH_3I) production by kelp and associated microbes, Mar. Biol., 98, 477–482, 1988.

Manley, S. L., Goodwin, K., and North, W. J.: Laboratory production of bromoform, methylene bromide, and methyl-iodide by macroalgae and distribution in nearshore southern california waters, Limnol. Oceanogr., 37, 1652–1659, 1992.

Martino, M., Mills, G. P., Woeltjen, J., and Liss, P. S.: A new source of volatile organoiodine compounds in surface seawater, Geophys. Res. Lett., 36, L01609, doi:10.1029/2008GL036334, 2009.

McGivern, W. S., Sorkhabi, O., Suits, A. G., Derecskei-Kovacs, A., and North, S. W.: Primary and secondary processes in the photodissociation of chbr3, J. Phys. Chem. A, 104, 10085–10091, doi:10.1021/jp0005017, 2000.

McGregor, H. V., Dima, M., Fischer, H. W., and Mulitza, S.: Rapid 20th-century increase in coastal upwelling off northwest africa, Science, 315, 637–639, doi:10.1126/science.1134839, 2007.

Minas, H. J., Codispoti, L. A., and Dugdale, R. C.: Nutrients and primary production in the upwelling region off northwest africa, Rapp. Proc. Verb. Reun. Cons. Inst. Expl. Mer., 180, 148–183, 1982.

Mittelstaedt, E.: Large-scale circulation along the coast of northwest africa, Rapp. Proc. Verb. Reun. Cons. Inst. Expl. Mer., 180, 50–57, 1982.

Montzka, S. A. and Reimann, S.: Ozone-depleting substances and related chemicals, Chapter 1 in Scientific Assessment of Ozone Depletion: 2010, Global Ozone Research and Monitoring Project, World Meteorological Organization (WMO), Geneva, Report No. 52, 2011.

Moore, R. M. and Zafiriou, O. C.: Photochemical production of methyl-iodide in seawater, J. Geophys. Res.-Atmos., 99, 16415–16420, doi:10.1029/94jd00786, 1994.

Moore, R. M., Geen, C. E., and Tait, V. K.: Determination of henry law constants for a suite of naturally-occurring halogenated methanes in seawater, Chemosphere, 30, 1183-1191, doi:10.1016/0045-6535(95)00009-w, 1995a.

Moore, R. M., Tokarczyk, R., Tait, V. K., Poulin, M., and Geen, C. E.: Marine phytoplankton as a natural source of volatile organohalogens, in: Naturally-produced organohalogens, edited by: Grimvall, A., and deLeer, E. W. B., Kluwer Academic Publishers, Dordrecht, The Netherlands, 283–294, 1995b.

Moore, R. M., Webb, M., Tokarczyk, R., and Wever, R.: Bromoperoxidase and iodoperoxidase enzymes and production of halogenated methanes in marine diatom cultures, J. Geophys. Res.-Oceans, 101, 20899–20908, doi:10.1029/96jc01248, 1996.

Moore, R. M. and Groszko, W.: Methyl iodide distribution in the ocean and fluxes to the atmosphere, J. Geophys. Res.-Oceans, 104, 11163–11171, doi:10.1029/1998jc900073, 1999.

Nightingale, P. D., Malin, G., and Liss, P. S.: Production of chloroform and other low-molecular-weight halocarbons by some species of macroalgae, Limnol. Oceanogr., 40, 680–689, 1995.

Nightingale, P. D., Malin, G., Law, C. S., Watson, A. J., Liss, P. S., Liddicoat, M. I., Boutin, J., and Upstill-Goddard, R. C.: In situ evaluation of air-sea gas exchange parameterizations using novel conservative and volatile tracers, Global Biogeochem. Cy., 14, 373–387, doi:10.1029/1999gb900091, 2000.

O'Brien, L. M., Harris, N. R. P., Robinson, A. D., Gostlow, B., Warwick, N., Yang, X., and Pyle, J. A.: Bromocarbons in the tropical marine boundary layer at the cape verde observatory - measurements and modelling, Atmos. Chem. Phys., 9, 9083–9099, doi:10.5194/acp-9-9083-2009, 2009.

O'Dowd, C. D., Jimenez, J. L., Bahreini, R., Flagan, R. C., Seinfeld, J. H., Hameri, K., Pirjola, L., Kulmala, M., Jennings, S. G., and Hoffmann, T.: Marine aerosol formation from biogenic iodine emissions, Nature, 417, 632–636, doi:10.1038/nature00775, 2002.

Pyle, J. A., Warwick, N., Yang, X., Young, P. J., and Zeng, G.: Climate/chemistry feedbacks and biogenic emissions, Philos. Trans. R. Soc. A-Math. Phys. Eng. Sci., 365, 1727–1740, doi:10.1098/rsta.2007.2041, 2007.

Quack, B. and Wallace, D. W. R.: Air-sea flux of bromoform: Controls, rates, and implications, Glob. Biogeochem. Cy., 17, 1023, doi:10.1029/2002gb001890, 2003.

Quack, B., Atlas, E., Petrick, G., Stroud, V., Schauffler, S., and Wallace, D. W. R.: Oceanic bromoform sources for the tropical atmosphere, Geophys. Res. Lett., 31, L23S05, doi:10.1029/2004gl020597, 2004.

Quack, B., Atlas, E., Petrick, G., and Wallace, D. W. R.: Bromoform and dibromomethane above the mauritanian upwelling: Atmospheric distributions and oceanic emissions, J. Geophys. Res.-Atmos., 112, D09312, doi:10.1029/2006jd007614, 2007a.

Quack, B., Peeken, I., Petrick, G., and Nachtigall, K.: Oceanic distribution and sources of bromoform and dibromomethane in the mauritanian upwelling, J. Geophys. Res.-Oceans, 112, C10006, doi:10.1029/2006jc003803, 2007b.

Richter, U.: Factors influencing methyl iodide production in the ocean and its flux to the atmosphere, PhD thesis, Mathematisch-Naturwissenschaftliche Fakultät der Christian-Albrechts-Universität zu Kiel, Christian-Albrechts-Universität zu Kiel, Kiel, 117 pp., 2004.

Richter, U. and Wallace, D. W. R.: Production of methyl iodide in the tropical atlantic ocean, Geophys. Res. Lett., 31, L23S03, doi:10.1029/2004gl020779, 2004.

Saiz-Lopez, A., Plane, J. M. C., Baker, A. R., Carpenter, L. J., von Glasow, R., Martin, J. C. G., McFiggans, G., and Saunders, R. W.: Atmospheric chemistry of iodine, Chem. Rev., 112, 1773–1804, doi:10.1021/cr200029u, 2012.

Salawitch, R. J., Weisenstein, D. K., Kovalenko, L. J., Sioris, C. E., Wennberg, P. O., Chance, K., Ko, M. K. W., and McLinden, C. A.: Sensitivity of ozone to bromine in the lower stratosphere, Geophys. Res. Lett., 32, L05811, doi:10.1029/2004gl021504, 2005.

Schall, C., Heumann, K. G., and Kirst, G. O.: Biogenic volatile organoiodine and organobromine hydrocarbons in the atlantic ocean from 42 degrees N to 72 degrees S, Fresenius J. Anal. Chem., 359, 298–305, 1997.

Schauffler, S. M., Atlas, E. L., Blake, D. R., Flocke, F., Lueb, R. A., Lee-Taylor, J. M., Stroud, V., and Travnicek, W.: Distributions of brominated organic compounds in the troposphere and lower stratosphere, J. Geophys. Res.-Atmos., 104, 21513–21535, 1999.

Smythe-Wright, D., Boswell, S. M., Breithaupt, P., Davidson, R. D., Dimmer, C. H., and Diaz, L. B. E.: Methyl iodide production in the ocean: Implications for climate change, Glob. Biogeochem. Cy., 20, GB3003, doi:10.1029/2005GB002642, 2006.

Solomon, S., Garcia, R. R., and Ravishankara, A. R.: On the role of iodine in ozone depletion, J. Geophys. Res.-Atmos., 99, 20491–20499, doi:10.1029/94JD02028, 1994.

Stemmler, I., Hense, I., Quack, B., and Maier-Reimer, E.: Methyl iodide production in the open ocean, Biogeosciences Discuss., 10, 17549–17595, doi:10.5194/bgd-10-17549-2013, 2013.

Taylor, B. B., Torrecilla, E., Bernhardt, A., Taylor, M. H., Peeken, I., Rottgers, R., Piera, J., and Bracher, A.: Bio-optical provinces in the eastern atlantic ocean and their biogeographical relevance, Biogeosciences, 8, 3609–3629, doi:10.5194/bg-8-3609-2011, 2011.

Tegtmeier, S., Kruger, K., Quack, B., Atlas, E. L., Pisso, I., Stohl, A., and Yang, X.: Emission and transport of bromocarbons: From the west pacific ocean into the stratosphere, Atmos. Chem. Phys., 12, 10633–10648, doi:10.5194/acp-12-10633-2012, 2012.

Tegtmeier, S., Krüger, K., Quack, B., Atlas, E., Blake, D. R., Boenisch, H., Engel, A., Hepach, H., Hossaini, R., Navarro, M. A., Raimund, S., Sala, S., Shi, Q., and Ziska, F.: The contribution of oceanic methyl iodide to stratospheric iodine, Atmos. Chem. Phys., 13, 11869–11886, doi:10.5194/acp-13-11869-2013, 2013.

Tokarczyk, R. and Moore, R. M.: Production of volatile organohalogens by phytoplankton cultures, Geophys. Res. Lett., 21, 285–288, 1994.

Tomczak, M.: The distribution of water masses at the surface as derived from t-s diagram analysis in the cineca area, Rapp. Proc. Verb. Reun. Cons. Inst. Expl. Mer., 180, 48–49, 1982.

Tomczak, M. and Godfrey, J. S.: Regional oceanography: An introduction, 2 ed., Daya Publishing House, Delhi, 2005.

Tran, S., Bonsang, B., Gros, V., Peeken, I., Sarda-Esteve, R., Bernhardt, A., and Belviso, S.: A survey of carbon monoxide and non-methane hydrocarbons in the arctic ocean during summer 2010, Biogeosciences, 10, 1909–1935, doi:10.5194/bg-10-1909-2013, 2013.

Tsuchiya, M., Talley, L. D., and McCartney, M. S.: An eastern atlantic section from iceland southward across the equator, Deep-Sea Res., 39, 1885–1917, doi:10.1016/0198-0149(92)90004-d, 1992.

Williams, J., Gros, V., Atlas, E., Maciejczyk, K., Batsaikhan, A., Scholer, H. F., Forster, C., Quack, B., Yassaa, N., Sander, R., and Van Dingenen, R.: Possible evidence for a connection between methyl iodide emissions and saharan dust, J. Geophys. Res.-Atmos., 112, D07302, doi:10.1029/2005jd006702, 2007.

Yokouchi, Y., Osada, K., Wada, M., Hasebe, F., Agama, M., Murakami, R., Mukai, H., Nojiri, Y., Inuzuka, Y., Toom-Sauntry, D., and Fraser, P.: Global distribution and seasonal concentration change of methyl iodide in the atmosphere, J. Geophys. Res.-Atmos., 113, D18311, doi:10.1029/2008JD009861, 2008.

Yokouchi, Y., Nojiri, Y., Toom-Sauntry, D., Fraser, P., Inuzuka, Y., Tanimoto, H., Nara, H., Murakami, R., and Mukai, H.: Long-term variation of atmospheric methyl iodide and its link to global environmental change, Geophys. Res. Lett., 39, L23805, doi:10.1029/2012GL053695, 2012.

Ziska, F., Quack, B., Abrahamsson, K., Archer, S. D., Atlas, E., Bell, T., Butler, J. H., Carpenter, L. J., Jones, C. E., Harris, N. R. P., Hepach, H., Heumann, K. G., Hughes, C., Kuss, J., Krüger, K., Liss, P., Moore, R. M., Orlikowska, A., Raimund, S., Reeves, C. E., Reifenhäuser, W., Robinson, A. D., Schall, C., Tanhua, T., Tegtmeier, S., Turner, S., Wang, L., Wallace, D., Williams, J., Yamamoto, H., Yvon-Lewis, S., and Yokouchi, Y.: Global sea-to-air flux climatology for bromoform, dibromomethane and methyl iodide, Atmos. Chem. Phys., 13, 8915–8934, doi:10.5194/acp-13-8915-2013, 2013.

3. Manuscript 3

Impact of the marine atmospheric boundary layer conditions on VSLS abundances in the eastern tropical and subtropical North Atlantic Ocean

S. Fuhlbrügge[1], K. Krüger[1], B. Quack[1], E. Atlas[2], H. Hepach[1], and F. Ziska[1]

[1] GEOMAR Helmholtz-Zentrum für Ozeanforschung Kiel, Kiel, Germany

[2] Rosenstiel School of Marine and Atmospheric Science, Miami, Florida, USA

Published in: Atmospheric Chemistry and Physics, 13, 6345-6357, doi:10.5194/acp-13-6345-2013, 2013.

Atmos. Chem. Phys., 13, 6345–6357, 2013
www.atmos-chem-phys.net/13/6345/2013/
doi:10.5194/acp-13-6345-2013
© Author(s) 2013. CC Attribution 3.0 License.

Atmospheric Chemistry and Physics
Open Access

Impact of the marine atmospheric boundary layer conditions on VSLS abundances in the eastern tropical and subtropical North Atlantic Ocean

S. Fuhlbrügge[1], **K. Krüger**[1], **B. Quack**[1], **E. Atlas**[2], **H. Hepach**[1], **and F. Ziska**[1]

[1]GEOMAR Helmholtz-Zentrum für Ozeanforschung Kiel, Kiel, Germany
[2]Rosenstiel School for Marine and Atmospheric Sciences, Miami, Florida, USA

Correspondence to: K. Krüger (kkrueger@geomar.de)

Received: 20 November 2012 – Published in Atmos. Chem. Phys. Discuss.: 5 December 2012
Revised: 13 May 2013 – Accepted: 30 May 2013 – Published: 4 July 2013

Abstract. During the DRIVE (Diurnal and Regional Variability of Halogen Emissions) ship campaign we investigated the variability of the halogenated very short-lived substances (VSLS) bromoform ($CHBr_3$), dibromomethane (CH_2Br_2) and methyl iodide (CH_3I) in the marine atmospheric boundary layer in the eastern tropical and subtropical North Atlantic Ocean during May/June 2010. The highest VSLS mixing ratios were found near the Mauritanian coast and close to Lisbon (Portugal). With backward trajectories we identified predominantly air masses from the open North Atlantic with some coastal influence in the Mauritanian upwelling area, due to the prevailing NW winds. The maximum VSLS mixing ratios above the Mauritanian upwelling were 8.92 ppt for bromoform, 3.14 ppt for dibromomethane and 3.29 ppt for methyl iodide, with an observed maximum range of the daily mean up to 50 % for bromoform, 26 % for dibromomethane and 56 % for methyl iodide. The influence of various meteorological parameters – such as wind, surface air pressure, surface air and surface water temperature, humidity and marine atmospheric boundary layer (MABL) height – on VSLS concentrations and fluxes was investigated. The strongest relationship was found between the MABL height and bromoform, dibromomethane and methyl iodide abundances. Lowest MABL heights above the Mauritanian upwelling area coincide with highest VSLS mixing ratios and vice versa above the open ocean. Significant high anticorrelations confirm this relationship for the whole cruise. We conclude that especially above oceanic upwelling systems, in addition to sea–air fluxes, MABL height variations can influence atmospheric VSLS mixing ratios, occasionally leading to elevated atmospheric abundances. This may add to the postulated missing VSLS sources in the Mauritanian upwelling region (Quack et al., 2007).

1 Introduction

Natural halogenated very short-lived substances (VSLS) contribute significantly to the halogen content of the troposphere and lower stratosphere (WMO, 2011). On-going environmental changes such as increases in seawater temperature and nutrient supply, as well as decreasing pH, are expected to influence VSLS production in the ocean. Thus, the oceanic emissions of VSLS might change in the future and, in connection with an altering efficiency of the atmospheric upward transport, might lead to significant future changes of the halogen budget of the troposphere/lower stratosphere (Kloster et al., 2007; Pyle et al., 2007; Dessens et al., 2009; Schmittner et al., 2008; Montzka and Reimann, 2011), as well as changes to the tropospheric oxidation capacity (Hossaini et al., 2012). Within the group of brominated VSLS, bromoform ($CHBr_3$) and dibromomethane (CH_2Br_2) are the largest natural sources for bromine in the troposphere and stratosphere. In combination with iodine compounds (i.e. methyl iodide, CH_3I), they can alter tropospheric oxidation processes, including ozone depletion (Read et al., 2008). The VSLS have comparably short tropospheric lifetimes (days to months); however, they can be rapidly transported by deep convection, especially in the tropics, to the upper troposphere and lower stratosphere and contribute to ozone depletion there (Warwick et al., 2006; WMO, 2007, 2011; Tegtmeier et al., 2012, 2013). Previous studies have reported distinctive halocarbon emissions in tropical coastal and shelf water regions due to high biological productivity, i.e. by macro algae, seaweed and phytoplankton (Gschwend et al., 1985; Manley and Dastoor, 1988; Sturges et al., 1992; Moore and Tokarczyk, 1993; Carpenter and Liss, 2000; Quack et al., 2007). Elevated mixing ratios of the compounds have been found within the marine atmospheric boundary layer (MABL) around the Cape Verde Islands with a mean (range) for $CHBr_3$ of 8 (2.0–43.7) ppt, CH_2Br_2 of 2 (0.7–8.8) ppt and CH_3I of 3 (0.5–31.4) ppt (O'Brien et al., 2009) and in the area of the Mauritanian upwelling with a mean (range) of $CHBr_3$ around 6 (3–12) ppt (Carpenter et al., 2007; Quack et al., 2007) and CH_2Br_2 of 2.4 (1.75–3.44) ppt by Quack et al. (2007). These mean mixing ratios from the tropical Atlantic Ocean agree well with other tropical oceanic areas (e.g. Atlas et al., 1993; Butler et al., 2007). Quack et al. (2004) suggested regionally enhanced biogenic production in the water column of the Mauritanian upwelling and a high sea-to-air flux of VSLS to be responsible for elevated tropospheric VSLS mixing ratios in this region. However, Carpenter et al. (2007) and Quack et al. (2007) both pointed out that the marine boundary layer height, besides additional potential coastal sources, may affect the tropospheric VSLS mixing ratios as well. The theory of warm offshore air flowing over cool water and creating a stable internal boundary layer, as suggested by Garratt (1990), applies well in the area of the cold Mauritanian upwelling. Here, the sea surface roughness and near surface turbulence reduce each other over the water, while the flow leads to a collapse of turbulence and a very stable stratification of the lowermost atmosphere, as was observed by Vickers et al. (2001) at the coast of the United States and modelled by Skyllingstad et al. (2005).

In this study, we present first results from the DRIVE (Diurnal and Regional Variability of Halogen Emissions) ship campaign during May/June 2010, comprising high-resolution meteorological and VSLS measurements. We investigate the meteorological constraints on the VSLS abundances and whether the cold waters upwelled along the Mauritanian coast have a verifiable influence on the atmospheric boundary layer height and therefore on the mixing of air within the lowermost troposphere. The accompanying study by Hepach et al. (2013) investigates the VSLS sources in the ocean and the sea-to-air fluxes in detail.

This paper begins with a short overview of the meteorological conditions during the DRIVE cruise, followed by a data and method description (Sect. 2.1). In Sect. 3 we present results from the meteorological and VSLS measurements and the influence of meteorology and MABL height on the VSLS mixing ratios and emissions. Finally, a summary is given in Sect. 4.

2 Data and methods

2.1 Cruise overview

During May/June 2010 the DRIVE (P399/2-3) campaign examined the formation and emission of halocarbons and reactive inorganic halogen compounds in the eastern tropical and subtropical North Atlantic Ocean (Bange et al., 2011) as part of the SOPRAN (Surface Ocean Processes in the Anthropocene: www.sopran.pangaea.de) project. The main objectives are to investigate the diurnal and regional variability of marine short-lived substances, as well as oceanic influences on the atmosphere.

The ship expedition was carried out on board the German research vessel (R/V) *Poseidon*. The cruise itself was split into two legs: P399/2 (31 May–17 June 2010) from Las Palmas to Las Palmas and P399/3 (19–24 June 2010) from Las Palmas to Vigo, Spain. For diurnal observations, hourly VSLS measurements were performed at six 24 h stations during leg P399/2. Positions and times of the 24 h stations are given in Table 1. The location of the 24 h stations were chosen to cover the nutrient-rich coastal upwelling region near the Mauritanian coast as well as the nutrient-poor regions near the Cape Verde Islands. In addition, 21 atmospheric VSLS samples were taken during the return from the last station in the Mauritanian upwelling region to Las Palmas (Gran Canaria). During the transit leg P399/3, an additional 20 atmospheric air samples were taken. All VSLS measurements were also integrated into the HalOcAt database used for the Ziska et al. (2013) climatology.

2.2 Meteorology and MABL height

Meteorological data have been collected by the automatic on-board weather station of the German Weather Service (DWD): air and water temperatures, wind speed and direction, humidity and air pressure were recorded once per second and are averaged to 10 min means for our analysis. GRAW DFM-06 radiosondes (http://www.graw.de) were launched from the working deck of R/V *Poseidon* at about 3 m above sea level during the cruise to profile the atmospheric composition of air temperature (resolution: 0.1 °C; accuracy: <0.2 °C), relative humidity (resolution: 1 %; accuracy: <5 %), and wind (wind speed accuracy: $<0.2\,\mathrm{m\,s^{-1}}$; horizontal position accuracy: <5 m) (http://www.gematronik.com/fileadmin/media/pdf/GRAW-Brochure_V01.30_en.pdf) from the sea level up to the middle stratosphere (∼30 km altitude). At the 24 h stations, the launch frequency was increased from one radiosonde per day at 12:00 UTC to four per day at 00:00, 06:00, 12:00 and 18:00 UTC, amounting to 41 launches for the whole cruise.

The atmospheric boundary layer height is determined using the approaches summarized by Seibert et al. (2000). These methods include practical and theoretical

Table 1. 24 h stations: position and date.

24 h station	Position	Date/Time
1st	17.6° N, 24.0° W	3 June (23:00 UTC)–4 June 2010 (22:00 UTC)
2nd	18.0° N, 21.0° W	6 June (19:00 UTC)–7 June 2010 (17:00 UTC)
3th	18.0° N, 18.0° W	8 June (18:00 UTC)–9 June 2010 (17:00 UTC)
4th	18.5° N, 16.5° W	10 June (12:00 UTC)–11 June 2010 (11:00 UTC)
5th	19.0° N, 16.5° W	11 June (16:00 UTC)–12 June 2010 (15:00 UTC)
6th	20.0° N, 17.25° W	13 June (04:00 UTC)–14 June 2010 (03:00 UTC)

determinations from radiosoundings. The vertical extension of the boundary layer is in general limited aloft by a temperature inversion or a stable layer, or by a significant reduction in air moisture. Two general types of boundary layers exist, the convective boundary layer (CBL), whose stable layer is found between the lower 100 m of the atmosphere and about 3 km height, and the stable boundary layer (SBL), characterized by a surface inversion. In the case of a CBL, it is recommended to take the height of the base of the inversion, increased by half of the inversion layer depth (Stull, 1988). For a SBL we assume the absence of turbulence and vertical mixing (Garratt, 1990) and further declare that the boundary layer stays close to the surface. According to this, we subjectively determined the height of the boundary layer in our study from the temperature and humidity profiles, and additionally from the bulk Richardson number of the following equation (Troen and Mahrt, 1986; Vogelezang and Holtslag, 1996):

$$Ri_\mathrm{B} = \frac{gz(\theta_z - \theta_s)}{\theta_s(u^2 + v^2)}. \tag{1}$$

The quantities g and z are the gravitation acceleration and the geometric height. $\theta_z\theta_z$ and θ_s θ_s are the virtual potential temperature at the height z and at the surface, and u and v are the zonal and meridional wind components. The virtual potential temperature can be regarded as a stability criterion for the atmosphere, considering the air moisture. It is constant with height for neutral conditions, increases for stable conditions and decreases if the air is statically unstable. To identify the boundary layer height theoretically, a fixed critical bulk Richardson number of $Ri_\mathrm{c} = 0.25$ is chosen as a threshold, following Sorensen (1998), where $Ri_\mathrm{B} \geq Ri_\mathrm{c}$. Due to missing wind data in the lowermost atmosphere during a number of radiosonde launches (failure of GPS sensor), we were not always able to determine Ri_B for the lower boundary layer. Therefore we use the subjectively determined boundary layer height for our investigations and calculate Ri_B to confirm our determined MABL height.

2.3 Air mass origin

For the analysis of the air mass origin, HYSPLIT trajectories (http://ready.arl.noaa.gov/HYSPLIT.php), based on NCEP/NCAR Reanalysis 1 (NNR), were calculated online. The NNR is a first-generation reanalysis from 1948 to the present and has a horizontal resolution of 208 km (T62) and 28 vertical levels (L28) with a model top at about 3 hPa. The data are globally distributed on a 2.5° latitude × 2.5° longitude Gaussian grid with a total of 144 × 73 grid points (Kalnay et al., 1996; Kistler et al., 2001).

2.4 VSLS measurements

A total of 187 air samples were taken on the monkey deck of R/V *Poseidon*, about 10 m above sea level. The air was pressurized up to 2 standard atmospheres in pre-cleaned stainless steel canisters, each with a volume of 2.6 L. The canisters were analysed within three months after the expedition at the Rosenstiel School for Marine and Atmospheric Sciences (RSMAS, Miami, Florida). The stability of the atmospheric samples has been demonstrated during more than 10 years of work with stainless steel canisters. The compounds reported here are typically stable for at least 6 months or more. The precision is estimated as an uncertainty of approximately 5 %, obtained from the standard variability during analysis and from examination of multiple samples within the same air mass. The analysis of the gases is performed with gas chromatography/mass spectrometry (GC/MS), while the calibration gases are standardized by gas chromatography with an atomic emission detector (AED) (Schauffler et al., 1999), and the entire standardization procedure was additionally adjusted to the NOAA scale in order to have better comparability to the NOAA measurements at surface stations. The preparation of standard gases is described in Montzka et al. (2003).

Our study concentrates on the atmospheric abundances of three VSLS: methyl iodide with a lifetime of ∼4 days (Solomon et al., 1994), bromoform of ∼26 days (Ko et al., 2003) and dibromomethane of ∼120 days (Ko et al., 2003).

Samples for dissolved halocarbons in sea water were taken from the continuously working pump from the ship's moon pool at a depth of 5 m on a nearly hourly basis at every 24 h station. A purge and trap system attached to a gas chromatograph with mass spectrometric detection in single-ion mode was used for analysis of the samples with a precision within 10 % determined from duplicates (Hepach et al., 2013).

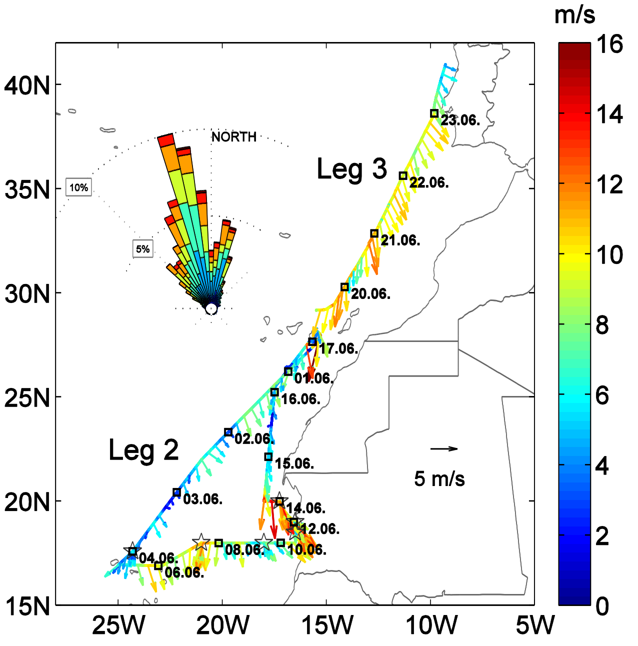

Fig. 1. DRIVE cruise track. In addition, the 3-hourly wind speed [$\mathrm{m\,s^{-1}}$], direction (10 min averages) and windrose for the whole cruise are shown.

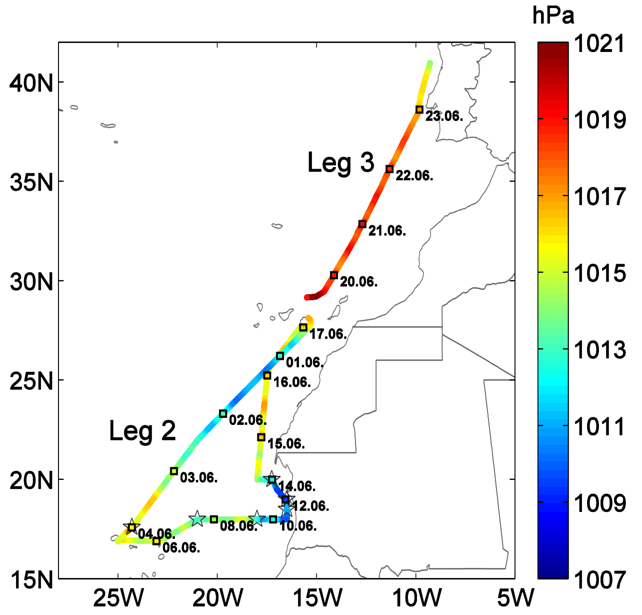

Fig. 2. 10 min average measurements of air pressure [hPa]. The stars indicate position and time of the diurnal stations.

2.5 Sea-to-air flux calculations

Sea-to-air fluxes (F) of methyl iodide, dibromomethane and bromoform were calculated with the air–sea gas transfer coefficient k_w and the air–sea concentration gradient Δc (Hepach et al., 2013):

$$F = k_w \cdot \Delta c \tag{2}$$

The parameterization of Nightingale et al. (2000), based on instantaneous wind speeds (10 min averages) and temperature-dependent Schmidt numbers according to Quack and Wallace (2003), was applied to determine k_w. Δc was calculated from the simultaneous water and air measurements at the 24 h stations.

3 Results

3.1 Meteorology

The cruise was mainly exposed to moderate weather conditions. Contrary to the climatological wind direction of northeasterly trade winds in the subtropics and westerlies north of 30° N during May/June, the mean absolute wind direction was NNW (Fig. 1) with a mean direction of 349° during leg 2 and 344° during leg 3. This caused a predominant influence of air masses with marine background conditions coming from the open North Atlantic Ocean. The mean wind speed during the whole cruise was moderate to fresh for both legs, with $7.4\,\mathrm{m\,s^{-1}} \pm 2.9\,\mathrm{m\,s^{-1}}$ during leg 2 and $9.3\,\mathrm{m\,s^{-1}} \pm 1.6\,\mathrm{m\,s^{-1}}$ during leg 3. The total air pressure difference of 13.4 hPa also reflects the moderate and steady weather conditions during the whole cruise with a minimum of 1007.6 hPa on 11 June 2010 close to the Mauritanian coast and a maximum air pressure of 1021 hPa at the beginning of leg 3 on 19 June 2010 close to the Canary Islands (Fig. 2). In addition, typical tropical diurnal variations up to 4 hPa (see also Krüger and Quack, 2012) due to atmospheric tides were observed in this study. The time series of 10 min average measured surface air temperature (T_{SAT}), sea surface temperatures (T_{SST}) and the difference ΔT (T_{SAT}–T_{SST}) are shown in Fig. 3. The temperature difference is related to the heat flux between atmosphere and ocean and indicates suppressing of convection, turbulence and therefore mixing within the boundary layer for a positive temperature difference (positive heat flux) and enhanced mixing for negative heat flux. As the ship cruise started to the south, the air and water temperatures increased until the maximum air temperature of 25.8 °C was recorded directly after the stop at Mindelo (Cape Verde Islands). On 11 June 2010, right after the 4th 24 h station, the ship reached the Mauritanian upwelling region at 18.75° N, 16.5° W. This is noticeable from the abrupt decrease in the water temperature and connected to an increase of the heat flux from the atmosphere to the ocean. After one day, the air temperature also drops, until T_{SAT} and T_{SST} stabilize between 18 °C and 20 °C (station 5). On 14 June 2010, after the ship has left the last 24 h station, the water temperature increases to about 23.5 °C. This increase coincides with a wind speed maximum of about $16\,\mathrm{m\,s^{-1}}$ from the north, indicating transport of water masses from outside the Mauritanian upwelling

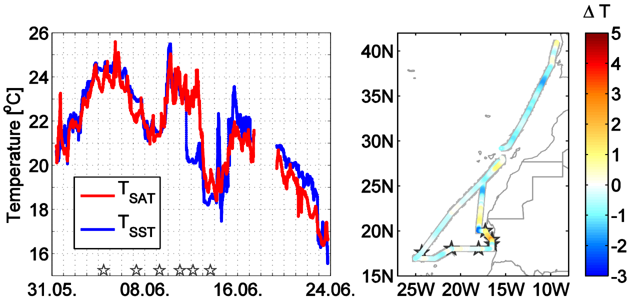

Fig. 3. Left: 10 min average measurements of T_{SAT} and T_{SST} [°C]. The stars indicate position and time of the diurnal stations. Right: the temperature gradient is given in [K].

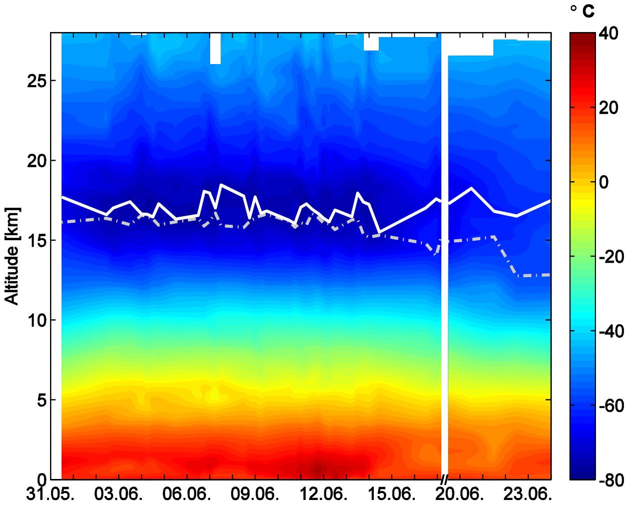

Fig. 4. Air temperature cross sections [°C] from radiosoundings for the whole cruise. Cold point tropopause and lapse rate tropopause are marked by the continuous and the dash-dotted lines, respectively. The measurement gap between leg 2 and 3 is shortened.

towards the ship, until the water temperature drops again to about 18 °C. On 15 June 2010 the ship left the Mauritanian upwelling region, indicated by increasing air and water temperatures until both decreased again while heading northward. A sudden decrease of the water temperature is also observed from 23 to 24 June 2010, as the ship enters the Iberian upwelling (Relvas and Barton, 2002).

3.1.1 Marine atmospheric boundary layer

In the following, we use the radiosonde measurements to analyse the state of the lower atmosphere. Profiles of air temperature along the cruise track are shown in Fig. 4. Lowest temperatures of −80 °C are observed between 2 and 15 June 2010 at 17 km height, indicating tropical air masses south of 25° N during leg 2. Two different tropopause definitions are used to identify the transition between tropical and extra-tropical air masses: the cold point tropopause (CPT; Highwood and Hoskins, 1998) and the lapse rate tropopause (LRT, WMO, 1957). During leg 2, the heights of the CPT and LRT are detected between 16 and 17 km altitude. A change of the atmospheric regime is reflected by the decrease of the LRT height to 15 km in contrast to the CPT height after 15 June 2010 at the end of leg 2, as the ship enters the extratropics. The air temperature profiles also reveal typical "trade inversions" (Neiburger et al., 1961) between 1 and 2 km height from the beginning of the cruise until 4 June and from 16 June 2010 until the end of the cruise. Beginning on 4 June 2010, the temperature inversions descend in height, until they migrate, due to cold upwelling deep water (Fig. 3) in the Mauritanian upwelling, to intense surface inversions. The neutral and stable stratification within the lower 3 km of the troposphere, and therefore the upper limit of the atmospheric boundary layer during the cruise, is shown by Fig. 5. The subjectively and theoretically derived MABL heights (see Sect. 2.2) show a good agreement with each other. Differences are found above the Mauritanian upwelling, due to missing near-surface winds for the calculation of the bulk Richardson number, but also at the end of leg 2 and the beginning of leg 3. This may be caused by our fixed Ri_{c}, which we took for convenience.

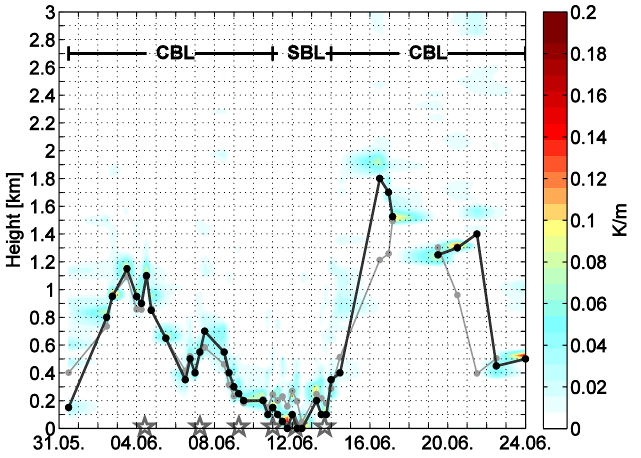

Fig. 5. Virtual potential temperature gradient (colour shading) with derived MABL heights (lines, in km). The black line shows the subjectively determined MABL height from temperature and humidity profiles, and the grey line is determined theoretically (Sect. 2.2). CBL and SBL identify convective and stable boundary layers. The 24 h stations are marked with stars.

Except for the area at and south of the upwelling, observed from 11 to 14 June 2010, where we observed a SBL, the cruise was predominantly characterized by CBLs, without distinct short time or diurnal variations, considering the launch frequencies. Boundary layer heights from the surface up to 400 m at the upwelling area and about 400–2000 m above the open ocean agree with heights derived from trajectory models from previous studies along the Mauritanian coast (Carpenter et al., 2007; Quack et al., 2007). During

Table 2. Observed mixing ratios [in ppt] of bromoform ($CHBr_3$), dibromomethane (CH_2Br_2), their ratio and methyl iodide (CH_3I) for the whole cruise, open ocean (leg 2 except stations 3–6, and leg 3) and coastal stations (stations 3–6). Given are the mean, the range and the standard deviation values.

	$CHBr_3$ (ppt)		CH_2Br_2 (ppt)		$\frac{CH_2Br_2}{CHBr_3}$	CH_3I (ppt)	
	Mean (range)	stdv of mean	Mean (range)	stdv of mean	Mean	Mean (range)	stdv of mean
Whole cruise	3.75 (0.48–9.9)	2.29	1.85 (0.89–3.14)	0.63	0.69	1.25 (0.51–3.29)	0.56
Open ocean	1.74 (0.48–9.9)	1.34	1.28 (0.89–2.70)	0.31	0.98	0.93 (0.51–2.11)	0.24
Coastal stations	5.60 (4.07–8.92)	1.06	2.37 (1.87–3.14)	0.31	0.43	1.55 (0.90–3.29)	0.62

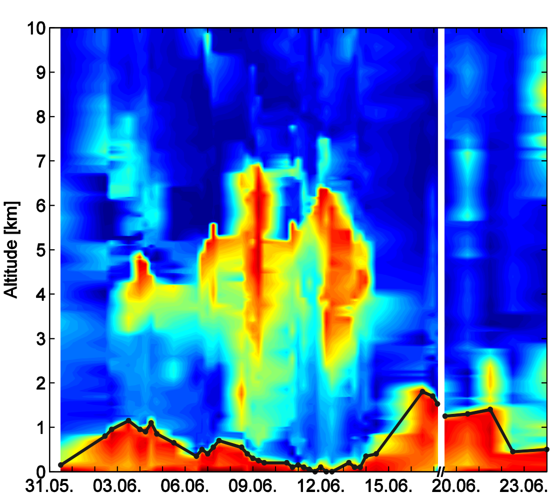

Fig. 6. Relative humidity cross sections [%] from radiosoundings for the whole cruise. The subjectively determined MABL height [km] is marked by the black line. The measurement gap between leg 2 and 3 is shortened.

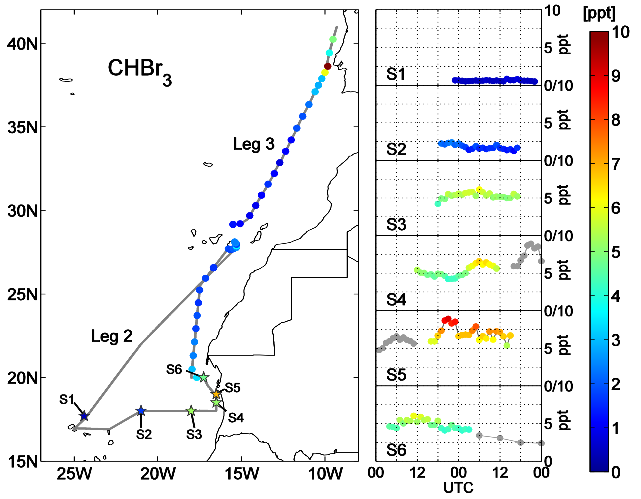

Fig. 7. Bromoform mixing ratios [ppt] measured during the DRIVE ship campaign from 31 May to 24 June 2010. Six 24 h stations (S1–S6) and measurements during transit are colour-coded according to the scale on the right side.

leg 3 the top of the boundary layer decreases from 1.4 km north of the Canary Islands to about 500 m near the coast of the Iberian Peninsula. The height of the MABL is also well reflected in the profiles of the relative humidity during the whole cruise as shown in Fig. 6. The increase of the surface/lowermost troposphere humidity between 15 and 22 June 2010 (Fig. 6) matches the observed elevation of the negative heat flux (Fig. 3). The height of the atmospheric boundary layer, determined from temperature observations, agrees very well with the surface maximum of relative humidity (Fig. 6). The vertical mixing within the MABL seems to be quite well reflected by the relative humidity observations. Especially the small extension of enhanced relative humidity above the surface of the Mauritanian upwelling from 11 to 12 June 2010 is consistent with the assumption of reduced vertical mixing (turbulence) in this area due to the positive heat flux, leading to a very stable and narrow MABL.

3.2 Atmospheric VSLS variability

The diurnal and regional variations of halogenated trace gas abundances in the MABL have been observed with hourly measurements at six 24 h stations near the Cape Verde Islands and in the Mauritanian upwelling. According to the regional distribution of the diurnal stations (Fig. 1), the first two stations (S1, S2) can be combined to an open ocean cluster. The following 4 diurnal stations are furthermore declared as coastal stations (S3–S6), since they show similar physical and biological characteristics (e.g. salinity and chlorophyll *a*) in the surface water (Hepach et al., 2013). Six-hourly measurements were also taken from 14 June 2010 after the 6th station to the coast of Gran Canaria and during leg 3 (19–23 June 2010). Also along the coast of Gran Canaria (17 June 2010) hourly samples were taken.

An increase of atmospheric mixing ratios from the Cape Verde Islands to the Mauritanian upwelling area is found for all three trace gases: bromoform (Fig. 7), dibromomethane (Fig. 8) and methyl iodide (Fig. 9). Within the open ocean cluster, the mixing ratios ranged 0.48–9.9 ppt

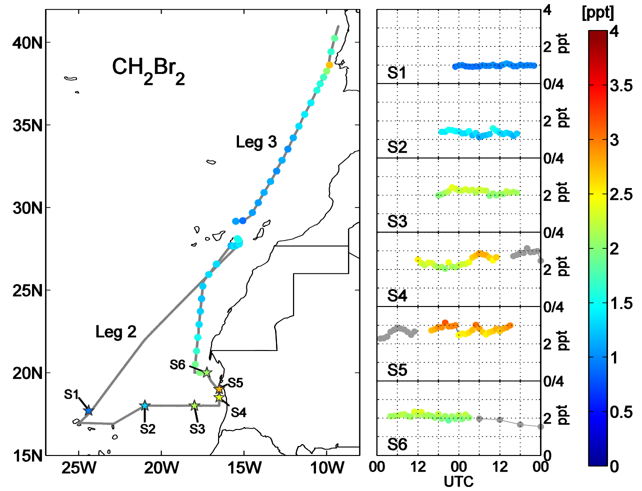

Fig. 8. Dibromomethane mixing ratios [ppt] measured during the DRIVE ship campaign from 31 May to 24 June 2010. Six 24 h stations (S1–S6) and measurements during transit are colour-coded according to the scale on the right side.

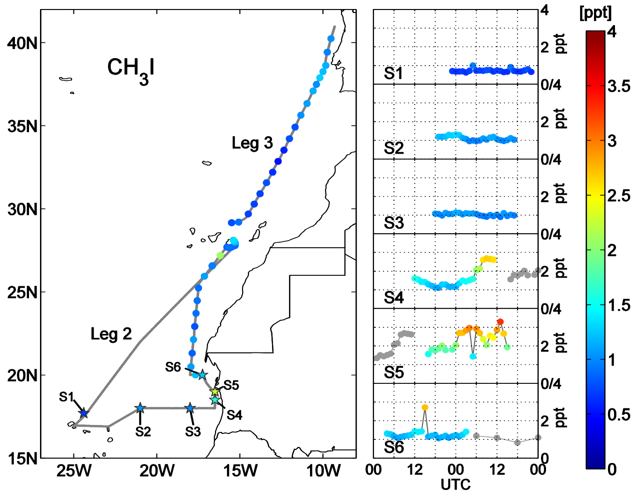

Fig. 9. Methyl iodide mixing ratios [ppt] measured during the DRIVE ship campaign from 31 May to 24 June 2010. Six 24 h stations (S1–S6) and measurements during transit are colour-coded according to the scale on the right side.

with a mean of 1.74 ppt for $CHBr_3$, 0.91–1.59 ppt with a mean of 1.28 ppt for CH_2Br_2, and 0.63–1.32 ppt with a mean of 0.93 ppt for CH_3I. The mixing ratio of CH_2Br_2 and $CHBr_3$ has often been observed to be around 0.1 in source areas, where the air has been influenced e.g. by fresh coastal emissions (Yokouchi, 2005 and references therein). The ratio increases towards the open ocean due to the different lifetimes of both compounds. A higher value implies an aged air mass and aged emission, while a lower value indicates fresher emissions and air masses. With an overall mean CH_2Br_2 / $CHBr_3$ ratio of 1.21 (Table 2) during stations 1 and 2, typical open ocean air masses were observed (Quack et al., 2004; Butler et al., 2007). At the third 24 h station, the bromocarbons increase to 4.22–6.12 ppt for $CHBr_3$ and 1.96–2.42 ppt for CH_2Br_2, while CH_3I mixing ratios remain at open ocean values. A mean CH_2Br_2 / $CHBr_3$ ratio of 0.41 now indicates fresher emissions. Slightly increased atmospheric mixing ratios of $CHBr_3$ with 4.21–6.58 ppt and of CH_2Br_2 with 2.04–2.87 ppt, and a CH_2Br_2 / $CHBr_3$ ratio of 0.46 are found at the 4th 24 h station. For the first time, the CH_3I mixing ratios show intense variations of 1.11–2.68 ppt at this coastal station. In addition, a diurnal pattern is striking for all three VSLS at this station (S4, Fig. 7). They show a slight decrease from 12:00 UTC to 00:00 UTC followed by an increase from 06:00 UTC to 09:00 UTC on the following day, which coincides with a decrease of the MABL height and the sunrise at about 06:30 UTC. The highest atmospheric mixing ratios for all three VSLS during leg 2 were observed during the 5th station at 19° N and 16.5° W. At this station also the most pronounced variations within one day are observed, with maximum mixing ratios of 8.92 ppt for $CHBr_3$, 3.14 ppt for CH_2Br_2 and 3.29 ppt for CH_3I. The extreme minimum of CH_3I at 05:00 UTC appears as an unreliable outlier due to the high variation of more than 1 ppt within two hours, which is nearly consistent with the whole diurnal variation of CH_3I at station 4. Although this station has the lowest CH_2Br_2 / $CHBr_3$ ratio of 0.40 during leg 2, this value is two to three times higher than previously reported ratios of 0.1–0.25 for coastal source regions in the North Atlantic Ocean and the northwest of Tasmania (Carpenter et al., 2003) and tropical islands and the open Pacific Ocean (Yokouchi et al., 2005), suggesting the presence of slightly aged air masses and emissions. While the ship moved away from the Mauritanian coast, southwest of the Banc d'Arguin National Park, the last coastal station (S6) shows an increase of the CH_2Br_2 / $CHBr_3$ ratio to 0.44 and a decrease of the trace gas mixing ratios to 4.85 ppt (range: 4.07–6.01 ppt) for bromoform, 2.11 ppt (1.87–2.34 ppt) for dibromomethane and 1.28 ppt (1.07–2.71 ppt) for methyl iodide. The extreme CH_3I maximum at 15:00 UTC appears again as an outlier. A further decrease of the atmospheric abundances is observed up to 22° N. Mixing ratios thereafter remain nearly constant to the Canary Islands, except for methyl iodide, which shows a maximum of 2 ppt southwest of Gran Canaria. Minor variations occur for all three VSLS at the Canarian coast, while the means of 2.29 ppt $CHBr_3$, 1.38 ppt CH_2Br_2 and 1.14 ppt CH_3I are in agreement with open ocean values and remain at this level until 35° N. An increase of the brominated halocarbons is observed as the cruise approaches the Portuguese coast. While dibromomethane only reaches 2.70 ppt, bromoform reaches the highest mixing ratio of 9.9 ppt during the whole DRIVE cruise close to Lisbon (Portugal), leading to a ratio of both compounds of 0.27. Raimund et al. (2011) related the increased abundances of halogenated trace gases in the Iberian upwelling system to strong intertidal coastal

Table 3. Correlation coefficients of bromoform ($CHBr_3$), dibromomethane (CH_2Br_2) and methyl iodide (CH_3I) mixing ratios with wind speed (w_{spd}), wind direction (w_{dir}), surface air pressure (p), surface air temperature (T_{SAT}), sea surface temperature (T_{SST}), temperature difference ($\Delta T = T_{SAT} - T_{SST}$), relative humidity ($U$), and MABL height. Whole cruise (leg 2 and 3) includes $n = 181$ samples for all parameters except MABL height (30 samples), open ocean (leg 2, except stations 3–6 and leg 3) includes $n = 85$ samples for all parameters except MABL height (15 samples) and coastal stations (stations 3–6) include $n = 96$ samples for all parameters except MABL height (15 samples). Bold coefficients have a p value of less than 5 %.

	$CHBr_3$			CH_2Br_2			CH_3I		
	Whole cruise	Open ocean	Coastal stations	Whole cruise	Open ocean	Coastal stations	Whole cruise	Open ocean	Coastal stations
w_{spd}	**0.23**	**0.23**	−0.17	**0.27**	**0.32**	−0.05	**0.24**	**0.37**	0.06
w_{dir}	**−0.49**	**−0.31**	0.04	**−0.52**	**−0.32**	−0.18	**−0.28**	−0.12	−0.01
p	**−0.76**	−0.01	**−0.53**	**−0.82**	−0.11	**−0.71**	**−0.64**	**−0.33**	**−0.52**
T_{SAT}	−0.04	**−0.68**	**0.42**	0.05	**−0.67**	**0.59**	**0.24**	**−0.26**	**0.48**
T_{SST}	**−0.45**	**−0.70**	−0.04	**−0.39**	**−0.69**	0.13	**−0.21**	**−0.24**	0.00
ΔT	**0.70**	0.17	**0.64**	**0.71**	0.18	**0.63**	**0.73**	−0.13	**0.68**
U	**0.52**	**0.47**	−0.16	**0.50**	**0.58**	**−0.32**	**0.21**	**0.50**	**−0.38**
MABL	**−0.81**	−0.32	**−0.60**	**−0.82**	−0.40	**−0.62**	**−0.64**	**−0.58**	**−0.70**

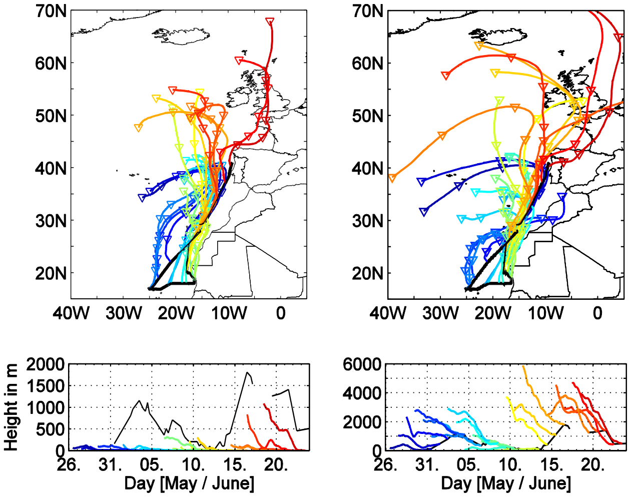

Fig. 10. HYSPLIT 5-day backward trajectories: initiated at the surface (left side) and at the top of the determined marine atmospheric boundary layer (right side) each day at 12:00 UTC. The colours of the trajectories indicate the time when the specific trajectory reached the ships position, e.g. blue at the beginning and red at the end of the cruise. The upper plots show the horizontal and the lower plots the vertical distribution of the trajectories. The black line indicates the height of the MABL. Trajectory and MABL heights are given in [m].

sources and advection of halocarbon-enriched coastal upwelling, but also anthropogenic sources as river outflow are likely (Quack and Wallace, 2003).

3.2.1 Air mass origin

Investigating the air mass history is a good way to reveal potential source regions (Fig. 10). Surface (STs) and boundary layer height trajectories (BLTs) indicate primarily northerly origin of air masses during the cruise. From 31 May to 3 June 2010 the air masses mainly arrive from the Azores. While the HYSPLIT model projects that the STs do not extend 100 m altitude, the BLTs arise from about 3 km height with little Moroccan influence. A high-pressure system, located between the Azores and the coast of Portugal, deflects the air masses up to 40° N–50° N, close to the coast of Portugal, and redirects, in combination with the trade winds, the air southwards to the ship. From 6 to 17 June 2010 the light blue, yellow and orange trajectories show a more varying origin, between 30° N and 60° N. Most of the STs descend from heights up to 300 m to the surface 1–2 days before hitting the ship. This air mass descent is typical for a high-pressure system. Reaching the ground, the surface inversions, as described in Sect. 3.1.1, prevent the air masses from ascending. The resulting stable, isolated and very low boundary layer leads to similar origins of offshore STs and BLTs. In the area of the Mauritanian upwelling, from 10 to 15 June 2010, the trajectories also pass the west coast of Mauritania and the western part of West Sahara within the last 24 h; however, the air approaches predominantly from the North Atlantic Ocean between 45° N and 60° N and west of Great Britain. These origins have also been observed in previous measurement campaigns (Quack et al., 2007; Carpenter et al., 2010). In comparison, the BLTs are spatially more widespread over the North Atlantic Ocean, indicating the higher wind speed in the free troposphere. At leg 3 the STs and BLTs have a mid- to polar latitude origin (30° N to 80° N); however, continental influences from northern Europe dominate for the BLTs east of the prime meridian.

3.3 Meteorological constraints on VSLS variability

To distinguish meteorological constraints on the VSLS abundances we correlate meteorological parameters with bromoform, dibromomethane and methyl iodide (Table 3). In the following we highlight the significant correlations. We find a weak but significant correlation between the trace gas abundances and the wind speed for the open ocean and for the whole cruise. In contrast, the wind direction reveals an overall anti-correlation of −0.5 for the brominated halocarbons and −0.3 for methyl iodide. This means increased VSLS abundances generally coincide with a westerly wind component and reduced abundances coincide with an easterly wind component during the whole cruise. To evaluate land–sea breeze constraints on the trace gas abundances, we take a look to stations 4 and 5. Indeed, both stations show typical land-sea breeze caused diurnal variations in wind speed and direction. The atmospheric abundances reveal significant high correlations of $r = 0.82$ for bromoform, $r = 0.73$ for dibromomethane and 0.82 for methyl iodide with the wind direction at station 4 in contrast to the overall anti-correlation (not shown here). At the 4th station, trace gas abundances increase with an increasing easterly component of the wind, while the abundances decrease with an increasing westerly wind component, related to differences in air mass origin (coastal versus open ocean), as also shown by the trajectories in Fig. 10. At the 5th station, 3-hourly trajectory calculations reveal ground-level air masses with potential coastal and anthropogenic influence along the coast of Western Sahara, with air masses from the open ocean leading to an increase of the dibromomethane abundances ($r = -0.55$) in contrast to the variations of bromoform and methyl iodide, which seem more related to local sources (not shown here). Anti-correlations of −0.6 to −0.8 are also found between the air pressure and the trace gases, caused by predominantly higher pressures at higher latitudes, and over open ocean, with lower VSLS abundances and vice versa for the coastal stations 3–6. At these stations, the anti-correlation is further dominated by the atmospheric tides of the air pressure and amounts to −0.5 for bromoform and methyl iodide and even −0.7 for dibromomethane. Whether or not this relation between the 12-hourly oscillations of sea level pressure and the trace gas variations can be generalized should be investigated in more detail in a future study. The relative humidity correlates with the trace gases in the open ocean with $r = 0.5$ to 0.6 and at the coastal stations with $r = -0.2$ to −0.4 (Table 3). The vertical distribution of the relative humidity has been a good indicator for mixing in and thickness of the MABL (Sect. 3.1.1), which may point to an additional correlation between the surface relative humidity and the VSLS abundances reflected by the high correlation for the whole cruise. However, over the upwelling areas this relationship does not hold. The cold upwelling water creates a positive ΔT and a negative sensible heat flux that suppresses convection and leads to a low relative humidity, which is in contrast to the VSLS abundances. This would explain the reversed correlation above the upwelling. The VSLS abundances are significantly anti-correlated with SAT and SST variations in the open ocean and correlated with SAT in the coastal upwelling. The sensible heat flux, reflected by the temperature difference ΔT (T_{SAT}–T_{SST}), correlates with r values of at least 0.7 for all trace gases during the whole cruise and at least 0.6 at the coastal stations. The combination of higher air and lower water temperatures coincides with increased trace gas abundances and vice versa, although this is inappropriate for evaporation. This shows that from surface relative humidity one cannot simply infer VSLS abundances or even the MABL height. The temperature difference ΔT further affects the atmospheric stability near the surface. The cold upwelling water at the Mauritanian upwelling converges with warm air from the African coast (Sect. 3.2.1) and creates a negative sensible heat flux between air and water, which cools the near-surface air layer. As a result, surface inversions, or at least a stable stratification of the lower atmosphere, are formed, which suppresses the vertical movement of air. The resulting reduced volume of air that is available for mixing leads to a low MABL height. An anti-correlation of −0.74 between ΔT and the MABL height at the coastal stations confirms this (not shown here). A comparison of bromoform, dibromomethane and methyl iodide with the MABL height during the whole cruise is shown in Fig. 11. Higher VSLS concentrations obviously coincide with a lower MABL height and vice versa. During leg 2 the highest mixing ratios are observed while the MABL height stays between the surface and 500 m in the area of the Mauritanian upwelling (stations 3–6). On the other hand, low mixing ratios measured over the open ocean coincide with a high boundary layer top. The transit towards Vigo (Spain) also shows a decrease of the MABL height and an increase of the three VSLS mixing ratios close to the Iberian coast. In contrast to the other meteorological parameters we derive anti-correlations between the atmospheric trace gas abundances and the MABL height for all regions, reflecting the distinct connection between these variables. The linear correlations of bromoform, dibromomethane and methyl iodide with the MABL height for the whole cruise are represented in Fig. 12a–c. Bromoform, with $r = -0.81$, and dibromomethane, with $r = -0.82$, show the

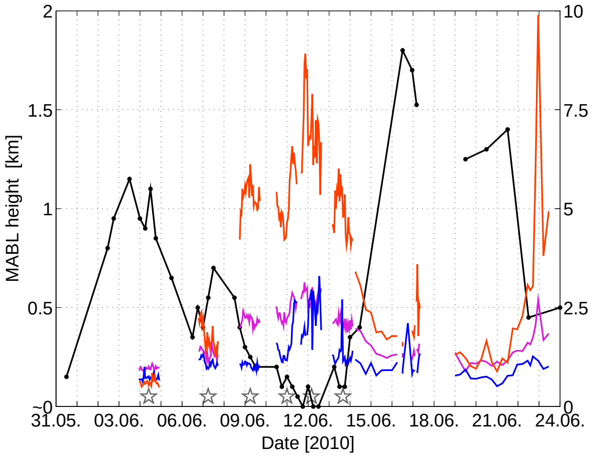

Fig. 11. Comparison of MABL height (left scale, in km) with bromoform, dibromomethane and methyl iodide mixing ratios (right scale, in ppt).

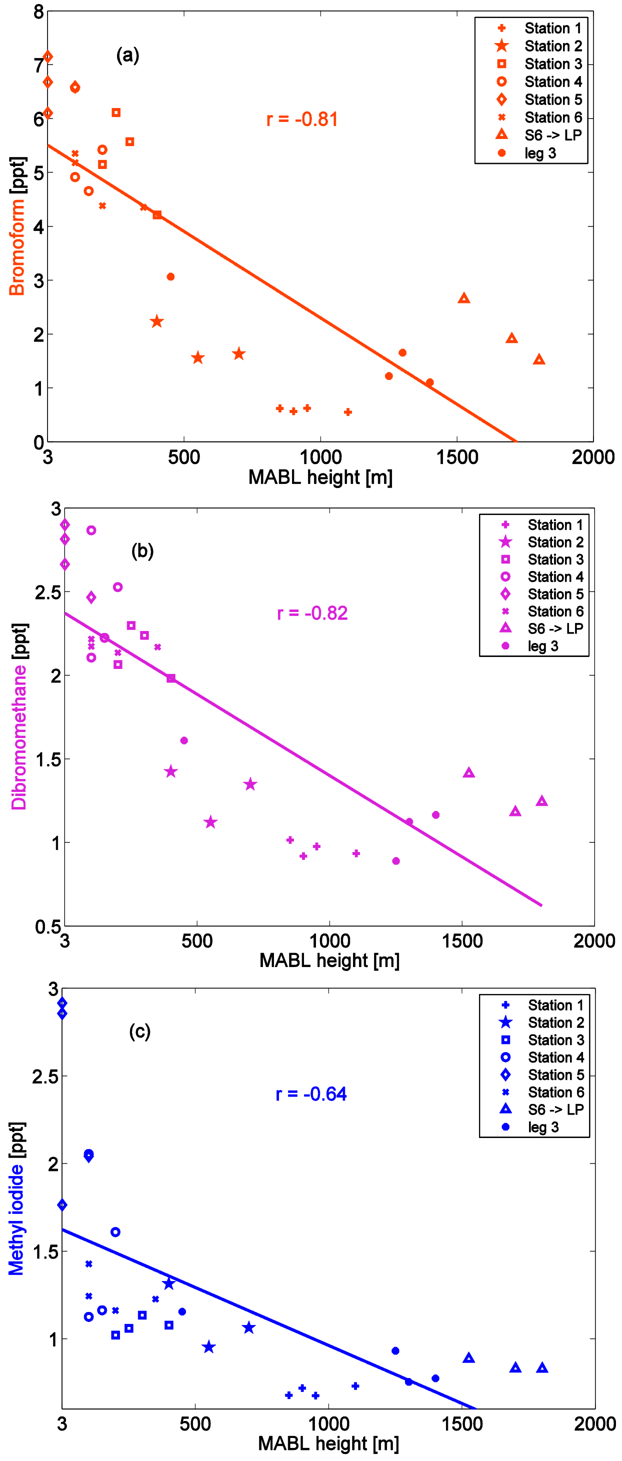

Fig. 12. Correlation between MABL height [m] and **(a)** bromoform, **(b)** dibromomethane and **(c)** methyl iodide abundances [ppt] for the whole cruise. The different markers reflect the different locations: leg 2 including stations 1–6, the transit between station 6 and Las Palmas, and leg 3. The according p values are less than 1 % for all three correlations, with each including 30 samples.

highest anti-correlations. Although the anti-correlation of methyl iodide, $r = -0.64$, is not as high as for the brominated halocarbons, it is significant at the 99 % level.

3.4 Correlations of meteorological parameters and atmospheric abundances with VSLS fluxes

The sea-to-air fluxes, which are calculated depending on wind speed and the concentration gradient Δc between sea water and air (Sect. 2.1), show significant correlations with wind speed and anti-correlations with MABL height (Table 4). The inverse relationship of atmospheric VSLS to MABL height as described in Sect. 3.3 should lead to lower sea-to-air fluxes, F, as lower MABL heights lead to higher atmospheric mixing ratios, decreasing the concentration gradient, Δc (Eq. 2). However, higher sea-to-air fluxes are observed in the lower MABL height areas for dibromomethane and bromoform, with an accordingly positive relationship of F to ΔT (Table 4). This is due to elevated sea water production of brominated VSLS in the cold waters, leading to a large increase in the concentration gradient, which masks the flux suppression by the higher atmospheric mixing ratios (Hepach et al., 2013). Also the elevated atmospheric mixing ratios of methyl iodide have no effect on the fluxes, because methyl iodide is strongly supersaturated in the sea surface water throughout the entire cruise. On the other hand, the observed sea-to-air fluxes reveal correlations with the atmospheric VSLS abundances (Table 5), showing that MABL height and sea-to-air fluxes in combination add to the VSLS variations in the atmosphere. The detailed analysis of the sea-to-air fluxes, their driving factors, such as the sea water concentrations, and their influences on the atmospheric VSLS abundances are discussed in detail in Hepach et al. (2013).

4 Summary

The diurnal and regional variability of atmospheric VSLS has been investigated during the DRIVE ship campaign in May/June 2010 in the eastern tropical and subtropical North Atlantic Ocean. Additionally, we analyse meteorological influences on the observed VSLS mixing ratios using simultaneous high-resolution data. VSLS measurements were conducted hourly at six 24 h stations and during passage from the coast of Mauritania to Vigo (Spain), resulting in a total of 187 atmospheric VSLS measurements during DRIVE. We concentrated our investigation on three trace gases: bromoform, dibromomethane and methyl iodide. Higher mean VSLS mixing ratios were found over the Mauritanian upwelling region (5.60 ppt, 2.37 ppt and 1.50 ppt for bromoform, dibromomethane and methyl iodide, respectively) than over the open ocean (1.74 ppt, 1.28 ppt and 0.93 ppt for bromoform, dibromomethane and methyl iodide, respectively). The upwelling region also shows diurnal variations of the VSLS with highest fluctuations between maximum and minimum

Table 4. Correlation coefficients of bromoform ($CHBr_3$), dibromomethane (CH_2Br_2) and methyl iodide (CH_3I) fluxes with wind speed (w_{spd}), wind direction (w_{dir}), surface air pressure (p), surface air temperature (T_{SAT}), sea surface temperature (T_{SST}), temperature difference ($\Delta T = T_{SAT} - T_{SST}$), relative humidity ($U$), and MABL height. Whole cruise (leg 2 and 3) includes $n = 109$ samples for all parameters except MABL height (21 samples), open ocean (leg 2 except stations 3–6 and leg 3) includes $n = 37$ samples for all parameters except MABL height (8 samples) and coastal stations (stations 3–6) include $n = 70$ samples for all parameters except MABL height (13 samples). Bold coefficients have a p value of less than 5 %.

	$CHBr_3$ flux			CH_2Br_2 flux			CH_3I flux		
	Whole cruise	Open ocean	Coastal stations	Whole cruise	Open ocean	Coastal stations	Whole cruise	Open ocean	Coastal stations
w_{spd}	**0.37**	0.19	**0.48**	**0.54**	**0.84**	**0.71**	**0.54**	**0.52**	**0.61**
w_{dir}	−**0.37**	0	0.06	−**0.51**	0.09	−0.13	0.07	−0.04	0.07
p	−**0.67**	−0.10	−**0.57**	−**0.81**	−**0.71**	−**0.73**	−0.08	−0.30	−0.14
T_{SAT}	−0.08	−0.13	0.15	−0.06	−**0.75**	**0.27**	−**0.20**	−**0.4**	−0.21
T_{SST}	−**0.54**	−0.29	−**0.31**	−**0.51**	−**0.84**	−0.17	−**0.24**	−**0.55**	−**0.36**
ΔT	**0.76**	**0.35**	**0.67**	**0.75**	−0.15	**0.63**	0.12	0.18	0.22
U	−0.04	−0.14	−**0.43**	−0.02	**0.65**	−**0.61**	−0.08	0.21	−**0.27**
MABL	−0.58	0.26	−**0.58**	−**0.68**	−**0.93**	−**0.68**	−0.27	−0.12	−**0.59**

Table 5. Correlation coefficients of bromoform ($CHBr_3$), dibromomethane (CH_2Br_2) and methyl iodide (CH_3I) fluxes with according mixing ratios. Whole cruise (leg 2 and 3) includes $n = 109$ samples, open ocean (leg 2 except stations 3–6 and leg 3) includes $n = 37$ samples and coastal stations (stations 3–6) include $n = 70$ samples. Bold coefficients have a p value of less than 5 %.

	$CHBr_3$ flux			CH_2Br_2 flux			CH_3I flux		
	Whole cruise	Open ocean	Coastal stations	Whole cruise	Open ocean	Coastal stations	Whole cruise	Open ocean	Coastal stations
$CHBr_3$ mixing ratio	**0.58**	−0.20	**0.33**	**0.68**	**0.60**	**0.39**	−0.08	0.22	−0.16
CH_2Br_2 mixing ratio	**0.61**	−0.05	**0.40**	**0.71**	**0.56**	**0.49**	−0.04	**0.33**	−0.08
CH_3I mixing ratio	**0.62**	−0.09	**0.50**	**0.66**	**0.62**	**0.51**	0.09	0.21	0.12

of 3.57 ppt for bromoform, 0.83 ppt for dibromomethane and 1.85 ppt for methyl iodide. A strong coastal gradient of the VSLS is also observed towards Lisbon (Portugal), where we detect the highest bromoform mixing ratio of the whole cruise of 9.8 ppt.

The air mass origin is investigated by 5-day backward trajectories starting at the surface and at the top of the determined marine atmospheric boundary layer. We identify a predominantly North Atlantic origin of the air due to the prevailing NW winds during the whole cruise, with minor coastal influence at the Mauritanian upwelling area.

To distinguish atmospheric constraints on the VSLS we compare several meteorological parameters with the trace gas abundances. Although we do not find an overall relationship with the wind, we detect a significant correlation between VSLS abundance and easterly wind direction changes ($r > 0.7$) at the 4th station, northwest of Nouakchott (Mauritania), which is linked to land–sea breeze influence. We find a strong anti-correlation between air–sea surface temperature difference and MABL height, derived from radiosoundings. The MABL heights are dependent on the location, as we determine heights from surface level to only 400 m in the upwelling region and between 400 and 1700 m over the open ocean. In the Mauritanian upwelling a stable boundary layer leads to stable atmospheric conditions near the surface, due to warm air flowing over cold upwelling water, suppressing the mixing of air. In the open ocean part of the cruise, the top of the MABL is limited by trade inversions. Overall a significant anti-correlation between the VSLS mixing ratios and the marine atmospheric boundary layer height is found. With correlation coefficients of $r = -0.81$ for bromoform, $r = -0.82$ for dibromomethane and $r = -0.64$ for methyl iodide, the MABL height appears to have a significant influence on the trace gas mixing ratios. This relationship may help explain observed events in the tropical eastern Atlantic with increased atmospheric VSLS mixing ratios in the Mauritanian upwelling. Whether this influence can also be found in different seasons or other oceanic regions should be addressed in future studies. Of particular interest would be to investigate other oceanic upwelling regions, which are expected to also have high VSLS sources as the Mauritanian upwelling/Cape Verde Islands region does.

Acknowledgements. We thank the authorities of Cape Verde, Mauritania, Portugal and Spain for the permissions to work in their territorial waters. We acknowledge the NOAA Air Resources Laboratory (ARL) for the provision of NCEP reanalysis data and the HYSPLIT transport and dispersion model used in this publication. We thank S. Tegtmeier for helpful comments and M. Toohey for proofreading. We acknowledge the support of the captain and crew of R/V *Poseidon* as well as Hermann Bange, chief scientist of P399 legs 2 and 3. We also thank the 3 anonymous reviewers and the editor Bill Sturges for the helpful comments. Financial support for this study was provided by the BMBF grant SOPRAN II FKZ 03F0611A. This work also contributes to European Union's

Seventh Framework Programme FP7/2007–2013 under grant agreement no. 226224 – SHIVA.

The service charges for this open access publication have been covered by a Research Centre of the Helmholtz Association.

Edited by: W. T. Sturges

References

Atlas, E., Pollock, W., Greenberg, J., Heidt, L., and Thompson, A.: Alkyl nitrates, nonmethane hydrocarbons, and halocarbon gases over the equatorial Pacific Ocean during SAGA-3, J. Geophys. Res.-Atmos., 98, 16933–16947, doi:10.1029/93JD01005, 1993.

Bange, H., Atlas, E., Bahlmann, E., Baker, A., Bracher, A., Cianca, A., Dengler, M., Fuhlbrügge, S., Großmann, K., Hepach, H., Lavrič, J., Löscher, C., Krüger, K., Orlikowska, A., Peeken, I., Quack, B., Schafstall, J., Steinhoff, T., Williams, J., and Wittke, F.: FS Poseidon cruise report P399 legs 2 and 3, 74, IFM-GEOMAR, Kiel, Germany, 2011.

Butler, J., King, D., Lobert, J., Montzka, S., Yvon-Lewis, S., Hall, B., Warwick, N., Mondeel, D., Aydin, M., and Elkins, J.: Oceanic distributions and emissions of short-lived halocarbons, Global Biogeochem. Cy., 21, doi:10.1029/2006GB002732, 2007.

Carpenter, L. and Liss, P.: On temperate sources of bromoform and other reactive organic bromine gases, J. Geophys. Res.-Atmos., 105, 20539–20547, doi:10.1029/2000JD900242, 2000.

Carpenter, L., Liss, P., and Penkett, S.: Marine organohalogens in the atmosphere over the Atlantic and Southern Oceans, J. Geophys. Res.-Atmos., 108, 4256, doi:10.1029/2002JD002769, 2003.

Carpenter, L., Wevill, D., Hopkins, J., Dunk, R., Jones, C., Hornsby, K., and McQuaid, J.: Bromoform in tropical Atlantic air from 25 degrees N to 25 degrees S, Geophys. Res. Lett., 34, L11810, doi:10.1029/2007GL029893, 2007.

Carpenter, L., Fleming, Z., Read, K., Lee, J., Moller, S., Hopkins, J., Purvis, R., Lewis, A., Muller, K., Heinold, B., Herrmann, H., Fomba, K., van Pinxteren, D., Muller, C., Tegen, I., Wiedensohler, A., Muller, T., Niedermeier, N., Achterberg, E., Patey, M., Kozlova, E., Heimann, M., Heard, D., Plane, J., Mahajan, A., Oetjen, H., Ingham, T., Stone, D., Whalley, L., Evans, M., Pilling, M., Leigh, R., Monks, P., Karunaharan, A., Vaughan, S., Arnold, S., Tschritter, J., Pohler, D., Friess, U., Holla, R., Mendes, L., Lopez, H., Faria, B., Manning, A., and Wallace, D.: Seasonal characteristics of tropical marine boundary layer air measured at the Cape Verde Atmospheric Observatory, J. Atmos. Chem., 67, 87–140, doi:10.1007/s10874-011-9206-1, 2010.

Dessens, O., Zeng, G., Warwick, N., and Pyle, J.: Short-lived bromine compounds in the lower stratosphere; impact of climate change on ozone, Atmospheric Science Letters, 10, 201–206, doi:10.1002/asl.236, 2009.

Garratt, J.: The internal boundary-layer – a review, Bound.-Lay. Meteorol., 50, 171–203, doi:10.1007/BF00120524, 1990.

Gschwend, P., Macfarlane, J., and Newman, K.: Volatile halogenated organic-compounds released to seawater from temperate marine macroalgae, Science, 227, 1033-1035, doi:10.1126/science.227.4690.1033, 1985.

Hepach, H., Quack B., Ziska F., Fuhlbrügge, S., Atlas, E. L., Peeken, I., Krüger, K., and Wallace, D. W. R.: Drivers of diel and regional variations of halocarbon emissions from the tropical North East Atlantic, in preparation, 2013.

Highwood, E. and Hoskins, B.: The tropical tropopause, Q. J. Roy. Meteorol. Soc., 124, 1579–1604, doi:10.1256/smsqj.54910, 1998.

Hossaini, R., Chipperfield, M., Dhomse, S., Ordonez, C., Saiz-Lopez, A., Abraham, N., Archibald, A., Braesicke, P., Telford, P., Warwick, N., Yang, X., and Pyle, J.: Modelling future changes to the stratospheric source gas injection of biogenic bromocarbons, Geophys. Res. Lett., 39, L20813, doi:10.1029/2012GL053401, 2012.

Kalnay, E., Kanamitsu, M., Kistler, R., Collins, W., Deaven, D., Gandin, L., Iredell, M., Saha, S., White, G., Woollen, J., Zhu, Y., Chelliah, M., Ebisuzaki, W., Higgins, W., Janowiak, J., Mo, K., Ropelewski, C., Wang, J., Leetmaa, A., Reynolds, R., Jenne, R., and Joseph, D.: The NCEP/NCAR 40-year reanalysis project, B. Am. Meteorol. Soc., 77, 437-471, doi:10.1175/1520-0477(1996)077<0437:TNYRP>2.0.CO;2, 1996.

Kistler, R., Kalnay, E., Collins, W., Saha, S., White, G., Woollen, J., Chelliah, M., Ebisuzaki, W., Kanamitsu, M., Kousky, V., van den Dool, H., Jenne, R., and Fiorino, M.: The NCEP-NCAR 50-year reanalysis: Monthly means CD-ROM and documentation, B. Am. Meteorol. Soc., 82, 247–267, doi:10.1175/1520-0477(2001)082<0247:TNNYRM>2.3.CO;2, 2001.

Kloster, S., Six, K., Feichter, J., Maier-Reimer, E., Roeckner, E., Wetzel, P., Stier, P., and Esch, M.: Response of dimethylsulfide (DMS) in the ocean and atmosphere to global warming, J. Geophys. Res.-Biogeosci., 112, G03005, doi:10.1029/2006JG000224, 2007.

Ko, M. K. W., Poulet, G., and Blake, D. R.: Very short-lived halogen and sulfur substances, Scientific assessment of ozone depletion: 2002, Global Ozone Research and Monitoring Project. Report No. 47, Chapter 2, World Meteorological Organization, Geneva, 2003.

Krüger, K. and Quack, B.: Introduction to special issue: the TransBrom Sonne expedition in the tropical West Pacific, Atmos. Chem. Phys. Discuss., 12, 1401–1418, doi:10.5194/acpd-12-1401-2012, 2012.

Manley, S. and Dastoor, M.: Methyl-iodide (CH3I) production by kelp and assoviated microbes, Marine Biol., 98, 477–482, doi:10.1007/BF00391538, 1988.

Montzka, S. A. and Reimann, S.: Ozone-depleting substances and related chemicals, Scientific Assessment of Ozone Depletion: 2010, Global Ozone Research and Monitoring Project – Report No. 52, Geneva, Switzerland, 2011.

Moore, R. and Tokarczyk, R.: Volatile biogenic halocarbons in the northwest Atlantic, Global Biogeochem. Cy., 7, 195–210, doi:10.1029/92GB02653, 1993.

Neiburger, M., Johnson, D., and Chien, C.: Studies of the structure of the atmosphere over the Eastern Pacific Ocean in summer: I. The inversion over the Eastern North Pacific Ocean, 1, Univ. of Calif., Publications in Meteorology, 94 pp., 1961.

Nightingale, P., Malin, G., Law, C., Watson, A., Liss, P., Liddicoat, M., Boutin, J., and Upstill-Goddard, R.: In situ evaluation of air-sea gas exchange parameterizations using novel conservative and volatile tracers, Global Biogeochem. Cy., 14, 373–387, doi:10.1029/1999GB900091, 2000.

O'Brien, L., Harris, N., Robinson, A., Gostlow, B., Warwick, N., Yang, X., and Pyle, J.: Bromocarbons in the tropical marine boundary layer at the Cape Verde Observatory – measurements and modelling, Atmos. Chem. Phys., 9, 9083–9099, doi:10.5194/acp-9-9083-2009, 2009.

Pyle, J., Warwick, N., Yang, X., Young, P., and Zeng, G.: Climate/chemistry feedbacks and biogenic emissions, Phil. Trans. Roy. Soc. a-Mathematical Phys. Eng. Sci., 365, 1727–1740, doi:10.1098/rsta.2007.2041, 2007.

Quack, B. and Wallace, D.: Air-sea flux of bromoform: Controls, rates, and implications, Global Biogeochem. Cy., 17, 1023, doi:10.1029/2002GB001890, 2003.

Quack, B., Atlas, E., Petrick, G., Stroud, V., Schauffler, S., and Wallace, D.: Oceanic bromoform sources for the tropical atmosphere, Geophys. Res. Lett., 31, L23S05, doi:10.1029/2004GL020597, 2004.

Quack, B., Atlas, E., Petrick, G., and Wallace, D.: Bromoform and dibromomethane above the Mauritanian upwelling: Atmospheric distributions and oceanic emissions, J. Geophys. Res.-Atmos., 112, D09312, doi:10.1029/2006JD007614, 2007.

Raimund, S., Quack, B., Bozec, Y., Vernet, M., Rossi, V., Garcon, V., Morel, Y., and Morin, P.: Sources of short-lived bromocarbons in the Iberian upwelling system, Biogeosciences, 8, 1551–1564, doi:10.5194/bg-8-1551-2011, 2011.

Read, K., Mahajan, A., Carpenter, L., Evans, M., Faria, B., Heard, D., Hopkins, J., Lee, J., Moller, S., Lewis, A., Mendes, L., McQuaid, J., Oetjen, H., Saiz-Lopez, A., Pilling, M., and Plane, J.: Extensive halogen-mediated ozone destruction over the tropical Atlantic Ocean, Nature, 453, 1232–1235, doi:10.1038/nature07035, 2008.

Relvas, P., and Barton, E.: Mesoscale patterns in the Cape Sao Vicente (Iberian Peninsula) upwelling region, J. Geophys. Res.-Ocean., 107, 3164, doi:10.1029/2000JC000456, 2002.

Schmittner, A., Oschlies, A., Matthews, H., and Galbraith, E.: Future changes in climate, ocean circulation, ecosystems, and biogeochemical cycling simulated for a business-as-usual $CO_{(2)}$ emission scenario until year 4000 AD, Global Biogeochem. Cy., 22, GB1013, doi:10.1029/2007GB002953, 2008.

Seibert, P., Beyrich, F., Gryning, S., Joffre, S., Rasmussen, A., and Tercier, P.: Review and intercomparison of operational methods for the determination of the mixing height, Atmos. Environ., 34, 1001–1027, doi:10.1016/S1352-2310(99)00349-0, 2000.

Skyllingstad, E., Samelson, R., Mahrt, L., and Barbour, P.: A numerical Modeling study of warm offshore flow over cool water, Mont. Weather Rev., 133, 345–361, doi:10.1175/MWR-2845.1, 2005.

Solomon, S., Garcia, R., and Ravishankara, A.: On the role of iodine in ozone depletion, J. Geophys. Res.-Atmos., 99, 20491–20499, doi:10.1029/94JD02028, 1994.

Sorensen, J.: Sensitivity of the DERMA long-range gaussian dispersion model to meteorological input and diffusion parameters, Atmos. Environ., 32, 4195–4206, doi:10.1016/S1352-2310(98)00178-2, 1998.

Stull, R.: An Introduction to Boundary Layer Meteorology, Kluwer Academic Publishers, Dordrecht, the Netherlands, 1988.

Sturges, W., Cota, G., and Buckley, P.: Bromoform emission from arctic ice algae, Nature, 358, 660–662, doi:10.1038/358660a0, 1992.

Tegtmeier, S., Krüger, K., Quack, B., Atlas, E. L., Pisso, I., Stohl, A., and Yang, X.: Emission and transport of bromocarbons: from the West Pacific ocean into the stratosphere, Atmos. Chem. Phys., 12, 10633–10648, doi:10.5194/acp-12-10633-2012, 2012.

Tegtmeier, S., Krüger, K., Quack, B., Atlas, E., Blake, D. R., Boenisch, H., Engel, A., Hepach, H., Hossaini, R., Navarro, M. A., Raimund, S., Sala, S., Shi, Q., and Ziska, F.: The contribution of oceanic methyl iodide to stratospheric iodine, Atmos. Chem. Phys. Discuss., 13, 11427–11471, doi:10.5194/acpd-13-11427-2013, 2013.

Troen, I., and Mahrt, L.: A simple-model of the atmospheric boundary-layer: Sensitivity to surface evaporation, Bound.-Lay. Meteorol., 37, 129–148, doi:10.1007/BF00122760, 1986.

Vickers, D., Mahrt, L., Sun, J., and Crawford, T.: Structure of offshore flow, Mon. Weather Rev., 129, 1251–1258, doi:10.1175/1520-0493(2001)129<1251:SOOF>2.0.CO;2, 2001.

Vogelezang, D., and Holtslag, A.: Evaluation and model impacts of alternative boundary-layer height formulations, Bound.-Lay. Meteorol., 81, 245-269, doi:10.1007/BF02430331, 1996.

Warwick, N., Pyle, J., Carver, G., Yang, X., Savage, N., O'Connor, F., and Cox, R.: Global modeling of biogenic bromocarbons, J. Geophys. Res.-Atmos., 111, D244305, doi:10.1029/2006JD007264, 2006.

WMO: Definition of the thermal tropopause, WMO Bulletin, 136–137, 1957.

WMO: Scientific Assessment of Ozone Depletion: 2006, Geneva, Switzerland, 572, 2007.

WMO: Scientific Assessment of Ozone Depletion: 2010, World Meteorological Organization, Geneva, 2011.

Yokouchi, Y., Hasebe, F., Fujiwara, M., Takashima, H., Shiotani, M., Nishi, N., Kanaya, Y., Hashimoto, S., Fraser, P., Toom-Sauntry, D., Mukai, H., and Nojiri, Y.: Correlations and emission ratios among bromoform, dibromochloromethane, and dibromomethane in the atmosphere, J. Geophys. Res.-Atmos., 110, D23309, doi:10.1029/2005JD006303, 2005.

Ziska, F., Quack, B., Abrahamsson, K., Archer, S. D., Atlas, E., Bell, T., Butler, J. H., Carpenter, L. J., Jones, C. E., Harris, N. R. P., Hepach, H., Heumann, K. G., Hughes, C., Kuss, J., Krüger, K., Liss, P., Moore, R. M., Orlikowska, A., Raimund, S., Reeves, C. E., Reifenhäuser, W., Robinson, A. D., Schall, C., Tanhua, T., Tegtmeier, S., Turner, S., Wang, L., Wallace, D., Williams, J., Yamamoto, H., Yvon-Lewis, S., and Yokouchi, Y.: Global sea-to-air flux climatology for bromoform, dibromomethane and methyl iodide, Atmos. Chem. Phys. Discuss., 13, 5601–5648, doi:10.5194/acpd-13-5601-2013, 2013.

4. Manuscript 4

Global sea-to-air flux climatology for bromoform, dibromomethane and methyl iodide

F. Ziska[1], B. Quack[1], K. Abrahamsson[2], S. D. Archer[3], E. Atlas[4], T. Bell[5], J. H. Butler[6], L. J. Carpenter[7], C. E. Jones[7,*], N. R. P. Harris[8], H. Hepach[1], K. G. Heumann[9], C. Hughes[10], J. Kuss[11], K. Krüger[1], P. Liss[12], R. M. Moore[13], A. Orlikowska[11], S. Raimund[14,], C. E. Reeves[12], W. Reifenhäuser[15,***], A. D. Robinson[8], C. Schall[16], T. Tanhua[1], S. Tegtmeier[1], S. Turner[12], L. Wang[17], D. Wallace[13], J. Williams[18], H. Yamamoto[19,****], S. Yvon-Lewis[20], and Y. Yokouchi[19]**

[1] GEOMAR, Helmholtz-Zentrum für Ozeanforschung Kiel, Kiel, Germany

[2] Department of Analytical and Marine Chemistry, Chalmers University of Technology and Gothenburg University, Gothenburg, Sweden

[3] Plymouth Marine Laboratory, Plymouth, PMI, Plymouth, UK now at Bigelow Laboratory of Ocean Sciences, USA

[4] Marine and Atmospheric Chemistry, Rosenstiel School of Marine and Atmospheric Science, University of Miami, MAC, Miami, USA

[5] Department of Earth System Science, University of California, UCI, Irvine, USA

[6] Earth System Research Laboratory, Global Monitoring Division, ESRL/NOAA, Boulder, USA

[7] Department of Chemistry, University of York, York, YO10 5DD, UK

[8] Department of Chemistry, University of Cambridge, Cambridge, CB2 1EW, UK, Cambridge, UK

[9] Institut für Anorganische Chemie und Analytische Chemie, Johannes Gutenberg-Universität, JGU, Mainz, Germany

[10] Laboratory for Global Marine and Atmospheric Chemistry, University of East Anglia, LGMAC/UEA, Norwich, UK

[11] Institut für Ostseeforschung Warnemünde, IOW, Rostock-Warnemünde, Germany

[12] School of Environmental Science, University of East Anglia, Norwich, UK

[13] Department of Oceanography, Dalhousie University, Halifax, B3H 4R2, Canada

[14] CNRS, UMR 7144, Equipe Chim Marine, Stn Biol Roscoff, 29680 Roscoff, France

[15] Bayerisches Staatsministerium für Umwelt und Gesundheit, Augsburg, Germany

[16] Fresenius Medical Care Deutschland GmbH, Frankfurterstrasse 6–8, 66606 St. Wendel, Germany

[17] Rutgers State University of New Jersey, New Brunswick, USA

[18] Max Planck Institute for Chemistry, Air Chemistry Department, MPI, Mainz, Germany

[19] National Institute for Environmental Studies, Tsukuba, Ibaraki 305-0053, Japan

[20] Department of Oceanography, Texas A&M University, College Station, USA

[*] now at: Graduate School of Global Environmental Studies, Kyoto University, Yoshida-Honmachi, Sakyo-ku, Kyoto 606-8501, Japan

[**] now at: GEOMAR, Helmholtz-Zentrum für Ozeanforschung Kiel, Kiel, Germany

[***] now at: Bayerisches Landesamt für Umwelt, Augsburg, Germany

[****] now at: Marine Works Japan, Ltd., Oppamahigashi, Yokosuka 237-0063, Japan

Published in: Atmospheric Chemistry and Physics, 13, 8915-8934, doi:10.5194/acp-13-8915-2013, 2013.

Atmos. Chem. Phys., 13, 8915–8934, 2013
www.atmos-chem-phys.net/13/8915/2013/
doi:10.5194/acp-13-8915-2013
© Author(s) 2013. CC Attribution 3.0 License.

Atmospheric Chemistry and Physics
Open Access

Global sea-to-air flux climatology for bromoform, dibromomethane and methyl iodide

F. Ziska[1], B. Quack[1], K. Abrahamsson[2], S. D. Archer[3,*], E. Atlas[4], T. Bell[5], J. H. Butler[6], L. J. Carpenter[7], C. E. Jones[7,], N. R. P. Harris[8], H. Hepach[1], K. G. Heumann[9], C. Hughes[10], J. Kuss[11], K. Krüger[1], P. Liss[12], R. M. Moore[13], A. Orlikowska[11], S. Raimund[14,***], C. E. Reeves[12], W. Reifenhäuser[15], A. D. Robinson[8], C. Schall[16], T. Tanhua[1], S. Tegtmeier[1], S. Turner[12], L. Wang[17], D. Wallace[13], J. Williams[18], H. Yamamoto[19,****], S. Yvon-Lewis[20], and Y. Yokouchi[19]**

[1]GEOMAR, Helmholtz-Zentrum für Ozeanforschung Kiel, Kiel, Germany
[2]Department of Analytical and Marine Chemistry, Chalmers University of Technology and Gothenburg University, Gothenburg, Sweden
[3]Plymouth Marine Laboratory, Plymouth, PMI, Plymouth, UK
[4]Marine and Atmospheric Chemistry, Rosenstiel School of Marine and Atmospheric Science, University of Miami, MAC, Miami, USA
[5]Department of Earth System Science, University of California, UCI, Irvine, USA
[6]Earth System Research Laboratory, Global Monitoring Division, ESRL/NOAA, Boulder, USA
[7]Department of Chemistry, University of York, York, YO10 5DD, UK
[8]Department of Chemistry, University of Cambridge, Cambridge, CB2 1EW, UK, Cambridge, UK
[9]Institut für Anorganische Chemie und Analytische Chemie, Johannes Gutenberg-Universität, JGU, Mainz, Germany
[10]Laboratory for Global Marine and Atmospheric Chemistry, University of East Anglia, LGMAC/UEA, Norwich, UK
[11]Institut für Ostseeforschung Warnemünde, IOW, Rostock-Warnemünde, Germany
[12]School of Environmental Science, University of East Anglia, Norwich, UK
[13]Department of Oceanography, Dalhousie University, Halifax, B3H 4R2, Canada
[14]CNRS, UMR7144, Equipe Chim Marine, Stn Biol Roscoff, 29680 Roscoff, France
[15]Bayerisches Landesamt für Umwelt, Augsburg, Germany
[16]Fresenius Medical Care Deutschland GmbH, Frankfurterstraße 6–8, 66606 St. Wendel, Germany
[17]Rutgers State University of New Jersey, New Brunswick, USA
[18]Max Planck Institute for Chemistry, Air Chemistry Department, MPI, Mainz, Germany
[19]National Institute for Environmental Studies, Tsukuba, Ibaraki 305-0053, Japan
[20]Department of Oceanography, Texas A&M University, College Station, USA
[*]now at: Bigelow Laboratory of Ocean Sciences, Maine, USA
[**]now at: Graduate School of Global Environmental Studies, Kyoto University, Yoshida-Honmachi, Sakyo-ku, Kyoto 606-8501, Japan
[***]now at: GEOMAR, Helmholtz-Zentrum für Ozeanforschung Kiel, Kiel, Germany
[****]now at: Marine Works Japan, Ltd., Oppamahigashi, Yokosuka 237-0063, Japan

Correspondence to: F. Ziska (fziska@geomar.de)

Received: 13 December 2012 – Published in Atmos. Chem. Phys. Discuss.: 27 February 2013
Revised: 14 July 2013 – Accepted: 21 July 2013 – Published: 6 September 2013

Published by Copernicus Publications on behalf of the European Geosciences Union.

Abstract. Volatile halogenated organic compounds containing bromine and iodine, which are naturally produced in the ocean, are involved in ozone depletion in both the troposphere and stratosphere. Three prominent compounds transporting large amounts of marine halogens into the atmosphere are bromoform ($CHBr_3$), dibromomethane (CH_2Br_2) and methyl iodide (CH_3I). The input of marine halogens to the stratosphere has been estimated from observations and modelling studies using low-resolution oceanic emission scenarios derived from top-down approaches. In order to improve emission inventory estimates, we calculate data-based high resolution global sea-to-air flux estimates of these compounds from surface observations within the HalOCAt (Halocarbons in the Ocean and Atmosphere) database (https://halocat.geomar.de/). Global maps of marine and atmospheric surface concentrations are derived from the data which are divided into coastal, shelf and open ocean regions. Considering physical and biogeochemical characteristics of ocean and atmosphere, the open ocean water and atmosphere data are classified into 21 regions. The available data are interpolated onto a $1° \times 1°$ grid while missing grid values are interpolated with latitudinal and longitudinal dependent regression techniques reflecting the compounds' distributions. With the generated surface concentration climatologies for the ocean and atmosphere, global sea-to-air concentration gradients and sea-to-air fluxes are calculated. Based on these calculations we estimate a total global flux of 1.5/2.5 $\mathrm{Gmol\,Br\,yr^{-1}}$ for $CHBr_3$, 0.78/0.98 $\mathrm{Gmol\,Br\,yr^{-1}}$ for CH_2Br_2 and 1.24/1.45 $\mathrm{Gmol\,Br\,yr^{-1}}$ for CH_3I (robust fit/ordinary least squares regression techniques). Contrary to recent studies, negative fluxes occur in each sea-to-air flux climatology, mainly in the Arctic and Antarctic regions. "Hot spots" for global polybromomethane emissions are located in the equatorial region, whereas methyl iodide emissions are enhanced in the subtropical gyre regions. Inter-annual and seasonal variation is contained within our flux calculations for all three compounds. Compared to earlier studies, our global fluxes are at the lower end of estimates, especially for bromoform. An under-representation of coastal emissions and of extreme events in our estimate might explain the mismatch between our bottom-up emission estimate and top-down approaches.

1 Introduction

Halogen (fluorine, chlorine, bromine, iodine)-containing volatile organic compounds play an important role in tropospheric (Vogt et al., 1999; von Glasow et al., 2004) and stratospheric chemical cycles (Solomon et al., 1994; Salawitch et al., 2005). The ocean is the largest source of natural bromine- and iodine-containing halocarbons (Quack and Wallace, 2003; Butler et al., 2007; Montzka and Reimann, 2011). When emitted into the atmosphere, these compounds, comprising mainly very short-lived species (VSLS) having an atmospheric lifetime of less than 0.5 yr, contribute to the pool of reactive halogen compounds via photochemical destruction and reaction with hydroxyl radicals (von Glasow, 2008). Deep convection, especially in the tropics, can transport VSLS above the tropical tropopause layer (Aschmann et al., 2009; Tegtmeier et al., 2012, 2013) and into the stratosphere, where they influence stratospheric ozone destruction (Salawitch et al., 2005; Sinnhuber et al., 2009). Reactive bromine and iodine are more efficient in destroying stratospheric ozone than chlorine (e.g. Chipperfield and Pyle, 1998).

The absence of global emission maps of VSLS as input for chemistry transport models and coupled chemistry climate models is a key problem for determining their role in stratospheric ozone depletion. The most widely reported short-lived halogenated compounds containing bromine in both the atmosphere and the ocean are bromoform ($CHBr_3$) and dibromomethane (CH_2Br_2). Together, they may contribute $\sim$ 15–40 % to stratospheric bromine (Montzka and Reimann, 2011), with $CHBr_3$ considered to be the largest single source of organic bromine (Penkett et al., 1985) to the atmosphere. Its production involves marine organisms such as macroalgae and phytoplankton (Gschwend et al., 1985; Nightingale et al., 1995; Carpenter and Liss, 2000; Quack et al., 2004). CH_2Br_2 is formed in parallel with biological production of $CHBr_3$ in seawater (Manley et al., 1992; Tokarczyk and Moore, 1994) and, therefore, generally correlates with oceanic and atmospheric bromoform (e.g. Yokouchi et al., 2005; O'Brien et al., 2009), although it occasionally shows a different pattern in the deeper ocean indicating its different cycling in the marine environment (Quack et al., 2007). Large variability in the $CH_2Br_2 : CHBr_3$ ratio has been observed in sea water and atmosphere, while elevated concentrations of both compounds in air and water are found in coastal regions, close to macroalgae and around islands, as well as in oceanic upwelling areas (Yokouchi et al., 1997, 2005; Carpenter and Liss, 2000; Quack and Wallace, 2003; Quack et al., 2007). Seasonal variations have been observed in coastal regions (Archer et al., 2007; Orlikowska and Schulz-Bull, 2009), however the database is insufficient to resolve a global temporal dependence. Anthropogenic sources, such as water chlorination, are locally significant, but relatively small on a global scale (Quack and Wallace, 2003). There is uncertainty in the magnitude of the global emission flux, and the formation processes are poorly known. Recent studies have revealed a missing source of $\sim$ 5 pptv inorganic bromine in the stratosphere, which could possibly be explained by the contribution of oceanic VSLS (Sturges et al., 2000; Sinnhuber and Folkins, 2006; Dorf et al., 2008).

Atmospheric modelling studies have derived top-down global estimates of between 5.4 and 7 $\mathrm{Gmol\,Br\,yr^{-1}}$ for bromoform and between 0.7 and 1.4 $\mathrm{Gmol\,Br\,yr^{-1}}$ for dibromomethane using different atmospheric transport models (Warwick et al., 2006; Kerkweg et al., 2008; Liang et al., 2010; Ordonez et al., 2012). Global bottom-up emission estimates based on the interpolation of surface atmospheric and oceanic measurements have yielded emission estimates of between 2.8 and 10.3 Gmol Br yr^{-1} for $CHBr_3$ and between 0.8 and 3.5 Gmol Br yr^{-1} for CH_2Br_2 (Carpenter and Liss, 2000; Yokouchi et al., 2005; Quack and Wallace, 2003; Butler et al., 2007). Additionally, a parameterization for oceanic bromoform concentrations covered by a homogenous atmosphere estimates a flux of 1.45 Gmol yr^{-1} for $CHBr_3$ between 30° N and 30° S (Palmer and Reason, 2009).

Methyl iodide is mainly emitted from the ocean and is characterized as a dominant gaseous organic iodine species in the troposphere (Carpenter, 2003; Yokouchi et al., 2008). This compound is involved in important natural iodine cycles, in several atmospheric processes such as the formation of marine aerosol (McFiggans et al., 2000), and has been suggested to contribute to stratospheric ozone depletion in case it reaches the stratosphere through deep convection (Solomon et al., 1994). Current model results of Tegtmeier et al. (2013) suggest an overall contribution of 0.04 ppt CH_3I mixing ratios at the cold point and a localized mixing ratio of 0.5 ppt. Enhanced oceanic concentrations of CH_3I are found in coastal areas where marine macroalgae have been identified as the dominant coastal CH_3I source (e.g. Manley and Dastoor, 1988, 1992; Manley and dela Cuesta, 1997; Laturnus et al., 1998; Bondu et al., 2008). Phytoplankton, bacteria and non-biological pathways, such as photochemical degradation of dissolved organic carbon, are significant open ocean sources (Happell and Wallace, 1996; Amachi et al., 2001; Richter and Wallace, 2004; Hughes et al., 2011). Terrestrial sources, such as rice paddies and biomass burning, are suggested to contribute 30 % to the total atmospheric CH_3I budget (Bell et al., 2002). Modelling studies and data interpolation estimate global CH_3I emissions between 2.4 and 4.3 Gmol I yr^{-1} (Bell et al., 2002; Butler et al., 2007; Ordonez et al., 2012). Smythe-Wright et al. (2006) extrapolated a laboratory culture experiment with *Prochlorococcus marinus* (kind of picoplankton) to a global CH_3I emission estimate of 4.2 Gmol I yr^{-1}, whereas the study of Brownell et al. (2010) disputed the result of Smythe-Wright et al. (2006) and suggests that *P. marinus* is not significant on a global scale.

This study presents the first global 1° × 1° climatological concentration and emission maps for the three important VSLS bromoform, dibromomethane and methyl iodide based on atmospheric and oceanic surface measurements available from the HalOcAt (Halocarbons in the Ocean and Atmosphere) database project (https://halocat.geomar.de/). According to current knowledge of the compounds' distributions and possible sources, we classify the data based on physical and biogeochemical characteristics of the ocean and atmosphere. The interpolation of the missing values onto the 1° × 1° grid with two different regression techniques is analysed. Based on the generated marine and atmospheric surface concentration maps, global climatological emissions are calculated with a commonly used sea-to-air flux parameterization applying temporally highly resolved wind speed, sea surface temperature, salinity and pressure data. The results are compared to estimates of other studies, and the temporal and spatial variability of the climatological sea-to-air flux are discussed. The aim of this study is to provide improved global sea-to-air flux maps based on in situ measurements and on known physical and biogeochemical characteristics of the ocean and atmosphere in order to reduce the uncertainties in modelling the contribution of VSLS to the stratospheric halogen budget (Hamer et al., 2013; Hossaini et al., 2013; Tegtmeier et al., 2013).

2 Data

In this study, $CHBr_3$, CH_2Br_2 and CH_3I data are extracted from the HalOcAt database (https://halocat.geomar.de/, see Supplement for a list of all data). The database currently contains about 200 contributions, comprising roughly 55 400 oceanic and 476 000 atmospheric measurements from a range of oceanic depths and atmospheric heights of 19 different halocarbon compounds (mainly very short-lived brominated and iodinated trace gases) from 1989 to 2011. The dataset mainly consists of data from coastal stations, ship operations and aircraft campaigns. The individual datasets are provided by the dataset creators. Since the compound distribution is too variable and the current data are too sparse to identify a robust criterion for quality check and data selection, no overall quality and intercalibration control on the database exists. Future work is planned to use common standards and perform laboratory intercalibrations (Butler et al., 2010; Jones et al., 2011). Thus, we use all available surface ocean values to a maximum depth of 10 m (5300 data points) and atmospheric values to a maximum height of 20 m (4200 data points) from January 1989 until August 2011 (Fig. 1) for the calculation of the climatological concentrations. For sea-to-air flux calculations (see Sect. 3.5), 6-hourly means of wind speed (U), sea level pressure (SLP) and sea surface temperature (SST) are extracted from the ERA-Interim meteorological assimilation database (Dee et al., 2011) for the years 1989–2011 (1° × 1°), whereas salinity (SSS) is taken from the World Ocean Atlas 2009 (Antonov et al., 2010).

3 Methodology

3.1 Approach

The high variability of VSLS (especially for $CHBr_3$) in both ocean and atmosphere is not explicable with any correlation to common parameterizations. Production pathways with associated production rates and reliable proxies for the compounds' distributions are not available. We tested correlations, multiple linear regressions and polynomial fits with biological and physical parameters (e.g. chlorophyll a, SST,

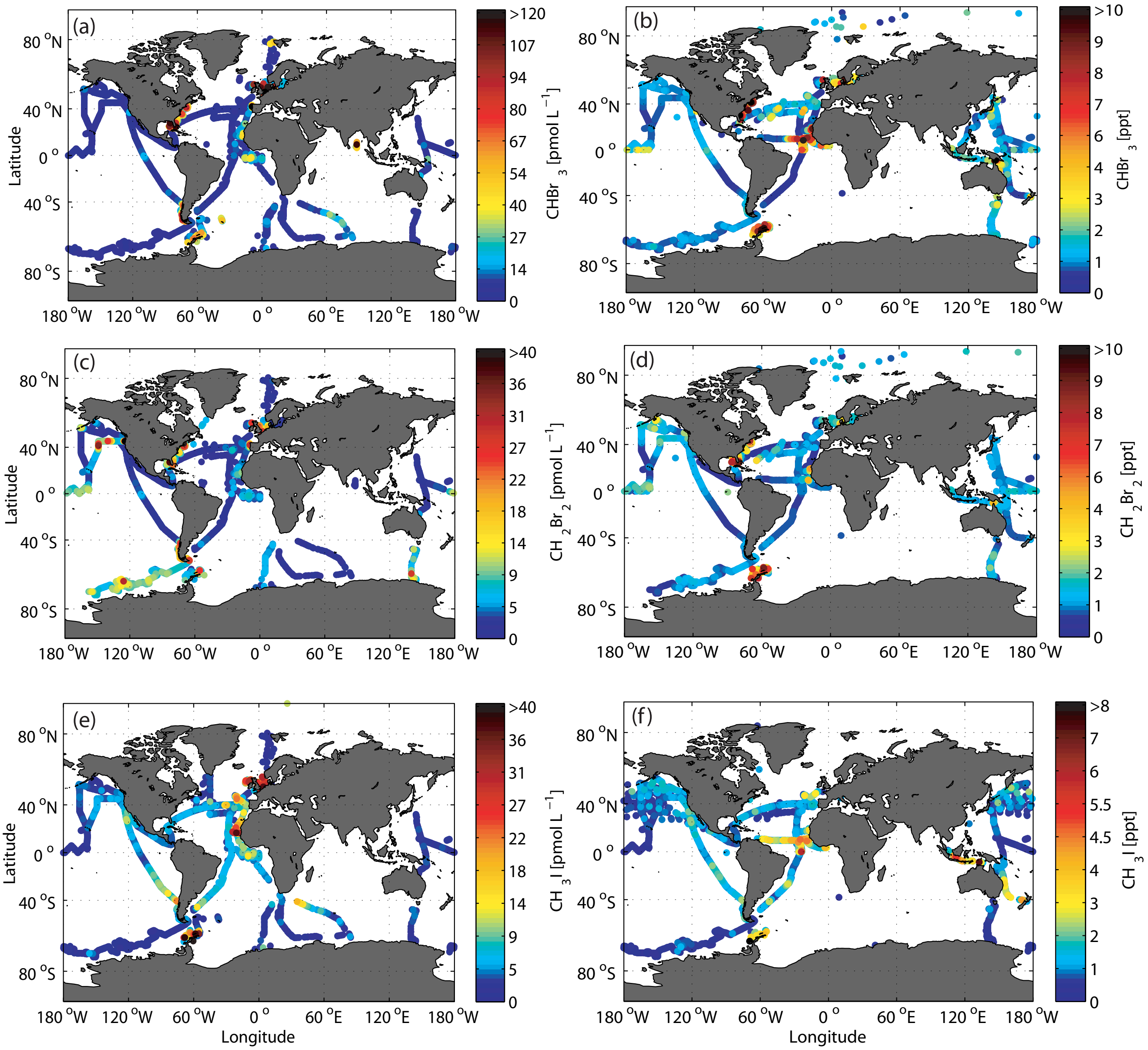
(a)
(b)
(c)
(d)
(e)
(f)
80 °N
40 °N
0 °
40 °S
80 °S
Latitude
180 °W
120 °W
60 °W
0 °
60 °E
120 °E
180 °W
Longitude
CHBr 3 [pmol L−1]
>120
107
94
80
67
54
40
27
14
0
CHBr 3 [ppt]
>10
9
8
7
6
4
3
2
1
0
CH 2Br 2 [pmol L−1]
>40
36
31
27
22
18
14
9
5
0
CH 2Br 2 [ppt]
CH 3I [pmol L−1]
CH 3I [ppt]
>8
7
6
5.5
4.5
4
3
2
1
0

Fig. 1. Global coverage of available surface seawater measurements in pmol L^{-1} and atmospheric measurements in ppt for bromoform **(a, b)**, dibromomethane **(c, d)** and methyl iodide **(e, f)** from the HalOcAt database project (data from 1989 to 2011).

SSS, SLP, mixed layer depth) to interpolate the data. Since none of the techniques provided satisfying results, we choose to simplify our approach. In order to compute climatological concentration maps, information on the compounds' distributions is extracted from the existing datasets of the HalOcAt database and the literature on source distributions. Both surface ocean and atmospheric $CHBr_3$ concentrations are generally higher in productive tropical regions, at coast lines and close to islands, while generally lower and more homogeneous concentrations are located in the open ocean (Fig. 1). The global ocean shows a latitudinal and longitudinal variation of biological regimes, driven by circulation and regionally varying nutrient input as well as light conditions. Productive eastern boundary upwelling, equatorial and high latitudinal areas are separated by low productive gyre regions. We therefore separated the ocean in different latitudinal bands and applied (multiple) linear regressions between the compounds' distributions and latitude and longitude (see more details in Sect. 3.3). The linear regressions reflect the underlying coarse distribution of the data, and their longitudinal and latitudinal concentration dependence within different biogeochemical and physical regimes appears to be the current best available approach for data analysis and interpolation. This approach is independent of additional variables, reasonably reflecting the current knowledge about the compounds' distributions considering different biogeochemical oceanic regions and minimizes the creation of non-causal characteristics. The existing data are interpolated onto a 1° × 1° grid. The missing grid values are filled using the latitudinal and longitudinal dependent regression techniques. The climatological oceanic and atmospheric surface concentration maps are used to calculate global fields of concentration gradients and sea-to-air fluxes.

3.2 Classification

All data are divided into coastal, shelf and open ocean regimes. The coastal area is defined as all first 1° × 1° grid points next to the land mask, while the shelf regime comprises all second grid points neighbouring the coastal one. The other grid points belong to the open ocean water and atmosphere regime. The data from coastal and shelf regions are very sparse. For this reason, they are only separated between Northern Hemisphere and Southern Hemisphere.

The open ocean water data are further divided into 4 regions for each hemisphere. The inner tropics (0 to 5°) include the equatorial upwelling regions with high biomass abundance and elevated $CHBr_3$ concentrations, especially in the eastern ocean basins. The subtropical gyres, with descending water masses and hence low biological production at the surface, are identified as the second region (5 to 40°). The third region comprises the temperate zones between 40 to 66° with higher climatological surface chlorophyll concentrations than in the gyre region and decreasing water temperature and increasing $CHBr_3$ concentrations towards higher latitudes. The fourth region (poleward of 66°) encompasses the polar Arctic and Antarctic with cold surface waters and occasional ice cover.

The open ocean atmosphere is classified in a slightly different way from that of the open ocean waters. The inner tropical region (here from 0 to 10°) is characterized by the intertropical convergence zone, upward motion, low pressure and deep convection. Additionally, each hemisphere is divided into 3 wind regimes: subtropics (10 to 30°), midlatitudes (30 to 60°) (westerlies, storm tracks) and polar regions (60 to 90°), characterized by distinctive air masses, wind directions and weather conditions.

The open ocean regimes (oceanic and atmospheric) are further subdivided into the Atlantic, Pacific, Indian and Arctic basins. Thus, the HalOcAt data is sorted into 21 different regions for surface open ocean water and atmosphere (see Tables S1 and S2 in the Supplement). Gridding the data and inserting missing values is described in the following section. Dibromomethane has been reported to have similar source regions as $CHBr_3$, (Yokouchi et al., 2005; O'Brien et al., 2009), while methyl iodide is reported to also have coastal, planktonic and photochemical sources (Hughes et al., 2011; Moore et al., 1994; Richter and Wallace, 2004). Both compounds are also tight to unrevealed direct or indirect biological processes. Thus, we divide the CH_2Br_2 and CH_3I data between the regions in the same way as we have classified the $CHBr_3$ data. The data density for dibromomethane and methyl iodide is equivalent to that of bromoform (Fig. 1).

3.3 Objective mapping

The original, irregular measurements from the HalOcAt database are transferred to a uniform global 1° × 1° grid using a Gaussian interpolation. Based on this technique the value at each grid point is calculated with the measurements located in a defined Gaussian range. The Gaussian bell radius is 3° for the surface open ocean water and atmosphere data and 1° for the coast and shelf region. The wider radius for the open ocean regimes are caused by the higher homogeneity of the data in this region. This kind of interpolation takes the spatial variance of the measurements into account. The smaller the distance between a given data point and the grid point, the greater is its weighting in the grid point calculation (Daley, 1991) (see Supplement for a list of all calculated atmospheric and oceanic grid points based on objective mapping). For grid points where no measurements are available within the Gaussian bell area, no concentration data can be calculated directly and a linear regression needs to be applied.

3.4 Linear regression

Data gaps on the 1° × 1° grid are filled based on a multiple linear regression technique using the original dataset, applying the functional relationship between latitude and longitude as predictor variables, x_1 and x_2, and compound concentration as the response variable, y (Fig. 2, for specific details see Sect. 3.5).

The regression coefficients for each defined oceanic and atmospheric region are given in Tables S1 and S2 in the Supplement. For regions where the spatial coverage of the data is extremely poor, a first order regression based on the latitude variable only is used. For regions without data or in case the interpolation does not produce reasonable results (e.g. concentrations calculated with the regression are negative), the linear regression of neighbouring open ocean regions of the same latitudinal band is used to fill the data gaps, assuming similar physical and biogeochemical conditions. For example, no data exist for the tropical Indian Ocean (0–5° N), thus, open ocean data from the tropical Atlantic and Pacific (0–5° N) are used to determine the missing values. Since data coverage in coastal and shelf regions is low, the regression coefficients are calculated over each entire hemisphere. Additionally, we apply the root mean square error (RMSE), calculated as the difference between the predicted values and the observed data, as a measure of accuracy. A small RMSE reflects a low bias and variance of the predicted values, with zero indicating that the regression techniques predict the observations perfectly.

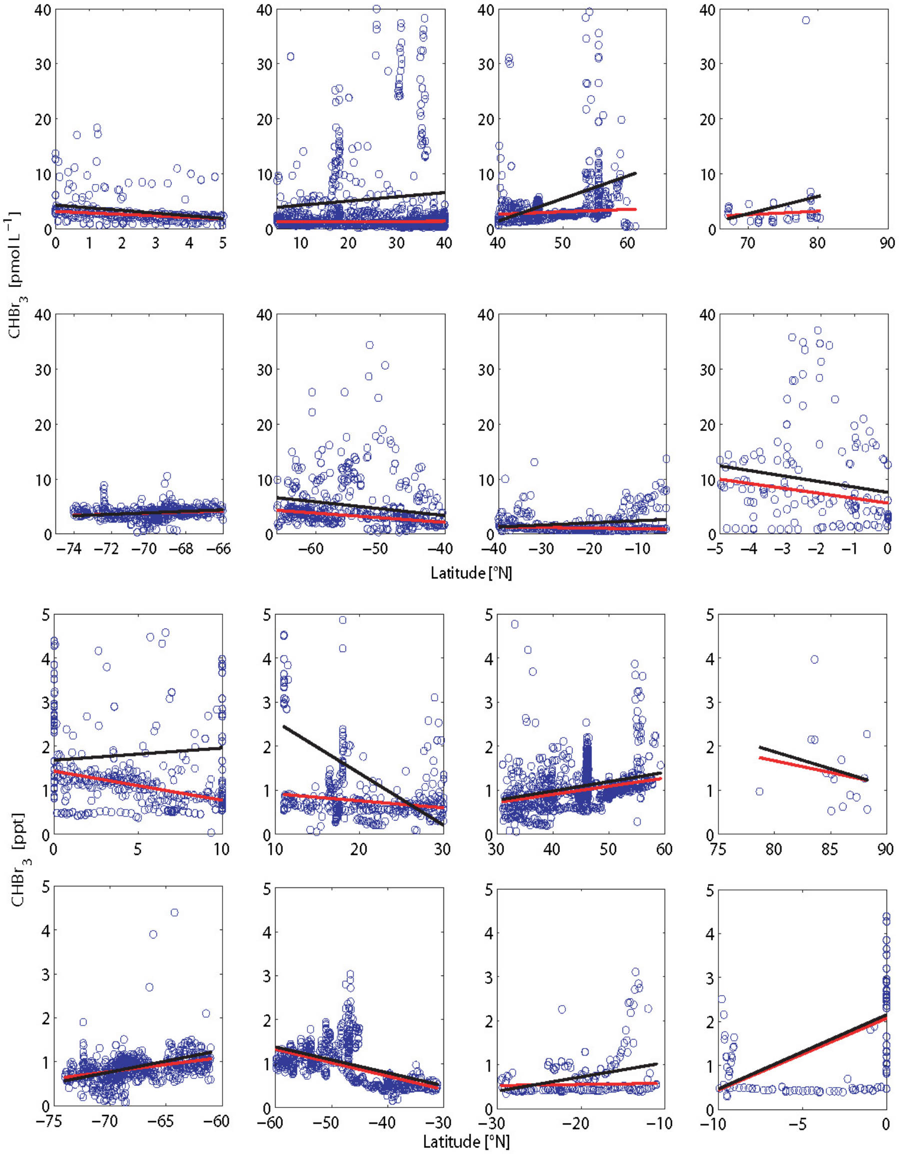

Fig. 2. Latitudinal distribution of open ocean water **(a)** (pmol L^{-1}) and atmosphere **(b)** (ppt) bromoform concentrations (blue circles) classified in eight different latitudinal bands. The robust fit (RF) (red line) and ordinary least squares (OLS) (black line) regression analyses are included.

3.5 Robust fit vs. ordinary least squares

In our study, two different regression techniques are applied. The ordinary least squares (OLS) technique contains the least squares method. This means that the sum of squared deviations between the empirical y values in the dataset and the predicted linear approximation is minimized.

The second method for calculating regression coefficients is the robust fit (RF) technique which is especially used for not normally distributed values. A regression analysis is *robust* if it is not sensitive to outliers. The calculation of the robust coefficients is based on the *iteratively reweighted least squares* process. In the first iteration each data point has equal weight and the model coefficients are estimated using ordinary least squares. In the following iterations, the weighting of the data points is recalculated so that the distant data points from the model regression from the previous iteration are given lower weight. This process continues until the model coefficients are within a predefined range. Our calculations are based on the most common general method of robust regression, the "M-estimation" introduced by Huber (1964).

Both regression methods are shown in Fig. 2 for all latitudinal divided open ocean water and atmospheric measurements for bromoform. The RF regression lines (red) are lower than the OLS (black) and occasionally show different

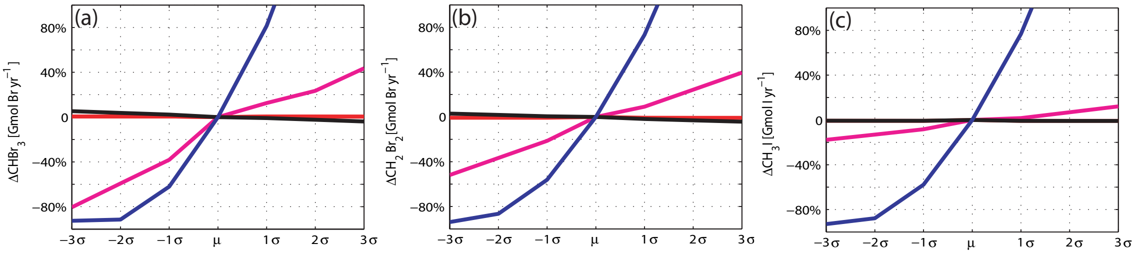

Fig. 3. The percentage change of the global oceanic emission for bromoform **(a)**, dibromomethane **(b)**, both in Gmol Br yr^{-1}, and methyl iodide **(c)**, in Gmol I yr^{-1}, based on individual input parameters: wind speed (blue), sea surface temperature (magenta), sea surface salinity (red) and sea level pressure (black). The input parameters are individually increased and decreased by their multiple standard deviations (-3σ to 3σ) while the other input parameters remain fixed (μ presents the oceanic emission using the mean input parameters).

trends. The reason for the large deviation between the RF and OLS regression is the different weighting of outliers. Outliers crucially influence the value of the OLS slope, whereas the RF regression is located at the largest data density and reduces the influence of outliers. While the RF captures background values, the OLS technique indicates the variability of the data. Based on the obtained concentration maps, global fluxes are calculated and compared to literature values (see Supplement for a list of all calculated atmospheric and oceanic grid points based on linear regression and objective mapping as well as on linear regression only).

3.6 Air–sea gas exchange and input parameters

Fluxes (F in pmol cm h^{-1}) across the sea–air interface are generally calculated as the product of the sea-to-air concentration difference and a gas exchange velocity. The partitioning of a gas between the water and gas phase is described by the dimensionless Henry's law constant (H) which highly depends on temperature and the molecular structure of the species. For our calculations, the Henry's law constants of Moore et al. (1995a, b) are used. The atmospheric mixing ratios (C_m in ppt) are converted to equilibrium water concentrations (C_a in pmol L^{-1}) and the deviation from the actual measured water concentration (C_w in pmol L^{-1}) describes the driving concentration gradient. The sea-to-air flux is negative if the transport is from the atmosphere to the ocean.

$$F = k(C_\mathrm{w} - C_\mathrm{a} H^{-1}) \tag{1}$$

$$C_\mathrm{a} = C_\mathrm{m} \cdot \mathrm{SLP}/(\mathrm{SST} + 273.15)/83.137 \tag{2}$$

$$H = \exp(-4973/(\mathrm{SST} + 273.15) + 13.16) \text{for } \mathrm{CHBr_3} \tag{3}$$

Several parameterizations for the air–sea gas exchange exist in the literature, which express the relationship between the gas exchange velocity (k in cm h^{-1}) and wind speed (e.g. Liss and Merlivat, 1986; Wanninkhof, 1992; Wanninkhof and McGillis, 1999; Nightingale et al., 2000). Experiments have shown that the dominant parameter influencing k is the wind speed. We chose to calculate the transfer coefficients based on the parameterization from Nightingale et al. (2000) with corrections for the water temperature and a Schmidt number (Sc) dependence for each gas (Quack and Wallace, 2003; Johnson, 2010).

$$k = (0.222U^2 + 0.333U)\mathrm{sqrt}(660 Sc^{-1}) \tag{4}$$

The dimensionless Schmidt number is the ratio of the diffusion coefficient of the compound (D in cm^2 s^{-1}) of interest and the kinematic viscosity (ν in cm^2 s^{-1}) of sea water, and depends mainly on the temperature and the salinity.

$$Sc = \nu / D \tag{5}$$

$$D = (193 \times 10^{-10} \times \mathrm{SST}^2 + 1686 \times 10^{-10} \times \mathrm{SST} + 403.42 \times 10^{-8}) \text{ for } \mathrm{CHBr_3} \tag{6}$$

The diffusion coefficients for the compounds were calculated according to Quack and Wallace (2003).

The gas exchange velocity and concentration gradient are dependent on SST, SSS, U and SLP as input parameters. During the initial stages of this study, we used climatological mean values (1989–2011) of the input parameters for our calculation of the global climatological emission estimates. A sensitivity study demonstrates how changes in the input parameters (climatological means) affect the global flux calculation for bromoform, dibromomethane and methyl iodide (Fig. 3). Each input parameter is individually increased and decreased by their multiple standard deviations (-3σ to 3σ) while the other input parameters remain fixed. The standard deviations are calculated for every grid point for the years 1989–2011. This study shows the importance of each input parameter for the flux variance. Sea surface salinity and sea level pressure affects the VSLS emission calculations least compared with the other parameters (Fig. 3). Changes in wind speed and sea surface temperature have strong influences on the bromoform sea-to-air flux. In general, a reduction/enhancement of the wind speed is directly accompanied by a decrease/increase in air–sea gas exchange coefficients, and higher/lower sea surface temperature leads to an increase/decrease of the concentration gradients as well as the air–sea gas exchange coefficients (Schmidt number).

The dependencies of the global dibromomethane emission variability on the individual input parameters are the same as described for bromoform. The global methyl iodide emissions are mainly influenced by variations of the wind speed, while the other parameters have less effect. The sensitivity study shows that marginal changes of the input parameters can lead to a significant variation of the global flux estimate.

Averaging over a long time period when producing climatological means involves smoothing extreme values, which is especially relevant for the wind speed (Bates and Merlivat, 2001). Since the air–sea gas exchange coefficient has a non-linear dependence on wind speed, the application of averaged data fields causes a bias towards a lower flux when compared to using instantaneous winds and averaging the emission maps afterwards (Chapman et al., 2002; Kettle and Merchant, 2005). To reduce the bias, we apply the highest available temporal resolution of the input parameters and calculate 6-hourly global emissions with 6-hourly means of U, SST, SLP and monthly means for the SSS (from January 1989 to December 2011). Finally, we sum the emissions for each month, calculate monthly average emissions over the twenty-one years and summarise these twelve averages to obtain the climatological annual emission.

4 Results and discussion

Marine (pmol L^{-1}) and atmospheric (ppt) global surface concentration maps of bromoform, dibromomethane and methyl iodide calculated with the RF regression are shown in Fig. 4 (surface ocean concentrations and mixing ratios calculated with the OLS technique are illustrated in the Supplement). Based on the RF and OLS marine and atmospheric concentration maps, global sea-to-air flux climatologies are calculated (Fig. 5).

4.1 Climatological concentration maps of $CHBr_3$ and CH_2Br_2

Marine surface concentrations of bromoform (Fig. 4) are higher in the equatorial region ($\sim 6\,\text{pmol L}^{-1}$), upwelling areas (e.g. the Mauritanian upwelling region $\sim 21\,\text{pmol L}^{-1}$), near coastal areas ($\sim 17$–$42\,\text{pmol L}^{-1}$) and in shelf regions ($\sim 8$–$32\,\text{pmol L}^{-1}$), consistent with macroalgal and anthropogenic sources along the coast lines as well as biological sources in upwelling areas (Carpenter and Liss, 2000; Quack and Wallace, 2003; Yokouchi et al., 2005; Quack et al., 2007; Liu et al., 2011). The coastal and shelf areas both show a positive latitudinal sea surface concentration gradient for bromoform and dibromomethane towards the polar regions. The coastal sea surface concentrations of bromoform are on average twice as high as in the shelf region. The open ocean generally has homogeneous concentrations between 0.5 and $4\,\text{pmol L}^{-1}$. Lower values are located especially in the subtropical gyres (~ 0.5–$1\,\text{pmol L}^{-1}$), most distinctly in the Atlantic, North Pacific and southern Indian Ocean.

Estimating global concentration maps based on an identified linear relationship is difficult in regions with sparse or missing data (e.g. Indian Ocean). Atlantic and Pacific Ocean data must be used to fill the data gap in the Indian Ocean, since no measurements exist there. Thus, we expect similar concentrations as in the other oceans. One dataset is available for the northern Indian Ocean (Yamamoto et al., 2001). The few measurements of bromoform in the Bay of Bengal are unusually high ($> 50\,\text{pmol L}^{-1}$) for an open ocean area. We decided to not include these outliers in our analysis, since our method would possibly overestimate water concentrations in the entire northern Indian Ocean using these data. The high concentrations in the equatorial region (the product of the other two basins) are approximately collocated with the upwelling season during the northeast monsoon, indicating higher productivity (Schott et al., 2002). The global ocean, and especially the Indian and Arctic, is data poor, and requires further sampling and evaluation to improve the predictions. Atmospheric surface mixing ratios of bromoform show similar distribution patterns. Higher atmospheric mixing ratios are located in the equatorial regions (1–3 ppt), around coastlines ($\sim$ 1-10 ppt) and upwelling regions (10–17 ppt), as well as in the northern Atlantic ($\sim$ 12–21 ppt), while lower mixing ratios are found above the subtropical gyres ($\sim$ 0.2–0.8 ppt).

The global surface oceanic concentration map of dibromomethane shows similar patterns as bromoform. Enhanced oceanic surface concentrations are located around the equatorial region (~ 6–$9\,\text{pmol L}^{-1}$), while low concentrations occur in the subtropical gyres (1–$2\,\text{pmol L}^{-1}$), similar to $CHBr_3$ in distribution, but with higher values. Dibromomethane concentrations in the coastal regions are significantly lower than those for bromoform. Distant from the coastal source regions CH_2Br_2 is mostly elevated in the atmosphere relative to $CHBr_3$, because it has a longer atmospheric lifetime than $CHBr_3$ (e.g. Brinckmann et al., 2012) ($CH_2Br_2 = 0.33$ yr, $CHBr_3 = 0.07$ yr, (Warneck and Williams, 2012).

Elevated marine dibromomethane concentrations are found in the Southern Ocean (4–$6\,\text{pmol L}^{-1}$). This area is characterized by several circumpolar currents separated by frontal systems, with seasonally varying ice coverage, and is known to experience enhanced biological production (Smith and Nelson, 1985). Sea-ice retreat and the onset of microalgae blooms have been related to an increase in marine surface bromocarbon concentrations (Hughes et al., 2009). However, this strong increase of CH_2Br_2 is currently not understood.

The climatological maps represent annual average values that may underestimate seasonal and short-term variations (Hepach et al., 2013; Fuhlbrügge et al., 2013). These variations currently cannot be reflected in the model, since knowledge about production processes and the influence of environmental values on the concentrations is incomplete.

4.2 Climatological concentration maps of CH_3I

The same classification and interpolation technique used for the bromocarbons reveal elevated marine and atmospheric concentrations of methyl iodide (2–9 pmol L^{-1}, 0.3–1.5 ppt) in the subtropical gyre regions of both hemispheres (Fig. 4). This is in contrast to the oceanic concentration maps of bromoform and dibromomethane, and is in agreement with reported production processes, such as photochemical oxidation of dissolved organic matter and iodide, as well as production from cyanobacteria (e.g. Richter and Wallace, 2004; Smythe-Wright et al., 2006).

Additionally, enhanced oceanic concentrations and atmospheric mixing ratios are found in the upwelling region off Mauritania and near the coastlines north of 40° ($\sim$ 9 pmol L^{-1}). Here in the region of offshore trade winds and dust export, the atmospheric methyl iodide from the ocean may be supplemented by input from land sources (Sive et al., 2007) as elevated air concentrations have been noted to be associated with dust events (Williams et al., 2007). The sharp concentration increase towards the coast, as observed for bromoform and dibromomethane, does not exist for methyl iodide. The open ocean concentrations are generally higher than the coastal values, except for the Northern Hemisphere. The elevated coastal oceanic concentrations might be due to the occurrence of macroalgae and anthropogenic land sources (e.g. Laturnus et al., 1998; Bondu et al., 2008) or to elevated levels of dissolved organic material (DOM) (e.g. Manley et al., 1992; Bell et al., 2002). The polar regions show generally homogenous and low concentrations of methyl iodide (Antarctic: $\sim$ 0.3 ppt, $\sim$ 1.5 pmol L^{-1}; Arctic: $\sim$ 1 ppt and $\sim$ 0.3 pmol L^{-1}).

4.3 Climatological emission maps of $CHBr_3$ and CH_2Br_2

Elevated bromoform fluxes from the ocean to the atmosphere are generally found close to coastlines, in equatorial and eastern boundary upwelling regions (e.g. the Mauritanian upwelling region) and a wide region of the southern Pacific (subtropical gyre). Very high sea-to-air fluxes ($>$ 1500 pmol m^{-2} h^{-1}) also occur in the Bay of Bengal, the Gulf of Mexico, the North Sea and the east coast of North America.

While they cover 16 % of the world ocean area, the coastal and shelf regions, with their high biological productivity, have enhanced concentrations of bromoform and dibromomethane and account for 67/78(RF/OLS) % of total Br emission attributable to $CHBr_3$ and 22/24 % of that attributable to CH_2Br_2. Most of the open ocean appears almost in equilibrium with the atmosphere, especially in the subtropical gyre regions. A $CHBr_3$ flux from the atmosphere to the ocean is seen in the entire Southern Ocean, the northern part of the Pacific and in some parts of the North Atlantic (e.g. east of North America).

Our open ocean flux of $CHBr_3$ is about 25 % of the global sea-to-air flux estimate, which is in agreement with the 20 % calculated by Butler et al. (2007) and the 33 % of Quack and Wallace (2003). This underlines that the coast and shelf regions play a significant role in the global bromoform budget. The tropics (20° N to 20° S, including open ocean, shelf and coastal area) represent the region with the highest bromoform emissions of 44/55 % (Table 3). This is in agreement with the top-down approach of 55.6 % between 20° N to 20° S published by Ordonez et al. (2012) and of 37.7 % for 10° N to 10° S from Liang et al. (2010). A decrease in the total emission towards the polar region is visible. Hence, the tropics are a “hot spot” for bromoform emissions.

Comparable with the sea-to-air fluxes based on the RF analysis, the emissions using the OLS method shows enhanced sea-to-air fluxes in the North Atlantic and all gyre regions, and an elevated sink in the Arctic region (Fig. 5). We estimate a global positive sea-to-air flux for $CHBr_3$ of $\sim$ 2.06 Gmol Br yr^{-1} (RF), $\sim$ 2.96 Gmol Br yr^{-1} (OLS); and a global sink, air-to-sea flux, for $CHBr_3$ of $\sim$ 0.56 Gmol Br yr^{-1} (RF), $\sim$ 0.47 Gmol Br yr^{-1} (OLS).

Differences between the distribution of source and sink regions and of CH_2Br_2 emissions calculated with the RF and OLS regression are less pronounced than those of $CHBr_3$ (Fig. 5). The Arctic Ocean acts mainly as a sink for atmospheric CH_2Br_2, most likely because of the low sea surface temperatures, low water concentrations and higher air concentrations. The Southern Ocean (south of 50° S) acts as a source to the atmosphere. The OLS based emissions show an enhanced source region in the southern Pacific due to elevated marine surface concentrations. We estimate a positive global CH_2Br_2 sea-to-air flux of $\sim$ 0.89 Gmol Br yr^{-1} (RF), $\sim$ 1.09 Gmol Br yr^{-1} (OLS); and an air-to-sea flux of $\sim$ 0.12 Gmol Br yr^{-1} (RF), $\sim$ 0.11 Gmol Br yr^{-1} (OLS).

Our total open ocean flux of 0.6–0.76 Gmol Br (CH_2Br_2) yr^{-1} is in agreement with the estimates of $\sim$ 0.7 Gmol Br yr^{-1}given by Ko et al. (2003) and 0.6 Gmol Br yr^{-1} given by Butler et al. (2007). The coast and shelf regions play a minor role for the global CH_2Br_2 budget compared to the open ocean, which contributes $\sim$ 77 % Gmol Br yr^{-1}. The global emission distribution for CH_2Br_2 and $CHBr_3$ is similar in the midlatitudes and the tropics. (Table 3). Enhanced source regions for the atmosphere are found in the tropical area contributing about 44/49 % between 20° N and 20° S. This is lower compared with the study of Ordonez et al. (2012) who calculated a contribution of 63.1 % from 20° N to 20° S. The CH_2Br_2 emissions decrease towards the polar regions.

4.4 Climatological emission maps of CH_3I

The global emissions of CH_3I reveal an opposite pattern compared with $CHBr_3$ and CH_2Br_2 (Fig. 5). The main difference is the enhanced emission in the subtropical gyre regions.

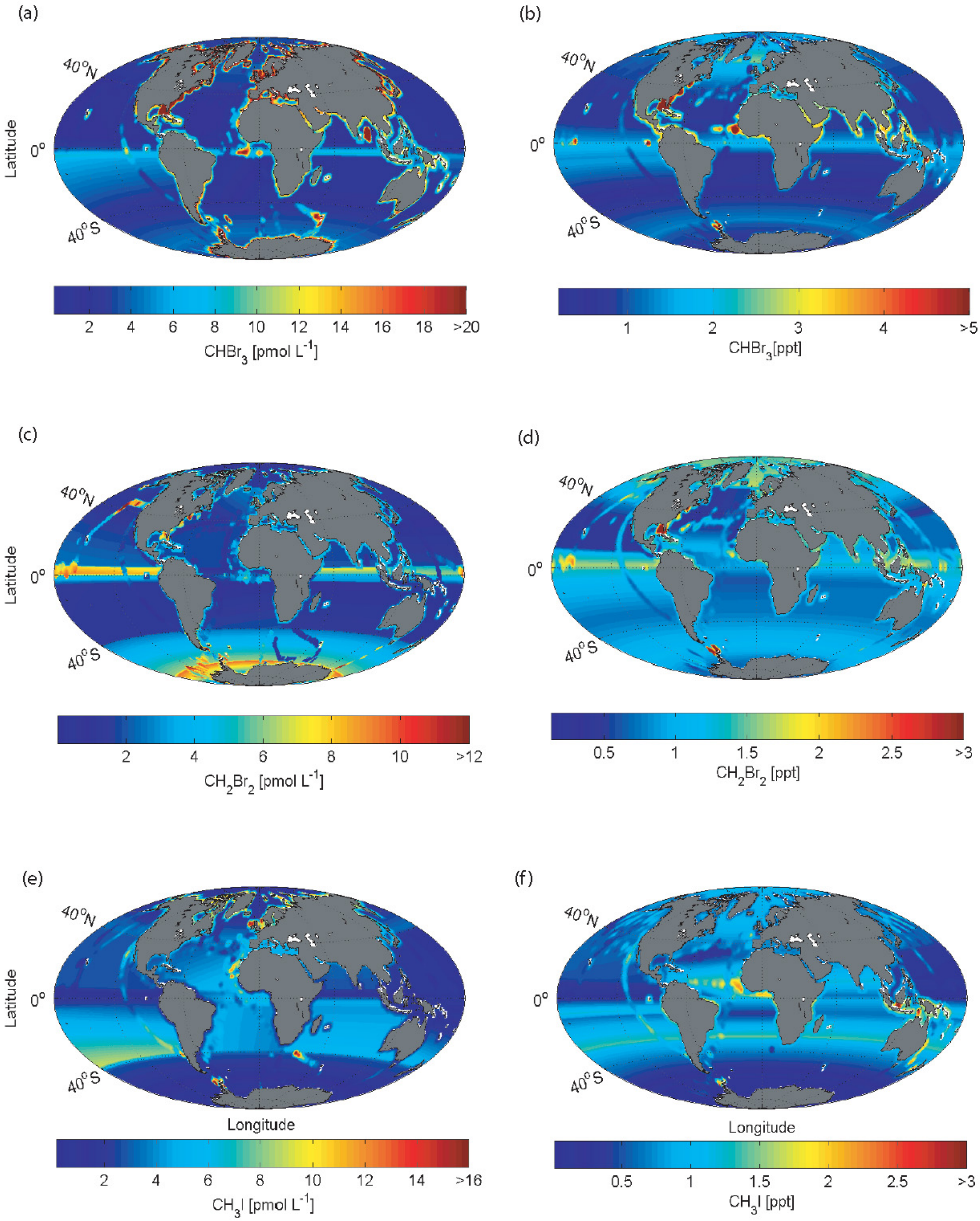
(a)
40°N
0°
40°S
Latitude
2 4 6 8 10 12 14 16 18 >20
CHBr3 [pmol L-1]
(b)
40°N
0°
40°S
1 2 3 4 >5
CHBr3[ppt]
(c)
40°N
0°
40°S
Latitude
2 4 6 8 10 >12
CH2Br2 [pmol L-1]
(d)
40°N
0°
40°S
0.5 1 1.5 2 2.5 >3
CH2Br2 [ppt]
(e)
40°N
0°
40°S
Latitude
Longitude
2 4 6 8 10 12 14 >16
CH3I [pmol L-1]
(f)
40°N
0°
40°S
Longitude
0.5 1 1.5 2 2.5 >3
CH3I [ppt]

Fig. 4. Global maps of marine concentrations (pmol L^{-1}) and atmospheric mixing ratios (ppt) for bromoform **(a, b)**, dibromomethane **(c, d)** and methyl iodide **(e, f)** based on the robust fit (RF) regression analyses. The concentration maps calculated with the OLS method are included in the Supplement (Fig. S3).

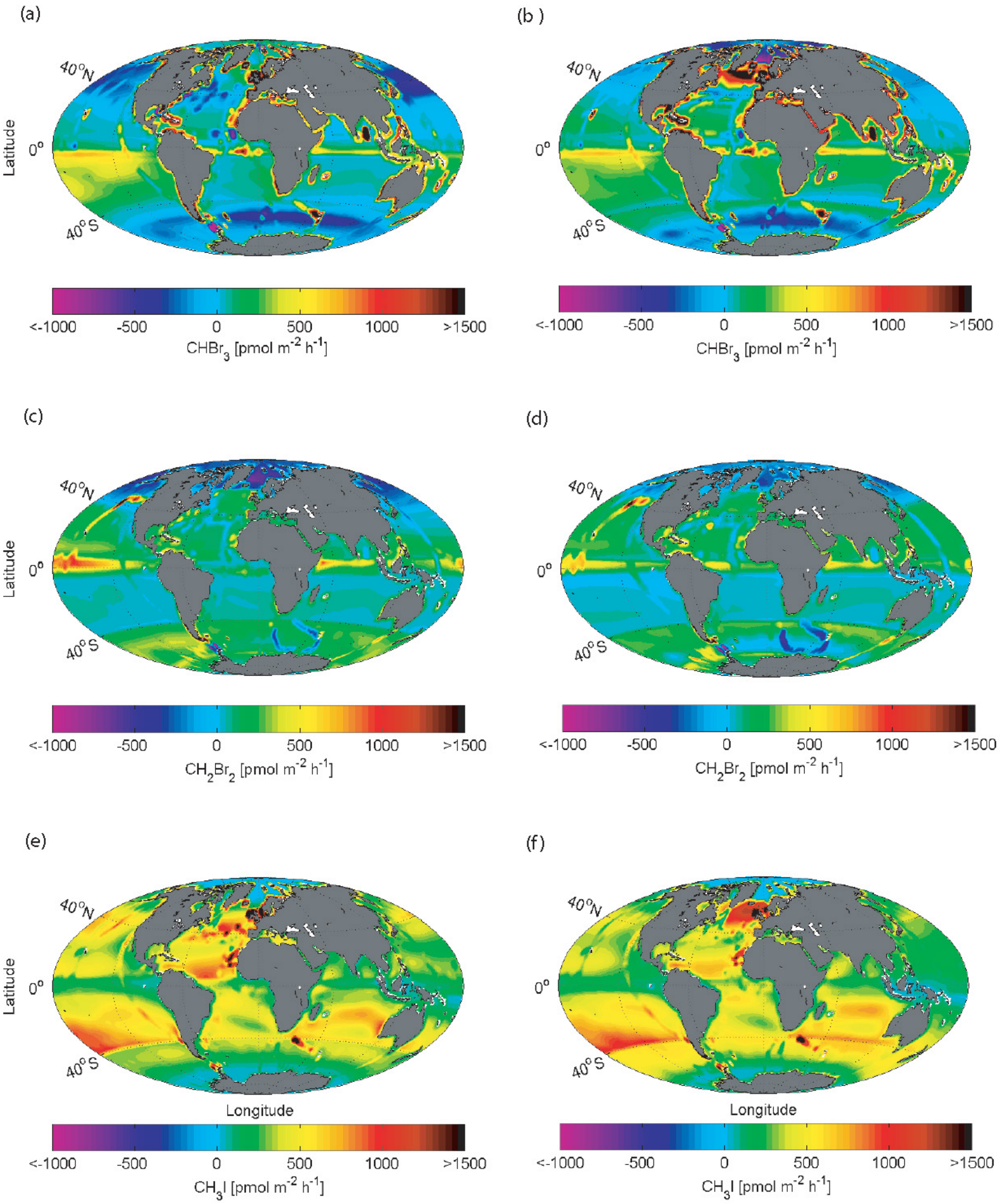
(a)
(b)
(c)
(d)
(e)
(f)
40°N
0°
40°S
Latitude
Longitude
<-1000
-500
0
500
1000
>1500
CHBr3 [pmol m-2 h-1]
CH2Br2 [pmol m-2 h-1]
CH3I [pmol m-2 h-1]

Fig. 5. Global sea-to-air flux climatology of bromoform **(a, b)**, dibromomethane **(c, d)** and methyl iodide **(e, f)** in pmol $\mathrm{m}^{-2}\,\mathrm{h}^{-1}$ based on the RF (**a, c, e**, left column) and OLS (**b, d, f**, right column) analyses.

Equatorial upwelling regions, as well as the Arctic and Antarctic polar regions, are mostly in equilibrium. In comparison with $CHBr_3$ and CH_2Br_2, the global CH_3I sea-to-air fluxes are generally positive, indicating the larger supersaturations of the oceanic waters. The OLS regression shows the North Atlantic to be a very strong source region for atmospheric methyl iodide. Coast and shelf regions transport only $\sim 13\,\%$ of I (CH_3I) to the atmosphere. The open ocean contribution of 87 % is more than the estimate from Butler et al. (2007) of 50 % open ocean emissions of methyl iodide. Possibly, the subtropical gyre regions are more distinctive source areas in our climatology than in Butler et al. (2007). The southern tropics and subtropics represent the regions with the highest emission strength, decreasing towards the polar areas (Table 3). We calculate a global sea-to-air flux for CH_3I of $\sim 1.24\,\mathrm{Gmol\,I\,yr^{-1}}$ (RF) and $\sim 1.45\,\mathrm{Gmol\,I\,yr^{-1}}$ (OLS).

4.5 Evaluation of RF and OLS results

All subtropical regions, and especially the equator, show a large temporal and spatial variability in the data, which is reflected in the enhanced RMSE parameter (Tables S1 and S2 in the Supplement). The wide concentration ranges might be caused by real variations between sampling in different seasons, where the seasonally varying strength and expansion of upwelling (equatorial and coastal) (Minas et al., 1982; Hagen et al., 2001) and solar flux may cause different concentrations of the compounds.

The evaluation of the two regression methods shows that RF is more representative of a climatology, since it is calculating a regression independently of outliers and weighted by the data distribution. In comparison, the OLS regression weights outliers, and, hence considers extreme data and variability more than the RF method (Fig. 2). The global appearances of RF and OLS maps are not extremely different (see Supplement). Nevertheless, they introduce slight differences in the concentration gradients and in the sea-to-air flux climatologies.

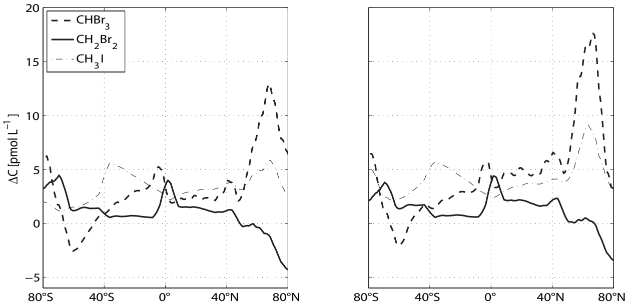

Fig. 6. Zonal mean concentration gradients for bromoform (dashed line), dibromomethane (solid line) and methyl iodide (dash-dotted line) in $\mathrm{pmol\,L^{-1}}$, calculated with RF (left side) and OLS (right side) methods.

The influence of the RF and the OLS regression for the global surface concentration distribution in atmosphere and ocean, which has consequences for the concentration gradient, is shown in Table 1 and Fig. 6. In general, the OLS technique calculates higher mean and median values, including the enhanced concentrations and outliers. Additionally, bromoform shows higher variance compared with the other compounds in both techniques and reflects the high data variability between coastal and open ocean bromoform concentrations. Further, the calculated concentration gradient from the OLS method exhibits stronger source (emission into the atmosphere) and weaker sink regions compared with RF, which is again most pronounced for bromoform (Fig. 6). The OLS and RF distribution (mean, median and standard deviation) for dibromomethane and methyl iodide are in closer agreement compared with bromoform. The reason for this smaller difference between RF and OLS is the occurrence of less extreme values in the concentration gradients for CH_2Br_2 and CH_3I compared with $CHBr_3$. The global surface emissions of bromoform, dibromomethane and methyl iodide yield a similar spatial distribution with both techniques (Table 2).

4.6 Comparison of estimation methods

In the following section we compare our emission climatology with recently published estimates, including different calculation techniques (i.e. bottom-up and top-down approaches), as well as laboratory experiments (Table 6). The global bromoform emission estimates show the largest difference between the studies.

Warwick et al. (2006) modelled surface mixing ratios using different emission scenarios and fitted them to the available atmospheric measurements. These scenarios applied different global emission estimates, e.g. the bottom-up estimate from Quack and Wallace (2003). The course resolution of 2.8° × 2.8° used in the Warwick study does not well resolve the coastal areas, which are thought to be the main source for bromoform. In addition the applied uniform interpolations do not reflect the actual conditions. In the results of Warwick et al. (2006), the coastlines further north and south of the tropics exhibit no enhanced atmospheric bromoform concentrations or emission to the atmosphere compared to the open ocean. This does not reflect the in situ measurements from the HalOcAt database. Based on local bromoform measurements in Southeast Asia, Pyle et al. (2011) reduced the emission estimate of Warwick et al. (2006) in this coastal area. This study shows the importance of local measurements for the improvement of global estimates. Other model studies based on the ideas of Warwick et al. (2006), e.g. Kerkweg et al. (2008), show the same underestimation of coastal emissions in the extra tropics. In contrast, Liang et al. (2010) consider all coastlines with enhanced emissions in their scenario; furthermore the finer classification of their emission scenario compared with Warwick et al. (2006) is

Table 1. Statistical moments: mean (μ), median, standard deviation (σ), minimum and maximum values of atmospheric mixing ratio (ppt) and oceanic concentration (pmol L^{-1}) climatologies of $CHBr_3$, CH_2Br_2 and CH_3I based on the RF and OLS regression analyses.

Compound	μ		Median		σ		Minimum		Maximum	
	RF	OLS	RF	OLS	RF	OLS	RF	OLS	RF	OLS
Atmosphere										
$CHBr_3$	0.9	1.1	1.0	1.6	1.2	1.6	0.01	0.03	53.1	53.1
CH_2Br_2	1.0	1.1	1.0	1.1	0.4	0.4	0.07	0.07	7.8	7.8
CH_3I	0.7	0.8	0.7	0.7	0.4	0.4	0.05	0.01	7.3	7.3
Ocean										
$CHBr_3$	5.9	9.3	3.1	4.4	9.8	14.6	0.29	0.19	823.0	823.0
CH_2Br_2	2.9	3.5	1.9	2.6	2.4	2.7	0.01	0.01	89.8	89.8
CH_3I	3.2	3.9	2.6	3.4	2.6	2.9	0.03	0.05	39.6	39.6

Table 2. Statistical moments: mean (μ), median, standard deviation (σ), minimum and maximum values for the calculated global sea-to-air flux climatologies of $CHBr_3$, CH_2Br_2 and CH_3I based on the RF and OLS regression analyses, in pmol m^{-2} h^{-1}.

Global Sea-to-Air	μ		Median		σ		Minimum		Maximum	
Flux Climatology	RF	OLS	RF	OLS	RF	OLS	RF	OLS	RF	OLS
$CHBr_3$	154.9	236.2	47.1	89.7	549.7	749.6	−5339	−5230	19 618	19 618
CH_2Br_2	76.5	112.4	79.3	78.8	237.9	258.4	−1687	−1714	3978	3978
CH_3I	329.6	405.0	307.3	385.2	289.8	348.3	−49	−55	4895	4878

Table 3. The emission distribution of $CHBr_3$, CH_2Br_2 and CH_3I calculated with two different regression methods (RF and OLS) for different latitudinal bands (see text for explanation), expressed as a percentage.

	$CHBr_3$		CH_2Br_2		CH_3I	
	RF	OLS	RF	OLS	RF	OLS
50–90° N	22.8	21.2	−9.7	−4.9	10.4	7.6
20–50° N	7.4	15.9	13.7	19.1	19.8	20.3
20° N–20° S	54.7	43.6	48.9	44.3	28.9	32.1
20–50° S	22.7	19.3	25.1	22.1	32.8	34.1
50–90° S	−7.6	0.007	22.0	19.5	8.2	5.9

similar to our study. Another comparable classification (latitudinal bands, higher emissions in coastal regions) is used in the model (top-down approach) by Ordonez et al. (2012), who parameterized oceanic polybromomethanes emissions based on a chlorophyll a (chl a) dependent source in the tropical ocean (20° N to 20° S). We also see the occurrence of enhanced bromoform, as well as dibromomethane emissions in tropical upwelling regions and in coastal regions, although a direct correlation between chl a and the VSLS compounds is not apparent from the observations (Abrahamsson et al., 2004; Quack et al., 2007b). Palmer and Reason (2009) developed a parameterization for $CHBr_3$ based on chl a (between 30° N and 30° S), including other parameters (mixed layer depth, sea surface temperature and salinity, wind speed). The correlation between his modelled values and observations is, with $r^2 = 0.4$, low, which reveals the deficiency of this method (and chl a).

In some studies local emission estimates are extrapolated to a global scale. Extrapolating near-shore emissions may significantly overestimate the global sea-to-air fluxes, since they generally include elevated coastal concentrations, which are not representative of the global ocean. Yokouchi et al. (2005) applied a coastal emission ratio of $CHBr_3/CH_2Br_2$ of 9, and a global emission of 0.76 Gmol Br yr^{-1} for CH_2Br_2 to infer a global $CHBr_3$ flux estimate of 10.26 ± 3.88 Gmol Br yr^{-1}. O'Brien et al. (2009) followed the same method and extrapolated local near-shore measurements in the region surrounding Cape Verde to a global scale using an emission ratio of $CHBr_3/CH_2Br_2 = 13$. The global fluxes from these studies are nearly four times higher than those calculated in our study. However, since the emission ratios of $CHBr_3$ to CH_2Br_2 are generally higher in coastal regions than in the other areas (Hepach et al., 2013), the calculated global flux for $CHBr_3$ could be an overestimation.

Butler et al. (2007) and Quack and Wallace (2003) interpolated oceanic and atmospheric in situ measurements for global emission estimates. Butler et al. (2007) subdivided the ocean into the main basins and calculated the fraction of each compound for each region as a percentage. Coastal areas were not considered. The extrapolation by Quack and Wallace (2003) contained most of the currently available

Table 4. Fluxes of bromine from $CHBr_3$ and CH_2Br_2 in Gmol Br yr^{-1}, and iodine from CH_3I in Gmol I yr^{-1}.

References	$CHBr_3$ Flux (Gmol Br yr^{-1})		CH_2Br_2 Flux (Gmol Br yr^{-1})		CH_3I Flux (Gmol I yr^{-1})		Approach
	Global		Global		Global		
Butler et al. (2007)	10.01		3.50		4.33		*bottom-up*
Liang et al. (2010)	5.38		0.71				*top-down*
O'Brien et al. (2009)	10.26						*bottom-up*
Yokouchi et al. (2005)	10.26						*bottom-up*
Warwick et al. (2006)	7.01		1.25				*top-down*
Pyle et al. (2011)	4.78		1.25				*top-down*
Quack and Wallace (2003)	10.01						*bottom-up*
Smythe-Wright et al. (2006)					4.18		*lab experiment*
Bell et al. (2002)					2.4		*model study*
Ordonez et al. (2011)	6.67		0.84		2.39		*top-down*
Kerkweg et al. (2008)	7.45		1.41				*top-down*
	Source	Sink	Source	Sink	Source	Sink	
This study RF	2.06	−0.56	0.89	−0.12	1.24	−0.00008	*bottom-up*
This study OLS	2.96	−0.47	1.09	−0.11	1.45	−0.0001	*bottom-up*

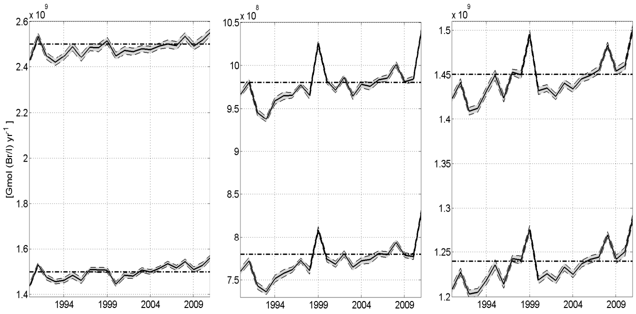

Fig. 7. Inter-annual sea-to-air flux variability over 1989–2011 (bold solid line) of bromoform (left), dibromomethane (centre) and methyl iodide (right) calculated with the two regression techniques (RF (lower panels) and OLS (upper panels)), in Gmol (Br/I) yr^{-1}. Additionally, the respective climatological value is marked (dash-dotted line) as well as the standard deviation (grey shaded).

published measurements and used a finer area classification for shore, shelf and open ocean regions as well as for latitudinal bands. Both bottom-up approaches applied a coarse data interpolation compared to the classification and regression techniques used in this study and appear too high.

We calculate a global CH_2Br_2 sea-to-air flux of 0.77–0.98 Gmol Br yr^{-1}, which is also in the lower (0.71–3.5 Gmol Br yr^{-1}) range of the other estimates (Table 4), but is in much closer agreement compared to the other compounds. Reasons for the good agreement with recent studies could be the longer atmospheric lifetime of CH_2Br_2 and the lower variance of sea water values which cause a more homogenous global distribution.

Some earlier emission estimations for CH_3I (1.05–10.5 Gmol I yr^{-1}) are given by Bell et al. (2002), who produced the first seasonal model simulation of global oceanic and atmospheric CH_3I surface concentrations. A low correlation between observations and modelled data was obtained ($r = 0.4$). The authors assumed a missing biological sink of CH_3I in the ocean that would have reduced their computed concentrations to better match the observations. Sink and source mechanisms for the formation of CH_3I are not fully understood, making it difficult to model CH_3I emissions based on source and sink parameterizations. In our study a global sea-to-air flux of 1.24–1.45 Gmol I yr^{-1} is estimated, which is within the lower range of earlier studies (Table 4). Our calculated climatology uses a larger dataset than the study of Bell et al. (2002). Ordonez et al. (2012) calculate a global CH_3I flux of the same magnitude as our study using a top-down approach with a modified global chemistry model that includes bromine and iodine chemistry. Smythe-Wright et al. (2006) calculated a global flux of iodine from *Prochlorococcus marinus* of ∼4.18 Gmol I yr^{-1} based on measurements from two cruises. The latter study assumes that this phytoplankton species is the major marine source of atmospheric CH_3I. The assumption of Smythe-Wright et al. (2006) that the oceanic surface (< 40° N and S) is covered with CH_3I-producing picoplankton might overestimate the global CH_3I sea-to-air flux. Calculations based on culture experiments from Brownell et al. (2010) demonstrate that *Prochlorococcus marinus* accounts only for 0.03 % of the global CH_3I budget and is not a globally significant source of CH_3I. Hughes et al. (2011) suggest different culture conditions as a possible explanation for the contradictory findings of the culture experiments. The bottle experiments of

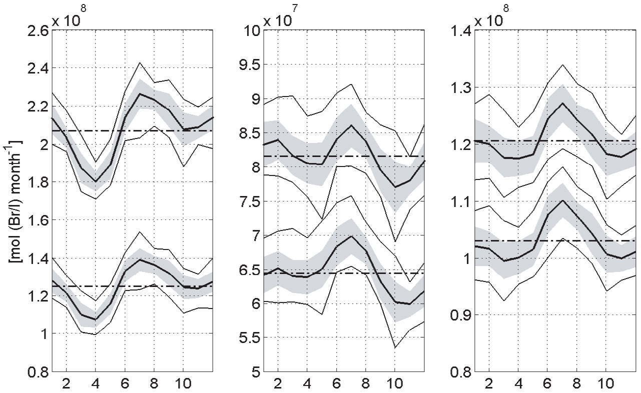

Fig. 8. Global monthly sea-to-air flux averages of bromoform (left), dibromomethane (centre) and methyl iodide (right) in mol (Br/I) month^{-1} (bold solid line) from 1989 to 2011, including their standard deviation (grey shaded area) and their minimum and maximum value (solid line). Additionally, the respective annual mean value is marked (dash-dotted line). The upper graphs show the oceanic emissions using the OLS regression technique and the bottom graphs the RF calculated fluxes.

Richter and Wallace (2004) suggested a photochemical production pathway of CH_3I in open ocean water which might also explain our surface distribution (enhanced emissions in the subtropical gyre regions).

The comparison of our global sea-to-air fluxes with other global estimates reveals the greatest discrepancy for bromoform. We have shown that bromoform levels are the most variable in the ocean and atmosphere. Possibly, the underrepresentation of extreme values generates too small concentration gradients, which reduces our total emission estimate. Especially in coastal and shelf regions, the 1° × 1° grid resolution cannot resolve these extreme concentrations and very likely leads to underestimated emissions.

5 Variability of the climatological sea-to-air fluxes

We calculate global emission fields using fixed oceanic concentrations and atmospheric mixing ratios and the highest available temporal resolution of the input parameters over the time period 1989–2011: 6-hourly means of U, SST, SLP and monthly means for the SSS. The global emissions of every time step are averaged over each month and the average monthly emissions are summed to the annual climatological emission. The climatologies thus include annual, seasonal and short timescale temporal variability.

5.1 Variability of the concentration data

The calculated global 1° × 1° maps of oceanic concentrations and atmospheric mixing ratios include in situ measurements from 1989 to 2011, illustrating a climatological year and covering the entire globe. Seasonally changing conditions, e.g. light and water temperature or biological species composition, which have an influence on the variability of the air and water concentrations in certain areas (Archer et al., 2007; Orlikowska and Schulz-Bull, 2009), are not considered because of the generally poor temporal data coverage. Fitting the in situ measurements onto our 1° × 1° grid (by using objective mapping) leads on average to a reduction of the initial atmospheric mixing ratios and oceanic concentrations of less than 1 %. The accuracy of the interpolation is limited by the sparse data coverage and the regression technique used. Seasonal and spatial accuracy could be improved if a larger dataset was available. Thus we recommend more measurements, especially in the ocean, as well as a refinement of process understanding. The temporal variability of the SST is considered in the concentration gradient, used in the sea-to-air flux calculation, by computing a new equilibrium concentration for every 6 h time step from 1989 to 2011.

5.2 Annual and seasonal variability

The inter-annual variability of the global sea-to-air flux from 1989 to 2011 is small and generally less than 5 % (Fig. 7). The halocarbons all show a positive trend towards 2011. Within a year, the global flux varies monthly for every halogenated compound (Fig. 8). The maximum global sea-to-air flux is most pronounced in July for all compounds, while the minimum is reached in March–April for $CHBr_3$ and CH_3I and in October for CH_2Br_2. The climatological monthly flux and the corresponding minimum and maximum monthly fluxes vary between 9 and 21 %. CH_3I shows the smallest mean deviation with 9 and 11 % for OLS and RF respectively, whereas the variation for CH_2Br_2 is between 14 and 17 % and for $CHBr_3$ between 17 and 21 %. Thus the seasonal variation of the global climatological flux is larger than the inter-annual variation, despite the shifting of the seasons (half a year) between the Northern Hemisphere and Southern Hemisphere. The global climatological fluxes, obtained from the sum of the monthly averages between 1989 and 2011, describe the current best possible estimates of the moderately varying annual and seasonal global emissions. However, the results do not consider a seasonally varying influence of either the water or the air concentration on the emission because the current sparse investigations do not allow a suitable parameterization of the VSLS yet.

5.3 Short time variability of fluxes

In situ fluxes from a cruise (TransBrom) between Japan and Australia in October 2009 are compared to the nearest grid points of our climatology (Fig. 9) as an example for the influence of short time variability. The TransBrom data include 105 $CHBr_3$ and CH_2Br_2 measurements and 96 CH_3I measurements, and are included in the climatology. The cruise transited through different biogeochemical regions with varying meteorological conditions influencing

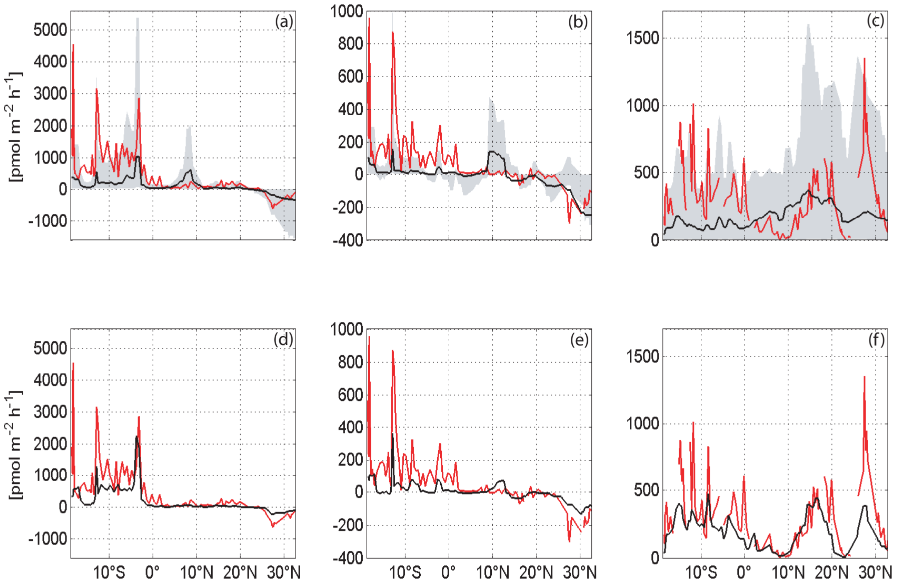

Fig. 9. The upper panels illustrate the comparison between our climatological estimate (black line) and the in situ sea-to-air fluxes from the TransBrom cruise (red line) for bromoform **(a)**, dibromomethane **(b)** and methyl iodide **(c)** in pmol m^{-2} h^{-1} (see more details in the text) including the climatological minimum and maximum values (grey shaded area). The lower panels represent the same in situ measurements compared to our model values using the nearest 6-hourly mean of SST, U and SLP and monthly mean of SSS with fixed mixing ratios and oceanic concentrations calculated with the RF method for bromoform **(d)**, dibromomethane **(e)** and methyl iodide **(f)** (the emissions using OLS look similar).

the strength of VSLS emissions (Krüger and Quack, 2012). The in situ and climatological sea-to-air fluxes for bromoform and dibromomethane compare very well in the Northern Hemisphere, where small concentration gradients are found in the open oceans. The enhanced emissions in the Southern Hemisphere encountered during the cruise are under-represented in the climatology. Comparison of the methyl iodide in situ fluxes and the climatology shows a similar trend, although the extreme values of the in situ measurements are highly under-represented in the climatological mean flux value. Our climatology underestimates the short-term measured fluxes by smoothing the values of the varying input parameters. The mean deviation between the climatology and the in situ fluxes during October 2009 is ∼ 120 % for $CHBr_3$, ∼ 20 % for CH_2Br_2 and ∼ 176 % for CH_3I, respectively.

We also calculate the sea-to-air fluxes using the nearest temporal and spatial 6-hourly means (highest available resolution) of SST, SLP and U, the monthly mean of the SSS and the climatological oceanic concentration and mixing ratios, and compare them to the measured fluxes (Fig. 9). The mean deviation between the 6-hourly means and the in situ fluxes for the three compounds is only ∼ 48 % for $CHBr_3$, ∼ 15 % for CH_2Br_2 and 51 % for CH_3I. These values show the good match between "modelled" and in situ measurements and validate the predictive capability of this approach. The climatological minimum and maximum values of the cruise nearest data points (Fig. 9, upper panel) reveal how variable the "modelled" fluxes can be at a single location. While most in situ fluxes are included in the 6 h minimum and maximum range from 1989 to 2011, it is also noteworthy that even with this high temporal (6 h) resolution of input parameters, the "modelled" fluxes can neither match the extreme values of the encountered in situ fluxes, nor do they resolve the high variability of the in situ fluxes completely. An additional factor for the under-representation of the extreme in situ values is the mean concentration gradient (1° × 1° resolution) in our "model". In the vicinity of source regions, e.g. coast lines, the water concentrations can vary by more than 100 % over short distances (Butler et al., 2006), which strongly influences the in situ fluxes and is likely not resolved in the model due to poor data coverage.

6 Summary and conclusion

Global sea-to-air flux climatologies (considering the time span from 1989 to 2011 of the three important short-lived halocarbons, bromoform, dibromomethane and methyl iodide) are calculated based on surface oceanic and atmospheric measurements from the HalOcAt database. The physical and biogeochemical factors of the compounds' distributions in ocean and atmosphere are also considered. Data are classified into coastal, shelf and open ocean regions, and are interpolated on a 1° × 1° grid. The missing grid values are filled with robust fit (RF) and ordinary least squares (OLS) regression techniques based on the latitudinal and longitudinal distribution of the compounds. The RF interpolation estimates background values, since it is weighted on the quantity of measurements, whereas the OLS regressions include extreme data and therefore represent our highest values. Global emission fields are calculated with a high temporal resolution of 6-hourly wind speed, sea surface temperature and sea level pressure data. The climatological annual global flux for 1989 to 2011 is obtained as sum of the monthly average fluxes. We estimate positive global sea-to-air fluxes of $CHBr_3$, CH_2Br_2 and CH_3I of 2.06/2.96, 0.89/1.09 Gmol Br yr^{-1} and 1.24/1.45 Gmol I yr^{-1}, based on RF/OLS respectively, which are all at the lower end of earlier studies. Previous global climatological estimate studies have not determined negative fluxes (flux into the ocean). We estimate negative global sea-to-air fluxes of $-0.47/-0.56$, $-0.11/-0.12$ Gmol Br yr^{-1} and $-0.08/-0.1$ Mmol I yr^{-1} for $CHBr_3$, CH_2Br_2 and CH_3I, respectively. The net oceanic emissions of our climatology are 1.5/2.5 Gmol Br yr^{-1} for $CHBr_3$, 0.78/0.98 Gmol Br yr^{-1} for CH_2Br_2, and 1.24/1.45 Gmol I yr^{-1} for CH_3I.

Our low bottom-up emission estimates, compared to recent top-down approaches, especially for bromoform, are most likely caused by an under-representation of extreme emissions. Observed high temporal and spatial in situ variances cannot be resolved in the $1^\circ \times 1^\circ$ grid climatology. It is still unclear how important extreme events are for the global bromoform budget, but we suggest that small spatial and temporal events of high oceanic bromoform emissions are important for the transport of bromine into the troposphere and lower stratosphere. The monthly variation of the global climatological flux (9–21 %) is contained within our calculations and it is larger than the inter-annual variability, which is generally less than 5 % for all three compounds.

Our global sea-to-air flux estimates can be used as input for different model calculations. The existing uncertainties can be reduced by enlarging of the HalOcAt database with more measurements, especially in ocean waters, common calibration techniques and more basic research into the underlying source and sink processes.

Supplementary material related to this article is available online at: http://www.atmos-chem-phys.net/13/8915/2013/acp-13-8915-2013-supplement.zip.

Acknowledgements. We thank all contributors sending their data to the HalOcAt database and for their helpful comments on the manuscript. We also thank our assisting student helpers Julian Kinzel, Christian Müller, Eike Hümpel, Anja Müller and Theresa Conradi who populated the database, which started in 2009. This work was financially supported by the WGL project TransBrom, the European commission under the project SHIVA (grant no. 226 224) and by the German Federal Ministry of Education and Research (BMBF) during the project SOPRAN (grant no: 03F0611A). SOLAS Integration (Surface Ocean Lower Atmosphere Study; http://www.bodc.ac.uk/solas_integration/) helped instigate this project and Tom Bell and Peter Liss were supported in this by a NERC UK SOLAS Knowledge Transfer grant (NE/E001696/1). Part of this project was supported by COST (European Cooperation in Science and Technology) Action 735, a European Science Foundation-supported initiative. Additionally, we would like to thank the ECMWF for providing the ERA Interim reanalysis data. We thank two anonymous reviewers for their useful comments and advice.

The service charges for this open access publication
have been covered by a Research Centre of the
Helmholtz Association.

Edited by: R. Volkamer

References

Abrahamsson, K., Bertilsson, S., Chierici, M., Fransson, A., Froneman, P. W., Loren, A., and Pakhomov, E. A.: Variations of biochemical parameters along a transect in the southern ocean, with special emphasis on volatile halogenated organic compounds, Deep-Sea Res. Part II, 51, 2745–2756, doi:10.1016/j.dsr2.2004.09.004, 2004.

Amachi, S., Kamagata, Y., Kanagawa, T., and Muramatsu, Y.: Bacteria mediate methylation of iodine in marine and terrestrial environments, Appl. Environ. Microbiol., 67, 2718–2722, doi:10.1128/aem.67.6.2718-2722.2001, 2001.

Antonov, J. I., Seidov, D., Boyer, T. P., Locarnini, R. A., Mishonov, A. V., Garcia, H. E., Baranova, O. K., Zweng, M. M., and Johnson, D. R.: World ocean atlas 2009, Volume 2: Salinity. S. Levitus Ed. NOAA Atlas NESDIS 69, U.S. Government Printing Office, Washington, DC, 184 pp., 2010.

Archer, S. D., Goldson, L. E., Liddicoat, M. I., Cummings, D. G., and Nightingale, P. D.: Marked seasonality in the concentrations and sea-to-air flux of volatile iodocarbon compounds in the western English Channel, J. Geophys. Res.-Oceans, 112, C08009, doi:10.1029/2006jc003963, 2007.

Aschmann, J., Sinnhuber, B.-M., Atlas, E. L., and Schauffler, S. M.: Modeling the transport of very short-lived substances into the tropical upper troposphere and lower stratosphere, Atmos. Chem. Phys., 9, 9237–9247, doi:10.5194/acp-9-9237-2009, 2009.

Bates, N. R. and Merlivat, L.: The influence of short-term wind variability on air-sea CO_2 exchange, Geophys. Res. Lett., 28, 3281–3284, doi:10.1029/2001gl012897, 2001.

Bell, N., Hsu, L., Jacob, D. J., Schultz, M. G., Blake, D. R., Butler, J. H., King, D. B., Lobert, J. M., and Maier-Reimer, E.: Methyl iodide: Atmospheric budget and use as a tracer of marine convection in global models, J. Geophys. Res.-Atmos., 107, 4340, doi:10.1029/2001jd001151, 2002.

Bondu, S., Cocquempot, B., Deslandes, E., and Morin, P.: Effects of salt and light stress on the release of volatile halogenated organic compounds by *Solieria Chordalis*: A laboratory incubation study, Bot. Mar., 51, 485–492, doi:10.1515/bot.2008.056, 2008.

Brinckmann, S., Engel, A., Bönisch, H., Quack, B., and Atlas, E.: Short-lived brominated hydrocarbons – observations in the source regions and the tropical tropopause layer, Atmos. Chem. Phys., 12, 1213–1228, doi:10.5194/acp-12-1213-2012, 2012.

Brownell, D. K., Moore, R. M., and Cullen, J. J.: Production of methyl halides by *Prochlorococcus* and *Synechococcus*, Glob. Biogeochem. Cy., 24, Gb2002, doi:10.1029/2009gb003671, 2010.

Butler, J. H., King, D. B., Lobert, J. M., Montzka, S. A., Yvon-Lewis, S. A., Hall, B. D., Warwick, N. J., Mondeel, D. J., Aydin, M., and Elkins, J. W.: Oceanic distributions and emissions of short-lived halocarbons, Glob. Biogeochem. Cy., 21, Gb1023, doi:10.1029/2006gb002732, 2007.

Butler, J. H., Bell, T. G., Hall, B. D., Quack, B., Carpenter, L. J., and Williams, J.: Technical Note: Ensuring consistent, global measurements of very short-lived halocarbon gases in the ocean and atmosphere, Atmos. Chem. Phys., 10, 327–330, doi:10.5194/acp-10-327-2010, 2010.

Carpenter, L. J.: Iodine in the marine boundary layer, Chem. Rev., 103, 4953–4962, doi:10.1021/cr0206465, 2003.

Carpenter, L. J. and Liss, P. S.: On temperate sources of bromoform and other reactive organic bromine gases, J. Geophys. Res.-Atmos., 105, 20539–20547, doi:10.1029/2000jd900242, 2000.

Chapman, E. G., Shaw, W. J., Easter, R. C., Bian, X., and Ghan, S. J.: Influence of wind speed averaging on estimates of dimethylsulfide emission fluxes, J. Geophys. Res.-Atmos., 107, 4672, doi:10.1029/2001jd001564, 2002.

Chipperfield, M. P. and Pyle, J. A.: Model sensitivity studies of arctic ozone depletion, J. Geophys. Res.-Atmos., 103, 28389–28403, doi:10.1029/98jd01960, 1998.

Daley, R.: Atmospheric data analysis, Cambridge University Press, Cambridge, England, 457 pp., 1991.

Dee, D. P., Uppala, S. M., Simmons, A. J., Berrisford, P., Poli, P., Kobayashi, S., Andrae, U., Balmaseda, M. A., Balsamo, G., Bauer, P., Bechtold, P., Beljaars, A. C. M., van de Berg, L., Bidlot, J., Bormann, N., Delsol, C., Dragani, R., Fuentes, M., Geer, A. J., Haimberger, L., Healy, S. B., Hersbach, H., Hólm, E. V., Isaksen, L., Kållberg, P., Köhler, M., Matricardi, M., McNally, A. P., Monge-Sanz, B. M., Morcrette, J.-J., Park, B.-K., Peubey, C., de Rosnay, P., Tavolato, C., Thépaut, J.-N., and Vitart, F.: The era-interim reanalysis: Configuration and performance of the data assimilation system, Q. J. Roy. Meteorol. Soc., 137, 553–597, doi:10.1002/qj.828, 2011.

Dorf, M., Butz, A., Camy-Peyret, C., Chipperfield, M. P., Kritten, L., and Pfeilsticker, K.: Bromine in the tropical troposphere and stratosphere as derived from balloon-borne BrO observations, Atmos. Chem. Phys., 8, 7265–7271, doi:10.5194/acp-8-7265-2008, 2008.

Fuhlbrügge, S., Krüger, K., Quack, B., Atlas, E., Hepach, H., and Ziska, F.: Impact of the marine atmospheric boundary layer conditions on VSLS abundances in the eastern tropical and subtropical North Atlantic Ocean, Atmos. Chem. Phys., 13, 6345–6357, doi:10.5194/acp-13-6345-2013, 2013.

Gschwend, P. M., Mac Farlane, J. K., and Newman, K. A.: Volatile halogenated organic-compounds released to seawater from temperate marine macro algae, Science, 227, 1033–1035, doi:10.1126/science.227.4690.1033, 1985.

Hagen, E., Feistel, R., Agenbag, J. J., and Ohde, T.: Seasonal and interannual changes in intense Benguela upwelling (1982–1999), Oceanol. Acta., 24, 557–568, doi:10.1016/s0399-1784(01)01173-2, 2001.

Hamer, P. D., Marécal, V., Hossaini, R., Pirre, M., Warwick, N., Chipperfield, M., Samah, A. A., Harris, N., Robinson, A., Quack, B., Engel, A., Krüger, K., Atlas, E., Subramaniam, K., Oram, D., Leedham, E., Mills, G., Pfeilsticker, K., Sala, S., Keber, T., Bönisch, H., Peng, L. K., Nadzir, M. S. M., Lim, P. T., Mujahid, A., Anton, A., Schlager, H., Catoire, V., Krysztofiak, G., Fühlbrügge, S., Dorf, M., and Sturges, W. T.: Modelling the chemistry and transport of bromoform within a sea breeze driven convective system during the SHIVA Campaign, Atmos. Chem. Phys. Discuss., 13, 20611–20676, doi:10.5194/acpd-13-20611-2013, 2013.

Happell, J. D. and Wallace, D. W. R.: Methyl iodide in the Greenland/Norwegian seas and the tropical Atlantic Ocean: Evidence for photochemical production, Geophys Res. Lett., 23, 2105–2108, doi:10.1029/96gl01764, 1996.

Hepach, H., Quack, B., Ziska, F., Fuhlbrügge, S., Atlas, E. L., Peeken, I., Krüger, K., and Wallace, D. W. R.: Drivers of diel and regional variations of halocarbon emissions from the tropical North East Atlantic, Atmos. Chem. Phys. Discuss., 13, 19701–19750, doi:10.5194/acpd-13-19701-2013, 2013.

Hossaini, R., Mantle, H., Chipperfield, M. P., Montzka, S. A., Hamer, P., Ziska, F., Quack, B., Krüger, K., Tegtmeier, S., Atlas, E., Sala, S., Engel, A., Bönisch, H., Keber, T., Oram, D., Mills, G., Ordóñez, C., Saiz-Lopez, A., Warwick, N., Liang, Q., Feng, W., Moore, F., Miller, B. R., Marécal, V., Richards, N. A. D., Dorf, M., and Pfeilsticker, K.: Evaluating global emission inventories of biogenic bromocarbons, Atmos. Chem. Phys. Discuss., 13, 12485–12539, doi:10.5194/acpd-13-12485-2013, 2013.

Huber, P. J.: Robust estimation of location parameter, Ann. Math. Stat., 35, 73–101, doi:10.1214/aoms/1177703732, 1964.

Hughes, C., Chuck, A. L., Rossetti, H., Mann, P. J., Turner, S. M., Clarke, A., Chance, R., and Liss, P. S.: Seasonal cycle of seawater bromoform and dibromomethane concentrations in a coastal bay on the western Antarctic Peninsula, Glob. Biogeochem. Cy., 23, Gb2024, doi:10.1029/2008gb003268, 2009.

Hughes, C., Franklin, D. J., and Malin, G.: Iodomethane production by two important marine cyanobacteria: *Prochlorococcus marinus* (ccmp 2389) and *Synechococcus sp* (ccmp 2370), Mar. Chem., 125, 19–25, doi:10.1016/j.marchem.2011.01.007, 2011.

Johnson, M. T.: A numerical scheme to calculate temperature and salinity dependent air-water transfer velocities for any gas, Ocean Sci., 6, 913–932, doi:10.5194/os-6-913-2010, 2010.

Jones, C. E., Andrews, S. J., Carpenter, L. J., Hogan, C., Hopkins, F. E., Laube, J. C., Robinson, A. D., Spain, T. G., Archer, S. D., Harris, N. R. P., Nightingale, P. D., O'Doherty, S. J., Oram, D. E., Pyle, J. A., Butler, J. H., and Hall, B. D.: Results from the first national UK inter-laboratory calibration for very short-lived halocarbons, Atmos. Meas. Tech., 4, 865–874, doi:10.5194/amt-4-865-2011, 2011.

Kerkweg, A., Jöckel, P., Warwick, N., Gebhardt, S., Brenninkmeijer, C. A. M., and Lelieveld, J.: Consistent simulation of bromine chemistry from the marine boundary layer to the stratosphere – Part 2: Bromocarbons, Atmos. Chem. Phys., 8, 5919–5939, doi:10.5194/acp-8-5919-2008, 2008.

Kettle, H. and Merchant, C. J.: Systematic errors in global air-sea CO_2 flux caused by temporal averaging of sea-level pressure, Atmos. Chem. Phys., 5, 1459–1466, doi:10.5194/acp-5-1459-2005, 2005.

Ko, M. K. W., Poulet, G., Blake, D. R., Boucher, O., Burkholder, J. H., Chin, M., Cox, R. A., George, C., Graf, H.-F., Holton, J. R., Jacob, D. J., Law, K. S., Lawrence, M. G., Midgley, P. M., Seakins, P. W., Shallcross, D. E., Strahan, S. E., Wuebbles, D. J., and Yokouchi, Y.: Very short-lived halogen and sulfur substances, in: Scientific assessment of ozone depletion: 2002, Global Ozone Res. Monit. Proj. Rep.47, World Meteorol. Org., Geneva, 2.1–2.57, 2003.

Krüger, K. and Quack, B.: Introduction to special issue: the TransBrom Sonne expedition in the tropical West Pacific, Atmos. Chem. Phys. Discuss., 12, 1401–1418, doi:10.5194/acpd-12-1401-2012, 2012.

Laturnus, F., Adams, F. C., and Wiencke, C.: Methyl halides from Antarctic macro algae, Geophys. Res. Lett., 25, 773–776, doi:10.1029/98gl00490, 1998.

Liang, Q., Stolarski, R. S., Kawa, S. R., Nielsen, J. E., Douglass, A. R., Rodriguez, J. M., Blake, D. R., Atlas, E. L., and Ott, L. E.: Finding the missing stratospheric Bry: a global modeling study of $CHBr_3$ and CH_2Br_2, Atmos. Chem. Phys., 10, 2269–2286, doi:10.5194/acp-10-2269-2010, 2010.

Liss, P. S. and Merlivat, L.: Air-sea gas exchange rates: Introduction and synthesis, in: The role of air-sea exchange in geochemical cycling, edited by: Buat-Ménard, P., D. Reidel, Hingham, Mass., 113–129, 1986.

Liu, Y., Yvon-Lewis, S. A., Hu, L., Salisbury, J. E., and O'Hern, J. E.: $CHBr_3$, CH_2Br_2, and $CHClBr_2$ in U.S. Coastal waters during the Gulf of Mexico and East Coast carbon cruise, J. Geophys. Res., 116, C10004, doi:10.1029/2010JC006729, 2011.

Manley, S. L. and Dastoor, M. N.: Methyl-iodide (CH_3I) production by kelp and associated microbes, Mar. Biol., 98, 477–482, doi:10.1007/bf00391538, 1988.

Manley, S. L. and dela Cuesta, J. L.: Methyl iodide production from marine phytoplankton cultures, Limnol. Oceanogr., 42, 142–147, 1997.

Manley, S. L., Goodwin, K., and North, W. J.: Laboratory production of bromoform, methylene bromide, and methyl-iodide by macro algae and distribution in near-shore southern California waters, Limnol. Oceanogr., 37, 1652–1659, 1992.

McFiggans, G., Plane, J. M. C., Allan, B. J., Carpenter, L. J., Coe, H., and O'Dowd, C.: A modeling study of iodine chemistry in the marine boundary layer, J. Geophys. Res.-Atmos., 105, 14371–14385, doi:10.1029/1999jd901187, 2000.

Minas, H. J., Packard, T. T., Minas, M., and Coste, B.: An analysis of the production-regeneration system in the coastal upwelling area off NW Africa based on oxygen, nitrate and ammonium distributions, J. Mar. Res., 40, 615–641, 1982.

Montzka, S. A. and Reimann, S.: Ozone-depleting substances and related chemicals, in, Scientific Assessment of Ozone Depletion: 2010, Global Ozone Research and Monitoring Project - Report No. 52, Chapt. 1, edited by: World Meteorological Project, Geneva Switzerland, 2011.

Moore, R. M. and Zafiriou, O. C.: Photochemical production of methyl-iodide in seawater, J. Geophys. Res.-Atmos., 99, 16415–16420, doi:10.1029/94jd00786, 1994.

Moore, R. M., Geen, C. E., and Tait, V. K.: Determination of Henry law constants for a suite of naturally-occurring halogenated methanes in seawater, Chemosphere, 30, 1183–1191, doi:10.1016/0045-6535(95)00009-w, 1995a.

Moore, R. M., Tokarczyk, R., Tait, V. K., Poulin, M., and and Geen, C. E.: Marine phytoplankton as a natural source of volatile organohalogens, in: Naturally-produced organohalogens, edited by: Grimvall, A., and deLeer, E. W. B., Kluwer Academic Publishers, D., 283–294, 1995b.

Nightingale, P. D., Malin, G., and Liss, P. S.: Production of chloroform and other low-molecular-weight halocarbons by some species of macro algae, Limnol. Oceanogr., 40, 680–689, 1995.

Nightingale, P. D., Malin, G., Law, C. S., Watson, A. J., Liss, P. S., Liddicoat, M. I., Boutin, J., and Upstill-Goddard, R. C.: In situ evaluation of air-sea gas exchange parameterizations using novel conservative and volatile tracers, Glob. Biogeochem. Cy., 14, 373–387, 2000.

O'Brien, L. M., Harris, N. R. P., Robinson, A. D., Gostlow, B., Warwick, N., Yang, X., and Pyle, J. A.: Bromocarbons in the tropical marine boundary layer at the Cape Verde Observatory – measurements and modelling, Atmos. Chem. Phys., 9, 9083–9099, doi:10.5194/acp-9-9083-2009, 2009.

Ordóñez, C., Lamarque, J.-F., Tilmes, S., Kinnison, D. E., Atlas, E. L., Blake, D. R., Sousa Santos, G., Brasseur, G., and Saiz-Lopez, A.: Bromine and iodine chemistry in a global chemistry-climate model: description and evaluation of very short-lived oceanic sources, Atmos. Chem. Phys., 12, 1423–1447, doi:10.5194/acp-12-1423-2012, 2012.

Orlikowska, A. and Schulz-Bull, D. E.: Seasonal variations of volatile organic compounds in the coastal Baltic sea, Environ. Chem., 6, 495–507, doi:10.1071/en09107, 2009.

Palmer, C. J. and Reason, C. J.: Relationships of surface bromoform concentrations with mixed layer depth and salinity in the tropical oceans, Glob. Biogeochem. Cy., 23, Gb2014, doi:10.1029/2008gb003338, 2009.

Penkett, S. A., Jones, B. M. R., Rycroft, M. J., and Simmons, D. A.: An interhemispheric comparison of the concentrations of bromine compounds in the atmosphere, Nature, 318, 550–553, doi:10.1038/318550a0, 1985.

Pyle, J. A., Ashfold, M. J., Harris, N. R. P., Robinson, A. D., Warwick, N. J., Carver, G. D., Gostlow, B., O'Brien, L. M., Manning, A. J., Phang, S. M., Yong, S. E., Leong, K. P., Ung, E. H., and Ong, S.: Bromoform in the tropical boundary layer of the Maritime Continent during OP3, Atmos. Chem. Phys., 11, 529–542, doi:10.5194/acp-11-529-2011, 2011.

Quack, B. and Wallace, D. W. R.: Air-sea flux of bromoform: Controls, rates, and implications, Glob. Biogeochem. Cy., 17, 1023, doi:10.1029/2002gb001890, 2003.

Quack, B., Atlas, E., Petrick, G., Stroud, V., Schauffler, S., and Wallace, D. W. R.: Oceanic bromoform sources for the tropical atmosphere, Geophys. Res. Lett., 31, L23s05, doi:10.1029/2004gl020597, 2004.

Quack, B., Atlas, E., Petrick, G., and Wallace, D. W. R.: Bromoform and dibromomethane above the Mauritanian upwelling: Atmospheric distributions and oceanic emissions, J. Geophys. Res.-Atmos., 112, D09312, doi:10.1029/2006jd007614, 2007a.

Quack, B., Peeken, I., Petrick, G., and Nachtigall, K.: Oceanic distribution and sources of bromoform and dibromomethane in the Mauritanian upwelling, J. Geophys. Res.-Oceans, 112, C10006, doi:10.1029/2006jc003803, 2007b.

Richter, U. and Wallace, D. W. R.: Production of methyl iodide in the tropical Atlantic Ocean, Geophys. Res. Lett., 31, L23s03, doi:10.1029/2004gl020779, 2004.

Salawitch, R. J., Weisenstein, D. K., Kovalenko, L. J., Sioris, C. E., Wennberg, P. O., Chance, K., Ko, M. K. W., and McLinden, C. A.: Sensitivity of ozone to bromine in the lower stratosphere, Geophys. Res. Lett., 32, L05811, doi:10.1029/2004gl021504, 2005.

Schott, F. A., Dengler, M., and Schoenefeldt, R.: The shallow overturning circulation of the indian ocean, Prog. Oceanogr., 53, 57–103, doi:10.1016/s0079-6611(02)00039-3, 2002.

Sinnhuber, B.-M. and Folkins, I.: Estimating the contribution of bromoform to stratospheric bromine and its relation to dehydration in the tropical tropopause layer, Atmos. Chem. Phys., 6, 4755–4761, doi:10.5194/acp-6-4755-2006, 2006.

Sinnhuber, B.-M., Sheode, N., Sinnhuber, M., Chipperfield, M. P., and Feng, W.: The contribution of anthropogenic bromine emissions to past stratospheric ozone trends: a modelling study, Atmos. Chem. Phys., 9, 2863–2871, doi:10.5194/acp-9-2863-2009, 2009.

Sive, B. C., Varner, R. K., and Mao, H.: A large terrestrial source of methyl iodide, Geophys. Res. Lett., 34, L17808, doi:10.1029/2007GL030528, 2007.

Smith, W. O. and Nelson, D. M.: Phytoplankton bloom produced by a receding ice edge in the Ross Sea – spatial coherence with the density field, Science, 227, 163–166, doi:10.1126/science.227.4683.163, 1985.

Smythe-Wright, D., Boswell, S. M., Breithaupt, P., Davidson, R. D., Dimmer, C. H., and Diaz, L. B. E.: Methyl iodide production in the ocean: Implications for climate change, Glob. Biogeochem. Cy., 20, Gb3003, doi:10.1029/2005gb002642, 2006.

Solomon, S., Garcia, R. R., and Ravishankara, A. R.: On the role of iodine in ozone depletion, J. Geophys. Res.-Atmos., 99, 20491–20499, doi:10.1029/94jd02028, 1994.

Sturges, W. T., Oram, D. E., Carpenter, L. J., Penkett, S. A., and Engel, A.: Bromoform as a source of stratospheric bromine, Geophys. Res. Lett., 27, 2081–2084, doi:10.1029/2000gl011444, 2000.

Tegtmeier, S., Krüger, K., Quack, B., Atlas, E. L., Pisso, I., Stohl, A., and Yang, X.: Emission and transport of bromocarbons: from the West Pacific ocean into the stratosphere, Atmos. Chem. Phys., 12, 10633–10648, doi:10.5194/acp-12-10633-2012, 2012.

Tegtmeier, S., Krüger, K., Quack, B., Atlas, E., Blake, D. R., Boenisch, H., Engel, A., Hepach, H., Hossaini, R., Navarro, M. A., Raimund, S., Sala, S., Shi, Q., and Ziska, F.: The contribution of oceanic methyl iodide to stratospheric iodine, Atmos. Chem. Phys. Discuss., 13, 11427–11471, doi:10.5194/acpd-13-11427-2013, 2013.

Tokarczyk, R. and Moore, R. M.: Production of volatile organohalogens by phytoplankton cultures, Geophys. Res. Lett., 21, 285–288, doi:10.1029/94gl00009, 1994.

Vogt, R., Sander, R., Von Glasow, R., and Crutzen, P. J.: Iodine chemistry and its role in halogen activation and ozone loss in the marine boundary layer: A model study, J. Atmos. Chem., 32, 375–395, doi:10.1023/a:1006179901037, 1999.

von Glasow, R.: Atmospheric chemistry – sun, sea and ozone destruction, Nature, 453, 1195–1196, doi:10.1038/4531195a, 2008.

von Glasow, R., von Kuhlmann, R., Lawrence, M. G., Platt, U., and Crutzen, P. J.: Impact of reactive bromine chemistry in the troposphere, Atmos. Chem. Phys., 4, 2481–2497, doi:10.5194/acp-4-2481-2004, 2004.

Wanninkhof, R.: Relationship between wind-speed and gas-exchange over the ocean, J. Geophys. Res.-Oceans, 97, 7373–7382, doi:10.1029/92jc00188, 1992.

Wanninkhof, R. and McGillis, W. R.: A cubic relationship between air-sea CO_2 exchange and wind speed, Geophys. Res. Lett., 26, 1889–1892, doi:10.1029/1999gl900363, 1999.

Warneck, P. and Williams, J.: The atmospheric chemist's companion-numerical data for use in the atmospheric sciences, Springer Science+Business Media B.V., 2012.

Warwick, N. J., Pyle, J. A., Carver, G. D., Yang, X., Savage, N. H., O'Connor, F. M., and Cox, R. A.: Global modeling of biogenic bromocarbons, J. Geophys. Res.-Atmos., 111, D24305, doi:10.1029/2006jd007264, 2006.

Williams, J., Gros, V., Atlas, E., Maciejczyk, K., Batsaikhan, A., Scholer, H. F., Forster, C., Quack, B., Yassaa, N., Sander, R., and Van Dingenen, R.: Possible evidence for a connection between methyl iodide emissions and Saharan dust, J. Geophys. Res.-Atmos., 112, D07302, doi:10.1029/2005jd006702, 2007.

Yamamoto, H., Yokouchi, Y., Otsuki, A., and Itoh, H.: Depth profiles of volatile halogenated hydrocarbons in seawater in the Bay of Bengal, Chemosphere, 45, 371–377, doi:10.1016/s0045-6535(00)00541-5, 2001.

Yokouchi, Y., Mukai, H., Yamamoto, H., Otsuki, A., Saitoh, C., and Nojiri, Y.: Distribution of methyl iodide, ethyl iodide, bromoform, and dibromomethane over the ocean (east and Southeast Asian seas and the western pacific), J. Geophys. Res.-Atmos., 102, 8805–8809, doi:10.1029/96jd03384, 1997.

Yokouchi, Y., Hasebe, F., Fujiwara, M., Takashima, H., Shiotani, M., Nishi, N., Kanaya, Y., Hashimoto, S., Fraser, P., Toom-Sauntry, D., Mukai, H., and Nojiri, Y.: Correlations and emission ratios among bromoform, dibromochloromethane, and dibromomethane in the atmosphere, J. Geophys. Res.-Atmos., 110, D23309, doi:10.1029/2005jd006303, 2005.

Yokouchi, Y., Osada, K., Wada, M., Hasebe, F., Agama, M., Murakami, R., Mukai, H., Nojiri, Y., Inuzuka, Y., Toom-Sauntry, D., and Fraser, P.: Global distribution and seasonal concentration change of methyl iodide in the atmosphere, J. Geophys. Res.-Atmos., 113, D18311, doi:10.1029/2008jd009861, 2008.

5. Manuscript 5

Numerical modeling of methyl iodide in the eastern tropical Atlantic

I. Stemmler[1], M. Rothe[1,*], I. Hense[1], and H. Hepach[2]

[1] Institute for Hydrobiology and Fisheries Science, CEN, University of Hamburg, Hamburg, Germany

[2] GEOMAR Helmholtz Centre for Ocean Research Kiel, Kiel, Germany

[*] now at: Leibniz Institute of Freshwater Ecology and Inland Fisheries, Berlin, Germany

Published in: Biogeosciences, 10, 4211 – 4225, doi:10.5194/bg-10-4211-2013, 2013.

Biogeosciences, 10, 4211–4225, 2013
www.biogeosciences.net/10/4211/2013/
doi:10.5194/bg-10-4211-2013
© Author(s) 2013. CC Attribution 3.0 License.

Biogeosciences
Open Access

Numerical modelling of methyl iodide in the eastern tropical Atlantic

I. Stemmler[1], **M. Rothe**[1,*], **I. Hense**[1], **and H. Hepach**[2]

[1]Institute for Hydrobiology and Fisheries Science, CEN, University of Hamburg, Hamburg, Germany
[2]GEOMAR Helmholtz Centre for Ocean Research Kiel, Kiel, Germany
[*]now at: Leibniz Institute of Freshwater Ecology and Inland Fisheries, Berlin, Germany

Correspondence to: I. Stemmler (irene.stemmler@zmaw.de)

Received: 19 December 2012 – Published in Biogeosciences Discuss.: 24 January 2013
Revised: 21 May 2013 – Accepted: 23 May 2013 – Published: 25 June 2013

Abstract. Methyl iodide (CH_3I) is a volatile organic halogen compound that contributes significantly to the transport of iodine from the ocean to the atmosphere, where it plays an important role in tropospheric chemistry. CH_3I is naturally produced and occurs in the global ocean. The processes involved in the formation of CH_3I, however, are not fully understood. In fact, there is an ongoing debate whether production by phytoplankton or photochemical degradation of organic matter is the main source term. Here, both the biological and photochemical production mechanisms are considered in a biogeochemical module that is coupled to a one-dimensional water column model for the eastern tropical Atlantic. The model is able to reproduce observed subsurface maxima of CH_3I concentrations. But, the dominating source process cannot be clearly identified as subsurface maxima can occur due to both direct biological and photochemical production. However, good agreement between the observed and simulated difference between surface and subsurface methyl iodide concentrations is achieved only when direct biological production is taken into account. Production rates for the biological CH_3I source that were derived from published laboratory studies are shown to be inappropriate for explaining CH_3I concentrations in the eastern tropical Atlantic.

1 Introduction

Methyl iodide (CH_3I) is one main carrier of iodine from the ocean to the atmosphere (Lovelock et al., 1973). Upon volatilization to the atmosphere it rapidly (within five days) transforms into reactive iodine species and impacts the tropospheric chemistry, such as the oxidative capacity and ozone depletion (e.g. Chameides and Davis, 1980; Solomon et al., 1994; Vogt et al., 1999). In coastal regions macro-algae were identified as significant methyl iodide sources (e.g. Manley and Dastoor, 1988; Nightingale et al., 1995; Carpenter, 2003), but they are not the major producers on the global scale due to their restricted distribution and small production rates (e.g. Giese et al., 1999; Wang et al., 2009). In the open ocean, CH_3I sources are unclear, and uncertainties remain with regard to origin of the source as well as production rates. Most studies suggested either a biological or a photochemical production pathway. Laboratory experiments in which filtered sea water was irradiated show photochemical production of CH_3I in absence of living phytoplankton cells that could account for at least 50 % of observed CH_3I emissions from the tropical Atlantic (Richter and Wallace, 2004). In addition, there is direct evidence for the biological production pathway (e.g. Moore and Tokarczyk, 1993; Manley and De La Cuesta, 1997); in particular the picocyanobacteria *Prochlorococcus* produce CH_3I (Brownell et al., 2010). The CH_3I production rates that have been independently derived for the same species by different research groups, however, are several orders of magnitude apart (Smythe-Wright et al., 2006; Brownell et al., 2010). While it was unclear whether differences in experimental setups in these laboratory studies can explain the discrepancies, a recent work provides an alternative explanation. Apparently, the production of methyl iodide is related to the health of these unicellular organisms; enhanced production rates by an order of magnitude have been recorded under stress conditions (Hughes et al., 2011). So far, oceanic CH_3I production has been quantified only in few modelling studies. Based on a very limited data set, best agreement between observations and model results from a global atmospheric chemistry-transport model (Bell et al., 2002) has been obtained when considering only a photochemical source instead of biological production. However, it has been criticized that the simulated photochemical source is too strong and the parametrization possibly too crude to represent CH_3I production (Moore, 2006). Since then more data on CH_3I in the environment have been collected and new insights in CH_3I production published. The existing uncertainties show the need to readdress the origin of oceanic CH_3I applying recent process understandings. Here, we present results from model experiments in which both the biological and photochemical production mechanisms are considered. We compare simulated concentrations of CH_3I with observations in sea water in order to assess distribution and strength of natural CH_3I sources in the ocean. A methyl iodide source and sink module is developed and coupled to a biogeochemical model as well as to the water column model GOTM. This model system is applied to simulate CH_3I concentrations in the eastern tropical Atlantic. By comparing observed and simulated vertical profiles of methyl iodide, we aim at identifying possible sources and sinks. Additionally, we want to quantify the air–sea flux of CH_3I and determine the sensitivity of this exchange process towards different parameterization for CH_3I production.

2 Material and methods

2.1 Model description

The physical model used is the "General Ocean Turbulence Model" (GOTM, Umlauf et al., 2005). GOTM is a one-dimensional water column model that mimics a number of hydrodynamic and thermodynamic processes related to vertical mixing in natural waters. It derives solutions for the one-dimensional versions of the transport equations of momentum, salt, and heat, and includes well-tested turbulence models. These models span the range from simple prescribed expressions for the turbulent diffusivities up to complex Reynolds-stress models with several differential transport equations to solve. We use a so-called two-equation model in which the turbulent kinetic energy (TKE) and the length scale of turbulence (l) are calculated from differential transport equations. They are described by a k-ε-type equation for TKE and a dynamic dissipation rate model for l (details in Umlauf et al., 2005). In line with Hense and Quack (2009) a minimum value of $10^{-5}\,\mathrm{m^2\,s^{-2}}$ for TKE is prescribed to parameterize the effects of double diffusion in the Cape Verde region.

Phytoplankton dynamics are simulated using a single column implementation of HAMOCC5.2 (Six and Maier-Reimer, 1996; Wetzel et al., 2006; Ilyina et al., 2013). HAMOCC is a marine carbon cycle model that includes a NPZD-type ecosystem model. The latter resolves exchange processes between several compartments: phytoplankton, zooplankton, sinking particulate organic carbon, a semi-labile dissolved organic carbon, and nutrients (iron, nitrate, and phosphate).

2.1.1 Methyl iodide modelling

The methyl iodide module considers several source and sink processes of CH_3I and has been implemented into the biogeochemical module HAMOCC. The methyl iodide concentration (c [$\mathrm{mmol\,m^{-3}}$]) evolves over time following production (P), degradation (S), air–sea exchange (F), as well as turbulent vertical diffusion (A_v-diffusion coefficient).

$$\frac{\mathrm{d}c}{\mathrm{d}t} = P - S + F_{\text{air–sea}} + \frac{\partial}{\partial z}\left(A_v \frac{\partial c}{\partial z}\right) \tag{1}$$

Two production mechanisms are implemented: photochemical production by radical recombination between methyl groups and iodine atoms (P_{photo}) and direct biological production by phytoplankton (P_{PP}). Photochemical production is parameterized using radiation (RAD) and a dissolved organic carbon concentration (DOC) (in $\mathrm{kmol\,P\,m^{-3}}$ as phosphorus is the model's internal "currency" of organic material. The model assumes a constant Redfield ratio of 1 : 106 for P : C in DOC). Here, (RAD) triggers the formation of methyl groups in the presence of organic matter and the production of iodine atoms from the photolysis of organic iodide. The photochemical production of methyl iodide concentration over time is then parameterized as follows:

$$P_{\text{photo}} = k_{\text{photo}} \cdot \mathrm{RAD} \cdot \mathrm{DOC}, \tag{2}$$

where k_{photo} is the photochemical production rate in $\mathrm{m^2\,mmol\,CH_3I\,(kmol\,P)^{-1}\,W^{-1}\,s^{-1}}$. RAD represents either UV light as parameterized in the photolysis (see below) or the photosynthetically active radiation (PAR) given by HAMOCC. Both are implemented as there is no experimental evidence that CH_3I production occurs preferentially under UV light (Richter and Wallace, 2004). The term DOC gathers a large variety of different substances with very different properties of different origin as "dissolved" is an operational definition for material passing a 0.45 µm filter. DOC can be directly produced in the ocean or originate from terrigenous decomposed plant material. Marine processes that form DOC include mainly extracellular release by phytoplankton, grazer mediated release and excretion, release via cell lysis, solubilization of particles, and bacterial transformation and release (Carlson, 2002). Relevant for CH_3I production are the DOC's photochemical properties, i.e. its ability to release methyl radicals. Photochemical transformation thereby can change the bioavailability of DOC in both directions – i.e. can make it more recalcitrant or more bioavailable

(Sulzberger and Durisch-Kaiser, 2009). To cover DOC pools of different lability two types of experiments with photochemical production of CH_3I are performed. In one group of experiments the semi-labile DOC (SLDOC) pool of pure marine origin as provided by HAMOCC is used as a source for methyl groups. In the second group of experiments the DOC concentration is set to a constant value of $40\,\mu\mathrm{mol\,C\,kg^{-1}}$. This mimics an unlimited supply of DOC and enables us to assess whether the spatio-temporal behaviour of DOC affects CH_3I production in the model. In the following this production pathway is referred to as photochemical production from refractory DOC (RDOC) as a very long life time of DOC would lead to almost uniform distribution in the ocean.

Direct biological production of CH_3I by phytoplankton is parameterized as follows:

$$P_{\mathrm{PP}} = k_{\mathrm{PP}} \cdot \mu(T,\, N,\, \mathrm{PAR}) \cdot \mathrm{PHY}. \tag{3}$$

Here, PHY is the phytoplankton concentration in $\mathrm{kmol\,P\,m^{-3}}$ and $\mu(T, N, \mathrm{PAR})$ is the actual growth rate of phytoplankton. The coefficient that specifies how much methyl iodide is produced during primary production is called k_{PP} ratio $[\mathrm{mmol\,CH_3I\,(kmol\,P)^{-1}}]$. This proportionality coefficient has been derived from two different laboratory studies: Moore et al. (1996) conducted incubation experiments with the phytoplankton species *Nitzschia* sp. and Smythe-Wright et al. (2006) incubated the cyanobacteria species *Prochlorococcus marinus*. Both measured an increase of methyl iodide concentration during the exponential growth phase of phytoplankton. In order to determine this coefficient, first the maximum specific growth rates ω in (d^{-1}) of these two species have been extracted from the exponential growth phase. The observed change in cell abundance is a function of the actual (net) growth rate μ. Since the maximum specific growth rate is required (see also Hense and Quack, 2009), a respiration rate of $1\,\%\ \mathrm{d}^{-1}$ is assumed.
Solving the ordinary differential equation for the experiment explained above,

$$\frac{\mathrm{dPHY}}{\mathrm{d}t} = \mu \cdot \mathrm{PHY} \tag{4}$$

and rearranging it to solve for μ

$$\mu = \frac{\ln\left(\frac{\mathrm{PHY}}{\mathrm{PHY_0}}\right)}{\Delta t} \tag{5}$$

the phytoplankton production within Δt is

$$\text{Phytoplankton production} = \omega \cdot \mathrm{PHY_0} \cdot e^{\omega \cdot \Delta t}, \tag{6}$$

with $\mathrm{PHY_0}$ and PHY accounting for the cell counts at the beginning and the end of the exponential growth phase; Δt is the time interval and $\omega = \mu + 0.01\,\mathrm{d}^{-1}$. Then the corresponding change of methyl iodide concentration ΔCH_3I in the same time interval Δt is determined in order to calculate the ratio between methyl iodide production and primary production k_{PP}:

$$k_{\mathrm{PP}} = \frac{\text{Methyl iodide production}}{\text{Phytoplankton production}} = \frac{\Delta \mathrm{CH_3I}}{\Delta t \cdot \omega \cdot \mathrm{PHY_0} \cdot e^{\omega \cdot \Delta t}}. \tag{7}$$

The resulting values for k_{PP} are 0.12 $\mathrm{mmol\,CH_3I\,(kmol\,P)^{-1}}$ for *Nitzschia* sp. and 1488.00 $\mathrm{mmol\,CH_3I\,(kmol\,P)^{-1}}$ for *Prochlorococcus marinus*, using typical cellular carbon contents for both species (Partensky et al. (1999): $50 \times 10^{-15}\,\mathrm{g\,C\,cell^{-1}}$ for *Prochlorococcus marinus*; $147 \times 10^{-12}\,\mathrm{g\,C\,cell^{-1}}$ for *Nitzschia* sp.; see also Hense and Quack, 2009) as well as the conversion factors from weight to molar units and the molar Redfield ratio ($\mathrm{P:C} = 1:106$). Under stress conditions the ratio between primary production and production of organic halogens significantly increases (Hughes et al., 2011). As picocyanobacteria are very abundant in the oligotrophic ocean (Partensky et al., 1999), and a large fraction of cells is in an unhealthy state (Agusti, 2004), we take nutrient limitation N_{lim} as a simple proxy for picocyanobacteria and for stress conditions to identify possible unhealthy cell states of phytoplankton:

$$N_{\mathrm{lim}} = \frac{N}{N + k_{\mathrm{N}}}, \tag{8}$$

where N is the nutrient concentration and k_{N} the half-saturation constant for nutrients. When enhanced production under nutrient limitation is simulated, k_{PP} varies between a minimum value under nutrient-rich conditions (N_{lim} =0.999) and a maximum value under extremely oligotrophic conditions (N_{lim}=0.001):

$$k_{\mathrm{PP}} = a \cdot \exp(-bN_{\mathrm{lim}}). \tag{9}$$

with

$$b = \frac{\ln\left(\frac{k_{\mathrm{PP_{min}}}}{k_{\mathrm{PP_{max}}}}\right)}{0.001 - 0.999} \tag{10}$$

and

$$a = \frac{k_{\mathrm{PP_{max}}}}{\exp(-b \cdot 0.001)}. \tag{11}$$

This non-linear approach was chosen to test the sensitivity versus minimum and maximum values of k_{PP} which can span several orders of magnitude. A linear approach here would over-represent the high values.

CH_3I degradation includes nucleophilic substitution with chloride S_{Cl}, hydrolysis S_{hyd}, and photolysis S_{phot}. Chloride substitution and hydrolysis are implemented as first-order processes with temperature-dependent decay rates:

$$S_{\mathrm{Cl}} = k_{\mathrm{Cl}}(T) \cdot c_{\mathrm{Cl}} \cdot c \tag{12}$$

and

$$S_{\mathrm{hyd}} = k_{\mathrm{hyd}}(T) \cdot c. \tag{13}$$

For chloride substitution a constant chloride ion sea water concentration of $c_{\mathrm{Cl}} = 0.54\,\mathrm{mol\,L^{-1}}$ was adopted, which is a typical value when assuming a mean sea water salinity $S = 35$ and a chloride ion proportion of 55 % (following the law of constant proportions after Dittmar, 1884). The reaction rate was derived by Elliott and Rowland (1993):

$$k_{\mathrm{cl}} = A \cdot \exp(-\frac{B}{T}), \tag{14}$$

with $A = 7.78 \times 10^{13}\,\mathrm{L\,mol^{-1}\,s^{-1}}$, and $B = 13518\,\mathrm{K}$; T is temperature in K. The reaction rates for hydrolysis were determined by Elliott and Rowland (1995) with $A = 1.7 \times 10^{12}\,\mathrm{s^{-1}}$, and $B = 13300\,\mathrm{K}$. Photolysis is implemented as proportional to UV attenuation (a_{uv} = 0.33m^{-1}), and irradiance (I) relative to its annual mean I_{ref}:

$$S_{\mathrm{photo}} = k_{\mathrm{uv}} \cdot \frac{I}{I_{\mathrm{ref}}} \exp(-a_{\mathrm{uv}} z). \tag{15}$$

The rate constant k_{uv} [s^{-1}] is estimated from atmospheric degradation rates (Rattigan et al., 1997) because reaction kinetics of methyl iodide photolysis in sea water are unknown. In particular, the e-folding time $(k_{\mathrm{uv}})^{-1}$ is set to 10 days assuming photo-dissociation of methyl iodide in water occurs at 50 % of the respective atmospheric rate. This approach was adopted from Carpenter and Liss (2000), who estimate kinetics of bromoform photolysis in water in a similar manner.

Gas exchange is calculated from the two-film model assuming methyl iodide gas exchange is controlled by the water side due to its low water solubility. Hence, the flux is calculated from a time-invariant field of atmospheric concentrations, solubility (Henry's law constant), bulk surface water concentrations, the Schmidt number, and a transfer velocity.

$$F_{\mathrm{air–sea}} = k_{\mathrm{w}} \cdot \left(c - \frac{c_{\mathrm{a}}}{H}\right) \tag{16}$$

The transfer velocity k_{w} depends on wind speed and is calculated according to Nightingale et al. (2000):

$$k_{\mathrm{w}} = \left(\frac{\mathrm{Sc}_{\mathrm{CH_3I}}}{600}\right)^{-\frac{1}{2}} \cdot \left(6.16 \times 10^{-7}\,\mathrm{s\,m^{-1}} \cdot {u_{10}}^2 + 9.25 \times 10^{-7} u_{10}\right), \tag{17}$$

with u_{10} denoting the wind speed at 10 m above the sea surface, and $\mathrm{Sc}_{\mathrm{CH_3}I}$ the Schmidt number for methyl iodide. The Schmidt number has been estimated from that of methyl bromide and the ratio of their molar volumes, as it has been done previously (e.g. Moore and Groszko, 1999):

$$\mathrm{Sc}_{\mathrm{CH_3I}} = \left(\frac{62.9}{52.9}\right)^{0.6} \cdot \left(2004 - 93.5\,{}^{\circ}\mathrm{C}^{-1} \cdot T + 1.39\,{}^{\circ}\mathrm{C}^{-2} \cdot T^2\right), \tag{18}$$

with T temperature in °C (5–30 °C). The temperature dependence of the solubility was determined by Moore et al. (1995):

$$H = \exp(13.32 - \frac{4338\,\mathrm{K}}{T}), \tag{19}$$

with T temperature in K.

Table 1. Parameter setup of the NPZD model, default HAMOCC values (Ilyina et al., 2013) and new values after tuning to fit observations close to Cape Verde.

Parameter	Default value	New value
Phytoplankton mortality rate (water column)[d^{-1}]	0.1	0.3
Maximum grazing rate [d^{-1}]	1.0	0.7
Initial slope of the P-I curve	0.02	0.025
Half saturation constant for nutrient uptake [kmol P m^{-3}]	1.0×10^{-8}	4.0×10^{-8}

2.2 Model setup

In order to receive a realistic simulation for a given oceanic region the model has to be configured for the conditions in a specific region. In this study, GOTM is configured for the Cape Verde region in the eastern tropical North Atlantic Ocean (latitude: 16° N, longitude: 24° W), like in Hense and Quack (2009). The physical model covers the upper 700 m of the ocean and has a vertical resolution of 2 m. The lower boundary of the model is set at this depth because here the nutrient maximum occurs and all diffusive fluxes vanish. A two-equation k-ε model with an algebraic second momentum closure is used, which is similar to Weber et al. (2007). For numerical integration a so-called quasi-implicit numerical scheme for the turbulence model with a time step of 1 h is used. The coupled physical–biogeochemical model is forced by climatological monthly mean data of 2 m atmospheric air temperature, air pressure, dew point temperature, 10 m zonal and meridional wind velocities, cloud cover, and precipitation based on the 40 yr ECMWF Re-analysis (ERA40) data (Uppala et al., 2005). The variables for water temperature and salinity are initialized with climatological profiles from the World Ocean Atlas (WOA01) (Conkright et al., 2002). The NPZD model parameters were tuned to closer match conditions at Cape Verde (see Appendix and Table 1).

For the calculation of the air–sea gas exchange a constant methyl iodide air concentration of $6.23 \times 10^{-8}\,\mathrm{mmol\,m^{-3}}$ is assumed which corresponds to 1.5 ppt at 20 °C and is the mean of observed base-level air concentrations of methyl iodide at Cape Verde during May and June 2007 (O'Brien et al., 2009). To account for lateral entry of higher-saline water, which is characteristic for the Cape Verde region, salinity and temperature values are restored towards climatological monthly means of WOCE (World Ocean Circulation Experiment; Global Data Resource) with a five day time scale, except for the upper 20 m of the water column. The dissolved inorganic nitrogen concentration is restored at the nutrient maximum to the observed value of 35.7 mmol N m^{-3}, and dissolved inorganic phosphate to an observed value of 2.23 mmol P m^{-3} with a time scale of one hour.

2.3 Observations

To evaluate the simulated CH_3I concentrations, model results are compared to observations from a ship cruise in the tropical northeast Atlantic close to Cape Verde – i.e. the Poseidon cruise P399/2 in April–June 2010 (Bange, 2011) (see Appendix A). Methyl iodide profiles have been obtained from three stations, one of which is located in an upwelling region and is therefore not further considered (since a 1-D water column model cannot simulate upwelling conditions). The other two stations are located at 17.6° N 24.3° W (St. 307 – in the following called CVOO, which stands for Cape Verde Ocean Observatory), and 18° N 21° W (St. 308).

Dissolved CH_3I was measured in sea water sampled in 500 mL amber glass bottles from 10 different depths at CVOO and station 308. These samples were taken from 10 L Niskin bottles that were installed on a 12-bottle rosette with a CTD (conductivity temperature depth). A purge and trap system attached to a gas chromatograph with mass spectrometer (GC-MS) and detection in single ion mode were used to analyse the samples. Eighty millilitres of the sampled water was heated up to 70 °C while being purged with a stream of helium at 30 $\mathrm{mL\,min^{-1}}$ in a glass chamber. Volatilized trace gases were trapped on glass beads at −100 °C and were desorbed onto a deactivated capillary in liquid nitrogen as second trap at 100 °C after one hour of purging. The trace gases were injected into the GC-MS after three minutes. Volumetrically prepared standards in methanol were used for quantification. Precision of the measurements is estimated to be 16 %, determined from duplicates with a detection limit of 0.05 $\mathrm{pmol\,L^{-1}}$ for CH_3I. Besides methyl iodide concentrations, phytoplankton pigments, temperature, and salinity profiles are available for the three stations. Phytoplankton pigments, i.e. total chlorophyll *a* concentrations, were converted into phytoplankton biomass by using a depth-dependent C : Chl ratio and assuming a P : C ratio of 1 : 106. The C : Chl ratio was calculated as described in Hense and Beckmann (2008) using modelled radiation profiles as irradiation was not measured. Calculated surface C : Chl ratios are much higher (>100 $\mathrm{g\,g^{-1}}$) than subsurface (minimum 25 $\mathrm{g\,g^{-1}}$) ratios (not shown).

2.4 Model experiments

GOTM is run in several experiments including different combinations of the CH_3I production processes (listed in Table 2). In the experiments E1 and E2 only direct production via phytoplankton growth is implemented and the production rates derived from laboratory studies by Moore et al. (1996) (E1) and Smythe-Wright et al. (2006) (E2) are tested. In experiment E3 the production rates by Moore et al. (1996) and Smythe-Wright et al. (2006) are used as the lower ($k_{\mathrm{PP_{min}}}$) and upper ($k_{\mathrm{PP_{max}}}$) boundaries of the variable biological production rate that mimics production by phytoplankton with consideration of stress. As the production rates for the photochemical production pathways (from SLDOC or RDOC) are unknown, they are derived from a parameter optimization. Thereby the parameter (set) that leads to the minimum root mean square deviation (RMSD),

$$\mathrm{RMSD} = 0.5\sqrt{\frac{1}{N_{\mathrm{depth}}}\sum\nolimits_{\mathrm{depth}}(m_{\mathrm{depth}} - o_{\mathrm{depth}})^2} + 0.5\sqrt{(\max(m) - \max(o))^2}, \qquad (20)$$

between modelled (m) and observed (o) (see Sect. 2.3) profiles and maxima is found using a gradient descent search. The step length, i.e. the incremental parameter change, is set to 10 % of the most successful parameter value of the previous iteration. Optimizing for both the overall RMSD and the deviation from the maximum ensures that when a subsurface maximum is simulated it will be of similar strength as in the observations, even when predicted at a different depth. Assuming that differences between CVOO and St. 308 are minor, no individual optimization for St. 308 was performed. The experiments Opt1–Opt4 include only one source process and the production rates are chosen by a parameter optimization. In the following, 1 denotes "normal" (not stressed) production by phytoplankton, 2 photochemical production through semi-labile DOC (SLDOC) degradation, 3 photochemical production through refractory DOC (RDOC) degradation, and 4 biological production with a variable production rate (i.e. with consideration of stress), where the lower and upper bounds are optimized. In the experiments Opt2 and Opt3, CH_3I production mechanisms through both UV and PAR were tested. In the experiment Opt123, three production processes are considered (i.e. biological and photochemical production from semi-labile and refractory DOC), and the respective rates are derived from a parameter optimization with three simultaneously varying parameters.

Table 2. CH_3I model parameter configurations of the different experiments. The unit of k_{PP} is [$\mathrm{mmol\,CH_3I\,(kmol\,P)^{-1}}$], the one of k_{photo} is [$\mathrm{m^2\,mmol\,CH_3I\,(kmol\,P)^{-1}\,W^{-1}\,s^{-1}}$].

Experiment ID	$k_{\mathrm{PP_{min}}}$	$k_{\mathrm{PP_{max}}}$	k_{photo} (SLDOC)	k_{photo} (RDOC)
E1	0.12	–	–	–
E2	1488.00	–	–	–
E3	0.12	1488.00	–	–
Opt1	56.00	–	–	–
Opt2	–	–	1.31×10^{-6}	-
Opt3	–	–	–	3.91×10^{-7}
Opt4	0.14	1204.80	–	–
Opt123	0.05	-	7.80×10^{-7}	1.26×10^{-7}

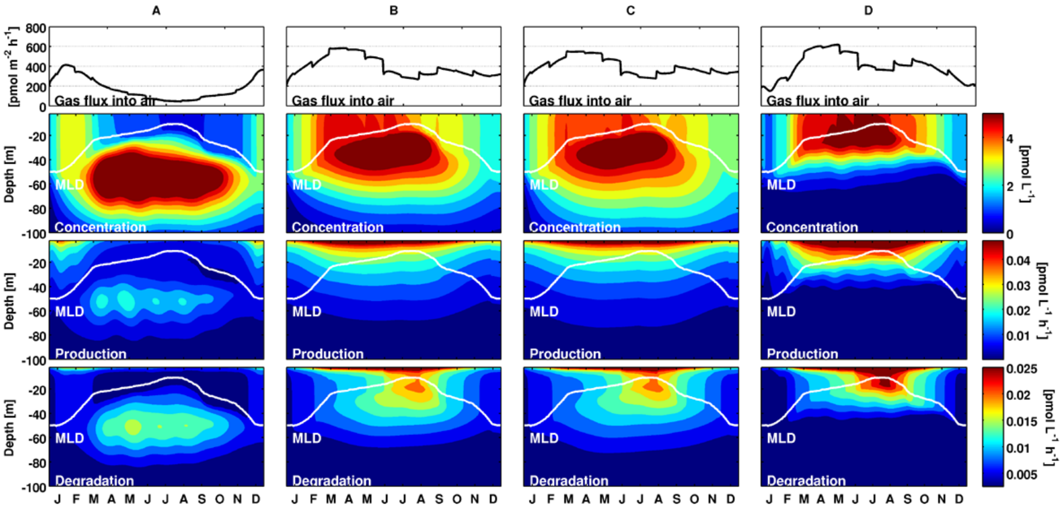

Fig. 1. Methyl iodide concentrations [pmol L^{-1}], production [pmol L^{-1} h^{-1}], degradation [pmol L^{-1} h^{-1}], and gas exchange [pmol m^{-2} h^{-1}] for the experiments Opt1 (column A), Opt2 (column B), Opt3 (column C), and Opt4 (column D).

3 Results

3.1 Seasonal cycle of CH_3I concentrations

In the experiments that include only biological production of CH_3I (Opt1, E1, E2), maximum production takes place between 50 and 80 m depth, i.e. where phytoplankton growth is largest (Fig. 1a). Consequently, a strong CH_3I subsurface maximum builds up over the year, with highest concentrations in the summer season (May–September). In Opt2 and Opt3, photochemical production was modelled using either PAR or UV. Of these experiments only those that use PAR show a subsurface CH_3I maximum (not shown). Location and cause of these maxima resulting from photochemical production are different from the experiments with biological production. Irrespective of the lability of the DOC pool considered, maximum CH_3I production occurs in the sunlit surface layers (Fig. 1c, d). The production is stronger in summer than in winter months, following the seasonal cycle of insolation. During times of deep mixing, i.e. in winter months, the CH_3I concentration is homogenous over the upper 50 m. When the mixed layer shallows, a pronounced subsurface maximum evolves, which is first situated at approximately 50 m depth, but later follows the mixed layer shallowing up to approximately 30 m depth. In the uppermost model levels the dominant sink processes for CH_3I are UV decay and gas exchange with the atmosphere. The subsurface maximum is not a result of a particularly strong local production (production always exceeds decay) but is caused by the stratification that shields the freshly produced CH_3I from gas exchange. When photochemical production is parameterized using light that is efficiently absorbed in the surface layers (i.e. UV light identical to the parameterization of photolysis) CH_3I production is restricted to the upper model levels and never takes place below the mixed layer. This inhibits the evolution of a subsurface maximum, and concentration maxima are always located in the mixed layer (not shown). Since subsurface maxima are observed, photochemical production by UV light seems unrealistic.

The experiments Opt2 and Opt3 show only minor differences, despite the different DOC pools considered as sources for available methyl groups. This is because the semi-labile DOC in HAMOCC shows a surface maximum throughout the year. Hence, the vertical distribution of CH_3I production in both experiments is limited by light absorption leading to similar seasonal patterns.

In Opt4, when biological production is simulated and calculated from different production rates in oligotrophic water and the residual water column, the distribution of CH_3I differs very much from that of "normal" biological production in e.g. Opt1 (Fig. 1d). Concentration maxima occur from May to September and stretch within the upper 40 m of the water column. Production is highest at the surface because nutrient scarcity (caused by strong stratification of the water) leads to a high CH_3I production: PP ratio k_{PP} (Fig. 2). At the surface k_{PP} is 4–6 times higher than in Opt1 and is more than 100 times lower than in Opt1 subsurface where maximum primary production occurs (Fig. 2a). The distribution of CH_3I in Opt123 is almost identical to Opt2 and Opt3 because k_{PP} is even smaller than in the experiment with the low biological production rate derived from laboratory experiments (E1, Table 2).

3.2 Evaluation of simulated CH_3I concentrations

In the experiments E1 and E2 – i.e. when considering only biological production using the rates derived from laboratory studies (Table 2) – different concentration distributions

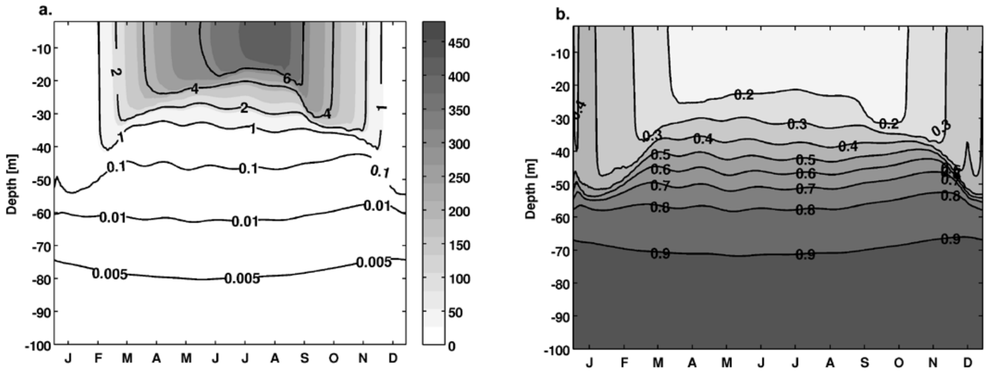

Fig. 2. Ratio between methyl iodide and primary production rate k_{PP} in Opt4 (**a**, grey shaded area, [mmol CH_3I (kmol P)$^{-1}$]), its relation to k_{PP} in Opt1 (i.e. $\frac{k_{\mathrm{PP}_{\mathrm{Opt4}}}}{k_{\mathrm{PP}_{\mathrm{Opt1}}}}$) (**a**, contour lines), and the nutrient limitation factor N_{lim} **(b)**.

evolve resulting from the balance between production, degradation and gas exchange with the atmosphere. In both experiments CH_3I production is tied to primary production, that has its maximum subsurface. Nevertheless, as a result of a low k_{PP}, production and therefore surface concentration are much too low in E1. This leads to an undersaturation of the ocean and a net influx of CH_3I from the atmosphere throughout the year. In contrast, in E2 a pronounced subsurface maximum of CH_3I develops that is too high. The observed maximum and mean concentrations are 5.66, 1.49 pmol L^{-1} at CVOO; and 3.34, 0.66 pmol L^{-1} at St. 308 (Table 3). The model in turn predicts for the respective month maximum and mean concentrations of 0.11, 0.02 pmol L^{-1} in E1; 173.2, 60.67 pmol L^{-1} in E2 for CVOO; 0.14, 0.004 pmol L^{-1} in E1; and 187.65, 70.43 pmol L^{-1} in E2 for St. 308. Only the surface value of E1 matches the observations at St. 308 within a factor of 2. But, this apparent match is insignificant considering the large discrepancy (between observations and E1 model results) in subsurface concentrations. Thus, in both experiments unrealistic concentrations of CH_3I occur. Mean and maximum values in the third experiment E3, which allows for a variable biological CH_3I production rate using the parameters from laboratory studies as lower and upper bounds, match observed mean and maximum values much better (i.e. within a factor of 2) than the ones of E1 and E2. But, the vertical profile differs from the observed one: the strong production at the surface leads to concentrations that are much too high (100 times compared to CVOO, 6-fold compared to St. 308; see Table 3).

Next, the model runs with parameter optimization for "normal" biological production, photochemical production (from RDOC and SLDOC), biological production with a variable k_{PP}, and combined biological and photochemical production were performed. For the experiment with mixed sources (Opt123) the optimization results in a very low biological production rate k_{PP} (Table 2), and consequently in a dominance of the photochemical production pathways. Therefore, the methyl iodide concentration evolves similarly to Opt2 and Opt3 (Fig. 1b, c).

Results of the experiments using optimized parameter values compared to observations are depicted in a Taylor diagram (Fig. 3). This shows the RMSD (Eq. 20) normalized to the observed mean concentration at CVOO and St. 308 (Fig. 3), the standard deviation across the profile normalized to the profiles' mean concentration, and the correlation coefficient between modelled and observed profile. Of course, correlation and standard deviation are weak measures for the match between model and observations here due to the low data resolution. Nevertheless, they can give a hint on the similarity of the shapes of modelled and observed profiles. Unfortunately, the temporal evolution of CH_3I concentration cannot be evaluated at all because there are no long-term CH_3I data that would allow for assessing the seasonal cycle in the eastern tropical Atlantic. Observed methyl iodide concentrations show a subsurface maximum at around 40–50 m at both stations (Fig. 4). Due to the parameter optimization, all of the experiments simulate CH_3I concentrations that are close to the observed maximum and mean values at CVOO, and match observed profiles much better than E1–3 (see Table 3). At CVOO the maximum concentration and concentrations below the maximum are well represented in almost all experiments, except Opt4 (Fig. 4). In the Taylor diagram, Opt2, Opt3, and Opt123 are clustered closely at approximately the same distance from the observations as their profiles are very much alike (Fig. 4). According to the Taylor diagram (Fig. 3a), Opt1 is closest to the observations as it is the only experiment that reproduces the observed vertical gradient with low surface and higher subsurface concentrations. This translates into a higher correlation coefficient and a lower RMSD. Surface concentrations of the experiments that are dominated by photochemical production (Opt2, Opt3, Opt123) are too high compared to observations (Fig. 4, Table 3). For Opt4, the optimization converged to values that are not very different from the values at E3 (Table 2)

Table 3. Observed and modelled concentrations at the surface, concentration minima, and maxima [$\mathrm{pmol\,L^{-1}}$]. Modelled values are means of the respective months at the depth of the observations.

	Maximum		Mean		Surface	
Experiment ID	CVOO	St. 308	CVOO	St. 308	CVOO	St. 308
E1	0.11	0.14	0.02	0.004	0.11	0.14
E2	173.20	187.65	60.67	70.43	28.64	38.16
E3	6.24	5.67	1.23	1.57	6.24	5.55
Opt1	6.52	7.08	2.30	2.68	1.18	1.57
Opt2	5.60	5.04	2.00	2.31	4.66	4.65
Opt3	5.36	4.98	2.14	2.46	4.52	4.37
Opt4	5.34	4.94	1.08	1.39	5.34	4.83
Opt123	5.07	4.62	1.89	2.18	4.24	4.19
Observation	5.66	3.34	1.49	0.66	0.06	0.9

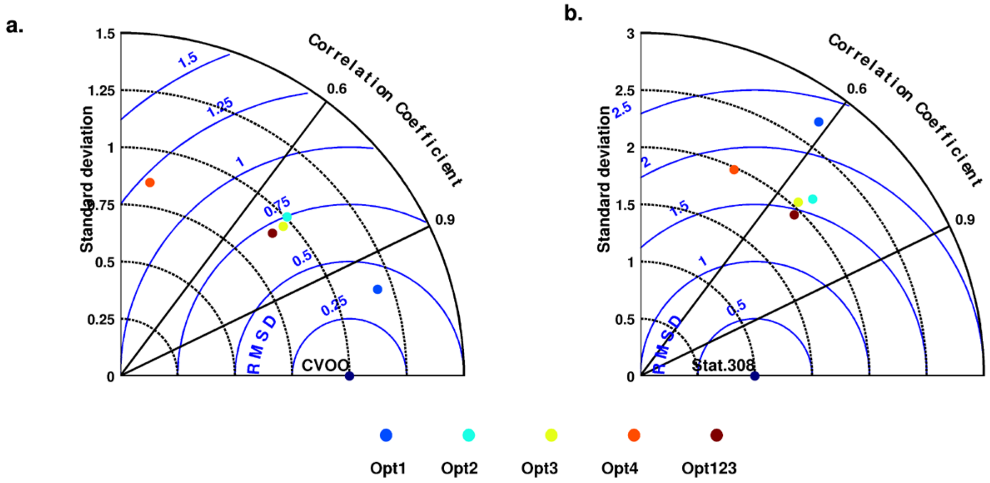

Fig. 3. Taylor diagrams for the different experiments showing the RMSD between modelled and observed profiles normalized with the observed mean concentration (blue circles), standard deviations of the individual profiles normalized with the one of the observations (black circles, ticks on the y-axis), and the linear correlation coefficient between model results and observations (angle between y- and x-axis). Note that all statistical parameters are derived from the vertical profiles, not from a time series. Observations are from CVOO **(a)** and St. 308 **(b)**.

and the representation of methyl iodide in that model experiment also did not improve much over the ones in E3. Compared to CVOO, most simulated vertical profiles show a too shallow maximum, with too low values below and too high surface values. Observations at St. 308 are generally worse represented by this model setup than observations at CVOO. A further parameter optimization would bring simulated concentrations closer to observed ones, but would not bring any further insights into CH_3I production. Also here (at St. 308) it is apparent that the experiment with CH_3I production by phytoplankton (Opt1) is the only one that can reproduce the sharp subsurface gradient of the observations when all others show rather high surface concentrations compared to the subsurface maximum (Fig. 4, Table 3).

3.3 Emissions

In all experiments with optimized production rates the ocean acts as a source of CH_3I to the atmosphere. Flux maxima for most experiments but Opt1 occur in spring (March–May, Fig. 5) due to high surface ocean concentrations during these times. In Opt1 highest emissions occur in winter (December, January, February), when both CH_3I production at the surface (Fig. 1a) and wind speed (Fig. 5) are high. The fluxes are of similar order of magnitude for all experiments (maxima at approximately 500 $\mathrm{pmol\,m^{-2}\,h^{-1}}$). The primary driver of direction and annual cycle of gas exchange is the concentration of CH_3I in the surface layer of the model. Hence, the ultimate reason for the difference among the experiments is that biological production is at its maximum in the ocean interior (at ca. 60 m) in summer, and at the surface in winter, whereas

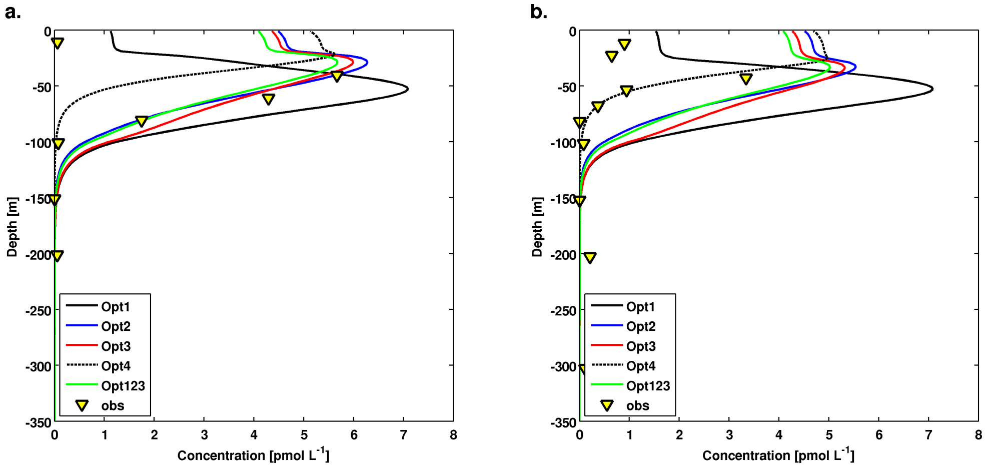

Fig. 4. Methyl iodide concentration profiles [pmol L^{-1}] from stations CVOO and St. 308 in the Cape Verde region. Observed data were collected during Poseidon cruise P399/2 in 2010. For the CVOO station only data from the upper 350 m of the water column are shown.

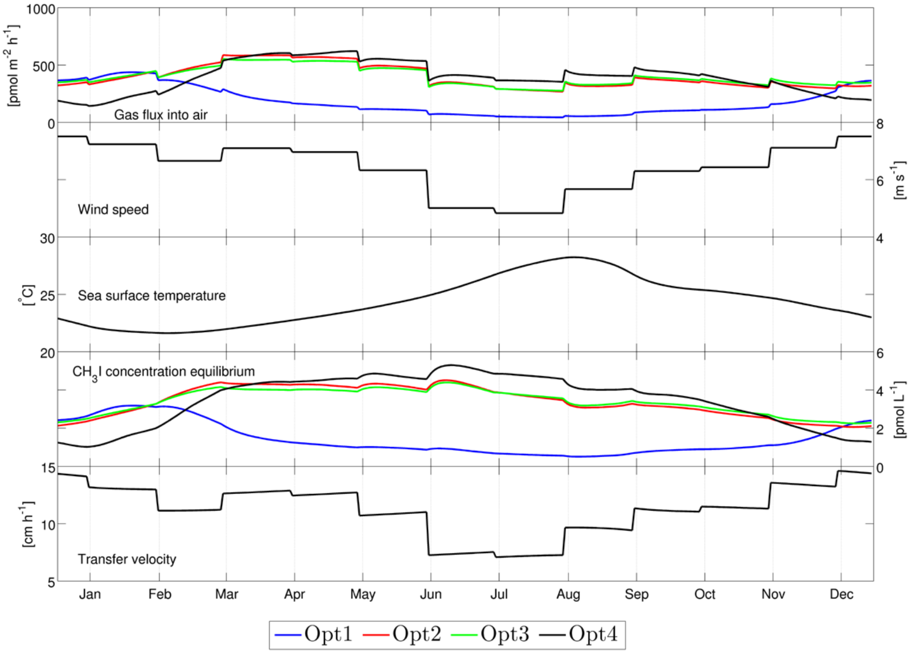

Fig. 5. Methyl iodide sea–air flux [pmol m^{-2} h^{-1}], wind speed [m s^{-1}], sea surface temperature [°C], CH_3I water and air concentration equilibrium $c_w - \frac{c_a}{H}$, [pmol L^{-1}], and gas transfer velocity [cm h^{-1}].

photochemical production is highest in the sun-lit surface layers during spring and summer. When production is limited to photochemical production, the seasonal cycle of the gas exchange is less pronounced (Fig. 5). This is because the temporal evolution of production is controlled by radiation, and hence strongest in summer, when low wind speeds lead to a lower transfer velocity. Other than by production and associated surface concentrations, the evolution of the fluxes is determined by wind speed and sea surface temperature. The low temporal resolution of wind speed (monthly means) via the transfer velocity shapes the month-to-month variation of the fluxes, which is characterized by an abrupt (non-smooth) transition from one month to the other (Fig. 5). Within individual months, temperature, which determines the solubility, and surface concentration control the deviation from equilibrium between atmosphere and ocean, and hence the evolution of sea–air fluxes.

4 Discussion

The profiles of temperature, salinity, phytoplankton, and nutrients at CVOO and St. 308 during P399/2 are similar to observations in Meteorcruise M55 (Wallace and Bange, 2004) and the World Ocean Atlas (Conkright et al., 2002); hence the observed profiles at these stations do not represent unusual environmental conditions. Therefore our results can be transferred to areas of the eastern tropical Atlantic where advection plays a minor role.

4.1 CH_3I production by phytoplankton

Modelling CH_3I distributions at CVOO and St. 308 using biological production rates derived from laboratory experiments (E1, E2) was not successful. The production rate as suggested by Moore et al. (1996) appears to be too low to reproduce observed CH_3I concentrations, whereas the production rate suggested by Smythe-Wright et al. (2006) seems to be too high. This does not imply that direct biological production of methyl iodide is unlikely. The parameter optimization for the cases where only biological production was included (Opt1) resulted in lowest RMSD values for a production rate in the order of magnitude of $10^{-6}\,\mathrm{mmol\,CH_3I\,(kmol\,P)^{-1}}$, and the overall shape of the vertical profiles was best reproduced. Hughes et al. (2011) suggested that the large discrepancies between the production rates from laboratory studies result from the different health conditions of the phytoplankton cells. As in nature the phytoplankton population can consist of mixed healthy and stressed cells (Agusti, 2004), it is not unrealistic to expect a bulk CH_3I production rate in between the two discussed. Here, we tested if enhanced production under oligotrophic conditions would result in a better representation of CH_3I profiles close to Cape Verde. But, even after optimization of the parameter setup this experiment did not reproduce observed concentrations satisfactorily.

The preliminary analysis of pigment measurements in the cruise report (Bange, 2011) indicates a high abundance of diatoms during P399/2, but also suggests the presence of *Prochlorococcus*, the plankton species that was shown to enhance CH_3I release during stress. Unfortunately, nothing is known about the cell physiological state of phytoplankton during the cruise. Hence, either nutrient scarcity is not a good proxy for stressed phytoplankton cells that produce more CH_3I than healthy ones and the chosen parameterisation of that factor is inadequate, or enhanced production by stressed cells is not relevant at these two stations. Since for both stations the same physical setup of GOTM is used, particularities of the two stations are not reflected by the model, e.g. if enhanced production by stressed picocyanobacteria would be more likely for St. 308 than for CVOO. In addition, the ecosystem model used is rather simple, and biological production of methyl iodide is described to be coupled to primary production of the bulk phytoplankton. Since *Prochlorococcus* is assumed to be the main producer of methyl iodide an explicit description of this phytoplankton group in the model might improve the overall representation of phytoplankton biomass and methyl iodide concentration. Yet, different ecotypes of *Prochlorococcus* exist (e.g. Johnson et al., 2006) and we cannot exclude that depth-dependent niche separation might also affect methyl iodide production and vertical distribution patterns of CH_3I concentrations. However, since our simulated subsurface CH_3I concentrations are in the same order of magnitude compared to observations (see Appendix A), we refrain from adding more complexity to the model system.

Another aspect in the evaluation of the simulated biologically produced CH_3I profile is the vertical distribution. In the experiments that include biological production of CH_3I using a constant production ratio, the depth of the maximum of primary production determines the depth of the maximum of CH_3I concentrations. As presented in Appendix A, the modelled phytoplankton concentration was compared to observed chlorophyll *a* data. Both show a subsurface maximum and are in the same order of magnitude. The exact location of the biomass maximum during the cruise, however, cannot be unambiguously assessed as the phytoplankton concentration in model units has to be diagnosed from an empirically derived depth-dependent relationship between chlorophyll and carbon. There is no doubt that the C : Chl ratio varies with depth (with higher values at the surface than subsurface), but there is no mechanistic understanding about the co-variation of carbon and chlorophyll with depth. Therefore, a match or mismatch of the exact location of the CH_3I maximum is not a good indicator for the model performance here.

4.2 Photochemical production of CH_3I

The experiments that are dominated by photochemical production are very successful in representing the subsurface CH_3I concentrations (below the maximum), and only the surface value is not represented by the model (Fig. 4). In particular, the concentrations at CVOO are well reflected by the model. But, simulated methyl iodide concentrations were found to be sensitive to the absorption properties of light. A subsurface maximum is only simulated during times of a shallow mixed layer and when using light that is penetrating deep enough to allow for production below the mixed layer. UV light gets absorbed readily in the water column, whereas other wavelengths show significant intensities down to approximately 100 m (e.g. PAR). Thus far, the photochemical production pathway has not yet been fully understood. Wang et al. (2009) found positive correlations of CH_3I concentrations with both PAR and UV light at 325 nm; Moore and Zafiriou (1994) detected methyl iodide production in laboratory studies when using light with a spectral distribution close to sunlight over the wavelength 280–1100 nm. Richter and Wallace (2004) tested CH_3I production under different light conditions to study the qualitative effect of UV light on production. They did not discover any significant differences in CH_3I production between the experiment with the full spectrum of light compared to the ones with reduced UV light. Photochemistry potentially impacts this production pathway twofold: on the one hand, the iodine atoms may originate from reaction of iodide with photochemically produced oxidants or photolysis of organic iodides, and on the other hand, the methyl radicals may originate from photolysis of humic material (Moore and Zafiriou, 1994). As photochemical production of e.g. OH^- from CDOM is more efficient for UV light (e.g. Loiselle et al., 2012) one could speculate about more significant differences in CH_3I production if the impact of light would be studied for various water depths. But for now, there is no experimental evidence that CH_3I production occurs preferentially under UV light. The sensitivity of the model results to the absorption characteristics suggest that further studies on the wavelength dependency of CH_3I production would be valuable.

4.3 Mixed biological and photochemical CH_3I sources

Similar to the experiments with photochemical CH_3I production, the mixed-source experiment, Opt123, shows highest discrepancies between modelled and observed concentrations at the surface. As the optimization is set up to find the minimum RMSD for both maximum and mean along the profile, the discrepancy in the surface value is not weighted strongly enough to force the mixed-source parameter optimization towards a biological production. Hence, one cannot conclude from the mere fact that the optimization suppressed biological production that photochemical production is the main source process of CH_3I here. As in oligotrophic waters, deep phytoplankton maxima regularly occur higher biologically mediated methyl iodide production at depth can hence not be excluded. Smythe-Wright et al. (2006) detected enhanced subsurface CH_3I concentrations where *Prochlorococcus* were largely abundant. They found much higher CH_3I concentrations during their cruise at Cape Verde compared to P399/2, although both cruises were conducted in the same season. In addition, Smythe-Wright et al. (2006) found elevated surface concentrations as well as associated high atmospheric levels. Thus, the variability might not be insignificant.

4.4 Gas exchange with the atmosphere

Gas exchange with the atmosphere depends on the deviations from equilibrium of marine and atmospheric methyl iodide concentrations, as well as on the wind-speed dependent transfer velocity. Saturation anomalies can be evaluated since they are derived frequently during ship cruises when atmospheric and oceanic CH_3I concentrations are measured simultaneously. Smythe-Wright et al. (2006) diagnose concentration anomalies of 40 $\mathrm{pmol\,L^{-1}}$ in May from data collected in the eastern Atlantic close to 20° N, resulting from very high CH_3I concentrations in water. Concentrations measured during P399/2 and our simulations show much lower values. The concentration anomaly between water and air of approximately 5–10 $\mathrm{pmol\,L^{-1}}$ modelled here is closer to what was estimated by Happell and Wallace (1996), Richter and Wallace (2004), or Chuck et al. (2005). Clearly, as model results were optimized for certain sea water concentrations, a direct comparison to other measured data is only possible when these coincide with the ones at P399/2. Chuck et al. (2005), for example, measured surface water concentration of approximately 5 $\mathrm{pmol\,L^{-1}}$ off Africa at 15–20° N, which is much higher than concentrations measured during P399/2. Thus, the variability of methyl iodide concentrations both in surface ocean and lower atmosphere concentrations is not insignificant.

Generally, the strength of modelled sea–air fluxes does not vary much among the experiments, but its seasonal cycle does. Even though the large differences in intensity of gas exchange for experiments that include different dominating source processes seems to be an inherent feature of production, the sea–air flux cannot be used to argue for a certain source type. This is because in the model sea–air exchange is only diagnosed from a constant atmospheric concentration. Using a model that includes the full cycling of CH_3I in both atmosphere and ocean would account for the variability of atmospheric CH_3I concentrations. But, the simulated seasonal cycle is not expected to change much when a model of atmospheric CH_3I cycling is added. This is because the saturation anomaly is mostly influenced by the oceanic values, due to the strong oversaturation of the ocean. Strong oversaturation has been found previously for both early summer month (May/June: O'Brien et al., 2009; Fuhlbrügge et al., 2012 and late fall (October/November: Butler et al., 2007). Furthermore, the measured mixing ratios both in May/June and October/November over the open ocean close to Cape Verde were in the range of 1–2 ppt (Butler et al., 2007; O'Brien et al., 2009; Fuhlbrügge et al., 2012). Hence, the expected seasonal variability of atmospheric concentrations will be much lower than the one of sea water concentrations (which show a factor of 6 between low summer and high winter values in the simulations). Here, monthly means were used to force the model at the atmospheric boundary (2 m temperature, wind speed, etc.). Usage of e.g. daily mean data would introduce higher temporal variability to the fluxes, but would not change the seasonal cycle, the magnitude of the mean fluxes or generate additional differences amongst the experiments.

High concentrations of methyl iodide in the surface ocean and lower atmosphere that have been observed occasionally in this region might also be the result of horizontal advection. Since we use a one-dimensional water column model, this non-local source cannot be represented by our model system. As a next step, we therefore aim to couple the biogeochemical module to a three-dimensional global ocean circulation model to account for horizontal and vertical advection.

5 Conclusions

The coupled biogeochemical–water column model that includes a methyl iodide compartment is able to reproduce observed subsurface maxima of CH_3I concentrations. However, our model results are not unequivocal. Subsurface maxima can occur due to direct biological and photochemical production. But, for the photochemical production pathway subsurface maxima strongly depend on the chosen light properties. Subsurface maxima can occur only if significant production occurs also below the mixed layer. This is not the case when only UV light is considered in the production mechanism. However, the gradient, i.e. the difference between surface and subsuface methyl iodide concentration, is best reproduced if direct biological production is taken into account. Although enhanced methyl iodide production is observed under stress conditions of picocyanobacteria, the parameterization of this process has not led to a model improvement at this particular site.

Overall, we conclude that the rates obtained from the laboratory experiments from Moore et al. (1996) are too low to explain the CH_3I concentration in the tropical northeast Atlantic. In contrast, the CH_3I production rates in this region cannot be as high as proposed by Smythe-Wright et al. (2006) at least not over longer times. The comparison of horizontal distribution patterns between simulated and observed CH_3I concentrations may provide further insights into the source of CH_3I.

Appendix A

Evaluation of the physical and biological state of model

For all simulations the model was restored towards salinity and temperature profiles from the tropical northeast Atlantic (see Sect. 2.4). But, this does not guarantee that the simulated ocean state is representing conditions during the Poseidon cruise (P399/2), in particular as those might be different for the two stations (CVOO, St. 308). Therefore, simulated temperature, salinity, and phytoplankton profiles in April and June are compared to observations taken during P399/2. At the CVOO station and at St. 308 temperature and salinity profiles are similar to the observed ones (Fig. A1a, b). The greatest mismatch occurs in the surface layer, where no restoring takes place. There, salinity and temperature are strongly influenced by vertical exchange via turbulence, surface fluxes (momentum, heat, radiation), which are a function of the forcing used. The forcing taken from climatological mean data cannot fully represent local conditions during the cruise. But, the use of other data sets and forcing fields (e.g. 2010 data of the NCEP global ocean data assimilation system (GODAS): http://www.esrl.noaa.gov/psd/data/gridded/data.godas.html, Behringer and Xue, 2004) has not improved the representation of observed profiles. Usage of the measured profiles would improve model results, but would introduce inconsistencies as in situ data would be treated as monthly means, and these data would have to be combined with other data as only observations for a limited time period in spring and summer are available. Modelled

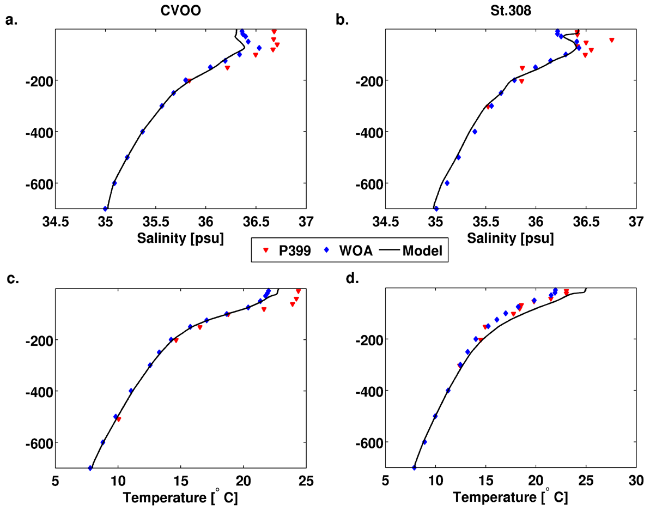

Fig. A1. Salinity [psu] **(a, b)** and temperature [°C] **(c, d)** profiles in April **(a, c)** and June **(b, d)**, model predictions (solid lines) and observations (red markers P399/2 cruise data, blue markers WOA data).

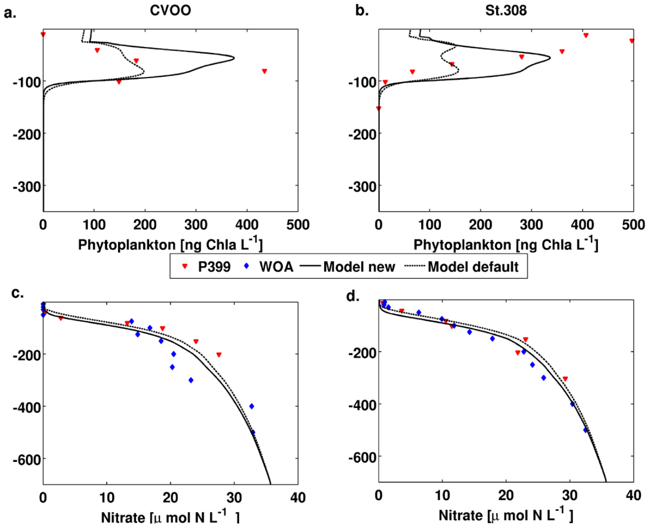

Fig. A2. Phytoplankton **(a, b)** and nutrient **(c, d)** concentrations in April **(a, c)** and June **(b, d)** [ng Chl *a* L^{-1}] – model-predicted (black solid lines new and dashed lines default parameter setup) and observed (red markers) profiles. Observations were taken from the Poseidon cruise P399/2 in 2010. Simulated phytoplankton concentrations have been converted to chlorophyll using a vertically dependent C : Chl ratio (e.g. Hense and Beckmann, 2008) and the Redfield ratio for conversion from carbon to phosphorus.

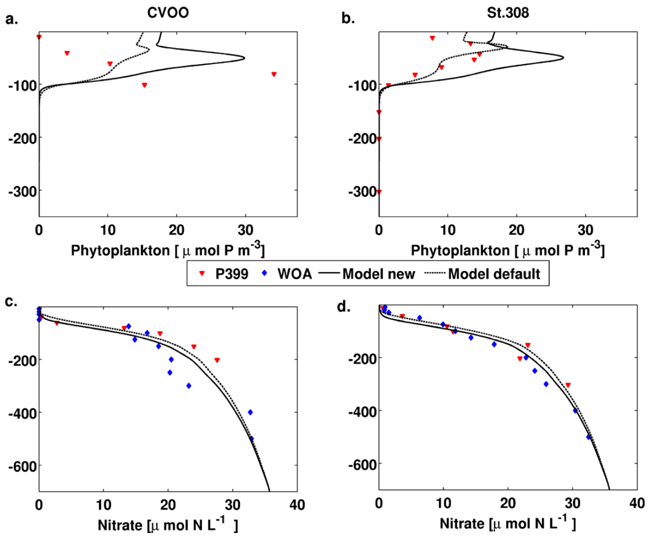

Fig. A3. Phytoplankton **(a, b)** and nutrient **(c, d)** concentrations in April **(a, c)** and June **(b, d)** [μmol P m^{-3}] – model-predicted (black solid lines new and dashed lines default parameter setup) and observed (red markers) profiles. Observations were taken from the Poseidon cruise P399/2 in 2010. Phytoplankton concentrations have been derived from chlorophyll, using a vertically dependent C : Chl ratio (e.g. Hense and Beckmann, 2008) and the Redfield ratio for conversion from carbon to nitrogen.

nutrient profiles (Fig. A2c, d) at CVOO and St. 308 closely match observed ones.

Modelled and observed phytoplankton biomass profiles (Fig. A3a, b) show similarities, but also significant differences. Similar to observations, the model predicts a subsurface phytoplankton maximum, but location and extent differ among the two stations and also compared to model results. Phytoplankton biomass is calculated from a depth-dependent C : Chl ratio. The ratio is derived from an empirical parameterization, which introduces uncertainties to the observations. Number (for model results), location, and strengths of subsurface maxima change when using biomass instead of chlorophyll as a measure for phytoplankton concentrations (compare Figs. A2 and A3). A direct comparison of model results to measured phytoplankton pigments on the other hand is not possible as chlorophyll is not a prognostic variable of the model. Nevertheless, modelled and observation-based phytoplankton concentrations are in the same order of magnitude and show a similar vertical profile. Unfortunately, there is no information on primary production available for the cruise P399/2. However, previous measurements in this region show values in the range between 0.3 to 2.6 $\mathrm{g\,C\,d^{-1}\,m^{-2}}$ (summer and fall for the oligotrophic/mesotrophic region; see Morel et al., 1996). Vertically integrated (0–100 m) daily primary production derived from our model ranges between 0.7 and 1.4 $\mathrm{g\,C\,d^{-1}\,m^{-2}}$. Thus, our model matches previously observed values well.

Acknowledgements. The authors are grateful to Ilka Peeken (Alfred Wegner Institute Bremerhaven) and Hermann Bange (GEOMAR Helmholtz Centre for Ocean Research Kiel) for providing phytoplankton pigment, salinity, and temperature data from the Poseidon cruise P399/2 and to Birgit Quack (GEOMAR Helmholtz Centre for Ocean Research Kiel) for valuable discussions. The constructive comments by C. Völker and an anonymous reviewer are gratefully acknowledged. The study was funded by the German BMBF project SOPRAN (Surface Ocean Processes in the Anthropocene) SOPRAN I 03F0462E, SOPRAN II 03F0611E; IH is financed through the Cluster of Excellence "CliSAP" (EXC177), University of Hamburg, funded through the German Science Foundation (DFG).

Edited by: X. Wang

References

Agusti, S.: Viability and niche segregation of *Prochlorococcus* and *Synechococcus* cells across the Central Atlantic Ocean, Aquat. Microb. Ecol., 36, 53–59, 2004.

Bange, H.: FS Poseidon Fahrtbericht/Cruise Report P399 - 2&3 : Eastern tropical North Atlantic; P399-2: 31.04.2010-17.06.2010 Las Palmas – Las Palmas (Canary Islands), P399-3: 18.-24.06.2010 Las Palmas (Canary Islands) – Vigo (Spain); DRIVE (Diurnal and RegIonal Variability of Halogen Emmissions), SOPRAN, Cruise Report 10.3289/ifm-geomar_rep_48_2011, IfM-Geomar Kiel, Kiel, http://oceanrep.geomar.de/12032/, 2011.

Behringer, D. and Xue, Y.: Evaluation of the Global Ocean Data Assimilation System at NCEP: The Pacific Ocean. Preprints, Eighth Symp. on Integrated Observing and Assimilation Systems for Atmosphere, Oceans, and Land Surface, Seattle, WA, Amer. Meteor. Soc., available at: http://www.cpc.ncep.noaa.gov/products/people/yxue/pub/13.pdf, 2004.

Bell, N., Hsu, L., Jacob, D., Schultz, M., Blake, D., Butler, J., King, D., Lobert, J., and Maier-Reimer, E.: Methyl iodide: Atmospheric budget and use as a tracer of marine convection in global models, J. Geophys. Res., 107, 8-1–8-12, 2002.

Brownell, D., Moore, R., and Cullen, J.: Production of methyl halides by *Prochlorococcus* and *Synechococcus*, Glob. Biogeochem. Cy., 24, GB2002, doi:10.1029/2009GB003671, 2010.

Butler, J.H.and King, D., Lobert, J.M.and Montzka, S., Yvon-Lewis, S., Hall, B., Warwick, N., Mondell, D., Aydin, M., and Elkins, J.: Oceanic distributions and emissions of short-lived halocarbons, Global Biogeochem. Cy., 21, GB1023, doi:doi:10.1029/2006GB002732, 2007.

Carlson, C.: Biogeochemistry of marine dissolved organic matter, chap. Production and removal processes, 91–152, Academic Press, An Elsevier Science Imprint, 2002.

Carpenter, L.: Iodine in the Marine Boundary Layer, Chem. Rev., 103, 4953–4962, 2003.

Carpenter, L. and Liss, P.: On temperate sources of bromoform and other reactive organic bromine gases, J. Geophys. Res., 105, 20539–20547, 2000.

Chameides, W. and Davis, D.: Iodine: Its Possible Role in Tropospheric Photochemistry, J. Geophys. Res., 85, 7383–7398, 1980.

Chuck, A., Turner, S., and Liss, P.: Oceanic distributions and air-sea fluxes of biogenic halocarbons in the open ocean, J. Geophys. Res., 110, 1–12, 2005.

Conkright, M. E., Locarnini, R. A., Garcia, H. E., O'Brien, T. D., Boyer, T. P., Stephens, C., and Antonov, J. I.: World Ocean Atlas 2001: Objective Analyses, Data Statistics, and Figures, CDROM Documentation, Tech. rep., National Oceanographic Data Center, Silver Spring, MD, USA, 2002.

Dittmar, W.: Part I. Report on researches into the composition of ocean-water, collected by H. M. S. Challenger, during the years 1873–1876, Physics and Chemistry, 1, 1–247, 1884.

Elliott, S. and Rowland, F.: Nucleophilic substitution rates and solubilities for methyl halides in seawater, Geophys. Res. Lett., 20, 1043–1046, 1993.

Elliott, S. and Rowland, F.: Methyl halide hydrolysis rates in natural waters, J. Atmos. Chem., 20, 229–236, 1995.

Fuhlbrügge, S., Krüger, K., Quack, B., Atlas, E., Hepach, H., and Ziska, F.: Impact of the marine atmospheric boundary layer on VSLS abundances in the eastern tropical and subtropical North Atlantic Ocean, Atmos. Chem. Phys. Discuss., 12, 31205–31245, doi:10.5194/acpd-12-31205-2012, 2012.

Giese, B., Laturnus, F., Adams, F. C., and Wiencke, C.: Release of Volatile Iodinated C_1–C_4 Hydrocarbons by Marine Macroalgae from Various Climate Zones, Environ. Sci. Technol., 33, 2432–2439, doi:10.1021/es980731n, 1999.

Happell, J. and Wallace, D.: Methyl iodide in the Greenland/Norwegian Seas and the tropical Atlantic Ocean: Evidence for photochemical production, Geophys. Res. Lett., 23, 2105–2108, 1996.

Hense, I. and Beckmann, A.: Revisiting subsurface chlorophyll and phytoplankton distributions, Deep-Sea Res. Pt. I, 55, 1193–1199, 2008.

Hense, I. and Quack, B.: Modelling the vertical distribution of bromoform in the upper water column of the tropical Atlantic Ocean, Biogeosciences, 6, 535–544, doi:10.5194/bg-6-535-2009, 2009.

Hughes, C., Franklin, D., and Malin, G.: Iodomethane production by two important marine cyanobacteria: *Prochlorococcus marinus* (CCMP 2389) and *Synechococcus* sp. (CCMP 2370), Mar. Chem., 125, 19–25, 2011.

Ilyina, T., Six, K. D., Segschneider, J., Maier-Reimer, E., Li, H., and Núñez-Riboni, I.: The global ocean biogeochemistry model HAMOCC: Model architecture and performance as component of the MPI-earth system model in different CMIP5 experimental realizations, JAMES, accepted, doi:10.1002/jame.20017, 2013.

Johnson, Z. I., Zinser, E., Coe, A., McNulty, N., Woodward, E., and Chisholm, S.: Niche partitioning among *Prochlorococcus* ecotypes along oceanscale environmental gradients, Science, 311, 1737–1740, 2006.

Loiselle, S., Vione, D., Minero, C., Maurino, V., Tognazzi, A., Dattilo, A. M., Rossi, C., and Bracchini, L.: Chemical and optical phototransformation of dissolved organic matter, Water Res., 46, 3197–3207, doi:10.1016/j.watres.2012.02.047, 2012.

Lovelock, J., Maggs, R., and Wade, R.: Halogenated hydrocarbons in and over the Atlantic [8], Nature, 241, 194–196, 1973.

Manley, S. and Dastoor, M.: Methyl iodide (CH_3I) production by kelp and associated microbes, Mar. Biol., 98, 477–482, 1988.

Manley, S. and De La Cuesta, J.: Methyl iodide production from marine phytoplankton cultures, Limnol. Oceanogr., 42, 142–147, 1997.

Moore, R.: Methyl halide production and loss rates in sea water from field incubation experiments, Mar. Chem., 101, 213–219, 2006.

Moore, R. and Groszko, W.: Methyl iodide distribution in the ocean and fluxes to the atmosphere, J. Geophys. Res., 104, 11163–11171, doi:10.1029/1998JC900073, 1999.

Moore, R. and Tokarczyk, R.: Volatile biogenic halocarbons in the northwest Atlantic, Global Biogeochem. Cy., 7, 195–210, 1993.

Moore, R. and Zafiriou, O.: Photochemical production of methyl iodide in seawater, J. Geophys. Res., 99, 16415–16420, 1994.

Moore, R., Geen, C., and Tait, V.: Determination of Henry's law constants for a suite of naturally occurring halogenated methanes in seawater, Chemosphere, 30, 1183–1191, 1995.

Moore, R., Webb, M., Tokarczyk, R., and Wever, R.: Bromoperoxidase and iodoperoxidase enzymes and production of halogenated methanes in marine diatom cultures, J. Geophys. Res., 101, 20899–20908, 1996.

Morel, A., Antoine, D., Babin, M., and Dandonneau, Y.: Measured and modeled primary production in the northeast Atlantic (EUMELI JGOFS program): the impact of natural variations in photosynthetic parameters on model predictive skill,, Deep-Sea Res. Pt. I, 43, 1273–1304, 1996.

Nightingale, P., Malin, G., and Liss, P.: Production of chloroform and other low-molecular-weight halocarbons by some species of macroalgae, Limnol. Oceanogr., 40, 680–689, 1995.

Nightingale, P. D., Malin, G., Law, C., Watson, A., Liss, P., Liddicoat, M., Boutin, J., and Upstill-Goddard, R.: In situ evaluation of air–sea gas exchange parameterizations using novel conservative and volatile tracers, Global Biogeochem. Cy., 14, 373–387, 2000.

O'Brien, L. M., Harris, N. R. P., Robinson, A. D., Gostlow, B., Warwick, N., Yang, X., and Pyle, J. A.: Bromocarbons in the tropical marine boundary layer at the Cape Verde Observatory – measurements and modelling, Atmos. Chem. Phys., 9, 9083–9099, doi:10.5194/acp-9-9083-2009, 2009.

Partensky, F., Hess, W., and Vaulot, D.: Prochlorococcus, a marine photosynthetic prokaryote of global significance, Microbiol. Mol. Biol. R., 63, 106–127, 1999.

Rattigan, O., Shallcross, D., and Cox, R.: UV absorption cross-sections and atmospheric photolysis rates of CF_3I, CH_3I, C_2H_5I and CH_2ICl, J. Chem. Soc.-Faraday T., 93, 2839–2846, 1997.

Richter, U. and Wallace, D.: Production of methyl iodide in the tropical Atlantic Ocean, Geophys. Res. Lett., 31, 1–4, 2004.

Six, K. and Maier-Reimer, E.: Effects of plankton dynamics on seasonal carbon fluxes in an ocean general circulation model, Global Biogeochem. Cy., 10, 559–583, 1996.

Smythe-Wright, D., Boswell, S., Breithaupt, P., Davidson, R., Dimmer, C., and Eiras Diaz, L.: Methyl iodide production in the ocean: Implications for climate change, Global Biogeochem. Cy., 20, GB3003, doi:10.1029/2005GB002642, 2006.

Solomon, S., Garcia, R., and Ravishankara, A.: On the role of iodine in ozone depletion, J. Geophys. Res., 99, 20491–20499, 1994.

Sulzberger, B. and Durisch-Kaiser, E.: Chemical characterization of dissolved organic matter (DOM): A prererquisite for understanding UV-induced changes of DOM absorption properties and bioavailabilty, Aquat. Sci., 71, 104–126, 2009.

Umlauf, L., Burchard, H., and Bolding, K.: GOTM -scientific documentation: version 3.2, Mar. Sci. Rep., 63, 1–346, 2005.

Uppala, S. M., Kållberg, P. W., Simmons, A. J., Andrae, U., Bechtold, V. D. C., Fiorino, M., Gibson, J. K., Haseler, J., Hernandez, A., Kelly, G. A., Li, X., Onogi, K., Saarinen, S., Sokka, N., Allan, R. P., Andersson, E., Arpe, K., Balmaseda, M. A., Beljaars,

A. C. M., Berg, L. V. D., Bidlot, J., Bormann, N., Caires, S., Chevallier, F., Dethof, A., Dragosavac, M., Fisher, M., Fuentes, M., Hagemann, S., Hólm, E., Hoskins, B. J., Isaksen, L., Janssen, P. A. E. M., Jenne, R., Mcnally, A. P., Mahfouf, J.-F., Morcrette, J.-J., Rayner, N. A., Saunders, R. W., Simon, P., Sterl, A., Trenberth, K. E., Untch, A., Vasiljevic, D., Viterbo, P., and Woollen, J.: The ERA-40 re-analysis, Q. J. Roy. Meteorol. Soc., 131, 2961–3012, doi:10.1256/qj.04.176, 2005.

Vogt, R., Sander, R., Von Glasow, R., and Crutzen, P.: Iodine chemistry and its role in halogen activation and ozone loss in the marine boundary layer: A model study, J. Atmos. Chem., 32, 375–395, 1999.

Wallace, D. R. and Bange, H.: Introduction to special section: Results of the Meteor 55: Tropical SOLAS Expedition, Geophys. Res. Lett., 31, L23S01, doi:10.1029/2004GL021014, 2004.

Wang, L., Moore, R., and Cullen, J.: Methyl iodide in the NW Atlantic: Spatial and seasonal variation, J. Geophys. Res., 114, C07007, doi:10.1029/2007JC004626, 2009.

Weber, L., Völker, C., Oschlies, A., and Burchard, H.: Iron profiles and speciation of the upper water column at the Bermuda Atlantic Time-series Study site: a model based sensitivity study, Biogeosciences, 4, 689–706, doi:10.5194/bg-4-689-2007, 2007.

Wetzel, P., Maier-Reimer, E., Botzet, M., Jungclaus, J., Keenlyside, N., and Latif, M.: Effects of ocean biology on the penetrative radiation in a coupled climate model, J. Climate, 19, 3973–3987, 2006.

6. Manuscript 6

The contribution of oceanic methyl iodide to stratospheric iodine

S. Tegtmeier[1], K. Krüger[1,*], B. Quack[1], E. Atlas[2], D. R. Blake[3], H. Boenisch[4], A. Engel[4], H. Hepach[1], R. Hossaini[5], M. A. Navarro[2], S. Raimund[1], S. Sala[4], Q. Shi[1], and F. Ziska[1]

[1] GEOMAR Helmholtz Centre for Ocean Research Kiel, Kiel, Germany

[2] Rosenstiel School of Marine and Atmospheric Science, University of Miami, Miami, Florida, USA

[3] University of California, Irvine, USA

[4] Goethe University Frankfurt am Main, Frankfurt, Germany

[5] Institute for Climate and Atmospheric Science, School of Earth and Environment, University of Leeds, Leeds, UK

[*] now at: University of Oslo, Oslo, Norway

Published in: Atmospheric Chemistry and Physics, 13, 11869-11886, doi:10.5194/acp-13-11869-2013, 2013.

Atmos. Chem. Phys., 13, 11869–11886, 2013
www.atmos-chem-phys.net/13/11869/2013/
doi:10.5194/acp-13-11869-2013
© Author(s) 2013. CC Attribution 3.0 License.

Atmospheric Chemistry and Physics
Open Access

The contribution of oceanic methyl iodide to stratospheric iodine

S. Tegtmeier[1], K. Krüger[1,*], B. Quack[1], E. Atlas[2], D. R. Blake[3], H. Boenisch[4], A. Engel[4], H. Hepach[1], R. Hossaini[5], M. A. Navarro[2], S. Raimund[1], S. Sala[4], Q. Shi[1], and F. Ziska[1]

[1]GEOMAR Helmholtz Centre for Ocean Research Kiel, Kiel, Germany
[2]Rosenstiel School of Marine and Atmospheric Science, University of Miami, Miami, Florida, USA
[3]University of California, Irvine, USA
[4]Goethe University Frankfurt am Main, Frankfurt, Germany
[5]Institute for Climate and Atmospheric Science, School of Earth and Environment, University of Leeds, Leeds, UK
[*]now at: University of Oslo, Oslo, Norway

Correspondence to: S. Tegtmeier (stegtmeier@geomar.de)

Received: 4 April 2013 – Published in Atmos. Chem. Phys. Discuss.: 30 April 2013
Revised: 14 October 2013 – Accepted: 6 November 2013 – Published: 9 December 2013

Abstract. We investigate the contribution of oceanic methyl iodide (CH_3I) to the stratospheric iodine budget. Based on CH_3I measurements from three tropical ship campaigns and the Lagrangian transport model FLEXPART, we provide a detailed analysis of CH_3I transport from the ocean surface to the cold point in the upper tropical tropopause layer (TTL). While average oceanic emissions differ by less than 50 % from campaign to campaign, the measurements show much stronger variations within each campaign. A positive correlation between the oceanic CH_3I emissions and the efficiency of CH_3I troposphere–stratosphere transport has been identified for some cruise sections. The mechanism of strong horizontal surface winds triggering large emissions on the one hand and being associated with tropical convective systems, such as developing typhoons, on the other hand, could explain the identified correlations. As a result of the simultaneous occurrence of large CH_3I emissions and strong vertical uplift, localized maximum mixing ratios of 0.6 ppt CH_3I at the cold point have been determined for observed peak emissions during the SHIVA (Stratospheric Ozone: Halogen Impacts in a Varying Atmosphere)-Sonne research vessel campaign in the coastal western Pacific. The other two campaigns give considerably smaller maxima of 0.1 ppt CH_3I in the open western Pacific and 0.03 ppt in the coastal eastern Atlantic. In order to assess the representativeness of the large local mixing ratios, we use climatological emission scenarios to derive global upper air estimates of CH_3I abundances. The model results are compared with available upper air measurements, including data from the recent ATTREX and HIPPO2 aircraft campaigns. In the eastern Pacific region, the location of the available measurement campaigns in the upper TTL, the comparisons give a good agreement, indicating that around 0.01 to 0.02 ppt of CH_3I enter the stratosphere. However, other tropical regions that are subject to stronger convective activity show larger CH_3I entrainment, e.g., 0.08 ppt in the western Pacific. Overall our model results give a tropical contribution of 0.04 ppt CH_3I to the stratospheric iodine budget. The strong variations in the geographical distribution of CH_3I entrainment suggest that currently available upper air measurements are not representative of global estimates and further campaigns will be necessary in order to better understand the CH_3I contribution to stratospheric iodine.

1 Introduction

It is currently believed that organic iodine compounds are not important for stratospheric ozone chemistry as a result of their very short lifetimes that allow only small fractions of the emitted iodine to reach the stratosphere (Aschmann et al., 2009; Montzka and Reimann, 2011). Emissions of iodinated compounds from the ocean into the atmosphere and subsequent strongly localized vertical transport in convective systems determines if and how much of the short-lived iodinated gases reach the upper tropical tropopause layer (TTL) and lower stratosphere. Both processes are highly variable in time and space and reliable global estimates should, if possible, be derived from frequent upper air observations and from model studies based on high resolution emission maps. In addition to the unknown variability of CH_3I in the TTL, uncertainties in the knowledge of the atmospheric lifetime of inorganic iodine (e.g., Dix et al., 2013) pose a major challenge for the quantification of the stratospheric iodine budget. If iodinated species reach the upper troposphere and lower stratosphere (UTLS), they might enhance ozone destruction due to the possible role of active iodine in rapid interhalogen reactions (Solomon et al., 1994).

Methyl iodide (CH_3I) is an important carrier of iodine from the surface to the free troposphere, where it plays an important role for ozone chemistry and oxidizing capacities (Chameides and Davis, 1980; Davis et al., 1996; McFiggans et al., 2000; O'Dowd et al., 2002; Saiz-Lopez et al., 2012; Vogt et al., 1999). CH_3I is emitted mainly from the ocean where biological sources in form of algae and phytoplankton (e.g., Hughes et al., 2011; Manley and Dastoor, 1987, 1988; Manley and de la Cuesta, 1997; Smythe-Wright et al., 2006) and non-biological sources in form of photochemical production (e.g., Butler et al., 2007; Chuck et al., 2005; Happell and Wallace, 1996; Moore and Zafiriou, 1994; Richter and Wallace, 2004; Yokouchi et al., 2008) have been identified. Note that current studies suggest that organic sources of iodine cannot explain iodine oxide concentrations in the lower troposphere over the tropical oceans (Jones et al., 2010; Mahajan et al., 2010) and that emissions of inorganic iodine following heterogeneous reactions at the ocean surface can account for a primary source of oceanic iodine emissions (Carpenter et al., 2013).

Global emission estimates are based on oceanic and atmospheric CH_3I concentrations obtained during ship cruises (*bottom-up*) and on model studies which are adjusted to CH_3I upper-air observations (*top-down*) (Montzka and Reimann, 2011). Oceanic and atmospheric surface CH_3I is characterized by a large spatial (e.g., Ziska et al., 2013) and temporal (e.g., Fuhlbrügge et al., 2013) variability. Additionally, differences between calibration scales, applied during past campaigns, might exist (Butler et al., 2007). Estimating local fluxes from observations and extrapolating them to a larger scale in order to derive global estimates may thus result in large uncertainties. Atmospheric modeling studies, on the other hand, prescribe global emissions with the emission strength chosen so as to reproduce atmospheric aircraft observations and might miss the importance of localized sources. As a result, emissions are poorly constrained and available global oceanic flux estimates based on the different approaches (top-down, bottom-up and laboratory experiments) range widely from 180 to 1163 $\mathrm{Gg\,I\,yr^{-1}}$. An overview of available global oceanic emission estimates in the literature is given in Table 1 in $\mathrm{Gg\,I\,yr^{-1}}$ and, for a better comparability with the ship campaign emissions presented in Sect. 3, in $\mathrm{pmol\,CH_3I\,m^{-2}\,h^{-1}}$. Additionally, terrestrial sources such as rice paddies, wetlands, and biomass burning, which are not well quantified yet, are assumed to contribute 80–110 $\mathrm{Gg\,I\,yr^{-1}}$ (Bell et al., 2002; Redeker et al., 2000; Sive et al., 2007).

Atmospheric mixing ratios of CH_3I in the marine boundary layer have been reported by a large number of measurement campaigns, and background values range between 0.4 and 1.6 ppt (Saiz-Lopez et al., 2012 and references therein). With increasing altitude the CH_3I abundance decreases and measurements from two aircraft campaigns reveal very little CH_3I in the TTL, with mean values of 0.01 ppt above 14 km (Montzka and Reimann, 2011). The two campaigns were conducted with the NASA WB57 high-altitude aircraft over Central America and the Gulf of Mexico, but due to the horizontal limitations of the campaign area, the results might not be representative of global CH_3I estimates in the TTL. The observational data obtained during the aircraft campaigns, combined with the outcome of model studies (Aschmann et al., 2009; Donner et al., 2007; Gettelman et al., 2009), lead to the conclusion that no more than 0.05 ppt of iodine enters the stratosphere in the form of the source gas CH_3I (Montzka and Reimann, 2011). If CH_3I is photolyzed before reaching the stratosphere, the generated inorganic iodine can be removed from the atmosphere by washout. It has been suggested recently that heterogeneous recycling of inorganic iodine on aerosol surfaces can occur (Dix et al., 2013), which could enable a longer atmospheric lifetime and possibly the direct entrainment of inorganic iodine into the stratosphere.

Once in the lower stratosphere, CH_3I will contribute to the inorganic iodine (I_y) budget, which is of interest due to the suggested efficiency of active iodine in destroying ozone (Davis et al., 1996; Solomon et al., 1994; WMO, 2007). Stratospheric iodine exists mostly in the form of free radicals (iodine atoms and iodine monoxide), so that the partitioning of free radicals to total halogen content is much higher for iodine than for chlorine or bromine (Brasseur and Solomon, 2005). Investigations of inorganic iodine species, in the form of iodine monoxide (IO) or iodine dioxide (OIO), in the lower stratosphere give an upper limit of IO of 0.3 ppt based on ground-based measurements (Wennberg et al., 1997) and 0.2 ppt based on solar-occultation balloon-borne measurements (Pundt et al., 1998). Other balloon campaigns in the upper TTL, however, detected no IO or OIO in the upper TTL above the detection limit at 0.1 ppt (Bösch et al., 2003; Butz et al., 2009). As a result, the total amount of stratospheric I_y is currently estimated to be below 0.15 ppt (Montzka and Reimann, 2011), arising from the detection limit of inorganic iodine (0.1 ppt) given by the latter studies and the iodine supply in form of CH_3I (0.05 ppt).

Due to its short lifetime of around 7 days (given in Montzka and Reimann, 2011), one expects CH_3I in the troposphere and TTL to exhibit significantly large variability. The amount of CH_3I transported from the ocean into the stratosphere is determined by oceanic emissions and the efficiency of atmospheric transport. In order to quantify the contribution of CH_3I to the stratospheric I_y budget, observations of CH_3I and IO with a good global coverage would be

Table 1. Global CH_3I emission estimates in the literature given in $Gg\,I\,yr^{-1}$ and additionally in $pmol\,CH_3I\,m^{-2}\,h^{-1}$.

CH_3I emission ($Gg\,I\,yr^{-1}$)	CH_3I emission ($pmol\,CH_3I\,m^{-2}\,h^{-1}$)	Reference	Approach
241	593	Liss and Slater (1974)	Bottom up
1163	2862	Rasmussen et al. (1982)	Bottom up
270–450	665–1107	Singh et al. (1983)	Bottom up
134	330	Campos et al. (1996)	Bottom-up
254	625	Moore and Groszko (1999)	Bottom up
272	670	Bell et al. (2002)	Bottom-up
180	443	Chuck et al. (2005)	Bottom up
531	1307	Smythe-Wright et al. (2006)	Lab-experiment
550	1354	Butler et al. (2007)	Bottom-up
272	748	Ordóñez et al. (2012)	Top-down
184	453	Ziska et al. (2013)	Bottom-up

necessary. While in the UTLS such observational evidence of global iodine abundances does not exist so far, recent measurements in the free troposphere over the Canary Islands (Puentedura et al., 2012) and the Pacific Ocean (Dix et al., 2013) report significant amounts of IO of up to 0.4 ppt and suggest that IO occurs in the lower troposphere on a global scale. At the surface, a variety of CH_3I data originating from ship campaigns and the resulting first global emission climatology (Ziska et al., 2013) are available. Here, we use in situ CH_3I measurements from three tropical ship campaigns, one in the eastern Atlantic and two in the western Pacific, and a Lagrangian transport model to analyze the characteristics and the variability of CH_3I transport from the ocean surface into the upper TTL. Furthermore, we derive upper air estimates of CH_3I abundances based on the global emission climatology and compare them to available upper air measurements that include new data from various aircraft campaigns. The ship and aircraft campaigns as well as the atmospheric transport model are introduced in Sect. 2. Estimates of atmospheric CH_3I abundances based on the individual ship campaigns are given in Sect. 3, while the model results based on global emissions, including their comparison to aircraft campaign data, are discussed in Sect. 4. We present the contribution of oceanic CH_3I to stratospheric iodine in the form of the model estimated CH_3I mixing ratios at the cold point. The summary and discussion of the key results can be found in Sect. 5.

2 Data and model

2.1 Ship campaigns

Oceanic CH_3I emissions from three tropical ship campaigns (Table 2), calculated from measurements of CH_3I mixing ratios in the surface water and atmosphere, are used in this study. The two ship campaigns TransBrom-Sonne and SHIVA-Sonne took place in the open and coastal western Pacific while the DRIVE campaign was located in the northeastern Atlantic (Fig. 1). During each cruise, surface air samples were collected every 1 to 3 h in pressurized stainless steel canisters and analyzed subsequently for CH_3I at the Rosenstiel School of Marine and Atmospheric Sciences (RSMAS) at the University of Miami by the group lead by Elliot Atlas. Surface water samples were collected simultaneously by a submersible pump at 5 m depth and analyzed on board using a purge-and-trap gas chromatography/mass spectrometry (GC/MS) analytical system (Quack et al., 2004). Both data sets were calibrated with a NOAA standard (Butler et al., 2007). The instantaneous CH_3I sea-to-air fluxes were calculated from the measured sea surface concentration and local atmospheric mixing ratios applying Henry's law constant from Moore et al. (1995) and the instantaneous 10 min average wind speed. Henry's law constant was calculated as a function of the 10 min average water temperature. The flux calculations are based on the transfer coefficient parameterization of Nightingale et al. (2000) adapted to CH_3I. For the parameterization, the transfer velocity at Schmidt number 660, which corresponds to CO_2 at 20 °C in seawater (Wanninkhof, 1992), was corrected by the CH_3I Schmidt number at the temperature of measurement. The ratio of the diffusion coefficients from CH_3Br (De Bruyn and Saltzman, 1997) and

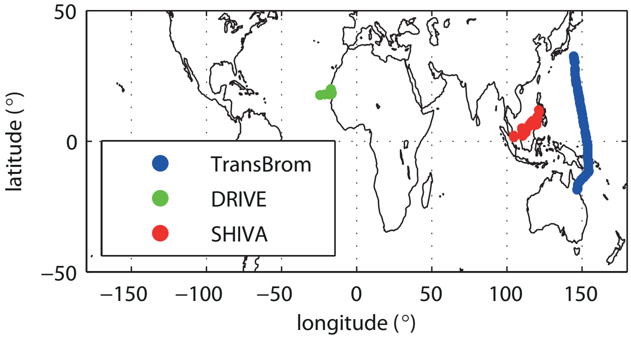

Fig. 1. Map of ship campaigns used in this study.

Table 2. Recent ship campaigns providing oceanic and atmospheric CH_3I measurements.

Campaign (R/V)	Full name	Route	Time period	References
TransBrom-Sonne (Sonne)	Very short lived bromine compounds in the ocean and their transport pathways into the stratosphere – Sonne	Western Pacific: Tomakomai, Japan – Townsville, Australia	2009 October	Krüger and Quack (2013)
DRIVE (Poseidon)	Diurnal and Regional Variability of Halogen Emissions	Atlantic: Las Palmas, Spain – Vigo, Spain	2010 May/June	Bange et al. (2011)
SHIVA-Sonne (Sonne)	Stratospheric Ozone: Halogen Impacts in a Varying Atmosphere – Sonne	Western Pacific: Singapore – Manila, Philippines	2011 November	Quack and Krüger (2013)

CH_3I, estimated according to Wilke and Chang (1955), was used as a function of temperature for the Schmidt-number correction (e.g., Richter and Wallace, 2004).

2.2 Aircraft campaigns

CH_3I measurements in the upper troposphere and TTL are currently available from seven aircraft campaigns. Three campaigns provide data from the surface up to the upper troposphere/lower TTL: the TC4-DC8 over Central America and the HIPPO and SHIVA campaigns which took place in the Pacific and western Pacific area, respectively. Note that SHIVA is a combined aircraft-, ship- and ground-based campaign with measurements both from the ship and from the aircraft used in this study. From the HIPPO mission, we use here the measurements obtained during the HIPPO2 campaign in 2009. CH_3I measurements in the upper TTL are available from Pre-AVE and TC4 campaigns. These two campaigns have been used to derive recent estimates of the upper air CH_3I abundance (Montzka and Reimann, 2011). In addition to the data used for the current upper TTL CH_3I estimate, observations from the ACCENT campaign in 1999 and from the ATTREX campaign in 2011 are included in our study. All four campaigns, which provide CH_3I measurements in the upper TTL, took place over the southern US and Central America. Detailed information about the aircraft missions, including location and time period, are presented in Table 3.

2.3 Global emission climatology

The global emission scenario from Ziska et al. (2013) is a bottom-up estimate of the oceanic CH_3I fluxes. Atmospheric and oceanic surface in situ measurements from the HalOcAt (Halocarbons in the ocean and atmosphere) database project (https://halocat.geomar.de) were used to generate global surface concentration maps. In a first step the surface measurements were classified based on physical and biogeochemical characteristics of the ocean and atmosphere important for the CH_3I distribution and sources. Within each classified region, the global $1° \times 1°$ grid was filled through the extrapolation of the in situ measurements based on the ordinary least square (OLS) regression technique. The estimated surface concentration maps do not provide any information on temporal variability, but represent climatological fields of a 20 yr time period. Based on the global concentration maps, the oceanic emissions were calculated with the transfer coefficient parameterization of Nightingale et al. (2000), adapted to CH_3I. The emission parameterization is based on 6 hourly meteorological ERA-Interim data (Dee et al., 2011), taking into account emission peaks related to maxima in the horizontal wind fields. The final emission climatology product is calculated as the 20 yr-average emission field. Emission peaks related to 6 hourly wind maxima are not present any more in the final 20 yr mean climatology; however, their existence in the temporally resolved emission fields counteracts a possible underestimation introduced by smoothing effects of the climatological approach.

2.4 Modeling atmospheric transport

The atmospheric transport of CH_3I from the oceanic surface into the upper troposphere and TTL is simulated with the Lagrangian particle dispersion model, FLEXPART (Stohl et al., 2005). This model has been validated based on comparisons with measurement data from three large-scale tracer experiments (Stohl et al., 1998) and on intercontinental air pollution transport studies (e.g., Forster et al., 2001; Spichtinger et al., 2001; Stohl and Trickl, 1999). FLEXPART is driven by meteorological fields from the ECMWF (European Centre for Medium-Range Weather Forecasts) numerical weather prediction model and includes parameterizations for moist convection (Forster et al., 2007), turbulence in the boundary layer and free troposphere (Stohl and Thomson, 1999), dry

Table 3. Aircraft campaigns with CH_3I measurements used in the study.

Campaign (Aircraft)	Full name	Max. altitude	Location	Time period	References
ACCENT (WB57)	Atmospheric Chemistry of Combustion Emissions Near the Tropopause	19 km	Southern US Central America	1999 April, September	http://espoarchive.nasa.gov/archive/browse/accent
Pre-AVE (WB57)	Pre-Aura Validation Experiment	19 km	Southern US Central America	2004 January–February	http://espoarchive.nasa.gov/archive/browse/pre_ave
TC4 (DC 8)	Tropical Composition, Cloud and Climate Coupling	12 km	Southern US Central America	2007 July–August	Toon et al. (2010)
TC4 (WB57)	Tropical Composition, Cloud and Climate Coupling	19 km	Southern US Central America	2007 August	Toon et al. (2010)
HIPPO2 (HIAPER)	HIAPER Pole-to-Pole Observations 2	14 km	Pacific	2009 November	Wofsy et al. (2011)
ATTREX (Global Hawk)	Airborne Tropical Tropopause Experiment	19 km	Eastern Pacific	2011 October–November	http://espo.nasa.gov/missions/attrex
SHIVA (Falcon)	Stratospheric ozone: Halogen Impacts in a Varying Atmosphere	14 km	Western Pacific (Maritime Continent)	2011 November	http://shiva.iup.uni-heidelberg.de/index.html

deposition and in-cloud as well as below-cloud scavenging, and the simulation of chemical decay.

We perform two different kinds of studies based on the different model setups, one using in situ emissions observed during individual ship campaigns and one using a global emission climatology. For the in situ experiments, the transport of CH_3I is simulated with a multitude of trajectories launched for each emission data point, as described in detail by Tegtmeier et al. (2012). The trajectories are assigned the amounts of CH_3I emitted from a $0.0002° \times 0.0002°$ grid box ($\sim 500\,m^2$) at the measurement location over one hour, as calculated from the observation-derived flux. Atmospheric mixing ratio profiles resulting from in situ emissions have been determined following the method described in Tegtmeier et al. (2012). The calculation of global CH_3I estimates is based on the emission climatology from Ziska et al. (2013). The oceanic sea-to-air flux is given globally on a $1° \times 1°$ grid. From each grid box 10 trajectories are released per day, carrying the according amount of CH_3I as prescribed by the emission scenario. While the simulations based on the in situ ship campaign data are carried out for the time period of the respective ship campaigns (see Table 2), the global simulations are run for the year 2009. Additionally, the global simulations are carried out for the time periods of the aircraft campaigns (see Table 3) in order to allow for a direct comparison between aircraft measurements and model results. The FLEXPART runs are driven by the ECMWF reanalysis product ERA-Interim (Dee et al., 2011), given at a horizontal resolution of $1° \times 1°$ on 60 model levels. Transport, dispersion and convection of the air parcels are calculated from the 6-hourly fields of horizontal and vertical wind, temperature, specific humidity, convective, and large scale precipitation and others. The vertical wind is calculated in hybrid coordinates mass consistently from spectral data by the preprocessor, which retrieves the meteorological fields from the ECMWF archives.

The atmospheric lifetime of CH_3I was assumed to be constant in the troposphere and set to 7 days according to current estimates (Montzka and Reimann, 2011). Trajectories were terminated after 20 days. For a sensitivity study, an altitude-dependent lifetime of CH_3I, derived by the TOMCAT chemical transport model (CTM) (Chipperfield, 2006), was also used. The CTM calculated tropospheric loss of CH_3I through photolysis, the major tropospheric sink, using the recommended absorption cross section data of Sander et al. (2011). The modeled CH_3I lifetime diagnosed by the CTM is relatively short ($\sim$ 2–3 days) in the tropical troposphere and thus this experiment is useful for examining the sensitivity of CH_3I loading in the upper troposphere to a range of lifetimes. Previously, CH_3I profiles from TOMCAT have been shown to agree well with aircraft observations in the tropical troposphere (Hossaini et al., 2012). The mass of the CH_3I carried by each air parcel is reduced at a rate corresponding to its chemical lifetime.

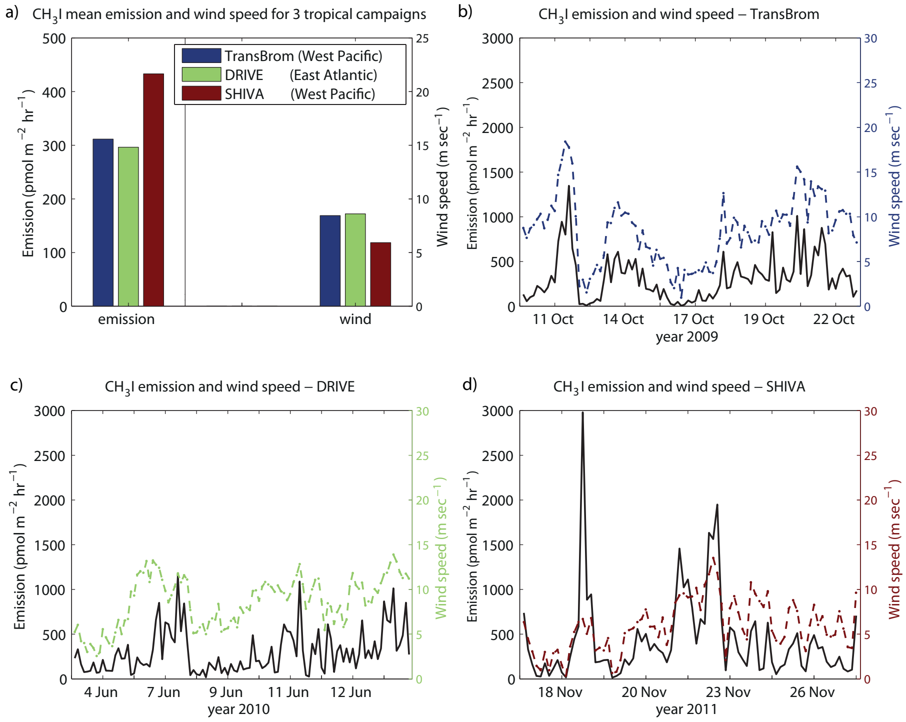

Fig. 2. Campaign-averaged CH_3I emissions and wind speed are shown for three tropical campaigns **(a)**. CH_3I emissions (black line), as well as the wind speed (colored line) are displayed as a function of time along the cruise track for TransBrom **(b)**, DRIVE **(c)**, and SHIVA **(d)**.

3 Atmospheric CH_3I transport based on individual ship campaigns

3.1 Comparison of three tropical campaigns

CH_3I emissions observed during the tropical ship cruises vary substantially from campaign to campaign. Figure 2a shows the campaign-averaged emissions for all three cruises, with stronger emissions for the coastal western Pacific campaign SHIVA-Sonne (referred to as SHIVA hereinafter) compared to the northeastern Atlantic campaign DRIVE and the open western Pacific campaign TransBrom-Sonne (referred to as TransBrom hereinafter). In contrast to global estimates (Table 1), the emissions observed during the three campaigns are small with mean values of 310 (DRIVE), 320 (TransBrom) and 430 (SHIVA) $\mathrm{pmol\,m^{-2}\,h^{-1}}$ just below the minimum global estimate (443 $\mathrm{pmol\,m^{-2}\,h^{-1}}$, Chuck et al., 2005) and three times smaller than the maximum global estimate (1354 $\mathrm{pmol\,m^{-2}\,h^{-1}}$, Butler et al., 2007).

Black lines in Fig. 2b–d give the emission strength along the cruise tracks and demonstrate the large variability of sea-to-air fluxes during the campaigns, with the measurement locations often about less than 100 km apart. CH_3I is generally oversaturated in oceanic surface waters. As a result, emission flux is primarily controlled by concentrations in water (rather than air) and the water–air exchange rate, which is in turn driven by the wind speed (Ziska et al., 2013). In addition to the emission time series, the wind speed along the cruise track (colored dashed lines) for the individual campaigns is presented in Fig. 2b–d. Particularly high emissions occur for the TransBrom cruise during times of high wind speeds, e.g., emissions of up to 1364 and 600 $\mathrm{pmol\,m^{-2}\,h^{-1}}$ were observed during the tropical storms Nepartak and Lupit on 12 October and 14 October 2009, respectively (Quack et al., 2013).

Among the different existing parameterizations, the here applied sea-to-air flux parameterization of Nightingale et al. (2000) predicts transfer velocities in the middle range (e.g., Carpenter et al., 2012) for wind speeds below 20 $\mathrm{m\,s^{-1}}$. All parameterizations gain uncertainty for wind speeds above 20 $\mathrm{m\,s^{-1}}$ and a possible overestimation of sea-to-air fluxes at these very high wind speeds has been suggested (McNeil and D'Asaro, 2007). While this needs to be kept in mind when fluxes at higher wind speeds are considered, for the here discussed cruises wind speeds are always below 20 $\mathrm{m\,s^{-1}}$ and the Nightingale parameterization has been applied throughout. CH_3I emissions during the DRIVE campaign are also determined by the large supersaturation in combination with varying wind speeds, with the largest emissions of up to 1146 $\mathrm{pmol\,m^{-2}\,h^{-1}}$ observed on 7 June 2010. For SHIVA, relatively high oceanic concentrations and warm water temperatures lead to very high supersaturations of methyl iodide in the coastal western Pacific and trigger large CH_3I emissions due to elevated wind speeds. Local peak emissions

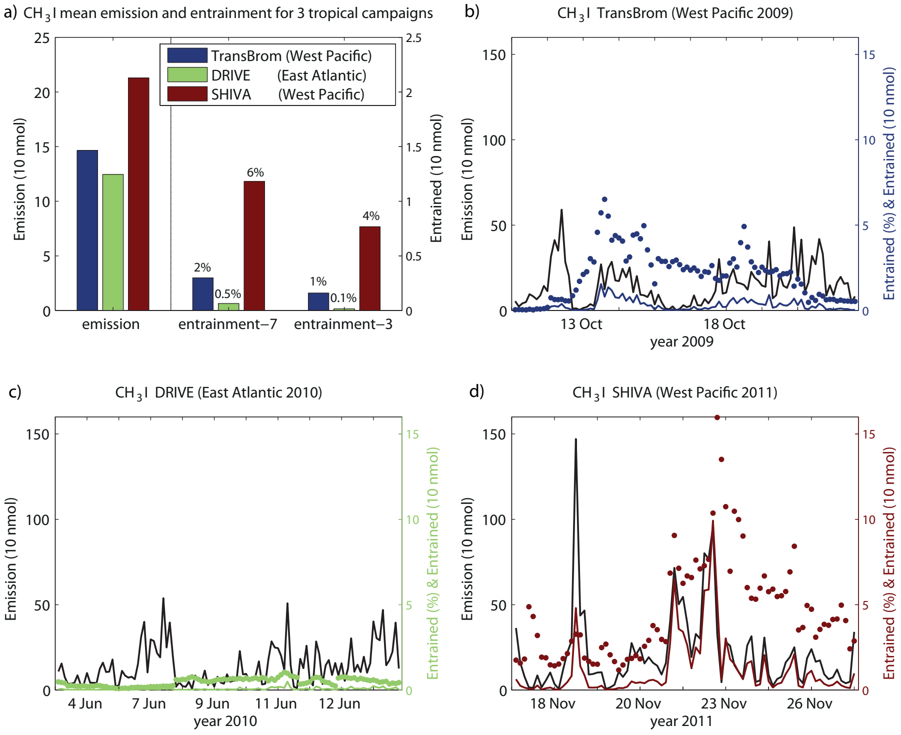

Fig. 3. Campaign-averaged CH_3I emissions and modeled entrainment above 17 km are shown for three tropical campaigns **(a)**. CH_3I emissions (black line) as well as the relative (colored dots) and total (colored line) amount of CH_3I entrained above 17 km are displayed as a function of time along the cruise track for TransBrom **(b)**, DRIVE **(c)**, and SHIVA **(d)**. Emissions are calculated from the observed flux for a time period of one hour and an area of 500 m^2 for each observation. CH_3I lifetime is prescribed with 7 days (entrainment-7 in panel **a** and all results in **b–d**) or with 2–3 days (entrainment-3 in **a**).

during SHIVA of up to 2980 $pmol\,m^{-2}\,h^{-1}$ (19 November 2011) exceed the maximum emissions observed during the other two campaigns and are among the largest local emissions observed so far (Ziska et al., 2013).

The amount of CH_3I that reaches the stratosphere has been estimated based on Lagrangian transport calculations with FLEXPART. CH_3I emissions in the FLEXPART runs are calculated from the observed flux for a time period of one hour and an area of 500 m^2 for each observation, presented in Fig. 3 as campaign averages (Fig. 3a) and as time series over the length of each individual campaign (Fig. 3b–d). The level above which no significant washout is expected is particularly important for stratospheric iodine chemistry, since all CH_3I which reaches this level before being photolyzed can be expected to contribute to the stratospheric I_y budget. While the exact altitude of the "no-washout level" is still under debate (Fueglistaler et al., 2009), we have chosen the cold point altitude as an upper estimate since no dehydration is expected to occur above. Based on evaluations of regular radiosonde measurements during the ship campaigns, the cold point is found at 17 km (Fuhlbrügge et al., 2013; Krüger and Quack, 2012). We quantify the contribution of CH_3I to stratospheric iodine based on the amount of CH_3I entrained above 17 km, which is calculated as the sum of CH_3I carried by all the computational particles across this altitude. Note that the altitude of the level above which no washout occurs is a source of uncertainty regarding our results of the CH_3I contribution to stratospheric iodine. If, for instance, heterogeneous recycling of iodine from aerosols back to the gas phase were to occur (Dix et al., 2013), the "no-washout level" would be lower than the cold point and, as a consequence, the CH_3I contribution to stratospheric iodine would be larger than estimated below. A simple sensitivity study reveals that approximately twice as much CH_3I is found to contribute to the stratospheric iodine if the "no-washout level" is set at 16 km instead of 17 km.

For all three campaigns the average amount of CH_3I being entrained above 17 km is shown in Fig. 3a. For the scenario of a uniform atmospheric lifetime of 7 days (WMO, 2011), about 0.5 % (DRIVE), 2 % (TransBrom) and 6 % (SHIVA) of the emitted CH_3I reaches the upper TTL and is projected to be entrained into the stratosphere. In order to investigate the sensitivity of our results to the prescribed atmospheric lifetime of CH_3I, we repeat the same calculation but using an altitude dependent CH_3I lifetime from the TOMCAT CTM. When the considerably shorter profile lifetime (2–3 days) is assumed, only 0.1 % (DRIVE), 1 % (TransBrom) and 4 % (SHIVA) of the emitted CH_3I are transported into the upper

TTL. The entrainment of CH_3I above 17 km based on the two different lifetimes reveals considerable differences, as one would expect, and illustrates the need for a better understanding of tropospheric CH_3I chemistry. While all the following results are based on assuming a CH_3I atmospheric lifetime of 7 days, the case study above provides an estimate of the sensitivity of our results (30–80 % less entrainment) to variations of the atmospheric lifetime (2.5–3 days instead of 7 days).

The efficiency of atmospheric CH_3I transport from the surface to the cold point (given by the percentage value of CH_3I reaching 17 km) during SHIVA (western Pacific) is 12 to 40 times larger than the efficiency of CH_3I transport during DRIVE (Atlantic). While these results are derived from model runs based on local campaign data, it is known from previous studies that the western Pacific is in general an important region for troposphere–stratosphere transport of short-lived compounds (e.g., Aschmann et al., 2009; Krüger et al., 2009; Levine et al., 2007) due to active deep convection (Fueglistaler et al., 2009 and references therein). For SHIVA, the large emissions together with the very efficient vertical transport lead to an overall large amount of CH_3I reaching the stratosphere. The absolute amounts of CH_3I being entrained above the cold point at 17 km are given in Fig. 3a for all campaigns, illustrating that 20 times more CH_3I is entrained for SHIVA compared to DRIVE and 4 times more when compared to TransBrom.

3.2 Possible connection between CH_3I emissions and atmospheric transport

Oceanic emissions and atmospheric transport vary from campaign to campaign but also considerably within each campaign. Dotted lines in Fig. 3b, c, and d give the transport efficiency along the cruise track and demonstrate its large variability from measurement side to measurement side. During DRIVE, the CH_3I troposphere–stratosphere transport is weak for the whole campaign and less than 1 % reaches the stratosphere (Fig. 3c). However, for the two western Pacific campaigns, the vertical transport is more efficient, lifting 1–16 % of emitted CH_3I from the surface to 17 km for SHIVA, and 0–6 % for TransBrom. While both ship campaigns took place in the western Pacific and encountered periods of strong convective activity, the amount of overshooting convection responsible for the transport of the short-lived CH_3I up to 17 km differs between the campaigns. An overall stronger vertical transport is predicted for the SHIVA campaign, which took place in the coastal regions of the maritime continent, an area well known for deep cumulus convection and heavy precipitation systems during boreal winter (Chang et al., 2005). For TransBrom, convection above the open ocean including tropical storm systems dominates the vertical transport from the surface to the cold point at 17 km. The total amount of CH_3I entrained above 17 km shows maximum values for cases when both variables, emission and transport efficiency, are large. For the SHIVA campaign, this coincidence is found for the event of the second largest emission on 22 November 2011, where the transport model estimates that around 10 % CH_3I could reach 17 km. For TransBrom, the largest total entrainment takes place on 14 October 2009 and is based on an average emission value during times of maximum efficiency of vertical transport.

In order to further analyze possible coincidences of strong emissions and efficient vertical transport, a correlation analysis has been applied to the two time series. For the entire time series covering the whole cruise length, no correlation exists for any of the three campaigns. However, when parts of the time series are analyzed, high correlations are found. For the TransBrom campaign, correlations between emissions and vertical atmospheric transport reach a maximum for two individual campaign sections (Fig. 4a). A very high correlation of 0.89 is found for the first section, comprising 16 data points collected over 2 days (red lines). A high correlation ($r = 0.69$) also exists for the subsequent cruise section extending from 13 October 2009 to 18 October 2009 based on 39 data points. All correlation coefficients are statistically significant at the 95 % confidence level based on the Student's t test. Scatter plots of the emissions versus vertical atmospheric transport show different relationships for the two periods, with linear fits resulting in slopes of 54 and 5, respectively.

Understanding the two different regimes occurring during TransBrom, which show correlations if analyzed separately, but lead to uncorrelated data sets when combined, requires some background information on the meteorological situation during the cruise (Krüger and Quack, 2012). The first cruise section extends north of the Intertropical Convergence Zone (ITCZ) from 32° N to 24° N, and model results suggest that vertical transport from the surface to 17 km is weak with less than 1 % of CH_3I being lifted by deep convection into the upper TTL. At the end of the first cruise section (12 October 2009, 27° N), the ship crossed the track of the tropical storm Nepartak and large horizontal wind speeds reaching values of 20.4 $\mathrm{m\,s^{-1}}$ were observed. Measurements were increased to an hourly frequency and peak emissions of oceanic CH_3I were reported during periods of maximum horizontal winds. Note that during the influence of Nepartak, the transport model shows strong convective activity, reaching only main convective outflow regions around 12 km and not the upper TTL, resulting in the weak transport efficiency discussed above. At the beginning of the second cruise section, the ship crossed the ITCZ and came close to the tropical storm Lupit (14 October 2009, 18° N), which developed into a super typhoon a couple of days later (Krüger and Quack, 2012). Similar to the situation during Nepartak, the strong horizontal wind speeds are accompanied by increased atmospheric trace gas concentrations and emissions. As opposed to the first cruise track section, atmospheric transport into the upper TTL is very efficient during the second cruise section, in accordance with its location within the ITCZ.

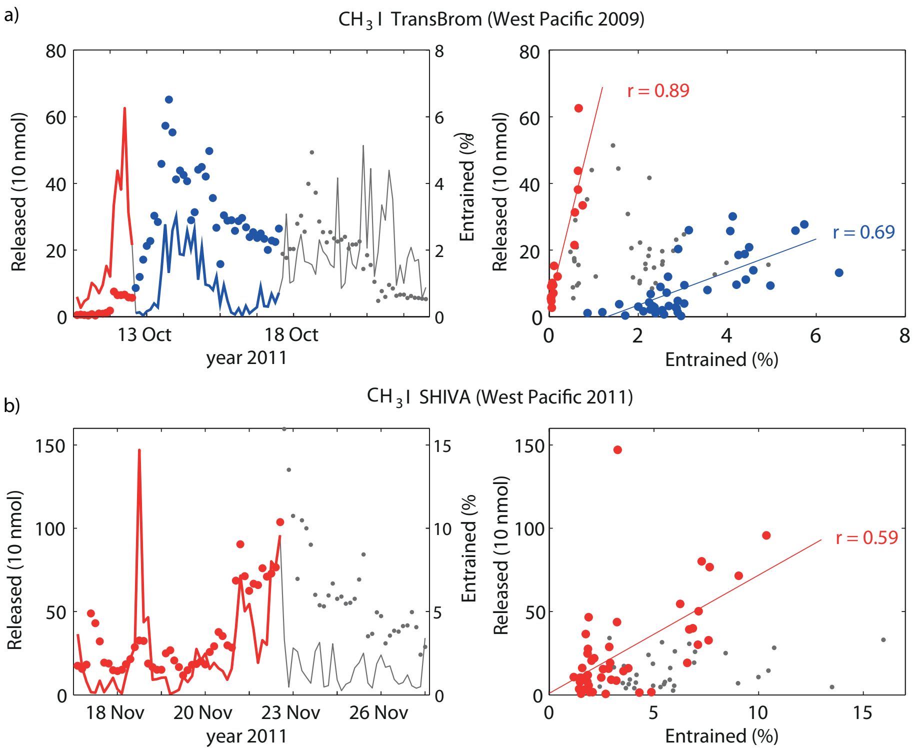

Fig. 4. The CH_3I observed emissions (line) and the modeled relative amount entrained above 17 km (dots) are shown for TransBrom **(a)** and SHIVA **(b)** as a function of time (left panels) and as a scatter plot (right panels). The subsets, for which correlations between the two functions have been identified, are color-coded in red and blue. The correlation coefficients (r) are given in the right panel.

Table 4. Correlation coefficients between CH_3I emission, horizontal wind speed and vertical transport efficiency (given by the relative amount of CH_3I entrained above 17 km). The coefficients are given for the entire TransBrom and SHIVA campaigns as well as for the subsets where correlations between the CH_3I emissions and vertical transport efficiency have been identified (TransBrom section 1 and 2, SHIVA section 1).

Correlation coefficients for various cruise sections	TransBrom section 1	TransBrom section 2	TransBrom entire	SHIVA section 1	SHIVA entire
CH_3I emission and horizontal wind speed	0.93	0.93	0.82	0.70	0.62
Horizontal wind speed and vertical transport	0.87	0.74	−0.29	0.73	0.49
CH_3I emission and vertical transport	0.89	0.69	−0.05	0.59	0.28

For the SHIVA campaign, the correlation between oceanic emissions and atmospheric transport reaches a maximum for the cruise section in the South China Sea from 17 November to 23 November 2011, comprising 47 data points. Figure 4b shows the two time series, oceanic emissions and troposphere–stratosphere transport efficiency, with the data during the respective cruise section displayed in red. The correlation ($r = 0.59$) results mostly from the fact that the large emissions on 21–22 November 2011 are accompanied by fast vertical transport. Note that for these two days high horizontal wind speeds of up to 13 $\mathrm{m\,s^{-1}}$ occurred, while the horizontal winds during the time period before were moderate, around 5 $\mathrm{m\,s^{-1}}$. After 23 November 2011, the horizontal winds and also the vertical transport continued to be large; however, due to lower oceanic concentrations and saturation anomalies the emissions are small compared with the first cruise section.

Based on two tropical campaigns in the western Pacific, three cruise sections have been identified that show a correlation between the amount of CH_3I emitted from the ocean and the fraction of emitted CH_3I transported from the surface to the cold point at 17 km. In general, CH_3I shows relatively uniform oceanic concentrations over the various cruise sections (Quack et al., 2013). Emission rates are mainly determined by the wind speed variations with high wind speeds resulting in a fast atmospheric outflow and an immediate replacement of the gas from the oceanic source. Such correlations between emissions and horizontal wind speeds have also been observed for other short-lived halogenated gases such as $CHBr_3$ and CH_2Br_2 in supersaturated coastal waters during tropical storm activities (Zhou et al., 2008). We find the strongest CH_3I emissions during tropical storms, which on the other hand can lead to intense vertical transport associated with developing tropical cyclones. It has been suggested that tropical cyclones could play an important role for troposphere–stratosphere exchange due to associated frequent convective overshooting (Rossow and Pearl, 2007) and due to contributing a disproportional large amount of the convection that penetrates the stratosphere (Romps and Kuang, 2009). The mechanism of strong horizontal winds triggering large emissions, on the one hand, and being associated with tropical convective systems, on the other hand, could provide a possible explanation of the identified correlations. Such a mechanism could also explain why data over longer time periods are uncorrelated if the meteorological or oceanic regime changes. Examples are the change in oceanic CH_3I concentration gradients during SHIVA on 23 November 2011 coinciding with the end of the correlation time period and the change of meteorological conditions during TransBrom on 14 October, across the ITCZ, coinciding with the switch between the two correlation regimes.

Correlation coefficients between all three quantities are presented in Table 4 for different sections of the two cruises. Evidently, in all cases there is a strong correlation between CH_3I emissions and the horizontal wind speed. When the horizontal surface wind is also strongly correlated with the efficiency of vertical transport, we find the above discussed correlation between CH_3I emissions and vertical transport. The fact that for these cases both quantities are highly correlated with the horizontal wind further strengthens the above suggested mechanism. For the entire TransBrom cruise, no correlation of the horizontal winds with the vertical transport can be found, probably due to the very different meteorological regimes. For the entire SHIVA campaign, the correlation between CH_3I emission and horizontal winds is somewhat weaker than for the other cases, probably because of a switch in the oceanic regime.

For the cruise sections where a correlation between emission and vertical transport could be identified, one also finds the overall largest amounts of CH_3I being transported into the stratosphere. For TransBrom, the maximum amount of 0.1 ppt CH_3I at 17 km (Fig. 5) is associated with emissions on 14 October 2009 and subsequent atmospheric transport influenced by the tropical storm Lupit. Atmospheric CH_3I abundance at 17 km averaged over the whole campaign amounts to 0.02 ppt. During SHIVA, very large peak emissions as well as very intense vertical transport result in model estimates of 0.6 ppt CH_3I at 17 km (Fig. 5), which is much larger than any values reported by high reaching aircraft measurements so far (Montzka and Reimann, 2011). The campaign average mixing ratio at 17 km is considerably lower, amounting to 0.07 ppt. During DRIVE, the maximum values at 17 km range around 0.03 ppt and mean values are in the order of 0.01 ppt (Fig. 5). Note that in the free troposphere, the CH_3I estimates are of similar order of magnitude as recent observations of inorganic iodine (Puentedura et al., 2012; Dix et al., 2013). In order to investigate whether the relatively large mixing ratios in the upper TTL estimated for the western Pacific emissions are isolated cases, strongly deviating from otherwise low CH_3I abundances, or if they occur frequently enough to impact global CH_3I, we analyze global model runs in the next section.

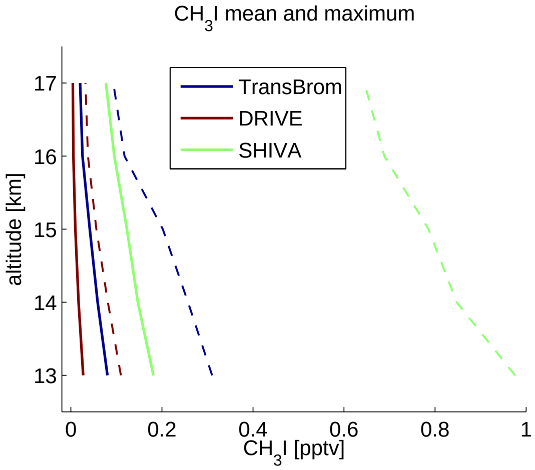

Fig. 5. Modeled CH_3I profiles based on observed emissions during the TransBrom, DRIVE and SHIVA ship campaigns. For all three campaigns mean values (solid lines) and maximum values (dashed lines) are given.

4 Global atmospheric CH_3I transport

4.1 Comparison with aircraft measurements in the lower TTL

The global contribution of CH_3I to the stratospheric iodine budget is estimated from FLEXPART model runs using a global emission climatology provided by Ziska et al. (2013) as input data. The emission maps have been derived from individual campaign measurements; however, as a result of the averaging process they do not represent the full spread of the original data. Furthermore, they do not include instantaneous peak emissions that might be correlated to the subsequent atmospheric transport, as illustrated above for individual campaigns. Figure 6 presents the 40° S–40° N section of

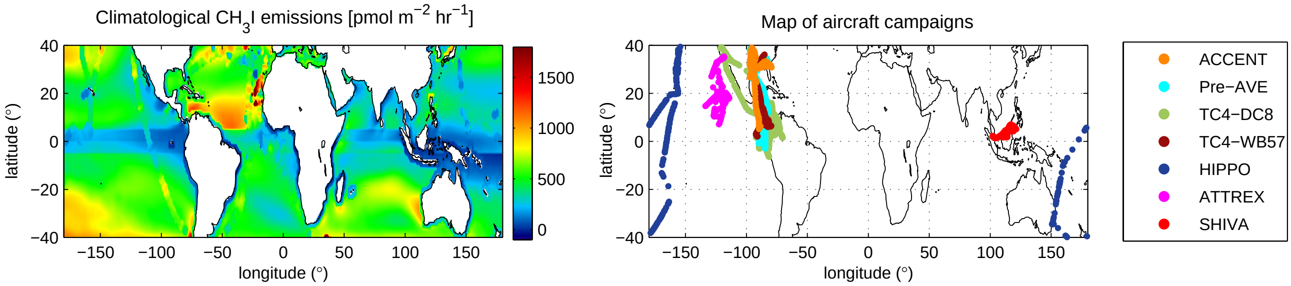

Fig. 6. Climatological CH_3I emissions [pmol m^{-2} h^{-1}] visualized between 40° S and 40° N on a 1° × 1° grid from Ziska et al. (2013) **(a)**. Locations of aircraft campaign measurements for the ACCENT, Pre-AVE, TC4, HIPPO2, ATTREX, and SHIVA missions **(b)**.

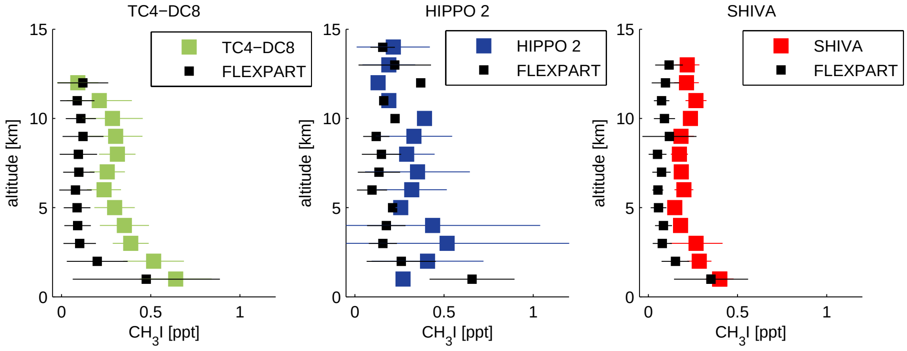

Fig. 7. Comparison between observed and modeled vertical profiles of CH_3I in the troposphere and lower TTL. Observations from all tropical flight sections of each aircraft campaign are used to find coincident model output. Observations and model results are averaged over all coincident data points in 1 km wide vertical intervals for TC4-DC8 (left panel), HIPPO2 (middle panel), and SHIVA (right panel). Horizontal bars indicate ±1 standard deviation.

the emission climatology. Due to supersaturated oceans the climatological emissions are nearly everywhere positive and only a very few grid points denote CH_3I sinks. Large oceanic sources are found in the subtropical gyre regions as well as in North Atlantic. The tropical western Pacific region shows particularly low CH_3I emissions. Recent observations in this region during the SHIVA ship campaign, which have not been included in the climatology compilation so far, suggest the climatology might underestimate western Pacific emissions.

We compare modeled CH_3I abundances to available aircraft measurements in the free troposphere and TTL region. A special focus is on the model-measurement comparison in the upper TTL and on the question whether the aircraft measurements available here are representative of existing global estimates. The comparison is based on model runs carried out for the time period of the respective campaign and uses global emission climatologies as input data. As a result we expect the modeled atmospheric transport to represent the atmospheric conditions during the campaign, even though the climatological emissions might deviate from the true local emissions present at the time. A geographic map of the flight tracks is shown in Fig. 6. In a first step, coincident data points for observations and model output are identified if they are less than 12 h apart and if their distance is less than 0.5° horizontally and less than 0.5 km vertically. Profile comparisons are determined for each campaign by taking the mean and standard deviation over all coincidences identified for the particular campaign data and for the corresponding model output.

The profile comparison for the three aircraft campaigns, which provide data in the free troposphere and lower UTLS, show in general a good agreement between the observations and the model results, with the latter being consistently lower (Fig. 7). For TC4-DC8, the modeled profile shows a steeper vertical gradient between 1 and 3 km than the observations, leading to some disagreement below 5 km. Above this level, model output and observations agree within their respective standard deviations. The HIPPO2 flight tracks extend over all tropical latitudes and campaign averaged profiles show a large variability below 10 km and around 13–14 km, which is also displayed although somewhat weaker by the model results. Mean values agree very well on some levels (e.g., above 10 km) but show larger discrepancies on other levels (e.g., 3–4 km). For SHIVA, the variability over all flight sections is small for observations and model results. In general, observed and modeled profiles show a very similar shape with FLEXPART results being slightly smaller consistently

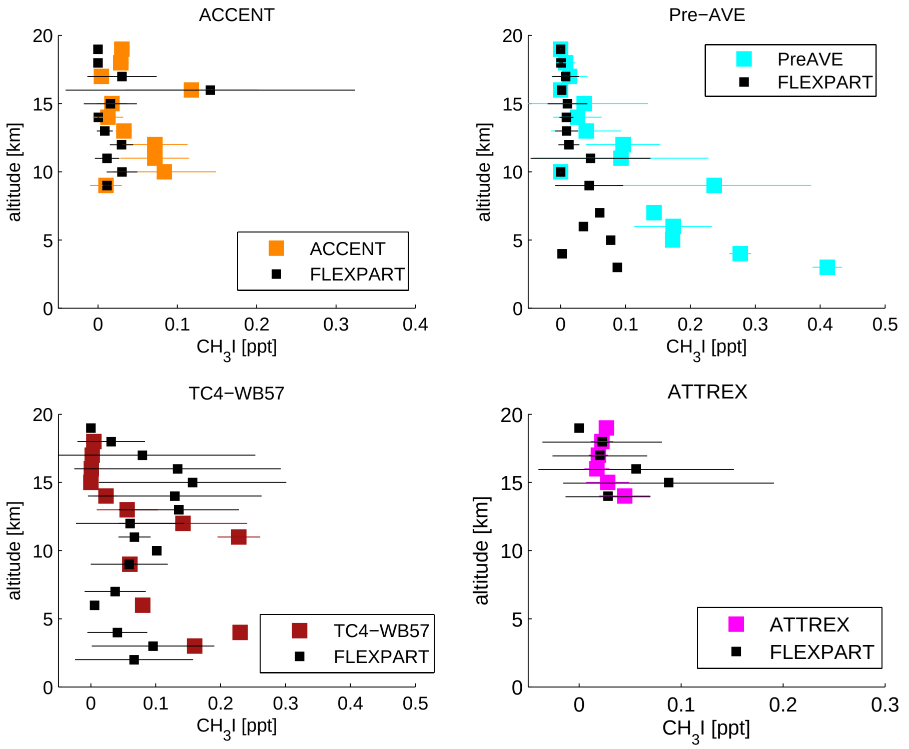

Fig. 8. Same as Fig. 7 for vertical profiles of CH_3I in the troposphere and TTL for the aircraft campaigns ACCENT, Pre-AVE, TC4-WB57, and ATTREX.

over the whole altitude range. The largest differences are found around 11 km. For some individual flights, convective outflow leads to observations of enhanced CH_3I between 10 and 12 km that result in a "C-shape" profile, a characteristic which is well captured by the model results (not shown here).

4.2 Comparison with aircraft measurements in the upper TTL

Model-measurement comparisons for the four campaigns conducted with the high-altitude aircraft sampling in the upper TTL and lower stratosphere are shown in Fig. 8. For three out of four campaigns, the modeled abundances above 10 km agree very well with the observations. For all three cases, the mixing ratios in the upper TTL are below 0.1 ppt, with the exception of the strongly enhanced mixing ratios at 16 km during ACCENT, which are reported by the observations and the model results. Largest discrepancies are found for the TC4-WB57 campaign, where basically no CH_3I was observed above 15 km while FLEXPART simulates mixing ratios around 0.1 ppt for the levels 13–17 km. Only below 10 and above 17 km does the model output agree well with the TC4-WB57 observations. A summary of the model-measurement comparison in the TTL is displayed in Fig. 9, where the modeled and observed profiles averaged over all four campaigns are displayed. FLEXPART overestimates the amount of CH_3I observed at 17–18 km (0.01 ppt) simulating a too strong CH_3I entrainment. However, the model results underestimate CH_3I at 19 km, which observations suggest to be around 0.02 ppt. Since CH_3I has no source in the atmosphere, one would expect to find lower values at higher altitudes. A horizontally moving aircraft, however, will probe different air masses at the different altitude levels, and a positive vertical gradient, as noted between 17 and 19 km, can occur. The overall comparison of the 17–19 km region gives a good agreement between observations (0.011–0.019 ppt) and model results (0.006–0.032 ppt).

4.3 Global CH_3I in the upper TTL

It is also of interest to estimate CH_3I abundances in regions where no in situ measurements in the upper TTL are available. The projected amount of CH_3I entrained into the stratosphere depends on various FLEXPART model parameters and their associated uncertainties such as in the convective parameterization and in the vertical transport driven by the vertical wind fields. The accurate representation of convection has been validated with tracer experiments and ^{222}Rn measurements (Forster et al., 2007). The application of transport timescales based on vertical heating rates instead of vertical wind fields in the TTL between 15 and 17 km results in only minor differences of VSLS entrainment (Tegtmeier et al., 2012). As discussed earlier, our results are also constrained by the prescribed CH_3I lifetime, which can

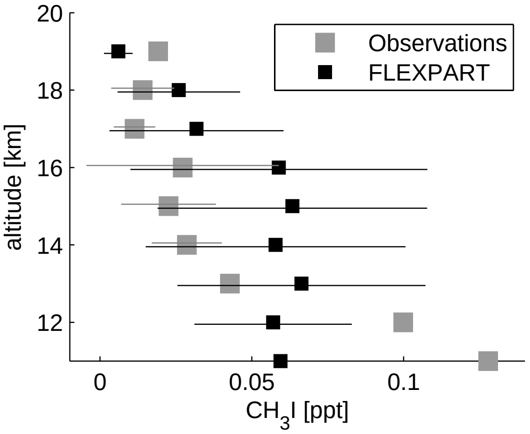

Fig. 9. Comparison between observed and modeled vertical profiles of CH_3I in the upper troposphere and TTL. Observations and model results are averaged over all data campaign-averaged profiles that include measurements in the upper TTL (ACCENT, Pre-AVE, TC4-WB57, and ATTREX). Horizontal bars indicate ±1 standard deviation.

cause variations of CH_3I entrainment into the stratosphere of around 50 %. However, the overall good agreement between model and observations in the eastern Pacific encourages the use of the FLEXPART model results for further analysis.

The western Pacific region is of particular interest for the troposphere–stratosphere transport, and we will evaluate how the FLEXPART results in this area compare to the model results and observations in the eastern Pacific. Such a comparison will allow speculations of how representative global estimates are of existing aircraft measurements. In Fig. 10a observations averaged over four tropical campaigns that crossed the eastern Pacific are displayed together with FLEXPART results averaged over three regions: the whole tropical belt (30° N–30° S), the tropical western Pacific, and the tropical eastern Pacific aircraft campaign area. While for the western Pacific and the tropical belt the 2009 annual mean is displayed, the eastern Pacific average is based on the months when aircraft measurements are available (see Table 3) in order to allow for a comparison of the modeled eastern Pacific mean values with the in situ observations. The observations and model results for the eastern Pacific agree quite well, as discussed above for the comparisons based on coincidences. While observations suggest 0.01 ppt CH_3I at 17 km, the modeled profile shows slightly larger values of 0.02 ppt. Overall, the comparison indicates that the available in situ measurements provide representative estimates of the mean CH_3I abundance in the eastern Pacific region. FLEXPART results for the western Pacific region show considerably larger mixing ratios, especially between 14 and 18 km with 0.08 ppt CH_3I at 17 km. The geographical distribution of the mixing ratios is displayed in Fig. 10b, indicating that the western Pacific region between 100° W and 150° E shows the largest CH_3I abundances. Our model does not take into account terrestrial CH_3I emissions and therefore the very-short lived CH_3I is projected to reach the cold point and enter the stratosphere mostly above the oceans.

The average entrainment of CH_3I into the stratosphere amounts to 0.04 ppt, as demonstrated by the tropical mean (30° S–30° N) CH_3I profile (Fig. 10a). In the annual mean distribution the entrainment is focused on the inner tropical latitude bands, mainly between 20° S and 20° N where the mean mixing ratio is about 0.05 ppt. Figure 11 provides information on the frequency occurrence of CH_3I mixing ratios at 17 km between 20° S and 20° N. As already evident from the geographical distribution of CH_3I abundances (Fig. 10), most values range between 0 and 0.1 ppt (82 %). However, a small amount of air is projected to carry larger amounts of CH_3I, with 5.5 % of air having mixing ratios larger than 0.2 ppt. Mixing ratios above 0.4 ppt occur only very rarely (0.6 %), while mixing ratios above 0.6 ppt occur only in less than 0.1 % of all air masses. The results from the global CH_3I model run show that the estimates from ship campaigns for TransBrom and SHIVA (0.02 and 0.07 ppt, respectively) are in the general range of values found in the western Pacific. Some in situ peak emissions observed during SHIVA combined with subsequent strong vertical transport lead to extremely high CH_3I abundances at 17 km ($\sim$ 0.6 ppt), which are expected to occur in less than 0.1 % of all events based on global model projections.

5 Summary and discussion

Our study follows a two-way approach for modeling upper air CH_3I abundances. One method uses highly localized CH_3I emissions estimated during three ship campaigns to study the detailed characteristics of CH_3I transport from the ocean surface through the TTL up to the cold point. The second approach uses global climatological emissions to estimate the global strength and geographical distribution of CH_3I entrainment into the tropical stratosphere. Model results are compared to measurements from high-altitude aircraft campaigns currently available in the eastern Pacific region.

The detailed analysis of CH_3I emissions and transport for three individual ship campaigns reveals that the emissions vary by about 50 % from campaign to campaign, but show much larger variations within one campaign. The large variability between measurements is supposedly related to the varying meteorological conditions, in particular to the variations of the horizontal winds. It is of interest to estimate to what degree one needs to know this variability in order to realistically simulate the CH_3I transport from the surface into the stratosphere. Especially if the CH_3I emissions and the intensity of vertical transport are correlated, coarse model simulations could potentially over- or underestimate atmospheric CH_3I abundances. While such correlations have not been observed over the entire length of one ship campaign,

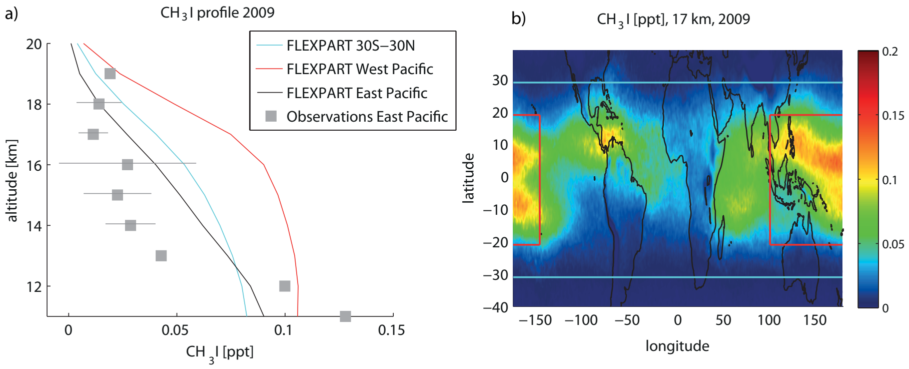

Fig. 10. Comparison between observed and modeled vertical profiles of CH_3I in the upper troposphere and TTL **(a)**. Observations are as in Fig. 7. Model output is averaged over the tropics (blue, 30° S–30° N) and the western Pacific (red, 100° W–150° E, 20° S–20° N) for 2009 and the eastern Pacific aircraft campaign region (green, 70–130° E, 6° S–30° N) for the months of available measurements. Modeled tropical distribution of CH_3I at 17 km for 2009 **(b)**.

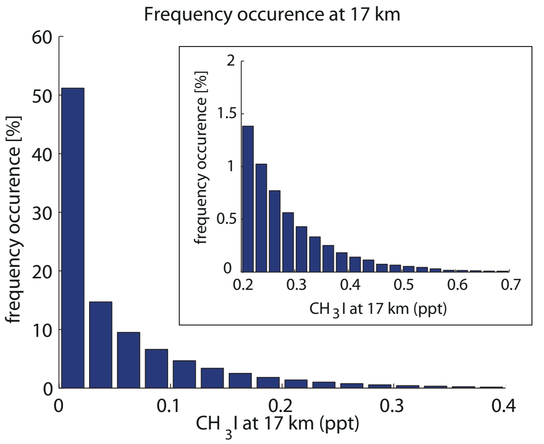

Fig. 11. Frequency occurrence of CH_3I abundances at 17 km in the tropics for 2009 based on climatological emissions. The inset panel provides a zoom-in for the range of larger mixing ratios 0.2–0.7 ppt.

individual sections with high correlations between emission and vertical transport have been identified. The analysis of the meteorological conditions during the campaigns leads to the hypothesis that the horizontal surface winds act as a connecting link between emission and transport. On the one hand, horizontal wind strength directly determines the emission strength by diluting CH_3I rich air and thereby controlling the uptake capacities of the atmosphere. Note that such mechanism works only for short-lived gases that are strongly supersaturated, as it is the case for CH_3I in most regions. Elevated oceanic concentrations and larger concentration gradients between sea water and air in source regions support this effect. On the other hand, horizontal wind variations depend on the meteorological conditions, such as convective systems or storm events. In particular, strong horizontal winds associated with tropical cyclones (i.e., typhoons) can indicate efficient vertical uplift possibly penetrating the stratosphere and thereby complete the line of argument connecting CH_3I emission strength and CH_3I troposphere–stratosphere transport. Note that for the DRIVE campaign with very little uplift of CH_3I into the upper TTL, emission and vertical transport are found to be uncorrelated. Determining the conditions that are required in order for the proposed mechanism to hold would require further analysis, ideally based on campaign data obtained during various meteorological situations.

The importance of the identified coincidences of strong emissions and efficient vertical transport for model simulations can be investigated with a simple test. For the campaign sections where a correlation between emission and transport was found, a considerable difference (of up to 70 %) would result when the transport simulations would have been initiated with one average emission instead of the highly variable emission time series. The opposite is true for campaign sections where emissions and vertical transport are uncorrelated. Here, model runs using one average emission lead to approximately the same amount of CH_3I at the cold point level as model runs using the spatially resolved emissions. If such correlations, as identified for parts of the tropical campaigns, were a more general phenomena, than global modeling studies should be based on highly resolved emissions scenarios instead of uniform background mixing ratios. However, CH_3I emission maps derived from observations can only be compiled in a climatological sense due to the low data density and cannot include information on the temporarily highly variable emission peaks. As a result, modeling studies based on climatological emission maps cannot fully take into account the simultaneous occurrence of large CH_3I emissions and strong vertical uplift and might therefore lead to an underestimation of stratospheric CH_3I. Model simulations could benefit from using the climatological surface concentration maps in order to calculate the emissions instantaneously. Parameterizations of CH_3I oceanic concentrations based on biogeochemical modeling (e.g., Stemmler et al., 2013) could help to further improve the modeling approach.

Our results indicate that a realistic simulation of current and future iodine loading in the troposphere and stratosphere requires, among many other factors, highly resolved and well constrained CH_3I emission scenarios. In particular, the simultaneous occurrence of large CH_3I emissions and strong vertical uplift during the developing tropical typhoon suggest that future changes in tropical cyclone activity (Murakami et al., 2011) might influence the contribution of CH_3I to stratospheric iodine in a changing climate.

Comparisons of aircraft measurements in the upper TTL with coincident model output give a good agreement with slightly larger CH_3I abundances in the model. In the eastern Pacific region, where aircraft campaigns are available, the observations and the model indicate that around 0.01 to 0.02 ppt of CH_3I enter the stratosphere. However, other tropical regions, which are subject to stronger convective activity, are suggested to have larger CH_3I entrainment, e.g., 0.08 ppt in the western Pacific. Note that our global climatological approach cannot account for any link between strong local emissions and vertical transport, which could lead to even larger entrainment, as discussed earlier. One example of such large entrainment is given by the peak emission and simultaneous strong vertical uplift during the SHIVA campaign, which results in a localized mixing ratio of 0.6 ppt, a magnitude larger than area-average mixing ratios. While our current understanding of the CH_3I contribution to stratospheric iodine is mostly based on above-mentioned measurements and on model results (Aschmann et al., 2009; Ordóñez et al., 2012), which range around 0.01 ppt, our model results suggest an overall tropical contribution of 0.04 ppt. This is in good agreement with a model study from Donner et al. (2007), who derived similar CH_3I mixing ratios at the cold point. Differences between existing model results can arise from different treatment of CH_3I emissions, convection and photochemistry in the models. Note that in addition to our insufficient knowledge of the direct CH_3I entrainment into the stratosphere, the atmospheric lifetime of inorganic iodine is a major uncertainty for the quantification of the stratospheric iodine budget. Our results show strong variations in the geographical distribution of CH_3I entrainment, suggesting that currently available upper air measurements are not representative of global estimates. Further aircraft campaigns for different emission regions and especially for different convective transport regimes will be necessary in order to better understand the CH_3I contribution to stratospheric iodine.

Acknowledgements. We thank the TransBrom, DRIVE and SHIVA team for collecting the samples and providing the oceanic VSLS measurements. The authors would also like to thank X. Zhu and L. Pope for their technical support in the analysis of the whole air samples, and R. Lueb, R. Hendershot, and S. Gabbard for support of the ATTREX and HIPPO airborne sample collections. We thank Ben Miller, Steve Montzka, and Fred Moore for contributing the CH_3I measurements from the HIPPO2 aircraft campaign. The authors are grateful to the ECMWF for making the reanalysis product ERA-Interim available. This study is carried out within the WGL project TransBrom and the EU project SHIVA (FP7-ENV-2007-1-226224) and contributes to the BMBF ROMIC grant THREAT 01LG1217A.

The service charges for this open access publication
have been covered by a Research Centre of the
Helmholtz Association.

Edited by: W. T. Sturges

References

Aschmann, J., Sinnhuber, B.-M., Atlas, E. L., and Schauffler, S. M.: Modeling the transport of very short-lived substances into the tropical upper troposphere and lower stratosphere, Atmos. Chem. Phys., 9, 9237–9247, doi:10.5194/acp-9-9237-2009, 2009.

Bange, H. W.: FS Poseidon cruise report P399 legs 2 and 3, IFM-GEOMAR report no. 48 Rep. 48, 74 pp., IFM-GEOMAR, Kiel, 2011.

Bell, N., Hsu, L., Jacob, D. J., Schultz, M. G., Blake, D. R., Butler, J. H., King, D. B., Lobert, J. M., and Maier-Reimer, E.: Methyl iodide: Atmospheric budget and use as a tracer of marine convection in global models, J. Geophys. Res., 107, 4340, doi:10.1029/2001JD001151, 2002.

Bösch, H., Camy-Peyret, C., Chipperfield, M. P., Fitzenberger, R., Harder, H., Platt, U., and Pfeilsticker, K.: Upper limits of stratospheric IO and OIO inferred from center-to-limb-darkening-corrected balloon-borne solar occultation visible spectra: Implications for total gaseous iodine and stratospheric ozone, J. Geophys. Res., 108, 4455, doi:10.1029/2002JD003078, D15, 2003.

Brasseur, G. and Solomon, S.: Aeronomy of the Middle Atmosphere, 2nd ed., Springer, New York, 2005.

Butler, J. H., King, D. B., Lobert, J. M., Montzka, S. A., Yvon-Lewis, S. A., Hall, B. D., Warwick, N. J., Mondeel, D. J., Aydin, M., and Elkins, J. W.: Oceanic distributions and emissions of short-lived halocarbons, Global Biogeochem. Cy., 21, GB1023, doi:10.1029/2006GB002732, 2007.

Butz, A., Bösch, H., Camy-Peyret, C., Chipperfield, M. P., Dorf, M., Kreycy, S., Kritten, L., Prados-Román, C., Schwärzle, J., and Pfeilsticker, K.: Constraints on inorganic gaseous iodine in the tropical upper troposphere and stratosphere inferred from balloon-borne solar occultation observations, Atmos. Chem. Phys., 9, 7229–7242, doi:10.5194/acp-9-7229-2009, 2009.

Campos, M. L. A. M., Nightingale, P. D., and Jickells, T. D.: A comparison of methyl iodide emissions from seawater and wet depositional fluxes of iodine over the southern North Sea, Tellus B, 48, 106–114, doi:10.1034/j.1600-0889.1996.00010.x, 1996.

Carpenter, L. J., Archer S. D., and Beale, R.: Ocean-atmosphere trace gas exchange, Chem. Soc. Rev., 41, 6473–6506, 2012.

Carpenter, L. J., MacDonald, S. M., Shaw, M. D., Kumar, R., Saunders, R. W., Parthipan, R., Wilson, J., and Plane, J. M. C.: Atmospheric iodine levels influenced by sea surface emissions of inorganic iodine, Nature Geosci., 6, 108–111, doi:10.1038/ngeo1687, 2013.

Chameides, W. L. and Davis, D. D.: Iodine: Its possible role in tropospheric photochemistry, J. Geophys. Res., 85, 7383, doi:10.1029/JC085iC12p07383, 1980.

Chang, C.-P., Harr, P. A., and Chen, H.-J.: Synoptic Disturbances over the Equatorial South China Sea and Western Maritime Continent during Boreal Winter, Mon. Weather Rev., 133, 489–503, doi:10.1175/MWR-2868.1, 2005.

Chipperfield, M. P.: New version of the TOMCAT/SLIMCAT offline chemical transport model: Intercomparison of stratospheric tracer experiments, Q. J. Roy. Meteorol. Soc., 132, 1179–1203, doi:10.1256/qj.05.51, 2006.

Chuck, A. L., Turner, S. M., and Liss, P. S.: Oceanic distributions and air-sea fluxes of biogenic halocarbons in the open ocean, J. Geophys. Res., 110, C10022, doi:10.1029/2004JC002741, 2005.

Davis, D., Crawford, J., Liu, S., McKeen, S., Bandy, A., Thornton, D., Rowland, F., and Blake, D.: Potential impact of iodine on tropospheric levels of ozone and other critical oxidants, J. Geophys. Res., 101, 2135, doi:10.1029/95JD02727, 1996.

De Bruyn, W. J. and Saltzman, E. S.: Diffusivity of methyl bromide in water, Mar. Chem., 57, 55–59, 1997.

Dee, D. P., Uppala, S. M., Simmons, A. J., Berrisford, P., Poli, P., Kobayashi, S., Andrae, U., Balmaseda, M. A., Balsamo, G., Bauer, P., Bechtold, P., Beljaars, A. C. M., van de Berg, L., Bidlot, J., Bormann, N., Delsol, C., Dragani, R., Fuentes, M., Geer, A. J., Haimberger, L., Healy, S. B., Hersbach, H., Hólm, E. V., Isaksen, L., Kållberg, P., Köhler, M., Matricardi, M., McNally, A. P., Monge-Sanz, B. M., Morcrette, J.-J., Park, B.-K., Peubey, C., de Rosnay, P., Tavolato, C., Thépaut, J.-N. and Vitart, F., The ERA-Interim reanalysis: configuration and performance of the data assimilation system, Q. J. Roy. Meteorol. Soc., 137, 553–597, 2011.

Dix, B., Baidar, S., Bresch, J. F., Hall, S. R., Schmidt, K. S., Wang, S., and Volkamer, R.: Detection of iodine monoxide in the tropical free troposphere, P. Natl. Acad. Sci. USA, 110, 2035–2040, doi:10.1073/pnas.1212386110, 2013.

Donner, L. J., Horowitz, L. W., Fiore, A. M., Seman, C. J., Blake, D. R., and Blake, N. J.: Transport of radon-222 and methyl iodide by deep convection in the GFDL Global Atmospheric Model AM2, J. Geophys. Res., 112, D17303, doi:10.1029/2006JD007548, 2007.

Forster, C., Wandinger, U., Wotawa, G., James, P., Mattis, I., Althausen, D., Simmonds, P., O'Doherty, S., Jennings, S. G., Kleefeld, C., Schneider, J., Trickl, T., Kreipl, S., Jäger, H., and Stohl, A.: Transport of boreal forest fire emissions from Canada to Europe, J. Geophys. Res., 106, 22887, doi:10.1029/2001JD900115, 2001.

Forster, C., Stohl, A., and Seibert, P.: Parameterization of Convective Transport in a Lagrangian Particle Dispersion Model and Its Evaluation, J. Appl. Meteorol. Climatol., 46, 403–422, doi:10.1175/JAM2470.1, 2007.

Fueglistaler, S., Dessler, A. E., Dunkerton, T. J., Folkins, I., Fu, Q., and Mote, P. W.: Tropical tropopause layer, Rev. Geophys., 47, RG1004, doi:10.1029/2008RG000267, 2009.

Fuhlbrügge, S., Krüger, K., Quack, B., Atlas, E., Hepach, H., and Ziska, F.: Impact of the marine atmospheric boundary layer conditions on VSLS abundances in the eastern tropical and subtropical North Atlantic Ocean, Atmos. Chem. Phys., 13, 6345–6357, doi:10.5194/acp-13-6345-2013, 2013.

Gettelman, A., Lauritzen, P. H., Park, M., and Kay, J. E.: Processes regulating short-lived species in the tropical tropopause layer, J. Geophys. Res., 114, D1330, doi:10.1029/2009JD011785, 2009.

Happell, J. D. and Wallace, D. W. R.: Methyl iodide in the Greenland/Norwegian Seas and the tropical Atlantic Ocean: Evidence for photochemical production, Geophys. Res. Lett., 23, 2105–2108, doi:10.1029/96GL01764, 1996.

Hossaini, R., Chipperfield, M. P., Feng, W., Breider, T. J., Atlas, E., Montzka, S. A., Miller, B. R., Moore, F., and Elkins, J.: The contribution of natural and anthropogenic very short-lived species to stratospheric bromine, Atmos. Chem. Phys., 12, 371–380, doi:10.5194/acp-12-371-2012, 2012.

Hughes, C., Franklin, D. J., and Malin, G.: Iodomethane production by two important marine cyanobacteria: Prochlorococcus marinus (CCMP 2389) and Synechococcus sp. (CCMP 2370), Marine Chem., 125, 19–25, doi:10.1016/j.marchem.2011.01.007, 2011.

Jones, C. E., Hornsby, K. E., Sommariva, R., Dunk, R. M., von Glasow, R., McFiggans, G., and Carpenter, L. J.: Quantifying the contribution of marine organic gases to atmospheric iodine, Geophys. Res. Lett., 37, L18804, doi:10.1029/2010GL043990, 2010.

Krüger, K. and Quack, B.: Introduction to special issue: the TransBrom Sonne expedition in the tropical West Pacific, Atmos. Chem. Phys., 13, 9439–9446, doi:10.5194/acp-13-9439-2013, 2013.

Krüger, K., Tegtmeier, S., and Rex, M.: Variability of residence time in the Tropical Tropopause Layer during Northern Hemisphere winter, Atmos. Chem. Phys., 9, 6717–6725, doi:10.5194/acp-9-6717-2009, 2009.

Levine, J. G., Braesicke, P., Harris, N. R. P., Savage, N. H., and Pyle, J. A.: Pathways and timescales for troposphere-to-stratosphere transport via the tropical tropopause layer and their relevance for very short lived substances, J. Geophys. Res., 112, D04308, doi:10.1029/2005JD006940, 2007.

Liss, P. S. and Slater, P. G.: Flux of Gases across the Air-Sea Interface, Nature, 247, 181–184, doi:10.1038/247181a0, 1974.

Mahajan, A. S., Plane, J. M. C., Oetjen, H., Mendes, L., Saunders, R. W., Saiz-Lopez, A., Jones, C. E., Carpenter, L. J., and McFiggans, G. B.: Measurement and modelling of tropospheric reactive halogen species over the tropical Atlantic Ocean, Atmos. Chem. Phys., 10, 4611–4624, doi:10.5194/acp-10-4611-2010, 2010.

Manley, S. L. and Dastoor, M. N.: Methyl halide production from the giant kelp, Macrocystis and estimates of global CH3X production by kelp, Limnol. Oceanogr., 32, 709–715, 1987.

Manley, S. L. and Dastoor, M. N.: Methyl iodide (CH3I) production by kelp and associated microbes, Marine Biol., 98, 477–482, doi:10.1007/BF00391538, 1988.

Manley, S. L. and De la Cuesta, J. L.: Methyl iodide production from marine phytoplankton cultures, Limnol. Oceanogr., 41, 142–147, 1997.

McFiggans, G., Plane, J. M. C., Allan, B. J., Carpenter, L. J., Coe, H., and O'Dowd, C.: A modeling study of iodine chemistry in the marine boundary layer, J. Geophys. Res., 105, 14371, doi:10.1029/1999JD901187, 2000.

McNeil, C. L. and D'Asaro, E. A.: Parameterization of air-sea gas fluxes at extreme wind speeds, J. Mar. Syst., 66, 110–121, 2007.

Montzka, S. A. and Reimann, S.: Ozone-depleting substances and related chemicals, in Scientific Assessment of Ozone Depletion: 2010, Global Ozone Research and Monitoring Project – Report No. 52, Geneva, Switzerland, 2011.

Moore, R. M. and Groszko, W.: Methyl iodide distribution in the ocean and fluxes to the atmosphere, J. Geophys. Res., 104, 11163, doi:10.1029/1998JC900073, 1999.

Moore, R. M. and Zafiriou, O. C.: Photochemical production of methyl iodide in seawater, J. Geophys. Res., 99, 16415, doi:10.1029/94JD00786, 1994.

Moore, R. M., Geen, C. E., and Tait, V. K.: Determination of Henry's Law constants for a suite of naturally occurring halogenated methanes in seawater, Chemosphere, 30, 1183–1191, doi:10.1016/0045-6535(95)00009-W, 1995.

Murakami, H., Wang, B., and Kitoh, A.: Future Change of Western North Pacific Typhoons: Projections by a 20-km-Mesh Global Atmospheric Model*, J. Climate, 24, 1154–1169, doi:10.1175/2010JCLI3723.1, 2011.

Nightingale, P. D., Malin, G., Law, C. S., Watson, A. J., Liss, P. S., Liddicoat, M. I., Boutin, J., and Upstill-Goddard, R. C.: In situ evaluation of air-sea gas exchange parameterizations using novel conservative and volatile tracers, Global Biogeochem. Cy., 14(1), 373–387, doi:10.1029/1999GB900091, 2000.

Ordóñez, C., Lamarque, J.-F., Tilmes, S., Kinnison, D. E., Atlas, E. L., Blake, D. R., Sousa Santos, G., Brasseur, G., and Saiz-Lopez, A.: Bromine and iodine chemistry in a global chemistry-climate model: description and evaluation of very short-lived oceanic sources, Atmos. Chem. Phys., 12, 1423–1447, doi:10.5194/acp-12-1423-2012, 2012.

O'Dowd, C. D., Jimenez, J. L., Bahreini, R., Flagan, R. C., Seinfeld, J. H., Hämeri, K., Pirjola, L., Kulmala, M., Jennings, S. G., and Hoffmann, T.: Marine aerosol formation from biogenic iodine emissions, Nature, 417, 632–636, 2002.

Puentedura, O., Gil, M., Saiz-Lopez, A., Hay, T., Navarro-Comas, M., Gómez-Pelaez, A., Cuevas, E., Iglesias, J., and Gomez, L.: Iodine monoxide in the north subtropical free troposphere, Atmos. Chem. Phys., 12, 4909–4921, doi:10.5194/acp-12-4909-2012, 2012.

Pundt, I., Pommereau, J. P., Phillips, C., and Lateltin, E.: Upper limits of iodine oxide in the lower stratosphere, J. Atmos. Chem., 30, 173–185, 1998.

Quack, B. und Krüger, K. (Eds.): RV SONNE Fahrtbericht/Cruise Report SO218 SHIVA 15.–29.11.2011 Singapore – Manila, Philippines Stratospheric Ozone: Halogens in a Varying Atmosphere Part 1: SO218 – SHIVA Summary Report (in German) Part 2: SO218 – SHIVA English reports of participating groups GEOMAR Report, N. Ser. 012, GEOMAR Helmholtz-Zentrum für Ozeanforschung, Kiel, Germany, 112 pp., doi:10.3289/GEOMAR_REP_NS_12_2013 (http://oceanrep.geomar.de/22284/), 2013.

Quack, B., Atlas, E., Petrick, G., Stroud, V., Schauffler, S., and Wallace, D. W. R.: Oceanic bromoform sources for the tropical atmosphere, Geophys. Res. Lett., 31, L23S05, doi:10.1029/2004GL020597, 2004.

Quack, B., Atlas, E., Krüger, K., Taylor, B., Dinter, T., Bracher, A., Petrick, G., Stange, K., Fuhlbrügge, S., Tegtmeier, S., Wache, S., and Wallace, D.: Distribution and air-sea fluxes of halocarbons through the Western Pacific, Atmos. Chem. Phys. Discuss., in preparation, 2013.

Rasmussen, R. A., Khalil, M. A. K., Gunawardena, R., and Hoyt, S. D.: Atmospheric methyl iodide (CH_3 I), J. Geophys. Res., 87, 3086, doi:10.1029/JC087iC04p03086, 1982.

Redeker, K. R., Wang, N.-Y., Low, J. C., McMillan, A., Tyler, S. C., and Cicerone, R. J.: Emissions of Methyl Halides and Methane from Rice Paddies, Science, 290, 966–969, doi:10.1126/science.290.5493.966, 2000.

Richter, U. and Wallace, D. W. R.: Production of methyl iodide in the tropical Atlantic Ocean, Geophys. Res. Lett., 31, L23S03, doi:10.1029/2004GL020779, 2004.

Romps, D. M. and Kuang, Z.: Overshooting convection in tropical cyclones, Geophys. Res. Lett., 36, L09804, doi:10.1029/2009GL037396, 2009.

Rossow, W. B. and Pearl, C.: 22-Year survey of tropical convection penetrating into the lower stratosphere, Geophys. Res. Lett., 34, L04803, doi:10.1029/2006GL028635, 2007.

Saiz-Lopez, A., Plane, J. M. C., Baker, A. R., Carpenter, L. J., Von Glasow, R., Martín, J. C. G., McFiggans, G. and Saunders, R. W.: Atmospheric chemistry of iodine, Chem. Rev., 112, 1773–804, doi:10.1021/cr200029u, 2012.

Sander, S., Friedl, R., Barker, J., Golden, D., Kurylo, M., Wine, P., Abbatt, J., Burkholder, J., Kolb, C., Moortgat, G., Huie, R., V. L. Orkin, "Chemical Kinetics and Photochemical Data for Use in Atmospheric Studies, Evaluation No. 17", JPL Publication 10-6, Jet Propulsion Laboratory, Pasadena, 2011.

Singh, H. B., Salas, L. J., and Stiles, R. E.: Methyl halides in and over the eastern Pacific (40° N–32° S), J. Geophys. Res., 88, 3684, doi:10.1029/JC088iC06p03684, 1983.

Sive, B. C., Varner, R. K., Mao, H., Blake, D. R., Wingenter, O. W., and Talbot, R.: A large terrestrial source of methyl iodide, Geophys. Res. Lett., 34, L17808, doi:10.1029/2007GL030528, 2007.

Smythe-Wright, D., Boswell, S. M., Breithaupt, P., Davidson, R. D., Dimmer, C. H., and Eiras Diaz, L. B.: Methyl iodide production in the ocean: Implications for climate change, Global Biogeochem. Cy., 20, GB3003, doi:10.1029/2005GB002642, 2006.

Solomon, S., Garcia, R. R., and Ravishankara, A. R.: On the role of iodine in ozone depletion, J. Geophys. Res., 99, 20491, doi:10.1029/94JD02028, 1994.

Spichtinger, N., Wenig, M., James, P., Wagner, T., Platt, U., and Stohl, A.: Satellite detection of a continental-scale plume of nitrogen oxides from boreal forest fires, Geophys. Res. Lett., 28, 4579–4582, doi:10.1029/2001GL013484, 2001.

Stemmler, I., Rothe, M., Hense, I., and Hepach, H.: Numerical modelling of methyl iodide in the eastern tropical Atlantic, Biogeosciences, 10, 4211–4225, doi:10.5194/bg-10-4211-2013, 2013.

Stohl, A. and Thomson, D. J.: A density correction for Lagrangian particle dispersion models, Boundary-Lay. Meteorol., 90, 155–167, doi:10.1023/A:1001741110696, 1999.

Stohl, A. and Trickl, T.: A textbook example of long-range transport: Simultaneous observation of ozone maxima of stratospheric and North American origin in the free troposphere over Europe, J. Geophys. Res., 104, 30445, doi:10.1029/1999JD900803, 1999.

Stohl, A., Hittenberger, M., and Wotawa, G.: Validation of the lagrangian particle dispersion model FLEXPART against large-scale tracer experiment data, Atmos. Environ., 32, 4245–4264, doi:10.1016/S1352-2310(98)00184-8, 1998.

Stohl, A., Forster, C., Frank, A., Seibert, P., and Wotawa, G.: Technical note: The Lagrangian particle dispersion model FLEXPART version 6.2, Atmos. Chem. Phys., 5, 2461–2474, doi:10.5194/acp-5-2461-2005, 2005.

Tegtmeier, S., Krüger, K., Quack, B., Atlas, E. L., Pisso, I., Stohl, A., and Yang, X.: Emission and transport of bromocarbons: from the West Pacific ocean into the stratosphere, Atmos. Chem. Phys., 12, 10633–10648, doi:10.5194/acp-12-10633-2012, 2012.

Toon, O. B., Starr, D. O., Jensen, E. J., Newman, P. A., Platnick, S., Schoeberl, M. R., Wennberg, P. O., Wofsy, S. C., Kurylo, M. J., Maring, H., Jucks, K. W., Craig, M. S., Vasques, M. F., Pfister, L., Rosenlof, K. H., Selkirk, H. B., Colarco, P. R., Kawa, S. R., Mace, G. G., Minnis, P., and Pickering, K. E.: Planning, implementation, and first results of the Tropical Composition, Cloud and Climate Coupling Experiment (TC4), J. Geophys. Res., 115, D00J04, doi:10.1029/2009JD013073, 2010.

Vogt, R., Sander, R., Von Glasow, R., and Crutzen, P. J.: Iodine Chemistry and its Role in Halogen Activation and Ozone Loss in the Marine Boundary Layer?: A Model Study, J. Atmos. Chem., 32, 375–395, 1999.

Wanninkhof, R.: Relationship between wind speed and gas exchange over the ocean, J. Geophys. Res., 97, 7373–7382, 1992.

Wennberg, P. O., Brault, J. W., Hanisco, T. F., Salawitch, R. J., and Mount, G. H.: The atmospheric column abundance of IO: Implications for stratospheric ozone, J. Geophys. Res., 102, 8887–8898, doi:10.1029/96JD03712, 1997.

Wilke, C. R. and Chang, P.: Correlation of diffusion coefficients in dilute solutions, AIChE (Am. Inst. Chem. Eng.) J., 1, 264–270, 1955.

WMO (World Meteorological Organization): Scientific Assessment of Ozone Depletion: 2006, Global Ozone Research and Monitoring Project – Report No. 50, Geneva., 2007.

Wofsy, S. C., HIPPO Sci Team, Cooperating Modellers Team and Satellite Team: HIAPER Pole-to-Pole Observations (HIPPO): fine-grained, global-scale measurements of climatically important atmospheric gases and aerosols., Philosophical Transactions Series A, Mathematical, physical, and engineering sciences, 369, 2073–2086, doi:10.1098/rsta.2010.0313, 2011.

Yokouchi, Y., Osada, K., Wada, M., Hasebe, F., Agama, M., Murakami, R., Mukai, H., Nojiri, Y., Inuzuka, Y., Toom-Sauntry, D., and Fraser, P.: Global distribution and seasonal concentration change of methyl iodide in the atmosphere, J. Geophys. Res., 113, D18311, doi:10.1029/2008JD009861, 2008.

Zhou, Y., Mao, H., Russo, R. S., Blake, D. R., Wingenter, O. W., Haase, K. B., Ambrose, J., Varner, R. K., Talbot, R., and Sive, B. C.: Bromoform and dibromomethane measurements in the seacoast region of New Hampshire, 2002–2004, J. Geophys. Res., 113, D08305, doi:10.1029/2007JD009103, 2008.

Ziska, F., Quack, B., Abrahamsson, K., Archer, S. D., Atlas, E., Bell, T., Butler, J. H., Carpenter, L. J., Jones, C. E., Harris, N. R. P., Hepach, H., Heumann, K. G., Hughes, C., Kuss, J., Krüger, K., Liss, P., Moore, R. M., Orlikowska, A., Raimund, S., Reeves, C. E., Reifenhäuser, W., Robinson, A. D., Schall, C., Tanhua, T., Tegtmeier, S., Turner, S., Wang, L., Wallace, D., Williams, J., Yamamoto, H., Yvon-Lewis, S., and Yokouchi, Y.: Global sea-to-air flux climatology for bromoform, dibromomethane and methyl iodide, Atmos. Chem. Phys., 13, 8915–8934, doi:10.5194/acp-13-8915-2013, 2013.

CONCLUSIONS AND OUTLOOK

V. Conclusions and outlook

The objectives of this thesis were to reduce uncertainties on factors influencing marine halocarbon emissions (Figure III-17), and they were summarized in eight research questions in section III.5. Substantial progress in elucidating these factors has been made, but at the same time, new research questions arise from the results presented here. The eight research questions were addressed in six manuscripts that focused on two upwelling systems in the tropical Atlantic, including a dataset from the equatorial Atlantic with the first direct measurements of oceanic $CHBr_3$, CH_2Br_2, CH_3I and CH_2I_2 from the ACT region. The Cape Verde region and the Mauritanian upwelling had been subject of previous studies, but the extensive dataset collected during the DRIVE campaign in the same region allowed for testing new hypotheses and drawing new conclusions. In the following, the eight research questions will be discussed.

1. Is the equatorial Atlantic a source for atmospheric halocarbons and how are they produced?

The equatorial Atlantic has been found to be a similar important source region for $CHBr_3$, CH_2Br_2 and CH_3I as other upwelling systems. Correlation analysis indicated a relationship of $CHBr_3$ and CH_2Br_2 to phytoplankton species, especially to the dominating *chrysophytes*, associated with water masses of the EUC. In contrast to the hypothesis that the distribution of CH_3I is mainly a result of photochemical formation, indicators, such as correlations with biological proxies, for biogenic formation were found. This source might be equally important as photochemical formation in the tropical ocean. Additionally, CH_2I_2 could be detected in the surface water although it had been hypothesized that it cannot reach the surface. However, photolytical destruction as the main sink process leads to low surface concentrations and consequently very low emissions.

2. How does halocarbon production below the mixed layer influence these emissions?

There is some uncertainty as to where halocarbon production takes place in the water column. Depth profiles measured during MSM18/3 showed maxima both within the mixed layer and below. Diapycnal fluxes of $CHBr_3$, CH_2Br_2, CH_3I and CH_2I_2 calculated here for the first time acted both as source and sink for mixed layer halocarbons. They were very low in comparison to the other sinks, leading to the conclusion that halocarbon production in the mixed layer compensates for sink processes such as sea-to-air flux. Mixing events could transport halocarbons produced below into the mixed layer in larger concentrations. The profiles observed during MSM18/3 indicate additional processes for CH_2Br_2 in comparison to $CHBr_3$ in deeper waters. These processes could be an additional source, the biologically mediated conversion from $CHBr_3$ possibly connected to heterotrophic processes, or a slower degradation of CH_2Br_2 in deeper layers.

3. **What influences emissions of $CHBr_3$, CH_2Br_2 and CH_3I from a tropical upwelling region on a diel and a regional scale?**

This question can now be answered for the Cape Verde and the Mauritanian upwelling region. $CHBr_3$ and CH_2Br_2 showed a distinct regional distribution during the DRIVE campaign strongly indicating biology as main driving factor for their concentrations: low $CHBr_3$ and CH_2Br_2 were found in the open ocean, while elevated concentrations that compare well to previous measurements were observed in the upwelling. The main driving factor for their emissions on a regional scale was their biologic production. Wind speed gained impact especially on CH_2Br_2 emissions with decreasing distance to the coast. In contrast to the equatorial Atlantic, CH_3I was ubiquitously distributed in the investigation area, suggesting photochemical formation as main driver for its oceanic concentrations. No main driver for its emissions was identified on a regional scale, but diel variations were strongly influenced by variability in oceanic concentrations. Additionally, the height of the marine atmospheric boundary layer (MABL) was identified as indirect impact factor for the oceanic emissions for the first time.

4. **Do coastal sources of $CHBr_3$ and CH_2Br_2 influence atmospheric abundances of these compounds in the Mauritanian upwelling?**

Atmospheric abundances of $CHBr_3$ and CH_2Br_2 above the Mauritanian upwelling were similarly elevated as during previous campaigns, however, trajectory analysis indicated only a small coastal influence. Significantly negative correlations of atmospheric $CHBr_3$, CH_2Br_2 and CH_3I with the height of the MABL were found: the largest atmospheric $CHBr_3$, CH_2Br_2 and CH_3I mixing ratios occurred simultaneously with the lower MABL height at a coastal station in the upwelling. At this same station, sea-to-air fluxes of these compounds, especially of $CHBr_3$ and CH_2Br_2, were at their maximum. A 1D box model simulation proved that the largely elevated atmospheric abundances of the three halocarbons could be solely explained by oceanic sources, contradicting the previously established hypothesis of additional coastal sources. For the first time, very good correlations between oceanic and atmospheric $CHBr_3$ and CH_2Br_2 were observed. Surprisingly, they could be explained very well within the known concepts of sea-to-air fluxes as described in section III.2., wind speed, and the MABL height.

5. **What are the meteorological constraints on atmospheric abundances and emissions of $CHBr_3$, CH_2Br_2 and CH_3I from coastal upwelling systems?**

One of the major meteorological constraints on atmospheric $CHBr_3$, CH_2Br_2 and CH_3I during the DRIVE campaign was the MABL height. Additionally, local influence of land-sea breeze circulations was found close to the coast, although local sea-to-air fluxes remain the main source for these compounds. The influence of the MABL was largest on emissions from $CHBr_3$ and CH_2Br_2 because they were not as strongly supersaturated as CH_3I.

6. **How do concentrations and emissions of the halocarbons from tropical upwelling systems in the Atlantic compare to a global perspective?**

The tropical ocean was identified to contribute largely to the global emission estimate of $CHBr_3$ and CH_2Br_2 with the tropical upwelling systems covered here as large sources in a global perspective. CH_3I was found to be most elevated in the subtropical gyres.

7. **Which processes lead to the observed depth profiles of CH_3I in the tropical open ocean?**

The model results for the depth profiles obtained in the Cape Verde region suggest that the observed profiles are produced from a combination of photochemical and biological production. This is in agreement with the results from the two campaigns in this thesis, which show that both biological and photochemical formation can dominate oceanic CH_3I concentrations. The results also suggest that production rates by *Prochlorococcus* for the tropical and subtropical oligotrophic Atlantic have previously been overestimated.

8. **How much CH_3I from the Cape Verde and Mauritanian upwelling region can reach the stratosphere and how does this compare to other tropical oceanic regions?**

CH_3I produced in the tropical Atlantic ocean can reach the stratosphere and is very likely to influence ozone chemistry. The entrainment of CH_3I above 17 km was in total higher for the tropical Pacific in comparison to the tropical Atlantic, which is due to the fact that the tropical deep convection in the West Pacific is much stronger than in the tropical Atlantic.

With the new findings from this thesis, we can now update Figure III-17.

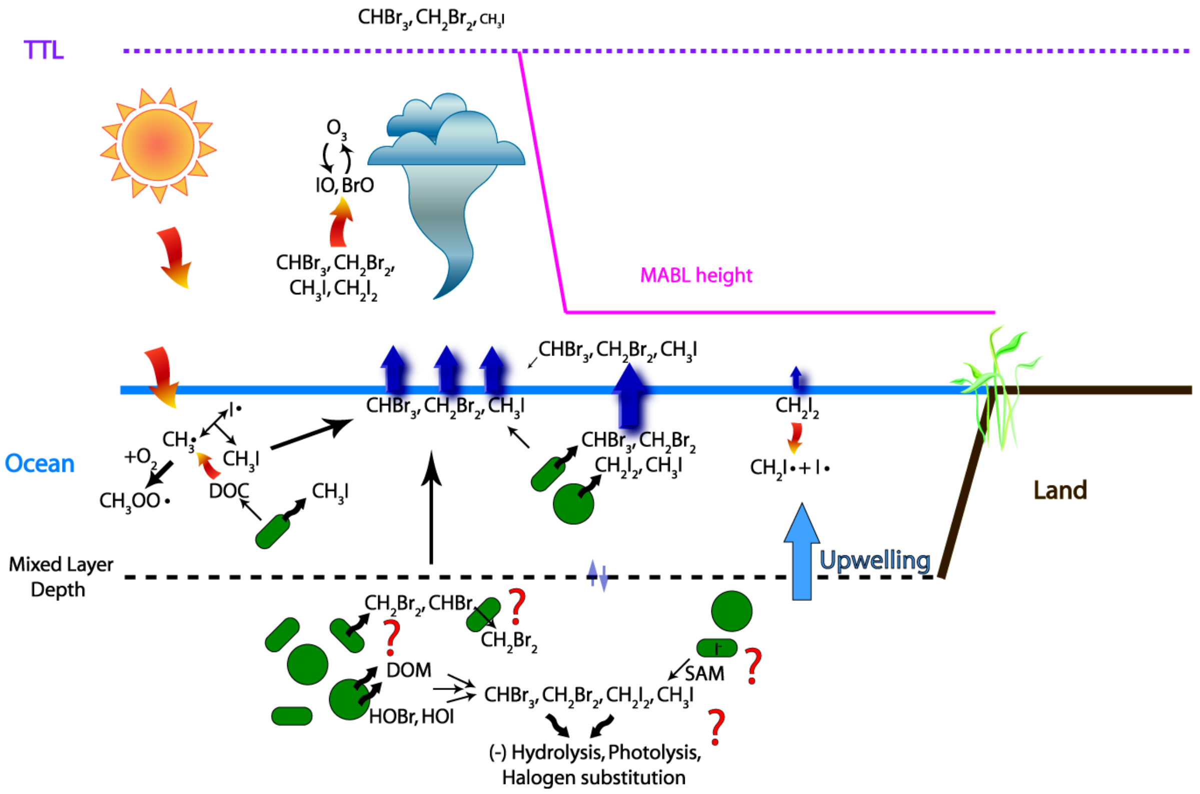
$CHBr_3$, CH_2Br_2, CH_3I
TTL
O_3
IO, BrO
$CHBr_3$, CH_2Br_2, CH_3I, CH_2I_2
MABL height
$CHBr_3$, CH_2Br_2, CH_3I
$CHBr_3$, CH_2Br_2, CH_3I
Ocean
CH_3•
I•
$+O_2$
CH_3I
CH_3OO•
DOC
CH_3I
$CHBr_3$, CH_2Br_2
CH_2I_2, CH_3I
CH_2I_2
CH_2I• + I•
Land
Upwelling
Mixed Layer Depth
CH_2Br_2, $CHBr_3$
?
?
CH_2Br_2
DOM
HOBr, HOI
I^-
SAM
?
$CHBr_3$, CH_2Br_2, CH_2I_2, CH_3I
?
(-) Hydrolysis, Photolysis, Halogen substitution

Figure V-1. Updated version of Figure III-17 with the results of this thesis, although some uncertainy still lies in every process. The question marks indicates processes that need much further investigation as described below.

The results of this thesis raise some more questions, additionally to the topics that could not be addressed yet (Figure V-1). There are indications that the emissions of halocarbons might increase in the future in upwelling systems due to enhanced land-sea temperature gradients and associated increasing wind speeds, as well as shifts in phytoplankton production. Overall, the phytoplankton production is projected to decrease in the open oceans (Falkowski et al., 1998; Misumi et al., 2014), but may increase in coastal upwelling systems (Lachkar and Gruber, 2012) with unknown consequences for the oceanic halocarbon production. More insight into the involved processes is severely needed to better estimate future changes. Incubation studies might be a good tool to investigate these. Some uncertainties include the location of the production, intra- or extracellular, which production pathways yield the largest amounts of these compounds, how species dependent the production is and why, as well as factors that enhance or decrease halocarbon release from phytoplankton, such as light of pH. The correlation analyses during the two campaigns indicate additional planktonic producers to *diatoms*. Hence, a useful experiment would include mono-cultural studies of phytoplankton species of each of the big phytoplankton groups to gain more knowledge on potentially different production rates. Field incubations with marked halocarbon isotopes could provide further insight into production and loss processes and their influence on halocarbon emissions. These experiments ideally include measurements of diapycnal mixing to evaluate the impact of physical constraints compared to chemical and biological production and losses of these compounds on a longer time scale. Furthermore, there are still large gaps in the global coverage of these measurements. Each new data point will help to further reduce the current uncertainties.

REFERENCES

VI. References

Abrahamsson, K., Lorén, A., Wulff, A., and Wangberg, S. A.: Air-sea exchange of halocarbons: The influence of diurnal and regional variations and distribution of pigments, Deep-Sea Res. Part II-Top. Stud. Oceanogr., 51, 2789-2805, 10.1016/j.dsr2.2004.09.005, 2004b.

Allonier, A. S., Khalanski, M., Camel, V., and Bermond, A.: Characterization of chlorination by-products in cooling effluents of coastal nuclear power stations, Mar. Pollut. Bull., 38, 1232-1241, 10.1016/s0025-326x(99)00168-x, 1999.

Amachi, S., Kamagata, Y., Kanagawa, T., and Muramatsu, Y.: Bacteria mediate methylation of iodine in marine and terrestrial environments, Applied and Environmental Microbiology, 67, 2718-2722, 10.1128/aem.67.6.2718-2722.2001, 2001.

Amachi, S., Muramatsu, Y., Akiyama, Y., Miyazaki, K., Yoshiki, S., Hanada, S., Kamagata, Y., Ban-nai, T., Shinoyama, H., and Fujii, T.: Isolation of iodide-oxidizing bacteria from iodide-rich natural gas brines and seawaters, Microb. Ecol., 49, 547-557, 10.1007/s00248-004-0056-0, 2005.

Archer, S. D., Goldson, L. E., Liddicoat, M. I., Cummings, D. G., and Nightingale, P. D.: Marked seasonality in the concentrations and sea-to-air flux of volatile iodocarbon compounds in the western english channel, J. Geophys. Res.-Oceans, 112, 10.1029/2006jc003963, 2007.

Aschmann, J., Sinnhuber, B. M., Atlas, E. L., and Schauffler, S. M.: Modeling the transport of very short-lived substances into the tropical upper troposphere and lower stratosphere, Atmos. Chem. Phys., 9, 9237-9247, 2009.

Aschmann, J., and Sinnhuber, B. M.: Contribution of very short-lived substances to stratospheric bromine loading: Uncertainties and constraints, Atmos. Chem. Phys., 13, 1203-1219, 10.5194/acp-13-1203-2013, 2013.

Beissner, R. S., Guilford, W. J., Coates, R. M., and Hager, L. P.: Synthesis of brominated heptanones and bromoform by a bromoperoxidase of marine origin, Biochemistry, 20, 3724-3731, 10.1021/bi00516a009, 1981.

Bell, N., Hsu, L., Jacob, D. J., Schultz, M. G., Blake, D. R., Butler, J. H., King, D. B., Lobert, J. M., and Maier-Reimer, E.: Methyl iodide: Atmospheric budget and use as a tracer of marine convection in global models, J. Geophys. Res.-Atmos., 107, 434010.1029/2001jd001151, 2002.

Blomquist, B. W., Fairall, C. W., Huebert, B. J., Kieber, D. J., and Westby, G. R.: Dms sea-air transfer velocity: Direct measurements by eddy covariance and parameterization based on the noaa/coare gas transfer model, Geophys. Res. Lett., 33, 10.1029/2006gl025735, 2006.

Bouwer, E. J., Rittmann, B. E., and McCarty, P. L.: Anaerobic degradation of halogenated 1- and 2-carbon organic compounds, Environ. Sci. Technol., 15, 596-599, 10.1021/es00087a012, 1981.

Bouwer, E. J., and McCarty, P. L.: Transformations of 1-carbon and 2-carbon halogenated aliphatic organic-compounds under methanogenic conditions, Applied and Environmental Microbiology, 45, 1286-1294, 1983.

Bravo-Linares, C. M., Mudge, S. M., and Loyola-Sepulveda, R. H.: Production of volatile organic compounds (vocs) by temperate macroalgae. The use of solid phase microextraction (spme) coupled to gc-ms as method of analysis, J. Chil. Chem. Soc., 55, 227-232, 2010.

Brownell, D. K., Moore, R. M., and Cullen, J. J.: Production of methyl halides by prochlorococcus and synechococcus, Glob. Biogeochem. Cycle, 24, 10.1029/2009gb003671, 2010.

Bumke, K., Schlundt, M., Kalisch, J., Macke, A., and Kleta, H.: Measured and parameterized energy fluxes estimated for atlantic transects of r/v polarstern, J. Phys. Oceanogr., 44, 482-491, 10.1175/jpo-d-13-0152.1, 2013.

Burreson, B., Moore, R., and Roller, P.: Haloforms in the essential oil of the alga asparagopsis taxiformis (rhodophyta), Tetrahedron Lett., 16, 473-476, 10.1016/S0040-4039(00)71897-1, 1975.

Butler, A.: Acquisition and utilization of transition metal ions by marine organisms, Science, 281, 207-210, 10.1126/science.281.5374.207, 1998.

Butler, J. H., King, D. B., Lobert, J. M., Montzka, S. A., Yvon-Lewis, S. A., Hall, B. D., Warwick, N. J., Mondeel, D. J., Aydin, M., and Elkins, J. W.: Oceanic distributions and emissions of short-lived halocarbons, Glob. Biogeochem. Cycle, 21, Gb102310.1029/2006gb002732, 2007.

Caniaux, G., Giordani, H., Redelsperger, J. L., Guichard, F., Key, E., and Wade, M.: Coupling between the atlantic cold tongue and the west african monsoon in boreal spring and summer, J. Geophys. Res.-Oceans, 116, 10.1029/2010jc006570, 2011.

Carpenter, L. J., Sturges, W. T., Penkett, S. A., Liss, P. S., Alicke, B., Hebestreit, K., and Platt, U.: Short-lived alkyl iodides and bromides at mace head, ireland: Links to biogenic sources and halogen oxide production, J. Geophys. Res.-Atmos., 104, 1679-1689, 1999.

Carpenter, L. J., and Liss, P. S.: On temperate sources of bromoform and other reactive organic bromine gases, J. Geophys. Res.-Atmos., 105, 20539-20547, 2000.

Carpenter, L. J., Malin, G., Liss, P. S., and Kupper, F. C.: Novel biogenic iodine-containing trihalomethanes and other short-lived halocarbons in the coastal east atlantic, Glob. Biogeochem. Cycle, 14, 1191-1204, 2000.

Carpenter, L. J., Hopkins, J. R., Jones, C. E., Lewis, A. C., Parthipan, R., Wevill, D. J., Poissant, L., Pilote, M., and Constant, P.: Abiotic source of reactive organic halogens in the sub-arctic atmosphere?, Environ. Sci. Technol., 39, 8812-8816, 10.1021/es050918w, 2005.

Carpenter, L. J., Wevill, D. J., Palmer, C. J., and Michels, J.: Depth profiles of volatile iodine and bromine-containing halocarbons in coastal antarctic waters, Mar. Chem., 103, 227-236, 10.1016/j.marchem.2006.08.003, 2007.

Carpenter, L. J., Jones, C. E., Dunk, R. M., Hornsby, K. E., and Woeltjen, J.: Air-sea fluxes of biogenic bromine from the tropical and north atlantic ocean, Atmos. Chem. Phys., 9, 1805-1816, 2009.

Carpenter, L. J., MacDonald, S. M., Shaw, M. D., Kumar, R., Saunders, R. W., Parthipan, R., Wilson, J., and Plane, J. M. C.: Atmospheric iodine levels influenced by sea surface emissions of inorganic iodine, Nature Geosci, 6, 108-111, http://www.nature.com/ngeo/journal/v6/n2/abs/ngeo1687.html#supplementary-information, 2013.

Chuck, A. L., Turner, S. M., and Liss, P. S.: Oceanic distributions and air-sea fluxes of biogenic halocarbons in the open ocean, J. Geophys. Res.-Oceans, 110, C1002210.1029/2004jc002741, 2005.

Cicerone, R. J., Heidt, L. E., and Pollock, W. H.: Measurements of atmospheric methyl-bromide and bromoform, J. Geophys. Res.-Atmos., 93, 3745-3749, 10.1029/JD093iD04p03745, 1988.

Class, T., and Ballschmiter, K.: Chemistry of organic traces in air ix: Evidence of natural marine sources for chloroform in regions of high primary production, Z. Anal. Chem., 327, 40-41, 10.1007/bf00474552, 1987.

Class, T., and Ballschmiter, K.: Chemistry of organic traces in air viii: Sources and distribution of bromo- and bromochloromethanes in marine air and surfacewater of the atlantic ocean, J. Atmos. Chem., 6, 35-46, 1988.

Collén, J., Ekdahl, A., Abrahamsson, K., and Pedersén, M.: The involvement of hydrogen-peroxide in the production of volatile halogenated compounds by meristiella gelidium, Phytochemistry, 36, 1197-1202, 10.1016/s0031-9422(00)89637-5, 1994.

Cota, G. F., and Sturges, W. T.: Biogenic bromine production in the arctic, Mar. Chem., 56, 181-192, 1997.

Daniel, J. S., Solomon, S., Portmann, R. W., and Garcia, R. R.: Stratospheric ozone destruction: The importance of bromine relative to chlorine, J. Geophys. Res.-Atmos., 104, 23871-23880, 10.1029/1999jd900381, 1999.

Dorf, M., Butz, A., Camy-Peyret, C., Chipperfield, M. P., Kritten, L., and Pfeilsticker, K.: Bromine in the tropical troposphere and stratosphere as derived from balloon-borne bro observations, Atmos. Chem. Phys., 8, 7265-7271, 10.5194/acp-8-7265-2008, 2008.

Dvortsov, V. L., Geller, M. A., Solomon, S., Schauffler, S. M., Atlas, E. L., and Blake, D. R.: Rethinking reactive halogen budgets in the midlatitude lower stratosphere, Geophys. Res. Lett., 26, 1699-1702, 1999.

Ekdahl, A., Pedersén, M., and Abrahamsson, K.: A study of the diurnal variation of biogenic volatile halocarbons, Mar. Chem., 63, 1-8, 1998.

Elliott, S., and Rowland, F. S.: Methyl halide hydrolysis rates in natural-waters, J. Atmos. Chem., 20, 229-236, 10.1007/bf00694495, 1995.

Fairall, C. W., Bradley, E. F., Hare, J. E., Grachev, A. A., and Edson, J. B.: Bulk parameterization of air–sea fluxes: Updates and verification for the coare algorithm, J. Clim., 16, 571-591, 10.1175/1520-0442(2003)016<0571:bpoasf>2.0.co;2, 2003.

Falkowski, P. G., Barber, R. T., and Smetacek, V.: Biogeochemical controls and feedbacks on ocean primary production, Science, 281, 200-206, 10.1126/science.281.5374.200, 1998.

Falkowski, P. G., and Raven, J. A.: Aquatic photosynthesis, Blackwell Science, Malden, 2007.

Farman, J. C., Gardiner, B. G., and Shanklin, J. D.: Large losses of toal ozone in antarctica reveal seasonal clox/nox interaction, Nature, 315, 207-210, 10.1038/315207a0, 1985.

Fedoseev, A.: Geostrophic circulation of surface waters on the shelf of north-west africa, Rapp. Proc. Verb. Reun. Cons. Inst. Expl. Mer., 159, 32-37, 1970.

Fenical, W.: Natural halogenated organics, in: Marine organic chemistry, edited by: Duursma, E. K., and Dawson, R., Elsevier, New York, 375-393, 1981.

Fielding, M., Gibson, T. M., and James, H. A.: Organic micropollutants in drinking water, Water Research Centre, Marlow, UK, 47, 1981.

Fogelqvist, E., Josefsson, B., and Roos, C.: Halocarbons as tracer substances in studies of the distribution patterns of chlorinated waters in coastal areas, Environ. Sci. Technol., 16, 479-482, 10.1021/es00102a010, 1982.

Fogelqvist, E.: Carbon-tetrachloride, tetrachloroethylene, 1,1,1-trichloroethane and bromoform in arctic seawater, J. Geophys. Res.-Oceans, 90, 9181-9193, 10.1029/JC090iC05p09181, 1985.

Fogelqvist, E., and Krysell, M.: Naturally and anthropogenically produced bromoform in the kattegatt, a semienclosed oceanic basin, J. Atmos. Chem., 13, 315-324, 10.1007/bf00057749, 1991.

Fueglistaler, S., Dessler, A. E., Dunkerton, T. J., Folkins, I., Fu, Q., and Mote, P. W.: Tropical tropopause layer, Rev. Geophys., 47, RG1004, 10.1029/2008rg000267, 2009.

Fuse, H., Inoue, H., Murakami, K., Takimura, O., and Yamaoka, Y.: Production of free and organic iodine by roseovarius spp, FEMS Microbiology Letters, 229, 189-194, 10.1016/s0378-1097(03)00839-5, 2003.

Garbe, C. S., Rutgersson, A., Boutin, J., de Leeuw, G., Delille, B., Fairall, C. W., Gruber, N., Hare, J. E., Ho, D. T., Johnson, M. T., Nightingale, P. D., Pettersson, H., Piskozub, J., Sahlée, E., Tsai, W.-T., Ward, B., Woolf, D. K., and Zappa, C. J.: Transfer across the air-sea interface, in: Ocean-atmosphere interactions of gases and particles, edited by: Liss, P. S., and Johnson, M. T., Springer Earth System Sciences, Norwhich, UK, 55-112, 2014.

Geen, C. E.: Selected marine sources and sinks of bromoform and other low molecular weight organobromines, PhD, Dalhousie University, Halifax, Halifax, Nova Scotia, 1992.

Giese, B., Laturnus, F., Adams, F. C., and Wiencke, C.: Release of volatile iodinated c1−c4 hydrocarbons by marine macroalgae from various climate zones, Environ. Sci. Technol., 33, 2432-2439, 10.1021/es980731n, 1999.

Goodwin, K. D., North, W. J., and Lidstrom, M. E.: Production of bromoform and dibromomethane by giant kelp: Factors affecting release and comparison to anthropogenic bromine sources, Limnol. Oceanogr., 42, 1725-1734, 1997a.

Goodwin, K. D., Lidstrom, M. E., and Oremland, R. S.: Marine bacterial degradation of brominated methanes, Environ. Sci. Technol., 31, 3188-3192, 10.1021/es970165g, 1997b.

Goodwin, K. D., Schaefer, J. K., and Oremland, R. S.: Bacterial oxidation of dibromomethane and methyl bromide in natural waters and enrichment cultures, Applied and Environmental Microbiology, 64, 4629-4636, 1998.

Grodsky, S. A., Carton, J. A., and McClain, C. R.: Variability of upwelling and chlorophyll in the equatorial atlantic, Geophys. Res. Lett., 35, L03610

10.1029/2007gl032466, 2008.

Grossmann, K., Friess, U., Peters, E., Wittrock, F., Lampel, J., Yilmaz, S., Tschritter, J., Sommariva, R., von Glasow, R., Quack, B., Kruger, K., Pfeilsticker, K., and Platt, U.: Iodine monoxide in the western pacific marine boundary layer, Atmos. Chem. Phys., 13, 3363-3378, 10.5194/acp-13-3363-2013, 2013.

Gschwend, P. M., Macfarlane, J. K., and Newman, K. A.: Volatile halogenated organic compounds released to seawater from temperate marine macroalgae, Science, 227, 1033-1035, 10.1126/science.227.4690.1033, 1985.

Hagen, E.: Northwest african upwelling scenario, Oceanol. Acta, 24, S113-S128, 2001.

Happell, J. D., and Wallace, D. W. R.: Methyl iodide in the greenland/norwegian seas and the tropical atlantic ocean: Evidence for photochemical production, Geophys. Res. Lett., 23, 2105-2108, 10.1029/96gl01764, 1996.

Hastenrath, S., and Lamb, P.: Dynamics and climatology of surface flow over equatorial oceans, Tellus, 30, 436-448, 1978.

Hayduk, W., and Laudie, H.: Prediction of diffusion-coefficients for nonelectrolytes in dilute aqueous-solutions, Aiche J., 20, 611-615, 10.1002/aic.690200329, 1974.

Helz, G. R., and Hsu, R. Y.: Volatile chlorocarbons and bromocarbons in coastal waters, Limnol. Oceanogr., 23, 858-869, 1978.

Hill, V. L., and Manley, S. L.: Release of reactive bromine and iodine from diatoms and its possible role in halogen transfer in polar and tropical oceans, Limnol. Oceanogr., 54, 812-822, 10.4319/lo.2009.54.3.0812, 2009.

Ho, D. T., Sabine, C. L., Hebert, D., Ullman, D. S., Wanninkhof, R., Hamme, R. C., Strutton, P. G., Hales, B., Edson, J. B., and Hargreaves, B. R.: Southern ocean gas exchange experiment: Setting the stage, J. Geophys. Res.-Oceans, 116, 10.1029/2010jc006852, 2011.

Holton, J. R., Haynes, P. H., McIntyre, M. E., Douglass, A. R., Rood, R. B., and Pfister, L.: Stratosphere-troposphere exchange, Rev. Geophys., 33, 403-439, 10.1029/95rg02097, 1995.

Hossaini, R., Chipperfield, M. P., Monge-Sanz, B. M., Richards, N. A. D., Atlas, E., and Blake, D. R.: Bromoform and dibromomethane in the tropics: A 3-d model study of chemistry and transport, Atmos. Chem. Phys., 10, 719-735, 2010.

Hossaini, R., Chipperfield, M. P., Feng, W., Breider, T. J., Atlas, E., Montzka, S. A., Miller, B. R., Moore, F., and Elkins, J.: The contribution of natural and anthropogenic very short-lived species to stratospheric bromine, Atmos. Chem. Phys., 12, 371-380, 10.5194/acp-12-371-2012, 2012.

Hughes, C., Malin, G., Nightingale, P. D., and Liss, P. S.: The effect of light stress on the release of volatile iodocarbons by three species of marine microalgae, Limnol. Oceanogr., 51, 2849-2854, 2006.

Hughes, C., Chuck, A. L., Rossetti, H., Mann, P. J., Turner, S. M., Clarke, A., Chance, R., and Liss, P. S.: Seasonal cycle of seawater bromoform and dibromomethane concentrations in a coastal bay on the western antarctic peninsula, Glob. Biogeochem. Cycle, 23, Gb2024

10.1029/2008gb003268, 2009.

Hughes, C., Franklin, D. J., and Malin, G.: Iodomethane production by two important marine cyanobacteria: Prochlorococcus marinus (ccmp 2389) and synechococcus sp (ccmp 2370), Mar. Chem., 125, 19-25, 10.1016/j.marchem.2011.01.007, 2011.

Hughes, C., Johnson, M., Utting, R., Turner, S., Malin, G., Clarke, A., and Liss, P. S.: Microbial control of bromocarbon concentrations in coastal waters of the western antarctic peninsula, Mar. Chem., 151, 35-46, http://dx.doi.org/10.1016/j.marchem.2013.01.007, 2013.

Hummels, R., Dengler, M., and Bourles, B.: Seasonal and regional variability of upper ocean diapycnal heat flux in the atlantic cold tongue, Prog. Oceanogr., 111, 52-74, 10.1016/j.pocean.2012.11.001, 2013.

Isemer, H.-J., Willebrand, J., and Hasse, L.: Fine adjustment of large scale air-sea energy flux parameterizations by direct estimates of ocean heat transport, J. Clim., 2, 1173-1184, 10.1175/1520-0442(1989)002<1173:faolsa>2.0.co;2, 1989.

Itoh, N., Tsujita, M., Ando, T., Hisatomi, G., and Higashi, T.: Formation and emission of monohalomethanes from marine algae, Phytochemistry, 45, 67-73, 10.1016/s0031-9422(96)00786-8, 1997.

Jaworske, D. A., and Helz, G. R.: Rapid consumption of bromine oxidants in river and estuarine waters, Environ. Sci. Technol., 19, 1188-1191, 10.1021/es00142a008, 1985.

Jenner, H. A., Taylor, C. J. L., vanDonk, M., and Khalanski, M.: Chlorination by-products in chlorinated cooling water of some european coastal power stations, Mar. Environ. Res., 43, 279-293, 10.1016/s0141-1136(96)00091-8, 1997.

Jones, C. E., and Carpenter, L. J.: Solar photolysis of ch_2i_2, ch_2ici, and ch_2ibr in water, saltwater, and seawater, Environ. Sci. Technol., 39, 6130-6137, 10.1021/es050563g, 2005.

Jones, C. E., and Carpenter, L. J.: Chemical destruction of ch3i, c2h5i, 1-c3h7i, and 2-c3h7i in saltwater, Geophys. Res. Lett., 34, 10.1029/2007gl029775, 2007.

Jones, C. E., Hornsby, K. E., Dunk, R. M., Leigh, R. J., and Carpenter, L. J.: Coastal measurements of short-lived reactive iodocarbons and bromocarbons at roscoff, brittany during the rhamble campaign, Atmos. Chem. Phys., 9, 8757-8769, 2009.

Jones, C. E., Hornsby, K. E., Sommariva, R., Dunk, R. M., Von Glasow, R., McFiggans, G., and Carpenter, L. J.: Quantifying the contribution of marine organic gases to atmospheric iodine, Geophys. Res. Lett., 37, L1880410.1029/2010gl043990, 2010.

Jones, C. E., Andrews, S. J., Carpenter, L. J., Hogan, C., Hopkins, F. E., Laube, J. C., Robinson, A. D., Spain, T. G., Archer, S. D., Harris, N. R. P., Nightingale, P. D., O'Doherty, S. J., Oram, D. E., Pyle, J. A., Butler, J. H., and Hall, B. D.: Results from the first national uk inter-laboratory calibration for very short-lived halocarbons, Atmos. Meas. Tech., 4, 865-874, 10.5194/amt-4-865-2011, 2011.

Jouanno, J., Marin, F., du Penhoat, Y., Sheinbaum, J., and Molines, J. M.: Seasonal heat balance in the upper 100 m of the equatorial atlantic ocean, J. Geophys. Res.-Oceans, 116, 10.1029/2010jc006912, 2011.

Karlsson, A., Auer, N., Schulz-Bull, D., and Abrahamsson, K.: Cyanobacterial blooms in the baltic - a source of halocarbons, Mar. Chem., 110, 129-139, 10.1016/j.marchem.2008.04.010, 2008.

Kerkweg, A., Jockel, P., Warwick, N., Gebhardt, S., Brenninkmeijer, C. A. M., and Lelieveld, J.: Consistent simulation of bromine chemistry from the marine boundary layer to the stratosphere - part 2: Bromocarbons, Atmos. Chem. Phys., 8, 5919-5939, 2008.

Klick, S., and Abrahamsson, K.: Biogenic volatile iodated hydrocarbons in the ocean, J. Geophys. Res.-Oceans, 97, 12683-12687, 10.1029/92jc00948, 1992.

Ko, M. K. W., and Poulet, G.: Very short-lived halogen and sulfur substances, chapter 2 in scientific assessment of ozone depletion: 2002, global ozone research and monitoring project, World Meteorological Organization (WMO), Geneva, Report No. 47, 2002.

Krysell, M.: Bromoform in the nansen basin in the arctic-ocean, Mar. Chem., 33, 187-197, 1991.

Krysztofiak, G., Catoire, V., Poulet, G., Marecal, V., Pirre, M., Louis, F., Canneaux, S., and Josse, B.: Detailed modeling of the atmospheric degradation mechanism of very-short lived brominated species, Atmos. Environ., 59, 514-532, 10.1016/j.atmosenv.2012.05.026, 2012.

Küpper, F. C., Schweigert, N., Gall, E. A., Legendre, J. M., Vilter, H., and Kloareg, B.: Iodine uptake in laminariales involves extracellular, haloperoxidase-mediated oxidation of iodide, Planta, 207, 163-171, 1998.

Kwok, W. M., Zhao, C. Y., Li, Y. L., Guan, X. G., and Phillips, D. L.: Direct observation of an isopolyhalomethane o-h insertion reaction with water: Picosecond time-resolved resonance raman (ps-tr3) study of the isobromoform reaction with water to produce a chbr2oh product, J. Chem. Phys., 120, 3323-3332, 10.1063/1.1640997, 2004.

Lachkar, Z., and Gruber, N.: A comparative study of biological production in eastern boundary upwelling systems using an artificial neural network, Biogeosciences, 9, 293-308, 10.5194/bg-9-293-2012, 2012.

Lana, A., Bell, T. G., Simó, R., Vallina, S. M., Ballabrera-Poy, J., Kettle, A. J., Dachs, J., Bopp, L., Saltzman, E. S., Stefels, J., Johnson, J. E., and Liss, P. S.: An updated climatology of surface dimethlysulfide concentrations and emission fluxes in the global ocean, Glob. Biogeochem. Cycle, 25, GB1004, 10.1029/2010gb003850, 2011.

Laturnus, F.: Volatile halocarbons released from arctic macroalgae, Mar. Chem., 55, 359-366, 1996.

Laturnus, F., Adams, F. C., Gomez, I., and Mehrtens, G.: Halogenating activities detected in antarctic macroalgae, Polar Biol., 17, 281-284, 10.1007/s003000050133, 1997.

Laube, J. C., Engel, A., Bonisch, H., Mobius, T., Worton, D. R., Sturges, W. T., Grunow, K., and Schmidt, U.: Contribution of very short-lived organic substances to stratospheric chlorine and bromine in the tropics - a case study, Atmos. Chem. Phys., 8, 7325-7334, 2008.

Leedham, E. C., Hughes, C., Keng, F. S. L., Phang, S. M., Malin, G., and Sturges, W. T.: Emission of atmospherically significant halocarbons by naturally occurring and farmed tropical macroalgae, Biogeosciences, 10, 3615-3633, 10.5194/bg-10-3615-2013, 2013.

Liang, Q., Stolarski, R. S., Kawa, S. R., Nielsen, J. E., Douglass, A. R., Rodriguez, J. M., Blake, D. R., Atlas, E. L., and Ott, L. E.: Finding the missing stratospheric br-y: A global modeling study of chbr3 and ch2br2, Atmos. Chem. Phys., 10, 2269-2286, 2010.

Lin, C. Y., and Manley, S. L.: Bromoform production from seawater treated with bromoperoxidase, Limnol. Oceanogr., 57, 1857-1866, 10.4319/1o.2012.57.06.1857, 2012.

Liss, P. S., and Slater, P. G.: Flux of gases across air-sea interface, Nature, 247, 181-184, 1974.

Liu, Y. N., Yvon-Lewis, S. A., Hu, L., Salisbury, J. E., and O'Hern, J. E.: Chbr(3), ch(2)br(2), and chclbr(2) in u.S. Coastal waters during the gulf of mexico and east coast carbon cruise, J. Geophys. Res.-Oceans, 116, C10004

10.1029/2010jc006729, 2011.

Lovelock, J. E., Maggs, R. J., and Wade, R. J.: Halogenated hydrocarbons in and over the atlantic, Nature, 241, 194-196, 10.1038/241194a0, 1973.

Lovelock, J. E.: Natural halocarbons in air and in the sea, Nature, 256, 193-194, 1975.

Luther, G. W.: Thermodynamic redox calculations for one and two electron transfer steps: Implications for halide oxidation and halogen environmental cycling, in: Aquatic redox chemistry, edited by: Tratnyek, P. G., Grundl, T. J., Haderlein, S. B., ACS Symposium Series; American Chemical Society, Washington, D.C., 2011.

Mabey, W., and Mill, T.: Critical-review of hydrolysis of organiccompounds in water under environmental-conditions, J. Phys. Chem. Ref. Data, 7, 383-415, 1978.

Manley, S. L., and Dastoor, M. N.: Methyl halide (ch3x) production from the giant-kelp, macrocystis, and estimates of global ch3x production by kelp, Limnol. Oceanogr., 32, 709-715, 1987.

Manley, S. L., and Dastoor, M. N.: Methyl-iodide (ch_3i) production by kelp and associated microbes, Mar. Biol., 98, 477-482, 1988.

Manley, S. L., Goodwin, K., and North, W. J.: Laboratory production of bromoform, methylene bromide, and methyl-iodide by macroalgae and distribution in nearshore southern california waters, Limnol. Oceanogr., 37, 1652-1659, 1992.

Manley, S. L.: The possible involvement of methylcobalamin in the production of methyl-iodide in the marine environment, Mar. Chem., 46, 361-369, 10.1016/0304-4203(94)90032-9, 1994.

Manley, S. L., and de la Cuesta, J. L.: Methyl iodide production from marine phytoplankton cultures, Limnol. Oceanogr., 42, 142-147, 1997.

Manley, S. L.: Phytogenesis of halomethanes: A product of selection or a metabolic accident?, Biogeochemistry, 60, 163-180, 10.1023/a:1019859922489, 2002.

Marandino, C. A., De Bruyn, W. J., Miller, S. D., and Saltzman, E. S.: Eddy correlation measurements of the air/sea flux of dimethylsulfide over the north pacific ocean, J. Geophys. Res.-Atmos., 112, 10.1029/2006jd007293, 2007.

Marshall, R. A., Harper, D. B., McRoberts, W. C., and Dring, M. J.: Volatile bromocarbons produced by falkenbergia stages of asparagopsis spp. (rhodophyta), Limnol. Oceanogr., 44, 1348-1352, 1999.

Martino, M., Liss, P. S., and Plane, J. M. C.: The photolysis of dihalomethanes in surface seawater, Environ. Sci. Technol., 39, 7097-7101, 10.1021/es048718s, 2005.

Martino, M., Liss, P. S., and Plane, J. M. C.: Wavelength-dependence of the photolysis of diiodomethane in seawater, Geophys. Res. Lett., 33, L06606

10.1029/2005gl025424, 2006.

Martino, M., Mills, G. P., Woeltjen, J., and Liss, P. S.: A new source of volatile organoiodine compounds in surface seawater, Geophys. Res. Lett., 36, L01609

10.1029/2008gl036334, 2009.

McConnell, O. J., and Fenical, W.: Antimicrobial agents from the marine red algae of the familiy bonnemaisoniacea, in: Marine algae in pharmaceutical science, edited by: Hoppe, H. A., Levring, T., and Tanaka, Y., Walter der Gruyter, Berlin, 479-500, 1979.

McGillis, W. R., Edson, J. B., Hare, J. E., and Fairall, C. W.: Direct covariance air-sea co2 fluxes, J. Geophys. Res.-Oceans, 106, 16729-16745, 10.1029/2000jc000506, 2001.

Merle, J.: Seasonal heat-budget in the equatorial atlantic-ocean, J. Phys. Oceanogr., 10, 464-469, 10.1175/1520-0485(1980)010<0464:shbite>2.0.co;2, 1980.

Miller, S., Marandino, C., de Bruyn, W., and Saltzman, E. S.: Air-sea gas exchange of co2 and dms in the north atlantic by eddy covariance, Geophys. Res. Lett., 36, 10.1029/2009gl038907, 2009.

Minas, H. J., Codispoti, L. A., and Dugdale, R. C.: Nutrients and primary production in the upwelling region off northwest africa, Rapp. Proc. Verb. Reun. Cons. Inst. Expl. Mer., 180, 148-183, 1982.

Misumi, K., Lindsay, K., Moore, J. K., Doney, S. C., Bryan, F. O., Tsumune, D., and Yoshida, Y.: The iron budget in ocean surface waters in the 20th and 21st centuries: Projections by the community earth system model version 1, Biogeosciences, 11, 33-55, 10.5194/bg-11-33-2014, 2014.

Mittelstaedt, E.: Large-scale circulation along the coast of northwest africa, Rapp. Proc. Verb. Reun. Cons. Inst. Expl. Mer., 180, 50-57, 1982.

Mohn, W. W., and Tiedje, J. M.: Microbial reductive dehalogenation, Microbiol. Rev., 56, 482-507, 1992.

Molina, M. J., and Rowland, F. S.: Stratospheric sink for chlorofluoromethanes - chlorine atomic-catalysed destruction of ozone, Nature, 249, 810-812, 10.1038/249810a0, 1974.

Molinari, R. L.: Observations of eastwars currents in the tropical south-atlantic ocean - 1978 - 1980, Journal of Geophysical Research-Oceans and Atmospheres, 87, 9707-9714, 10.1029/JC087iC12p09707, 1982.

Montzka, S. A., and Reimann, S.: Ozone-depleting substances and related chemicals, chapter 1 in scientific assessment of ozone depletion: 2010, global ozone research and monitoring project, World Meteorological Organization (WMO), Geneva, Report No. 52, 2011.

Moore, R. M., and Tokarczyk, R.: Volatile biogenic halocarbons in the northwest atlantic, Glob. Biogeochem. Cycle, 7, 195-210, 1993.

Moore, R. M., and Zafiriou, O. C.: Photochemical production of methyl-iodide in seawater, J. Geophys. Res.-Atmos., 99, 16415-16420, 10.1029/94jd00786, 1994.

Moore, R. M., Geen, C. E., and Tait, V. K.: Determination of henry law constants for a suite of naturally-occurring halogenated methanes in seawater, Chemosphere, 30, 1183-1191, 10.1016/0045-6535(95)00009-w, 1995a.

Moore, R. M., Tokarczyk, R., Tait, V. K., Poulin, M., and Geen, C. E.: Marine phytoplankton as a natural source of volatile organohalogens, in: Naturally-produced organohalogens, edited by: Grimvall, A., and deLeer, E. W. B., Kluwer Academic Publishers, Dordrecht, 283-294, 1995b.

Moore, R. M., Webb, M., Tokarczyk, R., and Wever, R.: Bromoperoxidase and iodoperoxidase enzymes and production of halogenated methanes in marine diatom cultures, J. Geophys. Res.-Oceans, 101, 20899-20908, 10.1029/96jc01248, 1996.

Moore, R. M., and Groszko, W.: Methyl iodide distribution in the ocean and fluxes to the atmosphere, J. Geophys. Res.-Oceans, 104, 11163-11171, 10.1029/1998jc900073, 1999.

Moore, R. M.: Methyl halide production and loss rates in sea water from field incubation experiments, Mar. Chem., 101, 213-219, 10.1016/j.marchem.2006.03.003, 2006.

Mtolera, M. S. P., Collén, J., Pedersén, M., Ekdahl, A., Abrahamsson, K., and Semesi, A. K.: Stress-induced production of volatile halogenated organic compounds in eucheuma denticulatum (rhodophyta) caused by elevated ph and high light intensities, Eur. J. Phycol., 31, 89-95, 10.1080/09670269600651241, 1996.

Nagata, T.: Production mechanisms of dissolved organic matter, in: Microbial ecology of the oceans, edited by: Kirchman, D. L., Wiley-Liss, New York, 121-152, 2000.

Nakano, Y., Enami, S., Nakamichi, S., Aloisio, S., Hashimoto, S., and Kawasaki, M.: Temperature and pressure dependence study of the reaction of io radicals with dimethyl sulfide by cavity ring-down laser spectroscopy, J. Phys. Chem. A, 107, 6381-6387, 10.1021/jp0345147, 2003.

Nightingale, P.: Air-sea gas exchange, in: Surface ocean - lower atmosphere processes, edited by: Le Quéré, C., and Saltzman, E. S., American Geophysical Union, Washington, DC, 69-97, 2009.

Nightingale, P. D., Malin, G., and Liss, P. S.: Production of chloroform and other low-molecular-weight halocarbons by some species of macroalgae Limnol. Oceanogr., 40, 680-689, 1995.

Nightingale, P. D., Malin, G., Law, C. S., Watson, A. J., Liss, P. S., Liddicoat, M. I., Boutin, J., and Upstill-Goddard, R. C.: In situ evaluation of air-sea gas exchange parameterizations using novel conservative and volatile tracers, Glob. Biogeochem. Cycle, 14, 373-387, 10.1029/1999gb900091, 2000.

O'Brien, L. M., Harris, N. R. P., Robinson, A. D., Gostlow, B., Warwick, N., Yang, X., and Pyle, J. A.: Bromocarbons in the tropical marine boundary layer at the cape verde observatory - measurements and modelling, Atmos. Chem. Phys., 9, 9083-9099, 10.5194/acp-9-9083-2009, 2009.

O'Dowd, C. D., Jimenez, J. L., Bahreini, R., Flagan, R. C., Seinfeld, J. H., Hameri, K., Pirjola, L., Kulmala, M., Jennings, S. G., and Hoffmann, T.: Marine aerosol formation from biogenic iodine emissions, Nature, 417, 632-636, 10.1038/nature00775, 2002.

Okumura, Y., and Xie, S. P.: Some overlooked features of tropical atlantic climate leading to a new nino-like phenomenon, J. Clim., 19, 5859-5874, 10.1175/jcli3928.1, 2006.

Orlikowska, A., and Schulz-Bull, D. E.: Seasonal variations of volatile organic compounds in the coastal baltic sea, Environ. Chem., 6, 495-507, 10.1071/en09107, 2009.

Page, G. W.: Comparison of groundwater and surface-water for patterns and levels of contamination by toxic-substances, Environ. Sci. Technol., 15, 1475-1481, 10.1021/es00094a008, 1981.

Paul, N. A., de Nys, R., and Steinberg, P. D.: Chemical defence against bacteria in the red alga asparagopsis armata: Linking structure with function, Marine Ecology Progress Series, 306, 87-101, 10.3354/meps306087, 2006.

Pedersén, M., Collén, J., Abrahamsson, K., and Ekdahl, A.: Production of halocarbons from seaweeds: An oxidative stress reaction?, Sci. Mar., 60, 257-263, 1996.

Penkett, S. A., Jones, B. M. R., Rycroft, M. J., and Simmons, D. A.: An interhemispheric comparison of the concentrations of bromine compounds in the atmosphere, Nature, 318, 550-553, 10.1038/318550a0, 1985.

Perry, D. L., Chuang, C. C., Jungclaus, G. A., and Warner, J. S.: Identification of organic compounds in industrial effluent discharges, U.S. Environmental Protection Agency, Columbus, Ohio, 1-72, 1979.

Philander, S. G. H., and Pacanowski, R. C.: A model of the seasonal cycle in the tropical atlantic ocean, Journal of Geophysical Research: Oceans, 91, 14192-14206, 10.1029/JC091iC12p14192, 1986.

Pyle, J. A., Ashfold, M. J., Harris, N. R. P., Robinson, A. D., Warwick, N. J., Carver, G. D., Gostlow, B., O'Brien, L. M., Manning, A. J., Phang, S. M., Yong, S. E., Leong, K. P., Ung, E. H., and Ong, S.: Bromoform in the tropical boundary layer of the maritime continent during op3, Atmos. Chem. Phys., 11, 529-542, 10.5194/acp-11-529-2011, 2011.

Quack, B., and Wallace, D. W. R.: Air-sea flux of bromoform: Controls, rates, and implications, Glob. Biogeochem. Cycle, 17, 102310.1029/2002gb001890, 2003.

Quack, B., Atlas, E., Petrick, G., Stroud, V., Schauffler, S., and Wallace, D. W. R.: Oceanic bromoform sources for the tropical atmosphere, Geophys. Res. Lett., 31, L23s0510.1029/2004gl020597, 2004.

Quack, B., Peeken, I., Petrick, G., and Nachtigall, K.: Oceanic distribution and sources of bromoform and dibromomethane in the mauritanian upwelling, J. Geophys. Res.-Oceans, 112, C1000610.1029/2006jc003803, 2007a.

Quack, B., Atlas, E., Petrick, G., and Wallace, D. W. R.: Bromoform and dibromomethane above the mauritanian upwelling: Atmospheric distributions and oceanic emissions, J. Geophys. Res.-Atmos., 112, D0931210.1029/2006jd007614, 2007b.

Raimund, S., Quack, B., Bozec, Y., Vernet, M., Rossi, V., Garcon, V., Morel, Y., and Morin, P.: Sources of short-lived bromocarbons in the iberian upwelling system, Biogeosciences, 8, 1551-1564, 10.5194/bg-8-1551-2011, 2011.

Rasmussen, R. A., and Khalil, M. A. K.: Gaseous bromine in the arctic and arctic haze, Geophys. Res. Lett., 11, 433-436, 10.1029/GL011i005p00433, 1984.

Richter, U., and Wallace, D. W. R.: Production of methyl iodide in the tropical atlantic ocean, Geophys. Res. Lett., 31, L23s0310.1029/2004gl020779, 2004.

Rook, J. J.: Formation of haloforms during chlorination of natural waters, Water Treat. Exam., 23, 234-243, 1974.

Saiz-Lopez, A., Plane, J. M. C., Baker, A. R., Carpenter, L. J., von Glasow, R., Martin, J. C. G., McFiggans, G., and Saunders, R. W.: Atmospheric chemistry of iodine, Chem. Rev., 112, 1773-1804, 10.1021/cr200029u, 2012.

Salawitch, R. J.: Atmospheric chemistry - biogenic bromine, Nature, 439, 275-277, 10.1038/439275a, 2006.

Compilation of henry's law constants for inorganic and organic species of potential importance in environmental chemistry, access: 15.05.2014, 1999.

Scarratt, M. G., and Moore, R. M.: Production of chlorinated hydrocarbons and methyl iodide by the red microalga porphyridium purpureum, Limnol. Oceanogr., 44, 703-707, 1999.

Schall, C., and Heumann, K. G.: Gc determination of volatile organoiodine and organobromine compounds in arctic seawater and air samples, Fresenius J. Anal. Chem., 346, 717-722, 10.1007/bf00321279, 1993.

Schall, C., Laturnus, F., and Heumann, K. G.: Biogenic volatile organoiodine and organobromine compounds released from polar macroalgae, Chemosphere, 28, 1315-1324, 1994.

Schall, C., Heumann, K. G., and Kirst, G. O.: Biogenic volatile organoiodine and organobromine hydrocarbons in the atlantic ocean from 42 degrees n to 72 degrees s, Fresenius J. Anal. Chem., 359, 298-305, 1997.

Schemainda, R., Nehring, D., and Schulz, S.: Ozeanologische untersuchungen zum produktionspotential der nordwestafrikanischen wasserauftriebsregion 1970 - 1973, Geodätischeund Geophysikalische Veröffentlichungen Reihe IV, 1-88, 1975.

Shi, Q., Petrick, G., Quack, B., Marandino, C., and Wallace, D.: Seasonal variability of methyl iodide in the kiel fjord, Journal of Geophysical Research: Oceans, 119, 1609-1620, 10.1002/2013jc009328, 2014.

Singh, H. B., Salas, L. J., and Stiles, R. E.: Methyl halides in and over the eastern pacific (40-degrees-n-32-degrees-s), Journal of Geophysical Research-Oceans and Atmospheres, 88, 3684-3690, 10.1029/JC088iC06p03684, 1983.

Sinnhuber, B. M., and Folkins, I.: Estimating the contribution of bromoform to stratospheric bromine and its relation to dehydration in the tropical tropopause layer, Atmos. Chem. Phys., 6, 4755-4761, 2006.

Smythe-Wright, D., Boswell, S. M., Breithaupt, P., Davidson, R. D., Dimmer, C. H., and Diaz, L. B. E.: Methyl iodide production in the ocean: Implications for climate change, Glob. Biogeochem. Cycle, 20, Gb300310.1029/2005gb002642, 2006.

Solomon, S., Garcia, R. R., and Ravishankara, A. R.: On the role of iodine in ozone depletion, J. Geophys. Res.-Atmos., 99, 20491-20499, 10.1029/94jd02028, 1994.

Solomon, S.: Stratospheric ozone depletion: A review of concepts and history, Rev. Geophys., 37, 275-316, 10.1029/1999rg900008, 1999.

Stramma, L., and Schott, F.: The mean flow field of the tropical atlantic ocean, Deep-Sea Res. Part II-Top. Stud. Oceanogr., 46, 279-303, 10.1016/s0967-0645(98)00109-x, 1999.

Tegtmeier, S., Kruger, K., Quack, B., Atlas, E. L., Pisso, I., Stohl, A., and Yang, X.: Emission and transport of bromocarbons: From the west pacific ocean into the stratosphere, Atmos. Chem. Phys., 12, 10633-10648, 10.5194/acp-12-10633-2012, 2012.

Theiler, R., Cook, J. C., and Hager, L. P.: Halohydrocarbon synthesis by bromoperoxidase, Science, 202, 1094-1096, 10.1126/science.202.4372.1094, 1978.

Tokarczyk, R., and Moore, R. M.: Production of volatile organohalogens by phytoplankton cultures, Geophys. Res. Lett., 21, 285-288, 1994.

Tomczak, M.: The distribution of water masses at the surface as derived from t-s diagram analysis in the cineca area, Rapp. Proc. Verb. Reun. Cons. Inst. Expl. Mer., 180, 48-49, 1982.

Tomczak, M., and Godfrey, J. S.: Regional oceanography: An introduction, in, 2 ed., Daya Publishing House, Delhi, 2005.

Urhahn, T., and Ballschmiter, K.: Chemistry of the biosynthesis of halogenated methanes: C1-organohalogens as pre-industrial chemical stressors in the environment?, Chemosphere, 37, 1017-1032, 10.1016/s0045-6535(98)00100-3, 1998.

Vogel, T. M., Criddle, C. S., and McCarty, P. L.: Es critical reviews: Transformations of halogenated aliphatic compounds, Environ. Sci. Technol., 21, 722-736, 10.1021/es00162a001, 1987.

Vogt, R., Sander, R., Von Glasow, R., and Crutzen, P. J.: Iodine chemistry and its role in halogen activation and ozone loss in the marine boundary layer: A model study, J. Atmos. Chem., 32, 375-395, 10.1023/a:1006179901037, 1999.

Voituriez, B.: Northern and southern equatorial undercurrents and the formation of tropical thermal domes, Oceanol. Acta, 4, 497-506, 1981.

Wanninkhof, R., Asher, W. E., Ho, D. T., Sweeney, C., and McGillis, W. R.: Advances in quantifying air-sea gas exchange and environmental forcing*, Annual Review of Marine Science, 1, 213-244, doi:10.1146/annurev.marine.010908.163742, 2009.

Weingartner, T. J., and Weisberg, R. H.: On the annual cycle of equatorial upwelling in the central atlantic-ocean, J. Phys. Oceanogr., 21, 68-82, 10.1175/1520-0485(1991)021<0068:otacoe>2.0.co;2, 1991.

Wever, R., and Krenn, B. E.: Vanadium haloperoxidases, in: Vanadium in biological systems: Physiologicy and biochemistry, Kluwer, Dordrech, 81-97, 1990.

Wever, R., Tromp, M. G. M., Krenn, B. E., Marjani, A., and Vantol, M.: Brominating activity of the seaweed ascophyllum nodosum: Impact on the biosphere, Environ. Sci. Technol., 25, 446-449, 1991.

White, R. H.: Analysis of dimethyl sulfonium compounds in marine-algae, J. Mar. Res., 40, 529-536, 1982.

Wilke, C. R., and Chang, P.: Correlation of diffusion coefficients in dilute solutions, Aiche J., 1, 264-270, 10.1002/aic.690010222, 1955.

Wong, G. T. F., and Cheng, X. H.: The formation of iodide in inshore waters from the photochemical decomposition of dissolved organic iodine, Mar. Chem., 74, 53-64, 10.1016/s0304-4203(00)00095-5, 2001.

Wuosmaa, A. M., and Hager, L. P.: Methyl-chloride transferase - a carbocation route for biosynthesis of halometabolites, Science, 249, 160-162, 10.1126/science.2371563, 1990.

Yamamoto, H., Yokouchi, Y., Otsuki, A., and Itoh, H.: Depth profiles of volatile halogenated hydrocarbons in seawater in the bay of bengal, Chemosphere, 45, 371-377, 10.1016/s0045-6535(00)00541-5, 2001.

Yang, M., Beale, R., Smyth, T., and Blomquist, B.: Measurements of ovoc fluxes by eddy covariance using a proton-transfer-reaction mass spectrometer - method development at a coastal site, Atmos. Chem. Phys., 13, 6165-6184, 10.5194/acp-13-6165-2013, 2013a.

Yang, M., Nightingale, P. D., Beale, R., Liss, P. S., Blomquist, B., and Fairall, C.: Atmospheric deposition of methanol over the atlantic ocean, Proceedings of the National Academy of Sciences, 10.1073/pnas.1317840110, 2013b.

Yang, X., Cox, R. A., Warwick, N. J., Pyle, J. A., Carver, G. D., O'Connor, F. M., and Savage, N. H.: Tropospheric bromine chemistry and its impacts on ozone: A model study, J. Geophys. Res.-Atmos., 110, D23311

10.1029/2005jd006244, 2005.

Yokouchi, Y., Hasebe, F., Fujiwara, M., Takashima, H., Shiotani, M., Nishi, N., Kanaya, Y., Hashimoto, S., Fraser, P., Toom-Sauntry, D., Mukai, H., and Nojiri, Y.: Correlations and emission ratios among bromoform, dibromochloromethane, and dibromomethane in the atmosphere, J. Geophys. Res.-Atmos., 110, D23309

10.1029/2005jd006303, 2005.

Yokouchi, Y., Osada, K., Wada, M., Hasebe, F., Agama, M., Murakami, R., Mukai, H., Nojiri, Y., Inuzuka, Y., Toom-Sauntry, D., and Fraser, P.: Global distribution and seasonal concentration change of methyl iodide in the atmosphere, J. Geophys. Res.-Atmos., 113, 10.1029/2008jd009861, 2008.

Yokouchi, Y., Saito, T., Ooki, A., and Mukai, H.: Diurnal and seasonal variations of iodocarbons (ch(2)cli, ch(2)i(2), ch(3)i, and c(2)h(5)i) in the marine atmosphere, J. Geophys. Res.-Atmos., 116, 10.1029/2010jd015252, 2011.

Yokouchi, Y., Ooki, A., Hashimoto, S., and Itoh, H.: A study on the production and emission of marine-derived volatile halocarbons, in: Western pacific air-sea interactions study, edited by: Uematsu, M., Yokouchi, Y., Watanabe, Y. W., Takeda, S., and Yamanaka, Y., TERRAPUB, Okusawa, 1-25, 2014.

Zafiriou, O. C.: Reaction of methyl halides with seawater and marine aerosols, J. Mar. Res., 33, 75-81, 1975.

Zafiriou, O. C., Blough, N. V., Micinski, E., Dister, B., Kieber, D., and Moffett, J.: Molecular probe systems for reactive transients in natural-waters, Mar. Chem., 30, 45-70, 10.1016/0304-4203(90)90061-g, 1990.

Zika, R. G., Gidel, L. T., and Davis, D. D.: A comparison of photolysis and substitution decomposition rates of methyl-iodide in the ocean, Geophys. Res. Lett., 11, 353-356, 10.1029/GL011i004p00353, 1984.

VII. Lists

1. List of Figures

Figure III-1. Contributions of different open ocean regions to emissions of $CHBr_3$ and CH_2Br_2 (warm colors – tropical regions, cold colors – temperate and polar regions). Modified from Butler et al. (2007). 15

Figure III-2. Exemplary profiles of $CHBr_3$ and CH_2Br_2 in the open ocean (a) and Chl *a* (b) at the Cape Verde Ocean Observatory (CVOO) from June 2010 (unpublished data)........ 16

Figure III-3. Methyl iodide biosynthesis using SAM-utilizing methyl transferases (Yokouchi et al., 2014)........ 21

Figure III-4. The production by phytoplankton leads to similar depth profiles as observed for $CHBr_3$ and CH_2Br_2 with pronounced maxima in the Chl *a* maximum (Moore and Groszko, 1999). 21

Figure III-5. CH_3I profiles from the tropical Atlantic (Happell and Wallace, 1996) 23

Figure III-6. Typical CH_2I_2 profile in the open ocean (a) in proximity to the Chl *a* maximum (b) at the CVOO from June 2010 (unpublished data). 25

Figure III-7. Two-layer model of a gas-liquid interface, *z* is the thickness of the transfer layer (Liss and Slater, 1974)........ 27

Figure III-8. Factors influencing the air-sea gas exchange of CO_2, modified from Garbe et al. (2014). 29

Figure III-9. Bromocarbons degrade on their way into the stratosphere. The decomposition products can react with e.g. clouds to form BrO which further can take part in ozone chemistry in the stratosphere (Salawitch, 2006)........ 31

Figure III-10. Catalytic ozone destroying cycles with involvement of bromine according to Daniel et al. (1999). *M* indicates a catalyzer........ 32

Figure III-11. Schematic of the atmospheric iodine photochemistry (Saiz-Lopez et al., 2012) with X and Y as halogen atoms and SOI standing for soluble organic iodine. 33

Figure III-12. Stratosphere-troposphere exchange modified from Holton et al. (1995). The thick line indicates the tropopause, the dark grey shaded area refers to the “lowermost stratosphere”, wavy doubleheaded arrows stand for meridional transport by eddy motions . 34

Figure III-13. The current system of the Atlantic with the positions of the two study regions of this thesis. Modified from Tomczak and Godfrey (2005). 35

Figure III-14. The currents in the Tropical Surface Water (TSW) from 0 – 100 m in boreal spring (a) and boreal fall (b), modified from Stramma and Schott (1999). 36

Figure III-15. SST distribution from 2001 from satellite (a), and the SST development from 2000 – 2009 in the section marked by stars (b), and the average annual SST cycle (c). Modified from Hummels et al. (2013). 36

Figure III-16. Tthe seasonal variability of the southern boundary of the Canary Current upwelling system (upper panel) (full dots – observed upwelling, circled dots – observed absence of upwelling), the frequency of occurrence of winds favorable for upwelling (lower panel), modified from Schemainda et al. (1975). The yellow mark indicates the season during which the DRIVE campaign took place. 37

Figure III-17. Summary of the processes that are still subjects of great uncertainty that contribute to halocarbon production and degradation in the tropical ocean as describe above.

The numbers at the processes indicate in which manuscript of the thesis they will be investigated.......... 38

Figure IV-1. Cruise track with measured SST in °C (small box) and the section (large box) during which halocarbons were sampled in both the sea surface and during CTD stations, plotted on monthly average Chl *a* for July 2011 derived from mapped level 3 MODIS Aqua Data.......... 47

Figure IV-2. Species composition (HL – high light, LL – low light) in a), SST (left side) and salinity (right side) during the cruise in b). In c) Chl *a* from underway sensor measurements (left side), and global radiation (right side). The halocarbon distribution is shown in d) for $CHBr_3$ and CH_2Br_2, and in e) for CH_3I and CH_2I_2. The top numbers mark the halocarbon CTD stations.......... 53

Figure IV-3. Selected CTD profiles (profiles 7, 9 and 10) of $CHBr_3$, CH_2Br_2, CH_3I, and CH_2I_2 in a – b), e – d), and i – j), along with temperature, salinity, and density (c, g and k), as well as raw chlorophyll in d), h), and l), and the mixed layer depth as black dashed line at the same stations.......... 57

Figure IV-4. Temperature-Salinity (T-S) plots for halocarbons (a – d, in pmol L^{-1}), and phytoplankton species (e – f, in µg Chl *a* L^{-1}). Square markers indicate surface values of halocarbons from underway measurements, circles are depth measurements from CTD profile, and the lines indicate the potential density – 1000.......... 58

Figure IV-5. Principal component analysis (PCA) of all halocarbon and phytoplankton species composition data, as well as temperature, salinity, and density for the 13 CTD stations.......... 61

Figure IV-6. Wind speed during the cruise (left side) along with sea-to-air fluxes calculated with sea surface water concentrations and mean atmospheric halocarbons from 10 air samples (right side) in a) for $CHBr_3$ and CH_2Br_2 and in b) for CH_3I and CH_2I_2. Numbers on the top indicate CTD stations.......... 62

Figure IV-7. Processes that were possibly involved in forming the observed depth profiles during the MSM18/3 cruise, including the processes that were taken into account for assessing the importance of diapycnal fluxes from below the thermocline into the mixed layer (including sea-to-air fluxes, nucleophilic chlorine substitution of CH_3I and photolysis of CH_2I_2). 70

Figure V-1. Updated version of Figure III-17 with the results of this thesis, although some uncertainy still lies in every process. The question marks indicates processes that need much further investigation as described below.......... 186

2. List of Tables

Table III-1. Henry's law coefficients for $CHBr_3$, CH_2Br_2, CH_3I and CH_2I_2. 28

Table III-2. Schmidt numbers for all four halocarbons 30

Table III-3. Local lifetimes of the four halocarbons (Montzka and Reimann, 2011). 30

Table IV-1. Mean (minimum – maximum) values of physical parameters (sea surface temperature (SST), salinity, and wind speed), biomass proxies (Chl *a* + Div *a*, and chl *a* determined from the continuously measuring fluorescence sensor), and sea surface concentrations, as well as sea-to-air fluxes of the four halocarbons $CHBr_3$, CH_2Br_2, CH_3I, and CH_2I_2 during the cruise MSM 18/3. 52

Table IV-2. Spearman's rank correlation coefficients r_s of halocarbons with different parameters and phytoplankton species. Numbers printed in bold are regarded as significant with $p < 0.05$. 56

Table IV- 3. Concentrations of $CHBr_3$, CH_2Br_2 and the sum of Chl *a* and div *a* averaged over different depths at every CTD station (1 – 13), as well as the mixed layer depth. If a range is not given, only one measurement point exists. Bold numbers indicate the maximum concentrations at this station. 59

Table IV- 4. Concentrations of CH_3I, CH_2I_2 and the sum of Chl *a* and div *a* averaged over different depths at every CTD station (1 – 13), as well as the mixed layer depth. If a range is not given, only one measurement point exists. Bold numbers indicate the maximum concentrations at this station. 60

Table IV-5. Diapycnal and sea-to-air fluxes at every CTD stations for the four halocarbons. The fluxes in bold provide the mixed layer with the corresponding halocarbon from below the mixed layer or from the atmosphere, while the negative fluxes losses from the mixed layer to below. 64

Table IV- 6. Averaged percentaged fractions of sinks during MSM18/3 for cases where diapycnal fluxes provided the mixed layer with halocarbons from below (first four columns, stations 1, 3 – 4, 9 – 11, 13 for $CHBr_3$, stations 1, 3 – 6, 9, 11, 13 for CH_2Br_2, stations 1, 9, 11 for CH_3I, and stations 1 – 9, 11 for CH_2I_2) and where halocarbons diffused out of the mixed layer (last four columns, stations 2, 5, 7 – 8, 12 for $CHBr_3$, satations 2, 7 – 8, 10, 12 for CH_2Br_2, stations 2 – 8, 10, 12 – 13 for CH_3I, stations 10, 11 – 12 for CH_2I_2). 71

3. List of Abbreviations

ACT	Atlantic Cold Tongue
BPO	Bromoperoxidase
Br^-	Bromide
BrO	Bromine oxide
Br_y	Inorganic bromine
CBr_2O	Carbonyl bromide
CCl_4	Tetrachloromethane
CFC	Chlorofluorocarbons
CH_2Br_2	Dibromomethane
CH_2ClI	Chloroiodomethane
CH_2I_2	Diiodomethane
CH_3Cl	Methyl chloride
CH_3I	Methyl iodide
CH_3O_2	Methyldioxy radical
CHBr2Cl	Dibromochloromethane
CHBr3	Bromoform
CHBrCl2	Bromodichloromethane
Chl *a*	Chlorophyll a
Cl^-	Chloride
CO_2	Carbon dioxide
CPO	Chloroperoxidase

DMSP	Dimethyl sulfoniopropionate
DOC	Dissolved organic carbon
DOI	Dissolved organic iodine
DOM	Dissolved organic matter
DRIVE	Diurnal and Regional Variability of Halogen Emissions
EUC	Equatorial Undercurrent
GOTM	General Ocean Turbulence Model
Halocarbons	Halogenated hydrocarbons
HalOcAt	Halocarbons in the Ocean and Atmosphere
HFC	Hydrofluorocarbons
HO_2	Hydroperoxyl radical
HOBr	Hypobromous acid
HOCl	Hypochlorous acid
HOI	Hypoiodous acid
HTMT	Halide ion thiol methyl transferase
I^-	Iodide
IO	Iodine oxide
IO_3^-	Iodate
IO_x	Active iodine
IPO	Iodoperoxidase
ITZC	Intertropical convergence zone
NACW	North Atlantic Central Water

NO	Nitroc oxide
NO_2	Nitrogen dioxide
O_2	Oxygen
O_3	Ozone
PFC	Perfluorocarbons
PG	Product gases
ROS	Reactive oxygen species
SACW	South Atlantic Central Water
SAH	S-adenosyl-L-homocysteine
SAM	S-adenosyl-L-methionine
SEC	South Equatorial Current
SECC	Sout Equatorial Countercurrent
SEUC	South Equatorial Undercurrent
SF6	Sulfur hexafluoride
SG	Source gases
SHIVA	Stratospheric Ozone: Halogen Impacts in a Varying Atmosphere
SOPRAN	Surface Ocean PRocesses in the ANthropocene
TSW	Tropical Surface Water
TTL	Tropical Tropopause Layer

VIII. Danksagung

Zuallererst möchte ich meiner Betreuerin Frau Dr. Birgit Quack danken, dass sie mir diese großartige Möglichkeit gegeben hat, ein sehr spannendes Thema zu bearbeiten. Dank ihrer Zusage habe ich viele großartige Erfahrungen gemacht, nette Menschen kennengelernt und sehr vieles neues gelernt. Vielen Dank für die vielen hilfreichen Gedanken während der Praktischen Arbeit und des Erstellens der Manuskripte und der Thesis. Ohne dich wäre diese Arbeit nicht möglich gewesen. Ich möchte Prof. Dr. Arne Körtzinger dafür danken, dass er zugestimmt hat, mein Doktorvater zu sein und zusammen mit Prof. Dr. Christa Marandino viele hilfreiche Ratschläge in meinen ISOS-Treffen gegeben hat. Vielen Dank, dass ihr euch bereit erklärt habt, diese Arbeit zu korrigieren.

Natürlich muss ich auch allen danken, die technisch zu dieser Arbeit beigetragen haben: Gert Petrick und Karen Stange. Vielen Dank für eure Hilfe im Labor und die Geduld, mir viele neue Dinge beizubringen. Außerdem würde ich an dieser Stelle gern dem Rest meiner Arbeitsgruppe, Franzi und Steffen, danken für Input während vieler Diskussionen. Außerdem danke ich den Fahrtleitern Prof. Dr. Hermann Bange, Arne und Birgit, sowie den Kapitänen, der Crew und der wissenschaftlichen Crew der vier Fahrten auf der FS Poseidon, FS Maria S. Merian, FS Sonne und FS Meteor, an denen ich teilgenommen habe. An dieser Stelle würde ich auch gern der gesamten Abteilung FB2-CH für die netten 4,5 Jahre danken.

Ein großes Dankeschön geht an meine Familie, ohne deren Unterstützung das alles nicht möglich gewesen wäre. Danke an meine Eltern und meine Schwestern, dass ihr mir selbst die merkwürdigsten Ideen nicht ausgeredet habt. Ich möchte gern meinem Büro, der HPA (in alphabetischer Reihenfolge: Annette, Cathleen, Kathrin, Meike und Sinikka, und natürlich dem ehemaligen Mitglied Björn), danken. Danke für eure Unterstützung während der ganzen Zeit, die ich in diesem Büro gesessen habe. Danke für die Korrekturen, die spannenden Gespräche und die moralische Unterstützung und dass ihr nicht an mir verzweifelt seid. Ohne euch wäre es nur halb so lustig gewesen. Für moralische Fahrtunterstützung (und lustige Diskussionsrunden) danke ich außerdem Anke und Tobi. Meinen Freunden, besonders dem Inner Circle, sowie Anne, Nadja und Silke, würde ich an dieser Stelle auch nochmals gern dafür danken, dass sie mich während der Arbeit unterstützt haben und nach all den Jahren immer noch mit mir befreundet sind.

Diese Arbeit wurde im Rahmen des Deutschen Verbundprojektes SOPRAN II (FKZ 03F0611A), unterstützt durch Bundesministerium für Bildung und Forschung (BMBF), und des EU-Projektes SHIVA (FP7-ENV-2007-1-226224) erstellt.

IX. Curriculum Vitae

Personal

Name: Helmke Hepach
Current adress: Weißenburgstr. 36, 24116 Kiel
Birth date: November 3rd 1984 (Berlin)
Nationality: German

Education

11/2009 – 06/2014	PhD Studies at the Christian-Albrechts-Universität zu Kiel under the supervision of Dr Birgit Quack and Prof Dr Arne Körtzinger
10/2004 – 10/2009	German Diplom (equivalent to a Master's degree) in Marine Environmental Sciences at the Carl von Ossietzky Universität (studies with emphasis on Marine Geochemistry, minors: physical and biological oceanography)
06/2004	German Abitur at the Heinrich Hertz Oberschule Berlin (high school with emphasis on Science and Mathematics)

Studies abroad

01/2009 – 06/2009	Research for the Diplom thesis at the University of British Columbia, Vancouver, Canada under the supervision of Prof. Dr. Philippe Tortell
01/2008 – 06/2008	Erasmus semester at the Università degli Studi di Perugia, Italy (internships in analytical environmental Chemistry and Geology)
08/2001 – 06/2002	Exchange year at the Jasper High School, Jasper, IN, USA

Awards

08/2011 – 09/2011	Selected participant at the SOLAS Summer School 2011, Cargèse, Corse, France
04/2009 – 06/2009	Scholarship for conducting research in a foreign country from the German Academic Exchange Service (DAAD)
01/2008 – 06/2008	Erasmus scholarship to study in Perugia, Italy

Work Experience

11/2009 – 05/2015	Research assistant at the GEOMAR Helmholtz centre for ocean research Kiel, Germany in the chemical oceanography department in the halocarbon working group
11/2008 – 12/2008	Internship at the Alfred Wegener Institute for Polar and Marine Research in Potsdam in the department "Atmospheric circulation"

07/2007 – 08/2009	Student assistant at the Postam Institute for Climate Impact Research (PIK), Potsdam in the department “Sustainable Solutions”

Campaigns

07/2014 – 08/2014	SO234 and OASIS-Sonne cruises onboard the RV Sonne (Durban, South Africa – Port Louis, Mauritius – Male, Maledives)
12/2012	M91 cruise onboard the RV Meteor (Callao, Peru – Callao, Peru)
11/2011	SHIVA-Sonne cruise onboard the RV Sonne (Singapore, Singapore – Manila, Philippines)
06/2011 – 07/2011	MSM18/3 cruise onboard the RV Maria S. Merian (Mindelo, Cape Verde – Libreville, Gabon)
05/2010 – 06/2010	DRIVE (Diurnal and RegIonal Variability of halogen Emissions) onboard the RV Poseidon (P399/2 and 3, Las Palmas, Spain – Mindelo, Cape Verde – Las Palmas, Spain – Vigo, Spain)
01/2009 – 06/2009	Several one-day cruises to the fjord Saanich Inlet on Vancouver Island, Canada

Publications

H. Hepach, B. Quack, S. Raimund, T. Fischer, A. Bracher: “*Halocarbon budget and sources in the equatorial Atlantic Cold Tongue*” – in preparation

H. Hepach, B. Quack, F. Ziska, S. Fuhlbrügge, E. L. Atlas, K. Krüger, I. Peeken, and D. W. R. Wallace: “*Driver of diel and regional variations of halocarbon emissions from the tropical North East Atlantic*” Atmos. Chem. Phys., 14, 1255-1275, doi:10.5194/acp-14-1255-2014, 2014.

S. Tegtmeier, K. Krüger, B. Quack, E. Atlas, D. R. Blake, H. Boenisch, A. Engel, H. Hepach, R. Hossaini, M. A. Navarro, S. Raimund, S. Sala, Q. Shi, and F. Ziska: “*The contribution of oceanic methyl iodide to stratospheric iodine*” Atmos. Chem. Phys. Discuss., 13, 11427-11471, doi:10.5194/acpd-13-11427-2013, 2013.

F. Ziska, B. Quack, K. Abrahamsson, S. D. Archer, E. Atlas, T. Bell, J. H. Butler, L. J. Carpenter, C. E. Jones, N. R. P. Harris, H. Hepach, K. G. Heumann, C. Hughes, J. Kuss, K. Krüger, P. Liss, R. M. Moore, A. Orlikowska, S. Raimund, C. E. Reeves, W. Reifenhäuser, A. D. Robinson, C. Schall, T. Tanhua, S. Tegtmeier, S. Turner, L. Wang, D. Wallace, J. Williams, H. Yamamoto, S. Yvon-Lewis, and Y. Yokouchi: “Global sea-to-air flux climatology for bromoform, dibromomethane and methyl iodide*” Atmos. Chem. Phys., 13, 8915-8934, doi:10.5194/acp-13-8915-2013, 2013.*

I. Stemmler, M. Rothe, I. Hense, and H. Hepach: "Numerical modeling of methyl iodide in the eastern tropical Atlantic" Biogeosciences, 10, 4211-4225, doi:10.5194/bg-10-4211-2013, 2013.

S. Fuhlbrügge, K. Krüger, B. Quack, E. Atlas, H. Hepach, and F. Ziska: “*Impact of the marine atmospheric boundary layer conditions on VSLS abundances in the eastern tropical and* *subtropical North Atlantic Ocean*” Atmos. Chem. Phys., 13, 6345-6357, doi:10.5194/acp-13-6345-2013, 2013.

X. Eidesstattliche Erklärung

Hiermit erkläre ich, dass ich die von mir vorgelegte Dissertation, bis auf die Beratung durch meine Betreuer, selbstständig und ohne Zuhilfenahme unerlaubte Hilfsmittel angefertigt habe. Alle benutzten Quellen und Hilfsmittel habe ich vollständig angegeben und die Zusammenarbeit mit anderen Wissenschaftlern habe ich kenntlich gemacht. Zudem versichere ich, dass diese Arbeit unter Einhaltung der Regeln guter wissenschaftlicher Praxis der Deutschen Forschungsgesellschaft verfasst wurde, und dass sie nach Form und Inhalt meine eigene Arbeit ist. Weder diese noch eine ähnliche Arbeit wurden an einer anderen Abteilung oder Hochschule im Rahmen eines Prüfungsverfahrens vorgelegt, veröffentlicht oder zur Veröffentlichung vorgelegt. Dies ist mein erstes und einziges Promotionsverfahren.

Kiel, den 21.05.2014

(Helmke Hepach)